



National Library
of Canada

Acquisitions and
Bibliographic Services Branch

395 Wellington Street
Ottawa, Ontario
K1A 0N4

Bibliothèque nationale
du Canada

Direction des acquisitions et
des services bibliographiques

395, rue Wellington
Ottawa (Ontario)
K1A 0N4

395 Wellington Street

395, rue Wellington

NOTICE

The quality of this microform is heavily dependent upon the quality of the original thesis submitted for microfilming. Every effort has been made to ensure the highest quality of reproduction possible.

If pages are missing, contact the university which granted the degree.

Some pages may have indistinct print especially if the original pages were typed with a poor typewriter ribbon or if the university sent us an inferior photocopy.

Reproduction in full or in part of this microform is governed by the Canadian Copyright Act, R.S.C. 1970, c. C-30, and subsequent amendments.

AVIS

La qualité de cette microforme dépend grandement de la qualité de la thèse soumise au microfilmage. Nous avons tout fait pour assurer une qualité supérieure de reproduction.

S'il manque des pages, veuillez communiquer avec l'université qui a conféré le grade.

La qualité d'impression de certaines pages peut laisser à désirer, surtout si les pages originales ont été dactylographiées à l'aide d'un ruban usé ou si l'université nous a fait parvenir une photocopie de qualité inférieure.

La reproduction, même partielle, de cette microforme est soumise à la Loi canadienne sur le droit d'auteur, SRC 1970, c. C-30, et ses amendements subséquents.

UNIVERSITY OF ALBERTA

AXIAL FATIGUE OF MULTI-LAYERED WIRE STRANDS

BY

PANAGIOTIS PAPANIKOLAS



A thesis submitted to the Faculty of Graduate Studies and Research in partial fulfillment of the requirements for the degree of DOCTOR OF PHILOSOPHY

DEPARTMENT OF CIVIL ENGINEERING

EDMONTON, ALBERTA

SPRING 1995



National Library
of Canada

Acquisitions and
Bibliographic Services Branch

395 Wellington Street
Ottawa, Ontario
K1A 0N4

Bibliothèque nationale
du Canada

Direction des acquisitions et
des services bibliographiques

395, rue Wellington
Ottawa (Ontario)
K1A 0N4

Vous le / Votre référence

Vous le / Notre référence

THE AUTHOR HAS GRANTED AN IRREVOCABLE NON-EXCLUSIVE LICENCE ALLOWING THE NATIONAL LIBRARY OF CANADA TO REPRODUCE, LOAN, DISTRIBUTE OR SELL COPIES OF HIS/HER THESIS BY ANY MEANS AND IN ANY FORM OR FORMAT, MAKING THIS THESIS AVAILABLE TO INTERESTED PERSONS.

L'AUTEUR A ACCORDE UNE LICENCE IRREVOCABLE ET NON EXCLUSIVE PERMETTANT A LA BIBLIOTHEQUE NATIONALE DU CANADA DE REPRODUIRE, PRETER, DISTRIBUER OU VENDRE DES COPIES DE SA THESE DE QUELQUE MANIERE ET SOUS QUELQUE FORME QUE CE SOIT POUR METTRE DES EXEMPLAIRES DE CETTE THESE A LA DISPOSITION DES PERSONNE INTERESSEES.

THE AUTHOR RETAINS OWNERSHIP OF THE COPYRIGHT IN HIS/HER THESIS. NEITHER THE THESIS NOR SUBSTANTIAL EXTRACTS FROM IT MAY BE PRINTED OR OTHERWISE REPRODUCED WITHOUT HIS/HER PERMISSION.

L'AUTEUR CONSERVE LA PROPRIETE DU DROIT D'AUTEUR QUI PROTEGE SA THESE. NI LA THESE NI DES EXTRAITS SUBSTANTIELS DE CELLE-CI NE DOIVENT ETRE IMPRIMES OU AUTREMENT REPRODUITS SANS SON AUTORISATION.

ISBN 0-612-01743-5

Canada

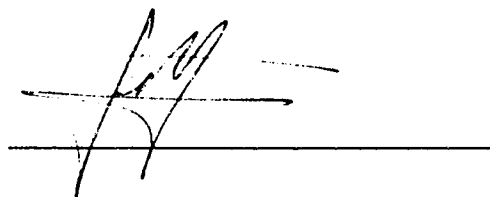
UNIVERSITY OF ALBERTA

RELEASE FORM

NAME OF AUTHOR: Panagiotis Papanikolas
TITLE OF THESIS: Axial Fatigue of Multi-layered Wire Strands
DEGREE: Doctor of Philosophy
YEAR THIS DEGREE GRANTED: 1995

Permission is hereby granted to the University of Alberta Library to reproduce single copies of this thesis and to lend or sell such copies for private, scholarly or scientific research purposes only.

The author reserves all other publication and other rights in association with copyright in the thesis, and except as hereinbefore provided neither the thesis nor any substantial portion thereof may be printed or otherwise reproduced in any material form whatever without the author's prior written permission.


A handwritten signature in black ink, appearing to be 'P. Papanikolas', is written over a horizontal line.

Panagiotis Papanikolas
Apt. 212, 10545 Saskatchewan Drive
Edmonton, Alberta
T6E 6C6, Canada

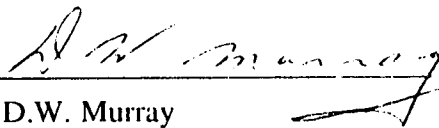
Date: APRIL 19/95

UNIVERSITY OF ALBERTA
FACULTY OF GRADUATE STUDIES AND RESEARCH

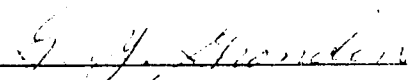
The undersigned certify that they have read, and recommend to the Faculty of Graduate Studies and Research for acceptance, a thesis entitled AXIAL FATIGUE OF MULTI-LAYERED WIRE STRANDS submitted by Panagiotis Papanikolas in partial fulfillment of the requirements for the degree of DOCTOR OF PHILOSOPHY.




Dr. G.L. Kulak — Supervisor



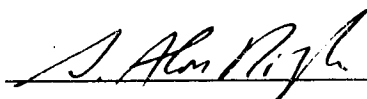
Dr. D.W. Murray



Dr. G.Y. Grondin



Dr. D.J. Steigmann



For Dr. M. Raof — External Examiner

Date April 10, 1995

Dedicated to the memory of my
father, Constantinos.

Abstract

A steel cable is a flexible load-transmitting element that is made up of a multitude of individual high strength wires laid out in a parallel fashion or helically around a center wire. Steel cables have both structural and industrial applications. Structural applications include use in suspension and cable-stayed bridges. The adequacy of cable-stayed and suspension bridges is dependent, among other things, on the axial fatigue performance of the cables. Presently, designers of bridges are working without adequate knowledge concerning the fatigue life of the principal components in these systems. The American Petroleum Institute and the Post-Tensioning Institute appear to provide the only specifications in North America that give simplified recommendations for the fatigue design of standing cables. However, the fatigue life obtained using these specifications differs significantly.

An investigation of the axial fatigue strength of multi-layered strands (bridge strands) is reported herein. The effects of stress range, cable make-up, and length to diameter ratio were experimentally investigated using sixteen full-size multi-layered wire strands. The strands tested in this program were of 45 or 25 mm diameter, had a length-to-diameter ratio of 75 to 133 and were subjected to a stress range of between 15% and 30% of the ultimate tensile strength of the strand.

Based on the limited number of specimens tested close to destruction, a failure criterion was derived. The effect of both the strand make-up and the stress range were found to be significant. For the lengths tested, the termination region had no influence on the fatigue life of the specimens. Fractographic examination revealed that wire breaks within the free length were due to localized fretting fatigue at the interlayer contact patches. Interlayer wire friction was also found to be the cause of multiple breaks that took place in individual wires. From a simulated two-block amplitude test, it was concluded that a linear damage cumulative hypothesis will underestimate the fatigue life.

The comparison of the data obtained herein with those from the literature concluded that the equation proposed by the American Petroleum Institute gives unsafe results for both high and low cycle fatigue. Finally, the extrapolation of the fatigue strength of multi-layered strands from test lengths to actual lengths was analytically investigated using the Castillo et al. statistical model. This statistical analysis showed that the effect of length diminishes as the probability of failure approaches zero. For design purposes, the effect of length was taken into account by using the 5% probability failure of an infinitely long cable.

Acknowledgments

The research described in this investigation was conducted with financial assistance received from the Natural Sciences and Engineering Research Council of Canada. The financial contribution and interest of Alberta Transportation and Utilities in conducting the acoustic emission non-destructive examination is greatly appreciated.

The author acknowledges financial support received in the form of Graduate Teaching Assistantship from the University of Alberta and scholarships from the following organizations: Faculty of Graduate Studies of the University of Alberta, the Canadian Institute of Steel Construction, and the American Hellenic Educational and Progressive Association.

The assistance of technicians in the Department of Civil Engineering, Department of Electrical Engineering, and the Department of Mining, Petroleum and Metallurgical Engineering of the University of Alberta is greatly appreciated.

The interest shown by Peter Johnson of Wrights Canadian Ropes is also acknowledged. Mr. Johnson advised the author of field practice of the cable industry and helped in the development of the socket detail. Dr. M.L. Wayman of the Department of Mining, Petroleum and Metallurgical Engineering freely assisted the author in the metallurgical examinations. Finally, the author wishes to express his deep appreciation to his research supervisor, Dr. G.L. Kulak, for his support and guidance throughout this study.

Table of Contents

Abstract.....	i
Acknowledgments.....	ii
List of Symbols.....	vii
1. Introduction.....	1
1.1 General Background.....	1
1.1.1 Definitions Related to Cables.....	1
1.1.2 Manufacturing Process, and Mechanical Properties.....	1
1.1.3 Basic Types of Cables and their Applications.....	3
1.1.3.1 Structural Strands and Structural Ropes.....	3
1.1.3.2 Locked Coil Strand.....	4
1.1.3.3 Parallel Bars.....	5
1.1.3.4 Parallel-Wire Strand.....	5
1.1.3.5 Parallel Strand Rope.....	7
1.1.4 Modulus of Elasticity and Elongation of a Cable.....	7
1.1.5 Cable Anchorages and Connections.....	8
1.1.5.1 General.....	8
1.1.5.2 Types of Sockets.....	9
1.1.6 Corrosion Protection.....	10
1.2 Statement of the Problem.....	11
1.2.1 Scope and Objectives.....	12
1.2.2 Organization of the Thesis.....	13
2. Literature Review.....	19
2.1 Performance of Existing Cables.....	20
2.2 Kinematics of Cables.....	20
2.3 Cables under Cycling Loading.....	21
2.3.1 Fatigue Failure Mechanism for Cables.....	21
2.3.2 Single Wire Axial Fatigue.....	22
2.3.3 Axial Fatigue Tests of Cables.....	23
2.3.4 Design Recommendations (S-N curves).....	30
2.3.5 Analytical Model for Axial Fatigue Life Prediction.....	32
2.4 Length Effect.....	33
2.4.1 Statistical Models.....	34

2.5	Wire Breakage Monitoring Methods	35
2.6	Summary	37
3.	Experimental Program.....	44
3.1	Introduction	44
3.2	Axial Fatigue Test Program	45
3.2.1	Development of the End Termination	45
3.2.2	Preparation of Specimens	46
3.2.3	Detection of Broken Wires.....	48
3.2.3.1	Accelerometer	48
3.2.3.2	Acoustic Emission System.....	49
3.2.3.2.1	Single Wire Tensile Test.....	50
3.2.3.2.2	Wave Attenuation Tests	50
3.2.3.2.3	Pulse Echo Test.....	51
3.2.4	Axial Fatigue Test Setup.....	51
3.3	Ancillary Tests	52
3.4	Metallography and Fractography	53
4.	Results of Experimental Program.....	74
4.1	Introduction	74
4.2	Acoustic Emission Calibration Test Results.....	74
4.2.1	Acoustic Emission Signal Characteristics	74
4.2.2	Signal Attenuation.....	75
4.2.3	Pulse Echo Test.....	75
4.3	Axial Fatigue Tests	76
4.3.1	Preliminary Test SP1	76
4.3.2	Series SP	78
4.3.3	Series SL	80
4.3.4	Series SS	81
4.4	Fractography.....	82
4.5	Metallography.....	83
4.6	Coupon Test Results.....	83
4.7	Chemical Analysis.....	84
4.8	Summary	84
5.	Discussion of Test Results.....	129
5.1	Introduction	129

5.2	Location of Wire Breaks.....	129
5.3	Modulus of Elasticity.....	131
5.4	Discard Criterion.....	134
5.5	Effect of Length of the Specimen.....	136
5.6	Regression Analysis and Effect of Strand Make-up.....	137
5.7	Effect of Stress Range on Fatigue Life.....	139
5.8	Effect of Specimen Temperature and Test Frequency.....	142
5.9	Performance of Cable Termination.....	143
5.10	Cumulative Fatigue Damage.....	143
6.	Comparison of Test Results with Work of Other Investigators.....	161
6.1	Introduction.....	161
6.2	Castillo et al. Statistical Model.....	161
6.2.1	Development of the Program FANOW.....	163
6.2.2	Castillo Model for the 45 mm Diameter Strand.....	164
6.2.3	Castillo Model for the 25 mm Diameter Strand.....	166
6.2.4	Castillo Model for all Tests Conducted at the University of Alberta.....	168
6.3	Inclusion of Previous Experimental Data.....	169
6.3.1	Experimental Work of Tilly (Ref. 16, Ref. 89).....	169
6.3.2	Experimental Work of Hobbs and Gavani (Ref. 64).....	170
6.3.3	Experimental Work of Raof (Ref. 72).....	172
6.4	Comparison of Test Data with Existing Design Curves.....	172
6.5	Simplified Design Equation.....	175
7.	Summary, Conclusions and Recommendations.....	186
7.1	Summary.....	186
7.2	Conclusions.....	188
7.2.1	Effect of Testing Parameters.....	188
7.2.2	Detection of Wire Breaks.....	189
7.2.3	Cumulative Fatigue Damage.....	189
7.2.4	Distribution of Wire Breaks and Failure Mechanism.....	189
7.2.5	Discard Criterion.....	190
7.2.6	Length Effect.....	190
7.3	Recommendations.....	191
7.3.1	Design Recommendations.....	191
7.3.2	Recommendations for Future Research.....	192

List of References	195
Appendix A. Test Data from Static Tests and Wire Breakage Detection	204
Appendix B. Statistical Analysis of Test Data.....	209
Appendix C. Experimental Data from Literature.....	217

List of Symbols

A	= Weibull shape or slope parameter in Castillo et al. model.
A_i	= Net steel area of a wire in layer i.
A_C	= Steel area of the core wire.
b_i	= Slope of regression line (Eq. 5.7).
B	= Asymptotic limit for Castillo et al. model.
C	= Parameter representing endurance limit in Castillo et al. model.
C_1	= Constant for Raoof analytical model (given by Eq. 2.9).
C_2	= Constant for Raoof analytical model (given by Eq. 2.10).
D	= Scale fitting parameter corresponding to a reference length L_0 (Castillo et al. model).
D_i	= Diameter of wire in layer i.
E	= Constant defining the S-N threshold curve (asymptotic curve) for Castillo et al. model.
$E(N; \Delta\sigma, L_0)$	= Cumulative distribution function of N for given $\Delta\sigma$ (Eq. 6.3).
E_s	= Modulus of elasticity for an individual steel wire (MPa).
$E_{full-slip}$	= Full-slip modulus of elasticity for a multi-layered wire strand (MPa) (Eq.5.1).
$E_{no-slip}$	= No-slip modulus of elasticity for a multi-layered wire strand (MPa) (Eq. 5.5).
$F_L(x)$	= Probability of failure function for a cable having length L. (Eq. 6.2).
$F_{L_0}(x)$	= Probability of failure function, for the sub-elements (i.e., test data) of length L_0 .
$F(\Delta\sigma; N, L_0)$	= Cumulative distribution function of $\Delta\sigma$ for given N (Eq. 6.4).
H	= Hruska parameter (given by Eq. 5.2).
K_a	= Surface finish factor for Raoof analytical model.
K_b	= Fretting fatigue parameter for Raoof analytical model.
K_c	= Core ion factor for Raoof analytical model.
$K_{P,L_0/L}$	= Constant used with Castillo et al. model, which depends on the probability of failure P and the cable ratio L_i/L .
K_S	= Stress concentration factor.
L	= Length of an actual cable.
L_0	= Length of a test specimen or sub-element.
n_i	= Number of wires in layer i.

N	= Fatigue life in cycles; Number of loading cycles; Total number of layers including the core wire.
N_c	= Fatigue life of a single galvanized wire.
N_{III}	= Threshold number of cycles in Castillo et al. model.
N_{i1}	= Number of cycles to failure at a stress range level i (Eq. 5.22).
N_i	= Fatigue life of a sub-element i .
P	= Probability of failure of an actual cable.
R	= Load range expressed as percentage of the minimum ultimate tensile strength.
s_b	= Standard deviation of the slope (given by Eq. 5.15).
s_e	= Standard error of estimate (given by Eq. 5.11).
S	= Non-dimensional stress factor.
S'	= Endurance limit of an individual wire.
S_1^i	= Nominal axial strain in individual wire.
S_e	= Reduced magnitude of endurance limit of a single wire due to interlayer contact and corrosion (Eq. 2.11).
S_f	= Equivalent fatigue stress in Raoof model (MPa)
S_r	= Stress range expressed as percentage of the minimum ultimate tensile strength.
S_{ult}	= Ultimate tensile strength of a single wire.
t	= Test statistic parameter (given by Eq. 5.14).
$t_{\alpha/2, n-2}$	= Student's distribution for a level of significance α and a number of degrees of freedom of $n-2$.
α_i	= Lay angle in layer i .
$\Delta\sigma$	= Stress range (MPa).
$\bar{\sigma}'$	= Nominal wire axial stress for Raoof model (MPa) (given by Eq. 2.13).
σ_m	= Mean stress (MPa).
σ_{max}	= Maximum static loading (in MPa).
σ'_a	= Amplitude axial stress of a wire (MPa) (given by Eq. 2.15).
σ'_m	= Mean nominal axial stresses of a wire (MPa) (given by Eq. 2.15).
σ'_{max}	= Maximum applied cycling stress (MPa)
σ'_{min}	= Minimum applied cycling stress (MPa)
$\bar{\sigma}'_{max}$	= Effective maximum von Mises contact stress (MPa).
σ_u	= Ultimate tensile strength (MPa).

Chapter 1

Introduction

1.1 General Background

1.1.1 Definitions Related to Cables

The term cable is defined in a general way to indicate any flexible tension member having a negligible resistance to bending. Cables have a high strength-to-weight ratio and have a variety of applications. The engineering applications of cables can be classified as structural (cable-stayed and suspension bridges, prestressing of concrete, mooring of offshore structures, etc.) and industrial (cranes, elevators, dragline excavators, winding system in mining, etc.). Depending on their use, cables can be grouped into two broad categories: running cables and standing cables. The principal distinguishing feature is that running cables move over a sheave, whereas standing cables are static.

The basic element of a cable is the steel wire. With the exception of parallel wire strand, a strand is an assembly of wires wound in an helical pattern around a central straight wire in one or more symmetrical layers forming a single or multi-layered wire strand. In the case of a parallel wire strand, the individual wires are arranged in a parallel configuration without the helical twist. Finally, a rope is composed of a plurality of strands helically wound around a core that could be either a strand or another rope.

1.1.2 Manufacturing Process, and Mechanical Properties of Steel Wires, Strands, and Ropes

The manufacturing process (Ref. 1) of steel wires starts at the rod-mill, where a continuous series of rollers reduce the billets to round rods having a diameter from about 5.5 mm to 18.6 mm. The rods are then heat-treated and quenched at a carefully controlled temperature in order to improve the tensile strength and to relieve the stress created during the hot rolling of the steel ingots into billets.

The rods are then inspected to ensure that all physical and chemical standards are met. The steel produced for cables has a chemical composition with considerably higher carbon content (0.8 percent carbon) than is allowed for structural steel (0.2 percent). Table 1.1, taken from Ref. 2, shows a comparison between the chemical composition of typical cable steel and structural steel.

After inspection, the rods are cleaned by dipping them in acid to remove mill scale, rinsed in water, neutralized, coated with a lubricant which facilitates the drawing process, and finally, coiled for shipment to the wire mill.

In the wire mill, wires are produced by cold drawing a rod through a series of dies. This process reduces the cross-sectional area of the rod by 65% to 75%, and also improves the internal structure of the steel and therefore increases the tensile strength. The quality control test program for the steel wire typically includes tension and torsion tests to determine uniformity and toughness and gauging to measure the diameter.

Before manufacturing structural strands and ropes, wires are usually coated (galvanized) with a layer of pure zinc. This coating gives the steel wire a measure of protection from atmospheric corrosion. Three different zinc coating categories exist. The most common is class A weight zinc-coated wires. Class B coating has twice and class C has three times the amount of zinc per square meter of wire surface of class A coating. The weight requirements of zinc coatings for various sizes of wires are specified in ASTM Standards A586-86 and A603-88 (Ref. 3, 4).

The mechanical properties of the finished zinc-coated drawn wire depend on the zinc coating class and the diameter of the wire. Table 1.2, reproduced from ASTM A586-86 (Ref. 3) and ASTM A603-88 (Ref. 4) Standards, gives the mechanical properties of zinc-coated wires. A comparison with typical values for mild and high strength structural steels is given in the same table.

Strands are produced from the individual wires that have been wound on steel spools before being placed in the cradle of the stranding machine. The stranding machine can rotate in either a clockwise or counterclockwise direction and the resulting strand is designated as either right lay or left lay, accordingly. The larger structural strands, referred to as multi-layered strands, are made by adding successive layers of wires. Strands having the wires of one layer crossing over those of the adjacent layer are referred to as a cross lay. Otherwise, the strand is referred to as an equal lay. The mechanical properties of a structural strand are given in ASTM Standard A586-86 (Ref. 3). Figure 1.1(a) shows a multi-layered wire strand consisting of six layers with a total of 91 wires.

A structural rope is made in a way similar to that described for structural strand. In this case, the individual wires are replaced by strands. These strands are placed into the cradles of a larger stranding machine. If the strands in a rope twist around the rope in a clockwise direction, the rope is in right hand lay. Conversely, if they twist in a counterclockwise

direction, the rope is in left hand lay. If the wires twist in the same direction as the strands themselves, the rope is said to be in Lang's lay, and if the wires twist in the opposite direction to the strands, the rope is said to be in ordinary lay. Depending the class of coatings of the wires, the mechanical properties of a rope vary, and in North American practice these properties are given by ASTM Standard A603-88 (Ref. 4). The cross-section of a structural rope is shown in Figure 1.1(b).

Note that, unless otherwise specified, structural strands and ropes are furnished with class A weight zinc-coated wires. However, where additional corrosion protection is required, structural strands may be ordered with class A coating on inner wires and either class B or class C coating for outer wires.

1.1.3 Basic Types of Cables and their Applications

In the following sections, the different types of cables, their advantages and their applications will be presented. In general, cables can be grouped in the following six categories, which are presented with their corresponding ASTM Standards :

- Structural helical strands, ASTM A586 (Ref. 3)
- Structural stranded ropes, ASTM A603 (Ref. 4)
- Locked-coil strands
- Parallel bars, ASTM A722 (Ref. 5)
- Parallel wires, ASTM A421 (Ref. 6)
- Parallel strands, ASTM A416 (Ref. 7)

1.1.3.1 Structural Strands and Structural Ropes

Structural helical strands and stranded ropes are the most commonly used types of cables. The manufacturing process and the structure of these cables were presented in Sections 1.1.1 and 1.1.2. The significant differences between strands and ropes that should be taken into consideration when selecting a cable are the following (Ref. 8, 9):

- A strand has a higher strength to size ratio than a rope. Based on the gross metallic area, the minimum ultimate tensile strength (UTS) of a strand is 1400 MPa (ASTM A586), while a rope should have a UTS of 1335 MPa (ASTM A603).
- A strand has a higher and more consistent modulus of elasticity than a rope. The modulus of elasticity of a strand (Ref. 8) ranges between 150 000 MPa to 185 000 MPa, while that of a rope is between 55 000 MPa and 140 000 MPa. See Table 1.3 for typical values of modulus of elasticity.

- A strand has a higher resistance to corrosion. This is due to the fact that outside surface is smoother than that of a rope and larger diameter steel wires are used. It therefore follows that the surface exposed to environmental effects is smaller, and this translates to an improved corrosion resistance. In addition, the smoother surface of the strand can more easily be protected with a paint covering.
- A strand has a better tension fatigue performance, while a rope has an improved bending fatigue behavior.

Strands are usually specified when a large force must be transferred and the flexibility or bending of the cable is not a major requirement. They may also be chosen in cases where the corrosion and the tension fatigue are of paramount consideration. In addition, strands use smaller accessories fittings (sockets, splices) because the strand diameter required for a given load is smaller than that of a rope. This explains why strands are generally preferred to ropes for standing structural applications, such as suspended or cable-stayed bridges.

On the other hand, ropes are specified when flexibility, bending and bending fatigue are important considerations in the application of the cable. Other advantages of a rope are that it is easier to handle in the field and the size of saddles for ropes are generally smaller because of its flexibility and bending capabilities. Ropes are therefore widely used in the materials handling industry (cranes, elevators, dragline excavators, winding, etc.), where cables have to bent and move over a sheave, drum or pulley.

1.1.3.2 Locked Coil Strand

Locked coil strand is also an helical type strand (Ref. 2). However, in this case different shapes of wires are used in the outer layers to form a strand with a smoother and tighter surface. The locked coil strand has a center portion composed of a number of round wires, several inner layers with wedge shaped wires, and outer layers consisting of wires with special Z- or S- shaped wires.

The advantages of this type of strand compared to the previously discussed structural strands (ASTM A586) arise from the application of the wedge and Z-shaped wires fitted tightly together in the outer layers. Those advantages are as follows:

- The density of a locked coil strand is approximately 85 to 90%, whereas helical strands of round wires have a density of about 70%. This results in smaller diameter cables for a given cross-sectional area. The minimum ultimate tensile strength based on the gross metallic area is 1570 MPa.

- Locked coil strands have an improved corrosion resistance by virtue of the tightly locked shaped wires in the exterior.
- Locked coil strands have a higher modulus of elasticity (170 000 MPa) than do structural strands and ropes.
- The special shaped wires of the outer layers also make the locked coil strands less sensitive to side pressure at saddles and anchorages because the wires have a genuine contact surface and not just a point contact, as in the case of round wires.

Locked coil strands were developed in Europe, where they have been extensively used in many of the early cable-stayed bridges. They are fabricated with diameters in the range of 40 mm to 120 mm. In contemporary design of cable-stayed bridges, locked coil strands are considered if for some reason a plastic pipe sheathing cannot be employed, in which case the locking and sealing features of the shaped wires will provide some inherent corrosion protection.

1.1.3.3 Parallel Bars

Parallel bar cables consist of high strength steel bars specified by ASTM A722-88a (Ref. 5). They are mostly intended for use in prestressed concrete construction. Two types of high strength steel bars are specified by ASTM A722-88a. A type I bar has a plain surface and a type II bar has surface deformations. The nominal diameter ranges from 15 to 36 mm and the minimum ultimate tensile strength is 1035 MPa. The modulus of elasticity of a parallel bar is 200 000 MPa. When high strength bars are used for cable-stays, type II is usually specified. In this case, the bars are coupled together in order to fabricate a stay. Because of the presence of couplers, the fatigue resistance of a parallel bar is lower than that of a wire strand.

1.1.3.4 Parallel-Wire Strand

The types of cables that were covered in the previous paragraphs are the so-called helical strands or cables. Because of the twisting of the layers, the helical strand becomes self-compacting and therefore the wires are held together naturally and without requiring application of a wrapping or bands around the strand. Another advantage of the helically wound cables is that each wire forms a spiral with its axis at the center of the strand: they are therefore easily curved around the reel, coil, saddle, or collars. Note that curving (or bending) of the helical strands or ropes does not require any elongation or contraction of the individual wires. The reduction of strength and stiffness in comparison with cables made out of straight wires and the fact that they require prestretching are the main two shortcomings of helically wound ropes.

In cases of bridges where cables do not need to move over a saddle and where large forces must be transferred by the cable (especially for the back stays of cable-stayed bridges), parallel wire cables have recently been introduced in bridge construction practice (Ref. 10). The major advantage of parallel wire cables is the improved strength and stiffness: since the wires are maintained straight, uniform stress is achieved. In fact, the elastic behavior of parallel wire cable approaches that of an individual wire (i.e., 200 000 MPa). In addition, pre-assembled parallel wire strands do not require any prestretching because there is no constructional stretch. (See Section 1.1.4 for the definition of constructional stretch).

Handling of parallel wire strands was the major disadvantage that excluded the use of those cables until the early 1960's. This problem is related to reeling, coiling and general bending of those cables, since the curving of a parallel-wire strand with undistorted cross-section will require an elongation of the wires at the outside and a corresponding contraction at the inside of the curve. However, this problem has been overcome by using larger diameter coils and reels.

In present practice, parallel wire strands follow the ASTM A421-80 Standard (Ref. 6), type BA wire, with minimum tensile strength of 1655 MPa and with a diameter ranging between 4.88 and 7.01 mm. See Table 1.3. Type BA wire has a cold-end deformation which is used for anchoring purposes. Note that the button-headed wires are individually anchored in the anchor socket, consequently requiring prefabrication of the stay. The minimum modulus of elasticity is 200 000 MPa, which is higher than the modulus of elasticity of a helically wound cable. In general, for suspension bridges 5 mm diameter wires are used for the parallel wire cables, whereas 7 mm diameter wires have been used in strands for the stays of multi-cable stayed systems.

In Japan, where the idea of using parallel-wire strands was first adopted, a trend towards using larger wires and strands is observed. Recently, another cable was developed, the semi-parallel wire strand (Ref. 10). It has its wires wound around the center wire with very large lays. This cable has all the advantages of the parallel wire strand plus the ability of holding the wires together without requiring any additional wrapping.

One of the main design considerations for a cable is its fatigue behavior. There can be a major difference in the axial fatigue behavior of stranded and parallel wire cables. When axial tension is applied to a stranded cable, high contact pressure develops at the interwire contact areas between wires of different layers. In addition, helically wound wires of adjacent layers have different lengths. Under cycling axial load, this will result in repetitive

movements at the interwire contact areas. The fatigue failure mode is therefore identified as localized fretting fatigue. By contrast, in the case of parallel wire strands a larger contact area along the length of adjacent wires exist. The interwire contact pressure will therefore be so low that fretting fatigue may not be developed. In the case of parallel wire strands, fatigue fractures are usually limited to the outside layer of the wires in the socket region. This is because of the high stress concentration experienced by those wires when transmitting the load from the termination to the free length of the cable.

1.1.3.5 Parallel-Strand Rope

Parallel strand cables are similar to parallel wire cables except that in this case the rope is composed of parallel strands instead of parallel wires. This rather recent innovation has been used for the individual stay cables of cable-stayed bridges. For this application, a 15.24 mm (0.6 in) diameter ASTM A416-88, Grade 270, seven-wire prestressing strand is used (Ref. 7). As shown in Table 1.3, this material has a minimum tensile strength of 1870 MPa and a modulus of elasticity in the order of 180 000 MPa. The relatively high breaking strength means that less volume of steel is used and, therefore, the stays weigh less. Another advantage of these cable stays is that they can be anchored individually or in groups, therefore giving the erection flexibility of prefabrication or *in situ* fabrication of the stay cable and its anchorages.

1.1.4 Modulus of Elasticity and Elongation of a Cable

The elongation of a stranded cable within the elastic range is due to two distinct types of stretch, namely constructional stretch and elastic stretch.

The constructional stretch is permanent and starts to develop as soon as the first load is applied to the cable. It is caused by the settlement of the wires in the strands and settlement of the strands in the rope as load is applied. The amount of permanent constructional stretch will be reflected in the rope classification and construction, rope-making techniques, range of load applied in service, and frequency of cycles of operation. In reality, most of it occurs within the first few days or weeks of operation, depending on the amount of load. Typical values of constructional permanent stretch are between 0.25% to 1% of the length of rope under load. The larger the load, the higher will be this percentage. A value 0.5% is often assumed for normal conditions.

For standing applications of steel wire ropes, a precise length and well-defined elastic properties are required. In order to achieve this condition, a process known as prestretching is used. With this process, the constructional stretch is removed by applying

predetermined loads within the elastic range and holding the load until the rope components adjust themselves and the rope stops deforming. Typical values of prestretching are 50% of nominal breaking load for strands and 40% of nominal breaking load for wire ropes. After removal from the prestretching bed, the cable is left with well-defined and uniform elastic properties.

The modulus of elasticity of a cable varies with the cable manufacturing process, the cable construction (type of cable), the metallic cross-sectional area, and is also dependent on the amount of zinc coating applied to the wires. The ASTM Standards specify minimum values to be used with various types, sizes and coatings. Table 1.3 gives typical values of the modulus of elasticity for different cable types, together with their minimum ultimate tensile strength.

Unlike the usual conventional tension test, the value for the modulus of elasticity for cables is determined using a gauge length of not less than 250 mm and is computed on the basis of the gross metallic area, which includes the zinc coating.

1.1.5 Cable Anchorages and Connections

1.1.5.1 General

The connection of the cable component to the rest of the structure is influenced by the fact that the force in a cable is concentrated within a small cross-sectional area. Furthermore, welding and bolting, which are commonly used to connect steel structural members, cannot be used to connect steel cables to other structural parts. In general, a cable connection should be able to provide full transfer of static and dynamic loads. Similar to any other structural connection, the general requirement is that the anchorage be capable of developing the tensile capacity of the cable. In addition, the type of anchorage selected should provide access for inspection, maintenance, or even replacement of the cable, protect the cable against accidental damage and corrosion, and provide sufficient space for initial tensioning and later adjustments. Finally, the erection procedure to be used should be considered when selecting the type of connection.

A cable termination (socket) is therefore a critical component which directly affects the structural performance of a cable. When the cable is exposed to a corrosive environment, terminations become even more critical. The termination is also the dampening point for any vibration induced in the cable and the point of maximum bending when displacement of the rope occurs perpendicular to its axis. In many instances, fatigue features related to the performance of a socket are the governing fatigue failure mechanisms of a cable assembly.

In the case of suspended and cable-stayed bridges, these two effects are found at the lower termination of a suspender or cable stay. This is due to the fact that moisture and corrosion products tend to run down the cable and collect at the mouth of the socket. This is also the point where the sheathing used for corrosion protection usually terminates. Furthermore, at the socket location the cable is altered in shape in order to transfer its load to the supporting structure, and it is known that locations of geometrical changes can often create stress concentrations and are therefore sites of potential failures.

It can be concluded that the decision as to the type of termination and the design of the socket detail is complicated and cannot be neglected when investigating the structural (static or fatigue) performance of a cable.

1.1.5.2 Types of Sockets

Two types of end fittings are commonly used and these are referred to as: swaged-type and poured-type sockets. The swaged sockets are used for small diameter cables, ranging from 12 mm to 38 mm diameter. The swaging process consists of carefully pressure squeezing a fitting over the cable in a hydraulic press in order not to damage the wires. Figure 1.2(a) shows a typical swaged socket.

The most common way of anchoring standing cables is by use of a poured socket. In its simplest form, a socket for a helical strand consists of a steel cylinder with a conical cavity in which the broomed end of the strand is inserted. Subsequently, the conical cavity is filled by pouring the socketing material. When the cable is subjected to tension, a wedge action will develop between the material inside the cone and the steel cylinder. This creates a tri-axial state of stress inside the socketing material which efficiently transfer the load from the cable to the socket. Depending upon the socketing material, two different types of poured-sockets can be used: hot-casting sockets and cold-casting sockets.

The socketing material in the case of hot-poured sockets consists of molten alloys made of zinc, lead, copper, or aluminum. The high pouring temperatures of those materials, which ranges between 350 and 450° C, can significantly reduce the fatigue strength of the wires at the socket. Figure 1.2(b) shows the typical dimensions for a poured bearing socket.

In order to improve the fatigue resistance of the anchor, experience has shown that it is preferable to use a cold casting material composed of epoxy resin, zinc dust, and small hardened steel balls. Parallel wire strands with epoxy resin and steel ball filled sockets were developed in Germany and they showed a better fatigue resistance than spiral strands. To reflect the higher fatigue resistance of this socket it is called HiAm socket, where HiAm

stands for *high amplitude*. Figure 1.2(c) shows a typical HiAm socket. The wires in the bundle are flared out slightly inside a steel casing and held against a steel plate by means of button heads at their ends. The conical space inside the steel casing is then filled with a mixture of steel pellets of 1.5-2.0 mm diameter and an epoxy-based resin. When the HiAm cable is loaded, arching action develops within the pellets in the resin mass inside the casing, thus transmitting the load to the anchor (Ref.10). Another type of parallel wire strand socket, termed NEW-PWS, was developed in Japan. It consists of epoxy resin and Zn-Cu alloy socketing material. Finally, by filling the well-known (from the prestressed concrete industry) BBRV-anchorage with a special epoxy compound, the high fatigue resistance BBRV-DINA anchorage was developed.

In addition to the requirements outlined above, the transition between cable and anchorage should have a certain flexibility so as to avoid high bending stresses caused by live load and wind load. At the same time, a device to prevent cable vibration from taking place at the anchorage may have to be provided. Vibration can cause excessive discomfort to users of the bridge, but, more importantly it can accelerate failure of the corrosion protection system (see Section 1.1.6). In addition, secondary bending stresses and vibrations induced around the neck of the socket have been found to be detrimental for the fatigue life of the cable assembly. A neoprene washer between the anchorage and the supporting frame can be used as a vibration damping device. In the case of the HiAm socket, a transition region consisting of zinc-copper alloy with epoxy resin is used around the neck of the socket in order to reduce the secondary bending stresses and the vibration.

1.1.6 Corrosion Protection

Corrosion protection of cables is essential because the main load-carrying components of a cable consist of wires of relatively small diameter and a small amount of corrosion could significantly reduce their strength. The problem of corrosion is further accentuated by the fact that cavities are present between all wires and the wires are inaccessible for inspection.

For normal conditions, no additional corrosion protection is required on the galvanized multi-layered strands, ropes, and locked-coil cables. This is illustrated in Figures 1.1(a) and 1.1(b). However, if the environment is very corrosive, additional protection may be provided by treating the completed galvanized cable with zinc dust paste and then wrapping it with soft-annealed galvanized wire.

Non-galvanized parallel bars, parallel wire strands, and parallel and semi-parallel cables can be protected by their insertion in polyethylene tubes which are then injected with corrosion

inhibiting materials such as portland cement milk, polymer concrete milk, tar epoxy, or an organic compound. For galvanized wires, a polyethylene sheathing can be used instead of a pipe. Figure 1.1(c) shows a typical corrosion protection system for a semi-parallel wire strand using a polyethylene pipe.

A survey conducted by Watson and Stafford (Ref. 11) indicated that vibrations of cables may cause cracking of both the grout and polyethylene casing, thereby opening up potential corrosion sites. The most recent development is a self-propelled jacketing machine that can hermetically seal cables by winding and folding tinned copper around them. Currently under development is a method that seals cables in a continuous (titanium grade) stainless coated carbon steel tubing, 3 mm thick, after all adjustment have been made (Ref. 11).

Until any of the innovative solutions to the corrosion problem are proven to be satisfactory in the long term, it is suggested that galvanized wires be used, that cement not be used, and that the cable and sockets be accessible for inspection and, if necessary, that there be provision for easy replacement.

1.2 Statement of the Problem

Spiral wire ropes made of high-tensile steel wires were first developed in 1834 by W.A. Albert, a senior mining engineer, and were used to provide ore haulage. The utilization of wire ropes in structural applications such as standing cables has proliferated since then. It has long been recognized that tensile force is the most efficient way to transmit a load because it gives maximum utilization of the cross-section. The applications of standing cables include stayed cable and suspension bridges, prestressing of concrete, mooring of offshore structures, and others.

The adequacy of cable-stayed and suspension bridges is dependent, among other things, on the axial fatigue performance of the cables. Presently, designers of bridges are working without adequate knowledge concerning the fatigue life of the principal component in these systems. This means that, although the design can be assumed to be satisfactory upon execution, the life of the structure cannot be predicted with the desired accuracy. Owners of such structures can expect to have to replace cables at intervals during the life of the structure.

The fatigue strength of cables can be influenced by the fatigue strength of the wire elements, the applied stress range, the applied mean load, the cable construction (i.e. lay direction and length, number of layers, etc.), the end termination, lubrication conditions, and by corrosion. In addition although a wire rope is essentially an element for

transmitting a tensile load, the rope construction is such that the individual wires in a rope are subjected to local bending and torsional moments and bearing loads, as well as to tension. Because the magnitude and distribution of stresses resulting from these loads determine the overall cable response, the identification of the fatigue failure of the entire assembly is a complex issue.

A limited number of mathematical models exist for the evaluation of the fatigue strength of a cable, and in the majority of cases they have been derived on the basis of a small number of physical tests. It is important that these models be confirmed or calibrated using a larger pool of test data. From the point of view of specifications, the most commonly used highway bridge specifications in North America (e.g. Ontario Highway Bridge Design Code (Ref. 12), American Association of State Highway and Transportation Officials (Ref. 13)) give no guidance for the axial fatigue design of bridge cables. The American Petroleum Institute (API, Ref. 14) and the Post-Tensioning Institute (PTI, Ref. 15) appear to be the only specifications in North America that give simplified recommendations for the fatigue design of non-running cables. The fatigue predictions obtained using these specifications differ significantly, and further investigation is needed. In many instances, bridge designers are forced to develop experimentally the fatigue strength information needed for a specific bridge, which is impracticable except for unusually large cables, or they have to rely on manufacturer's data.

In addition, in the design of cable-stayed bridges the fatigue strength of long cables is a major design criterion. Due to physical limitations of testing facilities, the available experimental results and the majority of the design recommendations have been obtained by tests on short specimens of wires or cables. These results must then be extrapolated to determine the fatigue strength of large cables, which may have lengths from ten to several hundred meters. The extrapolation required is far beyond the laboratory results, which implies a high risk. Recently, theoretical studies have been made to perform this extrapolation with models based on physical observations and statistical requirements. Those models need to be investigated, simplified, and incorporated into design recommendation for the fatigue strength of wire cables.

1.2.1 Scope and Objectives

The scope of the work presented herein is to develop design rules for the axial fatigue strength evaluation of standing multi-layered wire strands. In order to fulfill this scope, the research program was designed with the following objectives:

1. To conduct a literature survey in order to obtain and evaluate the experimental and analytical studies that already exist.
2. To design a testing apparatus capable of testing large diameter multi-layered strands that have a variety of lengths and are subjected to axial cyclic loading.
3. To establish a fatigue failure criterion (discard criterion).
4. To identify the fatigue failure mechanism.
5. To experimentally investigate the effect of strand make-up, strand diameter, stress range, and length-to-diameter ratio of the specimens upon the fatigue life of multi-layered cables.
6. To experimentally investigate and compare the most commonly available non-destructive procedures used to detect internal wire breakage during the fatigue test of a cable.
7. To compare and evaluate the present work in light of the results obtained by other researchers, and to attempt to pool the available fatigue data into one data base.
8. To investigate existing statistical models, which are used to extrapolate and to predict the fatigue strength of real cables based on laboratory test results of limited cable length and test duration.
9. To assess the existing fatigue design guidelines for multi-layered strands in light of the collected data base and the effect of length.

1.2.2 Organization of the Thesis

The organization of the thesis is indicated by its table of contents. In Chapter 2, a literature review is presented. This summarizes the research done in the area of fatigue of standing wire ropes and the existing fatigue design guidelines. Chapter 3 describes the experimental program that was used to investigate the failure mechanism and the effect of significant parameters such as stress range, strand make-up, and length-to-diameter ratio. Chapter 3 also presents the procedure used to assess the damage accumulated in a cable and to thereby establish a discard criterion. The test results are presented in tabular and graphical form in Chapter 4. The analysis performed on the test results in order to derive a common failure criterion and to quantify the effect of various parameters investigated in the test program is presented in Chapter 5. In Chapter 6, a statistical model is used in order to investigate the

size effect. A comparison of the test results with the test programs of other investigators and with the current design guidelines is also presented in Chapter 6. Finally, the summary, conclusions, and recommendations for further research are presented in Chapter 7.

The modulus of elasticity measurements and the wire breakage detection results that were obtained during the fatigue tests are tabulated in Appendix A. The statistical analysis used for the reduction of the test data is presented in Appendix B. Finally, Appendix C provides a summary of selected test data collected from the literature.

Table 1.1 Comparison of chemical composition of steel wire and structural steel

	Steel Wire (%)	Structural Steel Mild (%)	Structural Steel High Strength (%)
C	0.80	0.22	0.20
Si	0.20	0.40	0.15 – 0.40
Mn	0.60	0.50 – 1.50	1.50
Cu	0.05	–	–
Ni	0.05	–	–
Cr	0.05	–	–
P	0.03	0.04	0.03
S	0.02	0.05	0.04

Table 1.2 Mechanical properties of zinc-coated steel wire and comparison with typical structural steels

Zinc Class	Nominal Wire Diameter (mm)	Yield Strength (MPa)	Tensile Strength (MPa)	Elongation (%)	Modulus of Elasticity (MPa)
A	1.016 to 2.794	1030	1520	2.0	205 000
A	2.794 and larger	1100	1520	4.0	205 000
B	2.286 and larger	1030	1450	4.0	205 000
C	2.286 and larger	970	1380	4.0	205 000
Mild Structural Steel (300 W)		300	450 – 620	24	200 000
High Strength Structural Steel (700 Q)		700	800 – 950	18	200 000

Table 1.3 Mechanical properties for different types of cables

Type of Cable	Modulus of Elasticity (MPa)	Tensile Strength ¹ (MPa)	ASTM Standard
Structural Strand	158 600 – 165 500	1400	A586
Structural Rope	55 000 – 140 000	1335	A603
Locked Coil Strand	170 000	1570	–
Parallel Bars	200 000	1035	A722
Parallel Wire Strand	200 000	1655	A421
Parallel Strand Rope	180 000 – 190 000	1870	A416

- (1) The tensile strength reported here is the minimum guaranteed ultimate tensile strength based on the gross metallic area. Values presented herein are typical. They can vary with both diameter and amount of galvanizing.

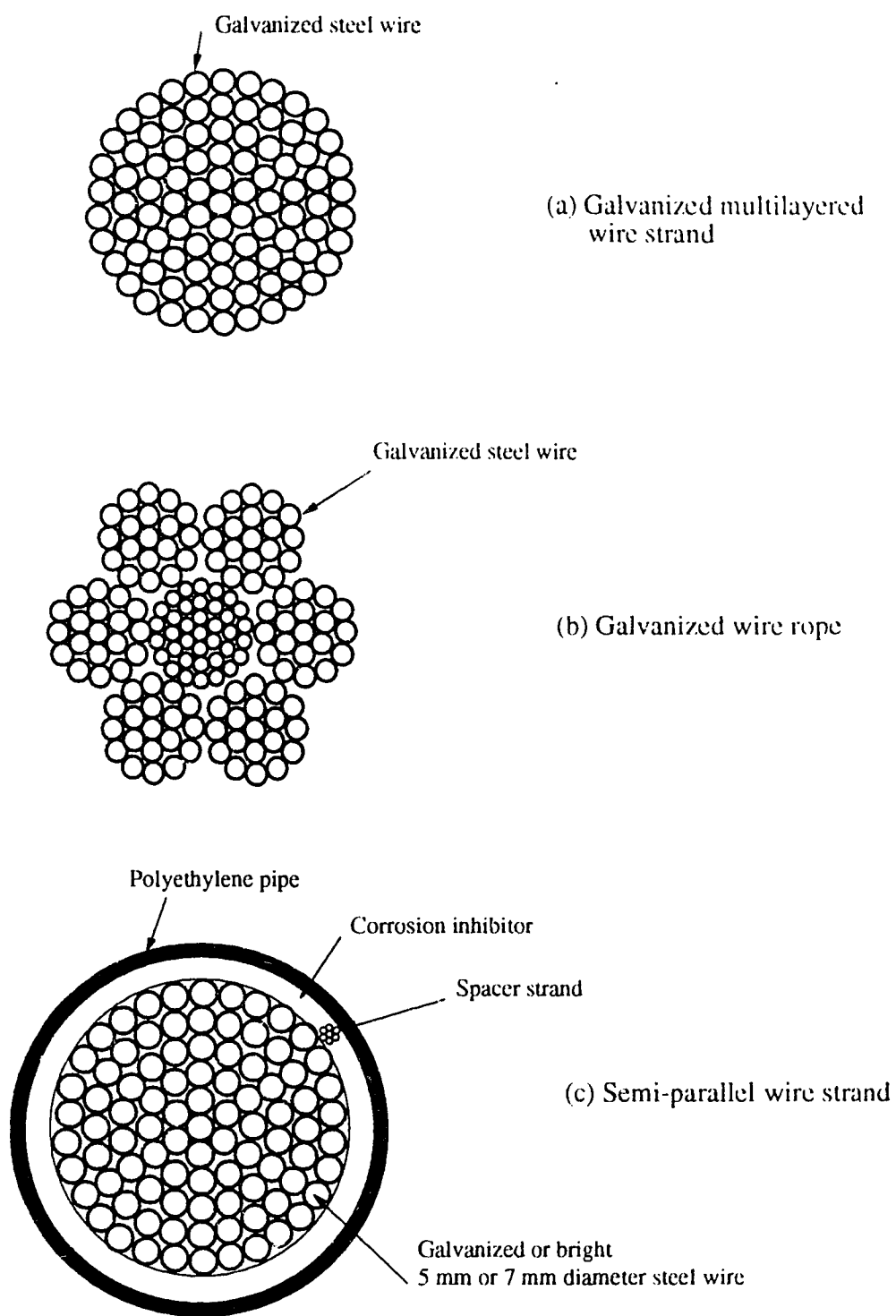
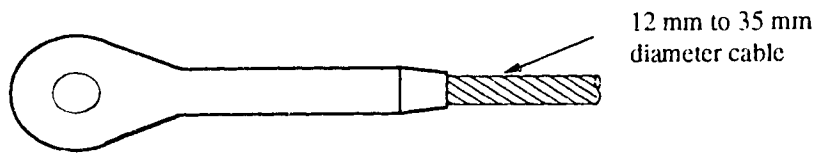
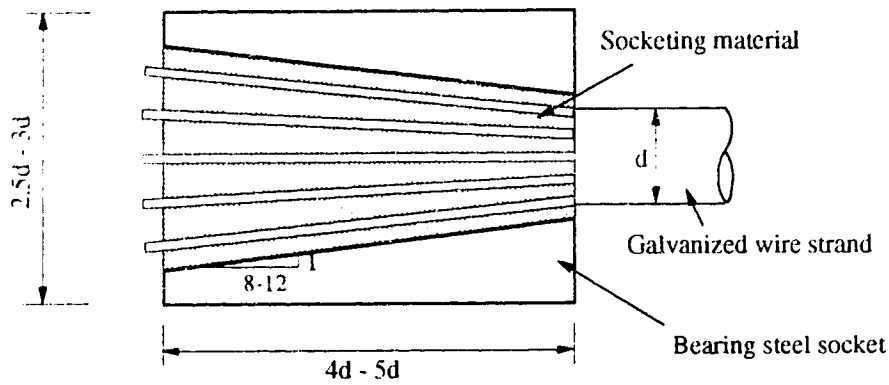


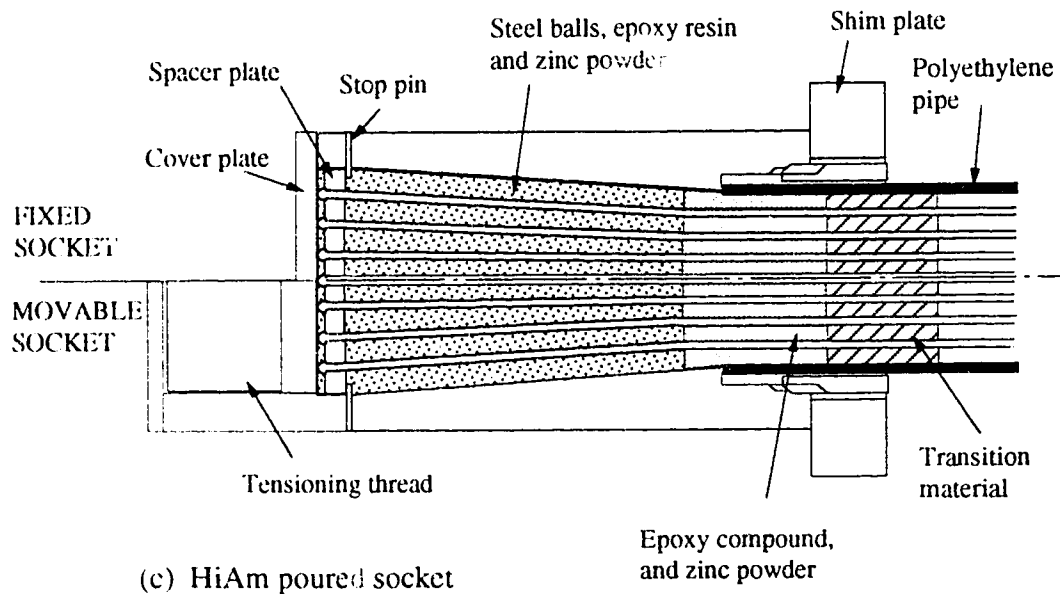
Figure 1.1 Different types of cables and their corrosion protection



(a) Typical swaged socket



(b) Typical dimensions of poured bearing socket



(c) HiAm poured socket

Figure 1.2 Types of sockets

Chapter 2 Literature Review

2.1 Performance of Existing Cables

There have been comparatively few well-documented studies on the performance of existing bridge cables, and some of the findings that have been reported are contradictory.

Watson and Stafford (Ref. 11) conducted a two-year survey on more than 100 cable-stayed bridges and concluded that most of them are in serious danger because of the amount of cable corrosion. In their pessimistic report, which stirred many comments from the engineering community, they stated that all existing methods of corrosion protection have failed. Furthermore, life expectancies of only about 20 years have been mentioned.

Tilly (Ref. 16) tabulated the results of a survey conducted on 11 British bridges which have galvanized and painted cables. Average life to replacement was reported to be 62 years. The most vulnerable location for corrosion and failure was found to be the point of entry of hanger or stay cables into the lower sockets. This is due to mechanical stress concentration in the vicinity of the socket and the fact that moisture and corrosion products tend to run down the cable.

The condition of the multi-layered strands that support a large radar-radio telescope after 20 years in service was reported by Phoenix et al. (Ref. 17). Wire breakage in this structure has been experienced since its construction. Twenty breaks were found over 5 000 wires in the 27 cables. All breaks occurred near the point where the wires enter the socket.

In the past, designers generally relied on manufacturer's data or developed their own permissible stress range in order to establish the fatigue strength of a cable. A knowledge of the fatigue design stress range is important to assess the condition of existing cables. Birdsall (Ref. 18) was able to obtain the design stress range of the cables in several bridges. The maximum reported value was 14% of the minimum ultimate tensile strength (UTS) of the cable and the smallest value was 5% of the UTS. Birkenmaier and Narayanan (Ref. 19) tabulated the design stress range of three cable-stayed bridges. The maximum stress range was 15% and the minimum 7.3% of the UTS. A summary of the individual data is given in Table 2.1.

In this Chapter, a review of the research related to the axial fatigue performance of standing cables will be presented. Although emphasis will be placed on the fatigue behavior of standing cables, related topics will also be discussed. These include the performance of cable subjected to static tensile loading, the axial fatigue of single wires, and non-destructive procedures for detection of broken wires.

2.2 Kinematics of Cables

The problems associated with a cable subjected to static load consist of determining the load distribution among the wires, the interwire/interlayer contact forces and associated relative displacements, the effective axial stiffness, and the lateral contraction of the cable assembly. This analytical evaluation of the kinematics of a cable loaded in tension or in bending is a complicated one, mainly due to the helical geometric configuration of the wires and the interwire/interlayer friction forces developed at the contact points between wires.

Hruska (Ref. 20) in 1951 assumed that each wire in a strand was subjected to tension only, and demonstrated that the tensile stresses vary in proportion to the square of the cosine of the lay angle. Hruska (Ref. 21) also derived a relationship between the radial clench forces and the axial force in the strand, and later he discussed the origin and consequences of the torque induced in a helical strand by an axial load (Ref. 22). However, he did not consider the actual stresses at the contact points between wires, which are required for the analytical prediction of the fatigue life of a cable. Leissa (Ref. 23), and Starkey and Cress (Ref. 24) were the first to attempt a theoretical study of interwire contact stresses. Although the analysis was limited to the special case where the wires cross at an included angle of twice the lay angle, it nevertheless demonstrated that contact stresses for crossed wires are significantly larger than those of parallel wires.

Studies by Durelli and Machida (Ref. 25), which included a test of an oversized epoxy model of a six-wire strand, emphasized the importance of bending and twisting moments in the six individual wires. However, it is doubtful whether these effects would be significant in a multi-layered strand, where the wire-to-strand diameter ratio is much smaller.

Costello and co-workers (Ref. 26–30) developed a theory to predict the static response of wire rope subjected to tension, torsion and bending. The cable is treated as a collection of thin wires and the general non-linear equations of equilibrium for each wire (as derived by Love, Ref. 31), including the effects of contact line loads, are solved. The frictional forces, which can be substantial, are neglected and both the unstressed and deformed configuration of wires are assumed to be helices. The bending and torsion in individual

wires can also be calculated using Costello et al. model. These forces are certainly significant in strands consisting of a few wires and for electro-mechanical cables with soft cores. In the large structural strands that form the subject of the present research, there are so many wires and the wire-to-strand diameter ratio is so small, that wire bending and torsion are thought to be of secondary importance in comparison with axial force and contact effects.

Knapp (Ref. 32) produced solutions for multi-layered strand using energy conservation principles. Friction forces and interwire contact deformations have been ignored in his model. Approximate linear equations suitable for hand calculations were also derived.

Hobbs and Raoof (Ref. 33), and Raoof and Hobbs (Ref. 34) developed a theoretical model for the analysis of a multi-layered strand. They used prestressed orthotropic sheet theory with compliance derived from consideration of contact stress theory. Friction forces and interwire contact deformation are included in their model. Axial, torsional, bending, and external pressure load cases have all been addressed (see also Ref. 35-37). After an extensive parametric study conducted by Raoof (Ref. 38, 39) and Raoof and Huang (Ref. 40), the complex mathematics involved in the model were simplified to the extent of obtaining reasonable estimates of the kinematical quantities using simple hand calculations. This model is able to predict axial stiffness, lateral contraction, wire strain, interwire forces and slippage, recovery length, and axial hysteresis.

2.3 Cables under Cycling Loading

2.3.1 Fatigue Failure Mechanism for Cables

The state of stress of a material subjected to cycling loading changes from the first cycle onwards. If flaws do not exist at the beginning, then hardening and softening processes lead initially to microscopic fatigue cracks. Inhomogeneities, such as inclusions, also lead to the formation of cracks because of the stress concentrations they cause. In wires, fatigue cracks start mainly at the surface: it is likely that, at this location, surface flaws or damage have arisen during fabrication, a certain surface roughness exists, the attack of any corrosive media takes place, and the highest loading often exists (Fuchs and Stephens, Ref. 41). Under the application of subsequent cyclic loading, the initiated or pre-existing micro-cracks will propagate to a critical size at which fracture occurs.

The literature contains considerable evidence (Ref. 33, 42 and 43) regarding the mode of fatigue failure of cables, and it is identified as fretting corrosion fatigue at the interlayer contact patches ("trellis" contact). At those contact surfaces, mechanical and physico-

chemical processes work together. Since at least one of the contact pairs is a metal, oxidation phenomena occur in the fretting regions, which are intensified by the oxidizing medium trapped in the gaps between the wires.

According to Waterhouse (Ref. 44) fretting fatigue strength decreases with increasing pressure and increasing relative displacement in the micro-meter (μm) range. Lubrication has a positive effect, since it reduces the friction force at the contact areas. Esslinger (Ref. 45) states that, for components subjected to fretting fatigue corrosion, an infinite life range (endurance limit) does not exist. In addition, the fretting fatigue resistance reduces with hardness, and, hence, with the strength of the material (Ref. 41). This reduction is also due to the fact that it can be expected that high strength cold-drawn materials, such as steel wires, can have a rough surface with surface imperfections (drawing marks) (Gabriel, Ref. 46).

The process of rupture of a steel wire by fatigue can be divided into two stages: the nucleation of a surface flaw and its propagation up to the critical size for which fracture of the wire takes place. Between the two stages there is a transition regime in which the mechanisms controlling each stage are operative at the same time (short crack regime). Research conducted by Verpoest et al. (Ref. 43) showed that fatigue failures of steel wires always propagated from pre-existing surface flaws with a depth of 25 to 125 μm . These micro-cracks were probably produced during the drawing process. Based on this observation, Verpoest suggested that the initiation period can be ignored. However, Llorca et al. (Ref. 47) postulated that fatigue fractures in cables is due to axial fatigue failure of individual wires and is not due to fretting fatigue at the interlayer contact patches. One of the experimental objective of the research presented herein was to investigate the fatigue failure mechanism. This was done by examining the fractured surfaces of failed specimens.

2.3.2 Single Wire Axial Fatigue

The fatigue properties of the basic wire material can be expected to have an influence upon the fatigue behavior of the cable assembly. Extensive experimental studies on individual wires subjected to fatigue have been carried out by many investigators, and the effects of parameters such as carbon content, method of manufacture, surface condition, and surface coatings on the fatigue life of wires have been summarized in a survey by Bahke (Ref. 48 and 49). During the drawing process of high strength, eutectoid carbon steel wires in which the cross-section is not reduced by more than 86%, the fatigue strength increases with tensile strength. In addition, for high strength steels, it is noted that differences in

surface roughness arising from fabrication and surface imperfections have a detrimental influence on the fatigue life (Gabriel, Ref. 46).

Castillo et al. (Ref. 50) performed 72 fatigue tests on individual wires with specimen lengths ranging from 140 to 8540 mm. These results showed a fatigue limit between 20% to 30% of the wire yield strength, depending on specimen length. Birkenmaier and Narayanan (Ref. 19) performed 210 fatigue tests on individual wires and found that the endurance limit (with 5% probability of rupture) was 24% of the wire yield strength (or 22% of the tensile strength). Similar values were found by Verpoest et al. (Ref. 43), who carried out fatigue tests on 2 mm diameter wires of different yield strengths.

Based on an extensive series of axial fatigue tests on 2 to 3 mm diameter hot-dipped galvanized wires, Watt (Ref. 51) suggested that the endurance limit is 27% of the ultimate tensile strength. Experimental data reported by Thorpe and Rance (Ref. 52) on hot-dipped wires having a diameter of 1.8 to 2.3 mm, which were tested in air, also yielded a similar conclusion. The test program included axial fatigue and fretting fatigue of individual wires in air and seawater. Parameters investigated included the method of galvanizing (hot-dipped and electro-deposition) and thickness of galvanizing (0.05 mm, 0.025 mm, and bare wires). They concluded that seawater reduces the fatigue life by an amount which increased with increasing mean stress and decreasing frequency. Since fretting fatigue of wires can be accompanied by corrosion, which is a time-dependent process, Thorpe and Rance suggested that testing should be carried out at realistic, in-service cycling loading frequencies. Thorpe and Rance also tried to correlate the fretting fatigue life of single wires with the fatigue life of a rope, although it was realized that the failure criterion is different.

Table 2.2 summarizes the experimental results on single wires. A large scatter of test results is evident, even for apparently identical materials and testing parameters.

Waterhouse et al. (Ref. 42) showed that hot-dip galvanizing produces a dramatic improvement in the fretting fatigue strength of wire specimens in seawater compared with ungalvanized specimens. However, in air it was found that the fretting fatigue strength was slightly lower for galvanized wire as compared with uncoated wire. This was attributed to the brittle alloy layer on the surface of the wire resulting from galvanizing.

2.3.3 Axial Fatigue Tests of Cables

It is the primary purpose of the literature survey to investigate the available experimental axial fatigue data on cables. In general, multi-layered strands have a significantly higher tensile fatigue performance than do wire ropes. Parallel wire ropes, on the other hand,

have a completely different failure mechanism from that of stranded cables. Fatigue data should therefore be categorized, depending the type of cable. As expected, the literature review also shows that the fatigue data often exhibit a large degree of scatter. Interpretation and correlation of results from different sources also presents difficulties. Poor test practices and inappropriate test parameters such as insufficient sample length, inclusion of specimens that failed prematurely at terminations, test frequency so high as to cause overheating of samples and loss of lubrication, and the use of different or undefined discard criteria (Potts et al., Ref. 53) all create problems in interpretation of results.

Waters et al. (Ref. 54) presented plots of cyclic tension rope fatigue data acquired from a literature review conducted by the United Kingdom National Laboratory. Because of confidentiality agreements, the testing parameters and procedures of many of the results presented by Waters et al. are not available. This makes the interpretation and comparison of the collected data extremely difficult.

Tilly (Ref. 16) investigated the axial fatigue performance of seven different steel cable constructions (three types of wire ropes and four types of spiral strands) that had diameters ranging from 35 mm to 70 mm. The cable lengths were 3000 mm, the cyclic ranges were 10% to 28% and the mean loads were 20% to 38% of the characteristic strength. It was found that, after the first wire fracture, up to twice as many additional cycles were required to reach five fractures, which was the failure criterion. It should also be noted that all specimens failed close to the termination.

Hanzawa et al. (Ref. 55, 56) conducted tests on 50 mm and 85 mm diameter ropes. Wire breakages were detected using both accelerometers and acoustic emission monitoring devices. The length of the test specimens ranged between 700 mm to 1810 mm, which gives a length-to-diameter ratio of 14 to 21. The stress ranges were between 10% to 40% of the breaking strength of the wire rope. Three different types of socketing material (Zn/Cu alloy, polyester, and epoxy) were used for the end fittings. It was concluded that breaks in the free length were due to interlayer fretting and occurred at high stress range, while those at the socket locations occurred at low stress range and were due to stress concentration. In addition, it was suggested that the fatigue performance of large diameter ropes could be estimated conservatively from fatigue tests on ropes of smaller diameter, since it was found that the larger the diameter, the greater the fatigue life. The epoxy resin proved satisfactory as a socketing material. The failure criterion used by Hanzawa et al. was 5% wire breakages per lay length.

Berge (Ref. 57 and 58) tested 32 mm and 76 mm diameter ropes in axial fatigue. The specimens had a length of 3000 mm and were tested at stress ranges between 16% to 24% of the characteristic load. All fractures occurred at positions that were more than 500 mm away from the sockets. With the exception of the 32 mm diameter (35x7) rope, the discard criterion used by Berge was the fracture of one outside strand. The axial fatigue strength was found to decrease significantly with the diameter (for ropes with similar construction). No difference was found between bright and galvanized ropes (in non-corroded state). An initial overloading of the ropes (up to about 80% of the minimum ultimate tensile strength) was found to be beneficial for the fatigue life of the rope.

Lucht and Donecker (Ref. 59) presented results of tension fatigue tests on wire ropes of various construction. Four different types of termination were used. The stress range varied between 6% to 99% of the ultimate tensile strength. The larger diameter ropes were suspender ropes removed from the Golden Gate Bridge after 35 years of service. The fatigue tests on the rope specimens were terminated after six visible wire breaks or at two million cycles, whichever occurred first. The results indicated that over 35 years of service had not degraded the fatigue life of the suspenders. Although, Lucht and Donecker did not give the lengths of the specimens tested, they concluded that "relatively short lengths used in testing prevent the rope from compensating for any slight misalignments of the sockets and thus reduces the fatigue life".

Waters, Eggar and Plant (Ref. 54) carried out tests on 127 mm and 62.5 mm diameter strands. Three samples of each size were tested, each at mean load of 40% of the minimum breaking load, and cycling ranges of 15%, 20% or 30% were applied to one sample of each size. Those experiments showed that large diameter cables had a markedly reduced fatigue life over half-size test specimens of the same construction when tested at the same percentage load levels. (Recall that Hanzawa et al. reached the converse conclusion.) Testing was discontinued when approximately fifteen wire breaks were observed in the outer layer. Periodically, the cycling test was interrupted and static tests were conducted up to the maximum fatigue load, in order to obtain the modulus of elasticity. It was found that the modulus of elasticity increased during the first 20 cycles and then remained constant until 6 to 10 wire breaks were observed. At that point, the modulus of elasticity started to reduce considerably as successive breakages occurred. The load range in which the static tests were conducted was not reported in the paper published by Waters et al. (Ref. 54). This is an important information, since unloading of the specimens during static test could change the interwire fretting locations and result in unrealistic high fatigue lives.

Casey and Waters (Ref. 60 and 61) conducted axial fatigue tests on 40 mm, 70 mm, and 127 mm diameter six stranded wire rope (6x41 construction with a 6x7 IWRC) having lengths of 3750 mm, 3600 mm, and 7000 mm, respectively. The ropes were loaded to $20\% \pm 15\%$ per cent of the manufacturer's stated minimum breaking load. From static tests, it was concluded that the stiffness increased and then remained relatively constant before starting to decrease at approximately 25% of the fatigue life for the 40 mm diameter rope, 30% for the 70 mm diameter ropes, and 35% for the 127 mm diameter ropes. The failure criterion relies on the identification of a property change point which is a function of load range and endurance. The property change point is defined as the point in life at which the degradation of the rope becomes measurable (Ref. 90).

Ronson (Ref. 62) presented prediction curves for tension fatigue performance of large diameter ropes and strands. Those curves are based on tests conducted by British Ropes Ltd. The stress range was found to have a much greater influence on the fatigue life than the level of mean load. Ronson believes that initial breaks occurred in the outer layer and tests were discontinued when 24 wires broke within a rope length of six times the rope diameter.

In a critical review of the existing experimental data and design curves, Raouf (Ref. 63) assembled a total of one hundred and ten test data on a wide variety of steel cable constructions (wire ropes, strands, and locked coil wires). Fatigue life on those tests was defined as the number of cycles to total failure. By using this rather extensive data bank, Raouf demonstrated that the API recommended design curve (see Ref. 14) is unconservative. Instead, it was shown that the design curve proposed by Tilly (see Ref. 16) does provide a reasonable lower bound solution to the available experimental and theoretical axial fatigue data. (A summary of the design methods for the prediction of axial fatigue life of cables is presented in Section 2.3.4). The axial fatigue data on multi-layered strands, reported by Raouf, will be summarized and further discussed in Chapter 6.

Hobbs and Ghavami (Ref. 64) published axial fatigue results on 15 multi-layered strands having 16 mm and 32 mm diameters. Twelve of these specimens were 16 mm diameter, had a test length of 1055 mm, and consisted of 19 x 3.2 mm diameter galvanized wires. Three others were 38 mm diameter specimens, which had a test length of 6000 mm, and were taken from an existing mast. They consisted of five layers of wires (92 in total), 3.5 mm in diameter, over a 5 mm diameter king wire. All specimens were terminated using zinc-poured sockets, and were tested using a pair of hydraulic actuators, each of 500 kN capacity. Wire failure observations were made "by ear, eye, and shock contact,"

and tests were discontinued when the specimens were no longer able to carry the applied mean load. Fatigue failures for all the specimens occurred at the strand/socket interface, with the first observed breakage invariably at the outer layer. A fracture at the socket of a 32 mm diameter strand and some pull-out failures in the zinc matrix of the sockets were signs of an under-designed termination. Nevertheless, the main conclusions drawn from the axial fatigue tests were that fatigue life seems to be insensitive to mean load and that the number of cycles from first wire fracture to overall failure increases with the number of wires. The latter could be explained by the fact that the loss of cross-section from one breakage is less significant for large diameter strand, which has more wires than the smaller diameter cable.

Significant aspects of accelerated block testing, such as the sequence of stress levels and periodic overloads, have been discussed by Yeung and Walton (Ref. 65). Although it was recognized that the load range is the dominant factor in tension fatigue, it was suggested that the contribution of mean loads could be included by using the concept of "an equivalent load range." Experimental substantiation for this was given by the test results on 32 mm diameter (1x17) and 51 mm diameter (1x139) strands tested at different mean loads (20% - 41% of the UTS) and load ranges (10%–28% of the UTS). Detailed information for the specimens (length, termination, etc.) and the failure criterion were not provided in the publication.

Potts et al. (Ref. 53) reported the results of a variable amplitude tension fatigue test program conducted at Reading University on 19 mm diameter ropes. The Miner damage summation was found to range between 1.25 and 1.43 at the time of failure. This indicated that the linear damage cumulative hypothesis consistently underestimated the total axial fatigue life. Use of the Miner rule will therefore provide designers with an additional margin of safety. Shifting of the fretting zone from one area to another as the different block loads were applied was used to explain the high values of the Miner summation.

Smith, Stonesifer, and Seibert (Ref. 66) investigated the effect of periodic overload on the fatigue life of wire rope. It was found that the fatigue life of the rope improves significantly with increased overloads (up to the yield strength of the rope). The optimum interval between overloads was suggested to be between 5000 and 20000 cycles, depending on the load range and overload. Ropes of various construction and diameters were investigated. The enhanced fatigue life resulting from periodic overloading was attributed to overload crack retardation and to readjustment of stresses within the rope by movement of contact points between wires during overloads. Continuing laboratory

studies conducted by the same research group (see Stonesifer and Smith, Ref. 67) on 1/4 in diameter ropes concluded that the major increase in life is achieved by the initial overload, with periodic overloading having only minor additional benefits. Furthermore, it was shown that an increase in mean load on a rope causes an increase in the endurance life. This was attributed to higher stiffness observed in wire rope as axial load increases. However, it was found that as the mean load is increased (above 25% of the minimum ultimate tensile strength, approximately) the effect of higher mean load begins to overshadow the effects of the reduced rope flexibility, and life then begins to decrease.

Nakamura and Hosokawa (Ref. 68) presented six tests on parallel wire strands (five specimens having 127 wires and one specimen with 91 wires) and five on semi-parallel wire strands having 139 wires. The galvanized high strength wires used were 7 mm in diameter. All specimens had sockets that used epoxy resin with Zn-Cu alloy (termed NEW-PWS) and a test length of 2500 mm. The semi-parallel strands were low-twist cables with an angle of twist of only 3.5°. The applied stress range was between 195 and 340 MPa, and the mean stresses were between 450 and 530 MPa. Wire breakages occurred both inside and outside the sockets. The discard criterion is not well-defined. Tests were discontinued when the number of cycles was between 0.52 and 5 million and the broken wires between 0% to 8.6%. Nevertheless, a specimen was considered to be damaged when 5% of the wires were broken. The tests results indicated that the fatigue life depends on the stress range, the mean stress level, and the ultimate strength of the wires. An expression was proposed to calculate the fatigue life of semi-parallel strands that use NEW-PWS sockets. Both the stress range and mean stress were found to influence the fatigue life of a cable.

Birkenmaier (Ref. 69), and Birkenmaier and Narayanan (Ref. 19) presented a study on the fatigue performance of HiAm and DINA socketed parallel wire cables (see Section 1.1.5.2) used for cable-stayed construction. It was emphasized that the stay tendons should be able to withstand both high permanent pretension forces and high cycling loads. Fatigue test results on a series of 14 identical, 19 wire (7 mm diameter) strands, fitted with HiAm anchorages and subjected to cyclic stresses between 260 MPa and 540 MPa were presented. The specimens were between 3 000 mm and 6 000 mm long, and the steel grade had a yield strength of 1 500 MPa and an ultimate strength of 1 700 MPa. The minimum stress was kept at 350 MPa. The discard criterion used was the number of cycles at the end of which the remaining static rupture load of the tendon is smaller than 90% of the ultimate tensile strength. Two million cycles was defined as infinite fatigue life. Since parallel wire strands consist of a plurality of single wires placed in a parallel

configuration, the fatigue failure mechanism of a parallel wire strand should be the same as that of an individual wire. By modifying the 5% fractile fatigue curve developed for single wires to fit the fatigue results on parallel wire strands, Birkenmaier and Narayanan (Ref. 19) derived a curve for the permissible stress range of HiAm parallel wire strands. It was also suggested that use of the Palmgren-Miner hypothesis for linear accumulation of damage was appropriate.

Birkenmaier and Narayanan (Ref. 19) also presented the fatigue results on five large diameter HiAm and DINA anchored parallel wire strands. The cable had from 19 to 295 wires of 7 mm in diameter. With the exception of one DINA specimen, where a stress range of 250 MPa was used, the stress range was 200 MPa. All tests were discontinued at two million cycles, and the maximum damage was found to be three broken wires in a 295 wire cable (1.0% breaks).

As part of the fatigue design of the Honshu-Shikoku railway / highway cable-stayed bridges, Takena et al. (Ref. 70) conducted eleven tests on large diameter parallel wire strands having HiAm and PWS sockets. The HiAm specimens consisted of 91 x 7 mm diameter wires (galvanized and not-galvanized) and the PWS specimens of 169 x 5 mm diameter galvanized wires. The minimum length-to-diameter ratio between sockets was 19. The cycling load corresponded to stresses between 148 MPa and 295 MPa. Almost all wire breakage occurred at or inside the sockets. The improved fatigue life of the HiAm cables in comparison with the PWS sockets showed that the soft epoxy resin in the front half of the HiAm sockets reduces the stress concentration caused by the anchoring of the cable, thereby enhancing the fatigue strength. Non-galvanized wires (even when covered with polyethylene jacket) are liable to have their fatigue strength reduced in a corrosive environment. Takena et al. found also that breakage in the free length was generally internal and occurred at large stress ranges (larger than 245 MPa). It is believed that they were caused by fretting. Since the stress range is generally smaller than 200 MPa in real bridges, the wire fractures can be expected to be concentrated in the anchor portion. Furthermore, ruptures in the anchor portion were confined to the outermost layer. As the diameter of cable increased, the life to first breakage was found to decrease. Finally, although most of the tests were discontinued when the number of breakage was less than 5%, Takena et al. proposed design life curves based on 5% wire breakage for HiAm sockets having 127 and 295 wires.

A graphical representation and a comparison between selected axial fatigue data on cables, obtained from the above literature review, will be presented in Chapter 6.

2.3.4 Design Recommendations (S-N curves)

A summary of the most commonly used design methods for the prediction of the axial fatigue life of cables is presented in this section.

(a) Tilly lower bound axial fatigue life curve (Ref. 16)

Based on the experimental work conducted at TRRL (Transport and Road Research Laboratory) on 35 and 70 mm diameter wire ropes and spiral strands, the following equation was proposed by Tilly (Ref. 16):

$$R^{3.3}N = 2 \times 10^9 \quad (2.1)$$

where R = load range expressed as percentage of the minimum ultimate tensile strength (UTS) and N = fatigue life in cycles. Equation (2.1) was based on a regression analysis of $\log N$ on $\log R$, and was found to give a lower bound line with 95% confidence limit. It was suggested that Eq. (2.1) could be used for the axial fatigue prediction of both wire ropes and multi-layered strands. Detailed description of the work conducted by Tilly was presented in Section 2.3.3.

(b) American Petroleum Institute (API) recommendations (Ref. 14)

The first edition of API-2FPI recommends the following axial fatigue life curve:

$$N \left(\frac{R}{100} \right)^{4.09} = 731 \quad (2.2)$$

where R and N are as defined above. As stated by API, Eq. (2.2) is based on wire rope test data from various sources. Most of the data were obtained from tests conducted in air for six-strand ropes with effects of corrosion not included. Although fatigue data on multi-layered wire strands were not considered by API, in the absence of better information, Eq. (2.2) was also recommended for the prediction of the axial fatigue life of multi-layered strands.

(c) Post-Tensioning Institute (PTI) recommendations (Ref. 15)

The PTI recommendations are based on data assembled by the PTI committee on the axial fatigue behavior of strand (see Ref. 71) and parallel wire stay cable systems (Ref. 19). It is assumed that the stay anchors will be designed to develop fatigue capabilities approaching those of the strand or wire in the free length of the stay cable. A design philosophy compatible with that of the American Association of State Highway and Transportation Officials (AASHTO, Ref. 13) was adopted. The allowable fatigue stress range values for

parallel six-wire strand stay cables are to be in accordance with AASHTO Category B, and differentiated between redundant or non-redundant load paths. Allowable fatigue stress range values for parallel wire stay cables are to be 35 MPa above the Category B values. Finally, the allowable fatigue stress range values for uncoupled and coupled bar stay cables are to be in accordance with AASHTO Category B and Category D values, respectively. A summary of the allowable design fatigue stress ranges for strand, wire and bar stay cables is presented in Table 2.3.

In addition, the PTI rules require that the fatigue strength of the proposed stay cable system shall be demonstrated for each project. Stay cables are to be tested with all their details (e.g., polyethylene pipe sheathing, grouted if required, socket detail with appropriate socketing material). At least three representative stay cable specimens, having lengths between 300 and 450 mm are to be tested for 2 million cycles, for an upper stress level of 0.45 UTS and a stress range 35 MPa greater than the allowable fatigue stress range values corresponding to the redundant load path case. A summary of stay test fatigue stress ranges for strand, wire and bar stay cables is also presented in Table 2.3.

(d) Nakamura and Hosokawa (Ref. 68)

Nakamura and Hosokawa suggested that the following relationship be used for axial fatigue life prediction of multi-layered wire strands.

$$S^3 N = 3\,000 \quad \text{for } N < 2 \times 10^6 \quad (2.3a)$$

$$S = 0.114 \quad \text{for } N \geq 2 \times 10^6 \quad (2.3b)$$

where N is the number of cycles and the non-dimensional stress factor, S , takes into account the effect of stress range (σ), ultimate strength (σ_u) and mean stress (σ_m). It is given by the expression:

$$S = \left(\frac{\sigma}{\sigma_u} \right) \left[1 - \left(\frac{\sigma_m}{\sigma_u} \right)^2 \right]^{-1} \quad (2.4)$$

Finally, Nakamura and Hosokawa modified Eq. (2.3) for the case of parallel wire strands with NEW-PWS sockets as follows:

$$S^3 N = 10\,000 \quad \text{for } N < 2 \times 10^6 \quad (2.5a)$$

$$S = 0.171 \quad \text{for } N \geq 2 \times 10^6 \quad (2.5b)$$

(c) Birkenmaier and Narayanan (Ref. 19)

For parallel wire strands with HiAm and DINA sockets, the following design recommendations were given by Birkenmaier and Narayanan:

$$\text{For static loading: } \sigma_{\max} \leq 0.45 \sigma_u \quad (2.6)$$

$$\text{For fatigue loading: } N = 10^6 \left(\frac{\max \Delta \sigma}{238} \right)^{-4.5} \quad \text{for } N < 10^6 \quad (2.7a)$$

$$\max \Delta \sigma = 238 \text{ MPa} \quad \text{for } N \geq 10^6 \quad (2.7b)$$

2.3.5 Analytical Model for Axial Fatigue Life Prediction

Raof (Ref. 72 and 73) proposed a theoretical model for prediction of axial fatigue life from first principles. It is based on the orthotropic sheet model (see Ref. 33, Ref. 34 and Section 2.2), which estimates the magnitude of interwire/interlayer normal contact forces. The failure criterion is fracture of the first wire. The fatigue life of a cable could therefore be estimated from the fatigue life of wire subjected to fretting fatigue (contact forces). The fatigue life, N_c , of galvanized wires under pure axial tension may be estimated from (Thorpe, Ref. 52):

$$N_c = 10^{-(C_2/C_1)} S_f^{(1/C_1)} \quad (2.8)$$

where,

$$C_1 = -\frac{1}{2.24} \log \left(\frac{0.344 S_{\text{ult}}}{S_e} \right) \quad (2.9)$$

$$C_2 = \log (0.344 S_{\text{ult}}) + 2.13 \log \left(\frac{0.344 S_{\text{ult}}}{S_e} \right) \quad (2.10)$$

S_{ult} is the ultimate tensile strength of a single wire, and S_e is the reduced magnitude of the endurance limit of a single wire due to interlayer contact (fretting fatigue), surface condition, and corrosion. The latter is given by:

$$S_e = K_a K_b K_c S' \quad (2.11)$$

In equation (2.11), S' is the endurance limit of an individual wire subjected to axial fatigue. Thorpe (Ref. 52) suggested that S' can be taken as approximately $0.27 S_{\text{ult}}$ (see also Table 2.2). The other terms are K_a , a surface finish factor ($0.5 \leq K_a \leq 1.0$), K_c , a corrosion parameter ($0.7 \leq K_c \leq 1.0$), and $K_b = 1/K_s$, a parameter to account for fretting fatigue.

The equivalent notch stress concentration factor, K_s , can be calculated from (Knapp and Chiu, Ref. 74):

$$K_s = \frac{\bar{\sigma}'_{\max}}{\bar{\sigma}'} \quad (2.12)$$

where, $\bar{\sigma}'$ is the nominal wire axial stress: $\bar{\sigma}' = E_s S_1^i$ (2.13)

The nominal axial strain in each wire, S_1^i , can be computed from Raof kinematics theory (see Ref. 33). In equation (2.12), the term $\bar{\sigma}'_{\max}$ is the effective maximum von Mises contact stress directly under the center of the trellis contact patches. Knowing the contact force at trellis points (Raof, Ref. 33), $\bar{\sigma}'_{\max}$ can be calculated from contact stress theories. Such a closed form (but lengthy) solution has been derived by Thomas and Hoersch and was graphically simplified by Seely and Smith (see Boresi et al., Ref. 75).

Finally, the equivalent fatigue stress, S_f , in expression (2.8) can be obtained from Goodman equation:

$$\frac{\sigma'_a}{S_f} + \frac{\sigma'_m}{S_{ult}} = 1 \quad (2.14)$$

where σ'_a and σ'_m are the amplitude and mean nominal axial stresses of a wire, respectively, given by:

$$\sigma'_a = \frac{\sigma'_{\max} - \sigma'_{\min}}{2} \quad \text{and} \quad \sigma'_m = \frac{\sigma'_{\max} + \sigma'_{\min}}{2} \quad (2.15)$$

The maximum and minimum nominal wire axial stresses, σ'_{\max} and σ'_{\min} , correspond to the maximum and minimum applied cycling load and, again, these can be calculated from Raof's kinematical theory.

2.4 Length Effect

Due to physical limitations of fatigue test facilities, the experimental results available are generally from short specimens of wires or cables (10 meters maximum). These results must then be extrapolated to determine the fatigue strength of large cables having lengths above 250 meters. The extrapolation required is far beyond the laboratory results, which implies an element of risk.

Experimental evidence suggests that axial fatigue life must be reduced as the length of the cable increases, but, because of physical testing restrictions, only small diameter cables have been used to investigate the influence of the L/D ratio. Birkenmaier and Narayanan

(Ref. 19) conducted tests on 7 mm diameter cold drawn high tensile steel wires having two different lengths (200 mm and 600 mm). Twenty-five specimens for each length were tested at stress ranges between 360 MPa and 600 MPa. The probability of failure at two million cycles increased for the longer specimens. Castillo et al. (Ref. 50) and Canteli et al. (Ref. 76) conducted carefully controlled experiments on 0.5 mm diameter wires and 15 mm strands having lengths between 500 and 10 400 mm. A typical comparative graph, giving the Weibull probability of rupture for two different lengths, is reproduced (from Ref. 76) in Figure 2.1. It can be clearly seen from this figure that as the length of the specimen increases, the probability of failure (at a given stress range) increases.

2.4.1 Statistical Models

The primary objectives for a statistical analysis of fatigue data are to estimate certain fatigue properties (e.g., endurance limit) of a material or component from a given set of data, to give procedures for comparing different sets of fatigue data, and to provide efficient information based on a limited number of test specimens. In addition, in order to account for the size effect, the statistical model should be able to extrapolate the fatigue strength of cables from short specimens to the real lengths, and to predict the fatigue life of a bridge cable based on tests of limited duration.

A review of the existing statistical models for fatigue analysis can be found in the work conducted by Castillo et al. (Ref. 50). According to Castillo, it is reasonable to take the size (length) effect into consideration using the *weakest link principle*. A real cable of length L can be subdivided into k smaller cables of length L_0 , connected in parallel series, and subjected to the same fluctuating stresses as the whole piece. The weakest link principle states that the fatigue strength of the cable is that of the weakest connected sub-element:

$$N^* = \min(N_1, N_2, \dots, N_k) \quad (2.16)$$

where N is the fatigue life of the whole cable, and N_1, N_2, \dots, N_k are the fatigue lives of the sub-elements.

It is generally accepted that the fatigue failures of wires and cables are due to fretting fatigue of pre-existing surface flaws, derived from the manufacturing process, handling and storage. If the distribution of flaws is random with respect to the length, it is reasonable to assume statistical independence between neighboring samples. The same distribution function could, therefore, be used for the fatigue strength of all sub-elements. Knowing

the probability of failure function, $F_{L_0}(x)$, for the sub-elements (i.e., test data) of length L_0 , the probability function, $F_L(x)$, of the cable with length L can be derived from the expression (Ref. 50):

$$F_L(x) = 1 - \left[1 - F_{L_0}(x) \right]^{(L/L_0)} \quad (2.17)$$

Castillo et al. (Ref. 50) noted that when the length of the sub-elements goes to zero ($L_0 \rightarrow 0$) or the number of pieces goes to infinity ($L/L_0 \rightarrow \infty$), the probability functions must be asymptotic. The only asymptotic family that is stable and compatible with respect to Eq. 2.17 and that best describes the non-linear experimental evidence of the fatigue life curve and the standard deviation was found to be the Weibull family. Accordingly, the following five-parameter statistical model was proposed by Castillo et al. (Ref. 50):

$$(N - B)(\Delta\sigma - C) = D \left\{ \left[-\frac{L_0}{L} \log(1 - P) \right]^{1/A} - E \right\} \quad (2.18)$$

where P is the probability of failure, L_0 is the reference length, and L the cable length. The five statistical parameters A, B, C, D, E are as:

A is the Weibull shape or slope parameter

B is the asymptotic N (cycles) limit

C is the endurance limit

D is the scale fitting parameter obtained for chosen reference length L_0

E is a constant defining the S-N threshold curve (asymptotic curve, zero probability of failure curve).

2.5 Wire Breakage Monitoring Methods

It is generally agreed that interlayer fretting fatigue between wires is the fundamental mechanism of fatigue failure in stranded cable subjected to fluctuating loading. Thus, the ability to detect internal breakage is important when assessing the condition of a cable during a fatigue test or in service.

For this purpose, a variety of non-destructive techniques have been used. They can be classified into two categories: methods that detect fractures of wires as they occur and those that detect fractures later. Acoustic emission and accelerometers are the most commonly used methods in the first group. Their applications are limited to short cables and they are extensively used for break detection during fatigue experiments. Electromagnetic methods are considered the most suitable for detection of existing wire ruptures and have been used

for inspection of cables in service (Tilly, Ref. 16). Nevertheless, conventional visual inspection is still the simplest and most commonly used method of assessing the condition of cable.

In order to carry out a reasonable visual inspection, the inspection speed must not exceed 0.3 m/sec (Babel, Ref. 77 and 78). Since high concentration is required during inspection, the inspection time of the testing person should be limited to 10 minutes. Since only surface flaws can be detected with this method, its use is of limited value (Weischedel, Ref. 79).

In the electromagnetic method, a static excitation is applied to the cable and the magnetic flux passing through the rope is measured. This magnetic flux is a function of the metallic area of the cable, and any change in the magnetic flux caused by a change in metallic area and/or broken wires will be detected. In practice, in order to assess the deterioration an initial "signature" would be taken from the new cable and all subsequent examinations would be compared to the original. The instrument can be mounted and slid along the cable relatively easily (Ref. 79). This technique has been extensively used in the mining industry, and it is a legal requirement in several countries (Ref. 62).

The European Working Group on Acoustic Emission (Ref. 80) defines acoustic emission as "the transient elastic waves resulting from local internal micro-displacements in a material. By extension, this term also describes the technical discipline and measurement technique relating to this phenomenon." For metals, microcracks emit sounds at frequencies outside the audible range, so that signals must be electronically processed in order to be detected. Those events are characterized by a number of parameters such as acoustic emission count, ring-down count, count rate, burst duration, maximum burst amplitude, burst rise-time, and so on. Definitions of terms related to acoustic emission (AE) can be found in Ref. 80.

Taylor and Casey (Ref. 81) and Casey et al. (Ref. 82) developed an AE device to detect wire breakage and conducted extensive tests on simple wires and ropes. The acoustic emission was found to accurately predict fractures of outer wires. For the 40 mm diameter rope tested, it was found that although the AE was able to provide warning of impending failure, no direct correlation was achieved between recorded events and wire breaks, mainly because of the occurrence of large numbers of wire breaks in the independent wire rope core. It was also observed that outer strand wire breaks occur relatively late in the life

of a rope undergoing tensile fatigue test. Babel (Ref. 77 and 78) also noted that wires break in the interior layers before breaks are detected on the surface layer.

Woodward (Ref. 83) also used acoustic emission to monitor the fatigue tests of 35 to 70 mm diameter ropes, multi-layered strands, and locked coil cables. A series of calibration tests were conducted in order to establish the properties of a wire fracture event, to determine the velocity of stress waves, to measure their attenuation, and to evaluate the coupling to be used between the transducers and the cable. In their tests, it appeared that a wire fracture event travels at a velocity of about 5.1 km/sec and has high amplitude, long duration, and large number of counts. The average ratio of acoustic events to total wire fractures was found to be 0.99 for multi-layered strands, 0.38 for ropes and 2.43 for locked coil cables. It was therefore concluded that acoustic emission is unlikely to be successful on locked coil and rope cables. Finally, it should be mentioned that the AE method is complicated, since it requires initial calibration tests, filtration of background noises, and special software to extract the events associated with wire fracture.

A simple way of detecting breakage of wires as they occur is by the use of accelerometers. An accelerometer is an electro-mechanical transducer that produces an electrical output proportional to the acceleration to which it is subjected. As a wire fractures, the accelerometer transducers are able to detect the corresponding shock wave. Hanzawa et al. (Ref. 55) used both accelerometers and AE to detect breakage on 50 mm to 85 mm diameter ropes. Good agreement between the two methods was observed. Takena et al. (Ref. 70) used accelerometers to detect wire breakage on large diameter HiAm parallel wire cables. Although the tests were discontinued after only few wire fractures and most of them were located at the outer layer, the ratio of prediction to actual ruptures was 100%.

2.6 Summary

This survey of the literature reveals that the kinematics of a multi-layered strand are characterized by uneven axial load distribution among the wires, interwire and interlayer contact and friction forces, and associated relative displacement of the wires.

The axial fatigue failure mechanism of wire ropes is identified as fretting fatigue at the interlayer and interwire contact patches. The most important factors that affect the performance of a stranded cable subjected to cyclic load have been found to be cable make-up, lubrication, corrosion protection and testing environment, axial fatigue behavior of individual wires, termination conditions, stress range, mean stress, length-to-diameter ratio, and frequency of testing.

A large amount of axial fatigue data on cables from different sources has been reported. Depending the type of cable, these data should be grouped in the following three categories: ropes, parallel-wire strands, multi-layered wire strands. Even after this classification, the fatigue data exhibit a large degree of scatter. This is mainly due to the different discard criteria used by researchers and to inappropriate test parameters, such as insufficient cable length and high test frequencies. A relatively short test length, for instance, prevents the rope from compensating for any slight misalignment of the sockets and specimen fails prematurely at the socket location. Test specimens should be long enough to accommodate the end effects and wire breaks should be distributed more or less uniformly between the anchor portion. Furthermore, sockets design for fatigue tests of cables should be similar to the ones used in real structures.

The fatigue failure criterion for steel cables is by nature more complex than that applied to conventional structural steel elements, where crack length (and cross-section loss) measurements may suffice for a quantitative fatigue damage assessment. Some of the difficulties are related to the interwire friction, which can allow load to redevelop in a given wire within a relatively short length. The influence of broken wires on the strength of a steel cable is, therefore, not directly equivalent to the loss of area of steel. For example, the literature review revealed that a cable that had been cyclically loaded to 70 percent of its expected fatigue life and had many wire breaks still possessed 100 percent of its static breaking strength (Ref. 66). Thus, remaining static strength should not be used as a discard criterion. Although the occurrence of an unacceptable number of wire breaks is by far the most common measure adopted for fatigue damage assessment, a large variety of criteria have been proposed without clearly demonstrating their derivation. In addition, very few investigators have tested cables to complete failure, and most of the reported fatigue data have been discontinued at two million cycles. It is considered that this is unrealistically low for steel cables. A well-defined discard criterion based on a damage parameter that describes the fatigue strength of a multi-layered strand is therefore required. In order to achieve this, some specimens should be tested to failure and the fatigue damage parameter closely monitored throughout the tests.

In order to establish a replacement criterion for a cable based on wire breaks, non-destructive procedures must be used to continuously detect internal and surface wire breaks during fatigue testing. The available non-destructive techniques have been reviewed and it appears that acoustic emission and accelerometers have been successfully used with constant amplitude fatigue tests.

Variable amplitude load testing demonstrated that the Miner linear damage cumulative theory gives conservative results. This is attributed to overload crack retardation and changing of the fretting locations between wires as the different load levels are applied.

Generally, only test results on short specimens of wires or cable are available. The size effect problem, which relates to the extrapolation of these results to determine the fatigue strength of cables with several hundred meters was also reviewed. This is usually done using statistical models. Castillo et al. (Ref. 50) have proposed a five-parameter model based on experimental observations and statistical requirements. This is a Weibull model and it takes the size effect into consideration, is based on the weakest link principle, and assumes statistical independence between the sub-elements that form the cable. This has been proven to be a reasonable assumption when relatively long test samples are used.

The recommended design procedures for the prediction of the axial fatigue life of cables have also been examined. The existing design "stress range vs. number of cycles" (S-N) curves were developed based on experimental data. The most commonly used highway bridge specifications in North America (e.g. Ontario Highway Bridge Design Code (Ref. 12), American Association of State Highway and Transportation Officials (Ref. 13)) give no guidance as to the fatigue life capability of steel cables. Only the Post-Tensioning Institute (PTI, Ref. 15) and the American Petroleum Institute (API, Ref. 14) give recommendations for the allowable fatigue stress range in cables. Equation 2.2 and Table 2.3 represent the recommendations of API and PTI, respectively.

Finally, an analytical model for the fatigue life prediction of multi-layered strands, based on first principles, has been developed by Raoof and co-workers. This model depends on a surface finish factor (ranging between 0.5 and 1.0) and accounts for the fretting fatigue by modifying the axial fatigue curve of single wires.

The proposed design procedures and Raoof's analytical model do not take into account the length effect, which has been shown to reduce significantly the fatigue life of a cable. Fatigue life "stress range vs. number of cycles" curves that account for the length effect need to be developed for the different types of cables.

Table 2.1 Design stress range of cables for several bridges (Ref.18 and 19)

Bridge	Type of Cable	Stress Range ¹
George Washington, U.S.A.	Suspender, rope	5%
Walt Whitman, U.S.A.	Suspender, rope	10%
Throg's Neck, U.S.A.	Suspender, rope	10%
Maysville, U.S.A.	Suspender, rope	12%
Odgenburg, Canada	Suspender, rope	14%
Davenport, U.S.A.	Suspender, rope	14%
Verrazano, U.S.A.	Suspender, rope	8%
Forth Road, Scotland	Suspender, rope	12%
Save, Yugoslavia	Stay, parallel wire	13%
Novi Sad, Yugoslavia	Stay, parallel wire	15%
Lyne, Great Britain	Stay, parallel wire	7%

(1) Percent of minimum ultimate tensile strength

Table 2.2 Experimental values for endurance limit of single wires

Ref., Year	Wire Diameter (mm)	Ultimate Strength (σ_u) (MPa)	Fatigue Limit (σ_f) (MPa)	σ_f / σ_u
(43, 1985)	2	1321	390	0.30 ¹
(43, 1985)	2	1469	366	0.25 ¹
(43, 1985)	2	1855	421	0.23 ¹
(43, 1985)	2	2099	471	0.22 ¹
(43, 1985)	2	2218	565	0.25 ¹
(50, 1985)	0.5	1700	415	0.24
(50, 1985)	0.5	1700	317	0.19
(50, 1985)	0.5	1700	294	0.17
(52, 1983)	1.8-2.3	1840	490	0.27
(19, 1982)	7	1783	378	0.22
(51, 1941)	2.1-3.1	1516-1722	441	0.27
(51, 1941)	2.1-3.1	1171-1309	403	0.33
(51, 1941)	2.1-3.1	758-827	322	0.41

(1) Residual stresses were removed

Table 2.3 Summary of fatigue stress range values as per PTI (MPa) ¹

Type of Stay	No. of Cycles (N)	Allowable Design Fatigue Stress Range (MPa)		Stay Test Fatigue Stress Range ^{2,4}	Component Fatigue Test Stress Range ^{3,4}
		Redundant Load Path	Non-redundant Load Path		
Strand or uncoupled bars AASHTO Category B	N > 2x10 ⁶	110	110	158.5	179
	2x10 ⁶	124	110		
	5x10 ⁵	189	124		
	1x10 ⁵	310	189		
Wire AASHTO Category B plus 35 MPa	N > 2x10 ⁶	145	145	193	282.5
	2x10 ⁶	158.5	145		
	5x10 ⁵	224	158.5		
	1x10 ⁵	344.5	224		
Bars with couplers AASHTO Category D	N > 2x10 ⁶	48	34	103	117
	2x10 ⁶	69	48		
	5x10 ⁵	110	69		

Notes: (1) Any flexural stress range in excess of 20 MPa shall be added to the axial fatigue stress range due to live load plus impact.

(2) To ensure fatigue quality of stays, it is recommended that the stay specimens be tested at 2x10⁶.

(3) Individual strand, bar, wire; or glued coupler bar respectively.

(4) Upper bound stress level shall be 45% of the yield strength.

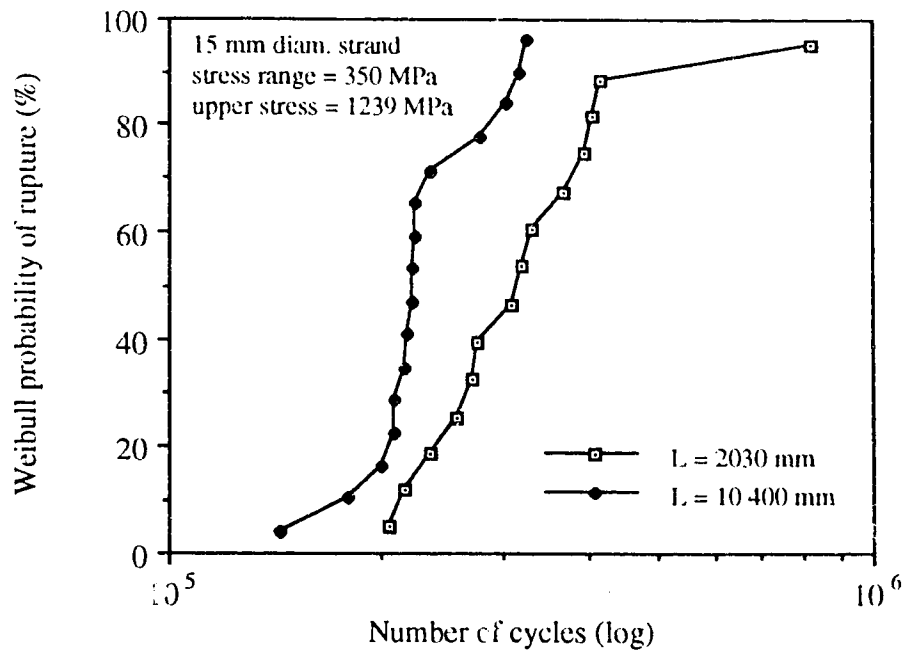


Figure 2.1 Experimental evidence of length effect (Ref. 76)

Chapter 3 Experimental Program

3.1 Introduction

The first objective of the test program was to establish a fatigue failure criterion. It is seldom practicable to run the fatigue test of a multi-layered structural strand to destruction. When the applied stress ranges are relatively low, a region of practical importance, the fatigue life to destruction can easily exceed ten million cycles. Thus, a discard criterion is desirable and the literature review indicated an inconsistency amongst the failure criteria used in the past. The most popular criteria are the first broken wire, 5% of wire breakages, and two million cycles. In order to assess the damage accumulated by a cable, the first series of tests were carried out to destruction and two potential discard criteria were carefully monitored. The number of wire breakages with respect to a minimum test length and the deterioration of the modulus of elasticity were the two parameters adopted for the damage assessment of a cable during axial fatigue test.

The literature review showed that there are very few fatigue data for large diameter cables. In addition, most fatigue data that are available are for high stress ranges or have been discontinued at two million cycles. In practical applications, low stress ranges predominate. In the fatigue loading of steel components subjected to fretting, it must be additionally taken into account that, even with small stress ranges, fractures can occur after two million cycles. It appears that an infinite life range (endurance limit) in the classical sense does not exist. Moreover, a cut-off of two million cycles is unrealistically low for steel cables in bridges. It was therefore considered important in this experimental study to obtain fatigue life data for large diameter strands operating in the low stress range region of the fatigue life (S-N) curve.

In Chapter 2, many parameters were identified as factors that can influence the axial fatigue performance of a cable. Based on their expected significance, the available experimental time, and the capabilities of the fatigue test equipment available, the parameters that were experimentally investigated are the stress range, the strand make-up, and strand diameter. Finally, the dependence of fatigue strength on the test length is not well established and is hardly ever treated in standards. In order to contribute towards the establishment of standard fatigue test procedures for cables, the effect of the length-to-diameter ratio (L/D) of the specimens was also experimentally investigated.

3.2 Axial Fatigue Test Program

Sixteen full-size multi-layered wire strands were tested in cycling tension fatigue. The parameters investigated are the stress range, the strand construction, and the specimen length-to-diameter ratio. The stress range varied between 15% and 30% of the ultimate tensile strength (UTS). Two different cable construction were used, as represented by a 45 mm and a 25 mm diameter strand. Finally, the length-to-diameter (L/D) ratio that was investigated ranged from 75 to 133.

The test program was subdivided into three series. Series SP, which was the reference series, consisted of eight specimens. The specimen was a 45 mm diameter galvanized strand conforming to ASTM Standard A586 (Ref. 3) and it consisted of 91 individual wires. The actual breaking strength of the cable, reported in the mill certificate, was 1842 kN. The specified minimum ultimate tensile strength (UTS) according to the ASTM Standard is 1673 kN. The gross metallic area, as defined in the ASTM Standard, is 1187 mm². The make-up of the cable is shown in Table 3.1, where measured values are given. The length of these specimens was approximately 3310 mm, giving a length-to-diameter ratio of 75. The mean stress was kept constant at a value of 350 MPa (25% of the UTS), while the stress range varied between 303 MPa (21.5% UTS) and 404 MPa (28.7% UTS). The testing parameters for Series SP are presented in Table 3.3.

Series SL and SS consisted of five and three specimens, respectively, each of 19 individual wires, 25 mm diameter galvanized strand, also conforming to ASTM Standard A586. The actual breaking strength of the cable, reported in the mill certificate, was 596 kN, whereas the ASTM specified minimum ultimate tensile strength is 543 kN. The gross metallic area, as defined in the ASTM Standard, is 387 mm². The make-up of the cable is shown in Table 3.2. Specimens of SL series had a length of approximately 3375 mm, giving a length-to-diameter ratio of 133, and those of SS series had a length of 2150 mm (L/D= 85). The mean stress was constant for all specimens at 361 MPa (25.8% of the UTS), and the stress range varied between 207 MPa (14.75% UTS) and 361 MPa (25.8% UTS). The testing parameters of SL and SS series are presented in Table 3.3.

3.2.1 Development of the End Termination

A split-bearing socket, which was designed and machined at the University of Alberta, was used for the end termination of the specimens. This socket, which was re-usable, is shown in Figure 3.1. (Fig. 3.1 identifies the 45 and 25 mm diameter sockets.) It consists of two steel plates which form a conical cavity and which are bolted together around the strand socket. The strand conical sockets were made independently by pouring the socketing

material into a mold around the splayed wires of the cable. The socketing material was so-called *wirelock cold socketing*, which contains polyester resin with hard inner fillers. Cold casting material has been found to give higher fatigue performance than the more commonly used zinc alloy hot-pouring metal. When the cable is subjected to tension, a wedge action develops between the material inside the cone and the split-bearing socket plates. This creates a tri-axial state of stress inside the socketing material, which efficiently transfers the load from the wires to the socket plates. Finally, the split socket plates transfer the load through the bearing face to the reaction beam. This type of reaction is consistent with how bridge strand would be anchored in a modern cable-supported bridge.

Preliminary dimensions for the conical cavity taken from Ref. 2 were presented in Figure 1.2(b) and also can be obtained from socket manufacturer's catalogues. The steel socket plates were checked for ring tension stress induced from the wedge action of the casting material and for bearing stresses at the interface of the socket with the supporting beam. The bolts connecting the two halves of the socket were designed to carry the splitting tensile force of the two plates.

It is important to note that for the 25 mm diameter socket, shown in Figure 3.1(b), a transition cylindrical region was introduced around the neck of the socket in order to try to minimize wire breakages that might occur at the termination region as a result of secondary bending stresses and vibration.

3.2.2 Preparation of Specimens

All specimens of a given diameter were taken from the same spool of cable. The 45 mm diameter cable was 73 meters long and the 25 mm diameter cable was 36.5 meters long. Both cables were coiled on shipping reels. The step-by-step procedure used for the preparation of testing samples is described in the following.

1. Unreeling

The cable was unreeled from the coil by holding the free end of the rope while the reel was rolled along the floor. The exact length of the specimen to be cut was then measured and marked.

2. Seizing

Before cutting the cable, even though it has been pre-formed it was carefully seized to prevent displacement or relative movement of the wires. If cables are not properly seized prior to cutting, wires and strands are apt to become slack, thereby upsetting the

uniformity of tension in the rope. This could result in overloading of some wires and underloading of others.

The cable was seized at each side of the cutting location for a length equal to twelve times its diameter. Figure 3.2 shows the special seizing device, which was developed at the University of Alberta, used to wrap the seizing wire around the rope in a close, tight winding. The direction of seizing was opposite to the lay of the rope. The 2 mm diameter seizing wire was tinned in order to be able to solder it.

3. Soldering

Soldering was applied on top of the seizing in order to hold it in place. For the soldering operation the specimen was heated at the seizing location with a hot copper block. A layer of non-acidic flux paste was then applied onto the seizing wire. Use of non-acidic flux is very important in order that there be no reaction of the acid with the galvanizing on the cable. Finally, the soldering was performed by melting a soldering bar with the help of the hot copper block.

4. Cutting

After seizing and soldering are completed the specimen was cut to its correct length by means of a saw cut rotating disk.

5. Socketing

The socketing operation can be subdivided into the following steps:

- The specimen is securely clamped (served) for a length of not less than three rope diameters with a special strand clamping device, fabricated at the University of Alberta. This serving device is shown in Figures 3.3 and 3.4. The same strand clamp was used for both 25 and 45 mm diameter cables by providing two different inserts for insertion between the strand and the specimen. The clamp was placed at a distance from the rope end equal to the length of the socket cone plus 10 mm.
- The individual wires at the end of the strand were unlayered and splayed as far down as the serving so that the cable end resembles a broom. This is shown in Figure 3.5 for the 45 mm diameter strand.
- The wires in the broom were cleaned thoroughly, using a proprietary degreasing solvent, so that all lubrication could be removed.
- The specimen was then positioned and clamped vertically. It is important that the rope below the socket be straight for a length equal to about twenty-four rope diameters. If cables are not properly straightened before socketing, secondary

bending stresses will be induced at the socket region during the axial fatigue loading. Figure 3.6 shows part of the vertical clamping device.

- The base of the socket was sealed with plasticine in order to prevent leakage of the resin.
- Figure 3.7 shows the aluminum molds that were used to pour the socketing material for both the 45 mm and the 25 mm diameter specimens. The split socket molds were sprayed with a silicon release agent and then installed on top of the strand serving device. A socket ready to be poured is shown in Figure 3.6. The wires in the broom had to be pulled back during this step so that they fit inside the mold without touching it.
- The last step in the socketing procedure is the mixing and pouring of the socketing material. The wirelock socketing material comes in pre-measured kits consisting of two containers, one with resin and one with granular compound. All of the granular compound is poured into a container containing all of the resin, and then it is mixed thoroughly for two minutes. Immediately after mixing, the mixture is slowly poured into the mold until the socket is full. After two hours, the mold could be removed and after twenty-four hours the socket is ready to be loaded. Figure 3.8 shows a finished socket for the 45 mm diameter multi-layered strand.

3.2.3 Detection of Broken Wires

During the axial fatigue tests, the wire breakages were detected by continuously monitoring the fatigue test by means of two different non-destructive test methods; acoustic emission system (AE) and accelerometers (ACC).

3.2.3.1 Accelerometers

An accelerometer is an electromechanical transducer that produces an electrical output proportional to the acceleration to which it is subjected. Its applications include shock and vibration measurements and analysis (see Section 2.5).

During the axial fatigue tests, two Brüel and Kjær delta shear accelerometers (Ref. 82), type 4370, were used to detect the shock corresponding to a wire breakage. The accelerometers were securely mounted on aluminum bracket devices, having a smooth flat surface, by means of threaded steel studs. They were located at a distance of approximately 500 mm away from the end terminations. In order to avoid ground loops that might give rise to noise in the measuring circuit, the accelerometers were electrically isolated from the specimen by means of mica washers. Rubber pads between the brackets and the specimen were used as couplants. Figure 3.9 shows an accelerometer connected to

a specimen. Charge pre-amplifiers were introduced between the accelerometers and the measuring set-up in order to convert the high output impedance of the accelerometer to a lower value and to amplify the relatively weak output signal from the accelerometers. A great advantage of the charge amplifier in comparison to a voltage amplifier is that very long cables can be used between the accelerometers and preamplifier without changing the sensitivity of the measuring system.

Finally, the pre-amplifiers were connected to two channels of a data acquisition system, DAS-8, which was loaded on a XT IBM compatible computer. The bit values of the two accelerometers could therefore be read. When the bit value of one of the two accelerometers exceeded a pre-set trigger value, the date, time, and maximum and minimum bit values were automatically recorded into a file. At the same time, another file having the bit data for both accelerometers for a period of 2.5 sec was generated, from which a bit versus cycles graph for the particular event could be plotted.

3.2.3.2 Acoustic Emission System

The acoustic emission (AE) technique that was described in Section 2.5 was used to detect, analyze and discriminate the transient elastic waves generated by the rapid release of energy as a wire fractures, during the fatigue test of a cable.

The acoustic emission (AE) monitoring system used for the detection of broken wires included (see Ref. 82):

- a dual-channel Monac AE surveillance unit
- two piezo-elastic type resonant transducers with frequency response band of 100 to 500 kHz and a resonant frequency of 250 kHz
- two transducer preamplifiers with 20 dB gain
- control software loaded on a IBM 386 personal computer
- a digital storage oscilloscope (PM3350A).

The AE system featured programmable pattern recognition capabilities. A 20/40 dB attenuator was built into the front of the main system amplifier. This added attenuation circuitry allowed the system to collect high amplitude AE signals from the wire breakage tests. Acoustic emission signals picked up by a transducer are amplified by the preamplifier. All the signals that pass a threshold value trigger the data collection circuit and are characterized by the monitoring unit on the basis of five signal pattern parameters: count, rise-time, peak amplitude, duration, and energy. Only those fitting the selected parameter window are saved by the computer as valid data.

A series of initial calibration tests, which are presented in the following sections (3.2.3.2.1 to 3.2.3.2.3), were required in order to characterize the features of AE signals from wire fractures and to study the AE signal propagation through cables. The values of the window parameters and the sort criteria were based on those preliminary tests.

3.2.3.2.1 Single Wire Tensile Test

Single wire specimens of 900 mm length were removed from the coil of the 45 mm diameter multi-layered strand. Two AE transducers were mounted on the wire using two specially designed flat clamps. A small notch was introduced at the center of the test specimen in order to ensure wire fracture at that location. The distance of each transducer to the center cut was 200 mm. The wire specimen was loaded using a testing machine of 1000 kN capacity. Background noises from the testing machine and grips were examined under a load of about 80% the ultimate wire strength. Individual wire specimens were loaded to failure and the signals from wire fracture were captured on both the AE unit and the oscilloscope. Figure 3.10 shows a wire specimen during the single wire tensile test.

3.2.3.2.2 Wave Attenuation Tests

Wave attenuation tests were performed on the 45 mm diameter strand using simulated AE signals obtained by breaking 2H, 0.7 mm pencil leads. The objective of these tests was to study the wave attenuation along the cable length, radially, and between the different layers of the cable. Attenuation was determined by comparing the signal parameters collected by the transducers.

A 300 mm long cable bundle was used in order to examine both the radial signal attenuation and the attenuation of the elastic wave between the six layers of the cable. The pencil lead was broken at one end of the cable on various wires located at different layers and angular orientations and signals were then picked up by a transducer on the external surface of the cable close to the other end. A test at a given location was repeated five times and the average value was then used for the final results.

The attenuation along the cable length was assessed using the 3300 mm long fatigue specimen SP2. Two transducers were mounted on the cable with half-circle clamps at distances of 300 mm and 1170 mm from the socket. Figure 3.11 shows the transducers and the 45 mm diameter cable used for the wave attenuation tests. Silicon grease was used as couplant between the cable and the clamp and between the clamp and the transducer. The breaking pencil lead test was conducted at various distances along the cable and the simulated AE signals were picked up by both transducers.

3.2.3.2.3 Pulse Echo Test

A pulse echo test was performed on the fatigue test specimen SP2 in order to investigate the possibility of using a pulse signal to detect broken wires inside a cable when one end of the cable is accessible. An acoustic emission transducer was mounted on the surface of the specimen. A pulse signal was simulated by breaking a 0.7 mm, 2H pencil lead. Upon breaking a pencil lead at the end of a specific wire in a cable bundle, two acoustic events are detected. One is detected when the pulse first passes the transducer and the second is detected when the pulse reflects from the other end of the wire. By calculating the time interval between the two recorded events, the location of a wire failure can be determined.

3.2.4 Axial Fatigue Test Setup

The axial fatigue tests of the sixteen full-scale multi-layered wire strands were carried out using the servo-hydraulically controlled fatigue equipment of the structural engineering laboratory at the University of Alberta. This system is driven by a large capacity pump (630 litres / sec).

Figure 3.12 illustrates the testing apparatus. It consists of a self-equilibrated frame that could be adjusted to accommodate cable lengths from 2 150 mm to 6 000 mm. The specimens, which were placed horizontally, were loaded in a load-control mode by means of two servo-hydraulically controlled actuators. Each actuator has a capacity of 530 kN and is capable of 150 mm stroke. An overall view of the testing frame is shown in Figure 3.13. The specimen was secured through the sockets to a fixed beam on one end and to a moving beam at the other. Such a detail is shown in Figure 3.14. The moving beam was supported on a rotating and sliding set of rollers, as shown in Figure 3.15. The actuators were secured with threaded rods on another beam and were pin-connected to the moving beam by means of a universal pin connection. In order for the actuators to be able to run in parallel load control mode, a stroke feedback circuit was built into the fatigue system to ensure in-phase stroke movements.

The constant amplitude cycling load had a sinusoidal shape and was applied to the specimen after it had been statically loaded up to the predetermined mean value. The testing frequency ranged between 1.5 Hz to 3.5 Hz, depending upon the characteristics of a given test specimen.

During the axial fatigue tests, the load range, static load, number of cycles, and frequency of testing were directly obtained from the control panel of the fatigue testing system. Additional instrumentation on the specimen consisted of:

- One linear variable differential transducer (LVDT) connected to the free length of the specimen. The LVDT was used to measure the elongation of the cable during the static tests.
- Two transducers used to measure the overall deformation of the specimen, including the end effects. They were only used during the static tests.
- Two piezo-elastic type resonant transducers, which were clamped to the cable at a distance of 500 to 700 mm away from the sockets. These transducers were part of the acoustic emission monitoring system used to detect wire breakages for the 45 mm diameter cables. (This was described in Section 3.2.3.2. See also Ref. 83.)
- Two accelerometers fitted close to the sockets of the test cables. These were used to detect the shock corresponding to a wire breakage. The accelerometers were mounted on all the specimens using a special clamping device. (The accelerometer system was described in Section 3.2.3.1.)
- A temperature probe was connected at the outside layer of some of the specimens. It was used to measure the change of cable temperature with respect to the ambient temperature during the cycling test. The ambient temperature was measured using an ordinary thermometer, and it recorded the temperature in the proximity of the testing area.

The deterioration of the stiffness of the specimen was determined by performing static tests at specific time intervals. Each static test was conducted at a load that was between the minimum and maximum values of the fluctuating load. With the exception of instances when there were problems with the fatigue test apparatus, the specimen was never unloaded during the test. The data taken during the static tests included the number of cycles at which the test was performed, the load applied, the free length elongation of the cable, and the elongation of the specimen including the end effects. Using this information, the modulus of elasticity, excluding and including the end effects, could be determined. This will be referred to as free length modulus of elasticity and overall modulus of elasticity, respectively. Figure 3.16 shows the instrumentation attached on a 45 mm diameter specimen.

3.3 Ancillary Tests

Three identical tensile coupon tests were conducted for the four different diameter wires. The specimens had a free length of 200 mm (between clamps) and were gripped by means of a modified standard grip of the kind used for prestressing strands. Those cylindrical grips have a diameter of 25 mm and a length of 75 mm.

The testing of the twelve coupons was done in a 1 000 kN testing machine and the testing procedure specified by ASTM Standard A586-86 (Ref. 3) was followed. The elongation of the coupon was measured by an electric clip-on extensometer of 50 mm gage length and the tests were run at a strain rate of about 5 $\mu\text{E}/\text{sec}$ in the elastic range. The load and the elongation from the autographic extensometer were recorded at regular intervals, using a multichannel data acquisition system. When the specimen had an extension of 0.7%, which corresponds to the starting of yielding, the cross-head was held in order to obtain a static stress value. Shortly after the ultimate stress level was reached, the extensometer was removed and the loading continued until the specimen ruptured. The ultimate tensile strength reached during test was obtained from the peak indicator of the testing machine. Figure 3.17 shows an individual coupon, with the extensometer, during a coupon test.

3.4 Metallography and Fractography

The objective of the metallographic study was to investigate the micro-structural uniformity between wires of different layers and to study the effect of the hot dip galvanizing and, most specifically, the possibility of existence of micro-cracks at the zinc-steel wire interface.

Three metallographic specimens were prepared from the 45 mm diameter strand. One sample was taken from the fourth layer of specimen SP2, another from the core wire of specimen SP4, and the third one from the outside layer.

Preparation of metallographic specimens requires five operations: sectioning, mounting, grinding, polishing, and etching. The micro-structural samples were shear cut to a length of about 25 mm.

The metallographic specimens were mounted in order to facilitate handling of the specimens during the subsequent steps of metallographic preparation and examination. Compression mounting was used for the three specimens since they were smaller than the standard 31 mm diameter mold. This involves mounting around the metallographic specimen by heat and pressure using Bakelite for molding material. The specimens were mounted while the wire axis was in a horizontal direction.

The subsequent grinding operation was performed until the mid-section of the specimen was reached. Another reason for grinding is to lessen the depth of deformed metal to the point where the last vestiges of damage can be removed by a series of polishing steps. Grinding was accomplished by abrading the specimen surface through a sequence of operations using progressively finer abrasive grit. Grit series from 40 mesh to 150 mesh

are usually regarded as coarse abrasive and grit sizes from 180 mesh through 600 mesh as fine abrasives. Each grinding step completely removed the deformed metal produced by the previous step.

Polishing is the final step in producing a surface that is flat, free of scratches, and mirror-like in appearance. Polishing was done in two stages. The first stage consisted of polishing with diamond compound abrasive and the final polishing was done with 0.05 micron particle size aluminum oxide.

In order to prepare the metallographic specimen for observation with the optical microscope, etching is necessary in order to reveal the structure. The principle of etching is based on preferential attack of one or more phases and grain boundaries because of differences in chemical composition, and to a lesser extent, because of differences in orientation. A two percent nital solution was used for etching the metallographic samples.

Fractured surfaces of broken wires and fretting areas were examined in the optical microscope or scanning electro-microscope in order to investigate the fretting fatigue mechanism and to observe the initiation, propagation and final fracture phases of a wire fatigue failure. No special surface preparation was performed in order that there be no alteration of the cracked area and to leave the corrosion associated with the fretting fatigue phenomenon, which was also shown on the fractographies.

Table 3.1 Strand make-up for the 45 mm diameter cable

Layer	No. of Wires	Lay Direction (1)	Wire Diameter (mm)	Lay Length (mm)	Strand O.D. (mm)	Lay Angle (degree)
1	30	LL	4.034	506	44.37	14.06
2	24	RL	4.034	395	36.27	14.38
3	18	LL	4.034	301	28.29	14.21
4	12	RL	4.034	206	20.16	13.82
5	6	RL	4.034	160	12.29	14.54
6	1	-	4.315	-	4.315	-

(1) LL=Left lay RL=Right lay

Table 3.2 Strand make-up for the 25 mm diameter cable

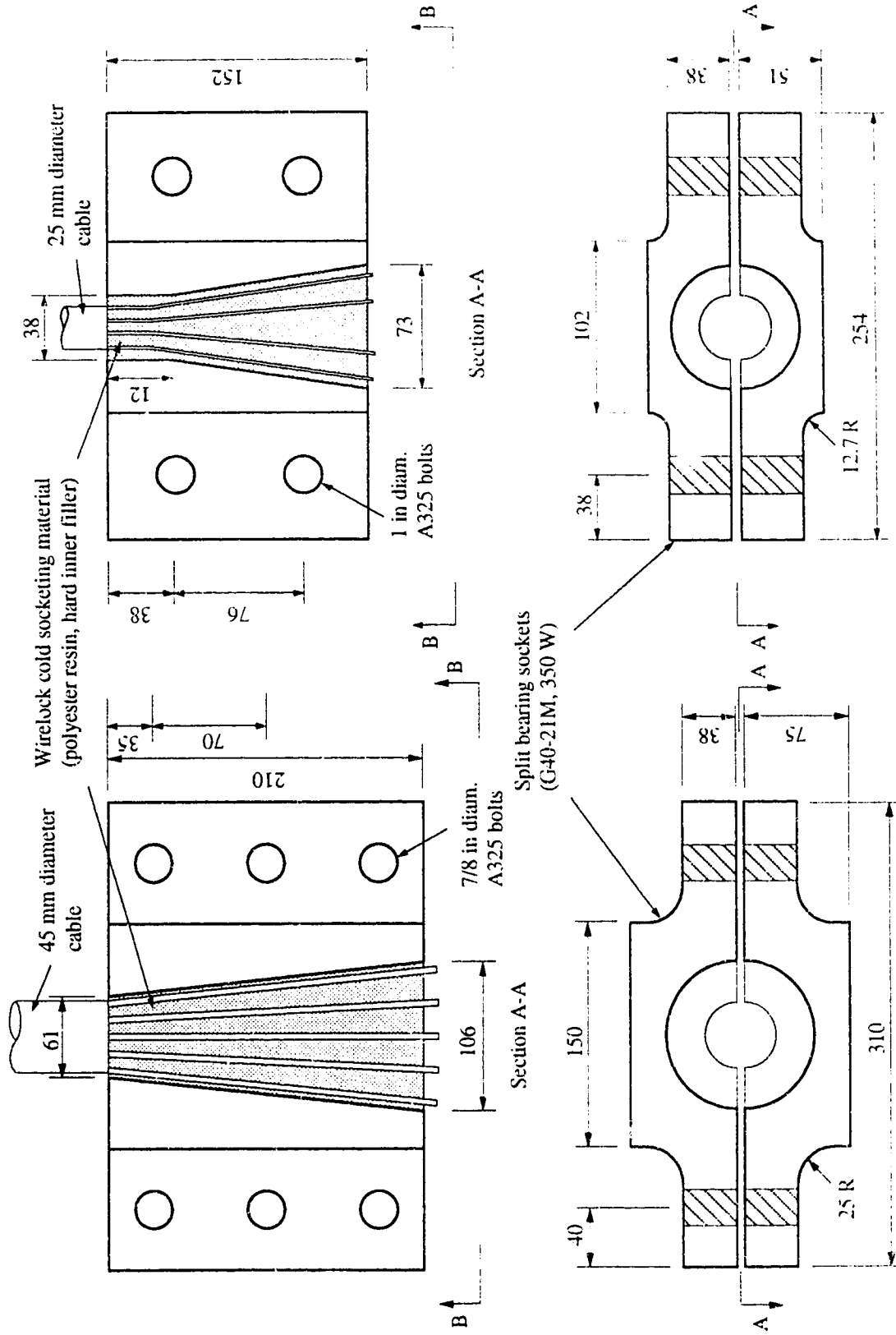
Layer	No. of Wires	Lay Direction (1)	Wire Diameter (mm)	Lay Length (mm)	Strand O.D. (mm)	Lay Angle (degree)
1	12	LL	5.056	263	25.34	13.62
2	6	RL	5.056	161	15.43	11.44
3	1	-	5.260	-	5.260	-

(1) LL=Left lay RL=Right lay

Table 3.3 Testing parameters for the axial fatigue test program

Specimen	Diameter (mm)	Length ⁽¹⁾ (mm)	Max. Stress (MPa)	Stress Range (MPa)
SP1	44.37	3315	505	303
SP2	44.37	3323	540	371
SP3	44.37	3336	540	371
SP4	44.37	3320	540	371
SP5	44.37	3323	505	303
SP6	44.37	3310	522	337
SP7	44.37	3328	522	337
SP8	44.37	3326	556	404
SL1	25.34	3357	517	310
SL2	25.34	3376	517	310
SL3	25.34	3379	465	207
SL4	25.34	–	517	310
SL5	25.34	3387	542	362
SS1	25.34	2153	542	362
SS2	25.34	2160	491	258
SS3	25.34	2152	517	310

(1) The length is measured from inside-to-inside of the sockets.



(a) Socket for 45 mm diameter cable

(b) Socket for 25 mm diameter cable

Figure 3.1 Split bearing sockets

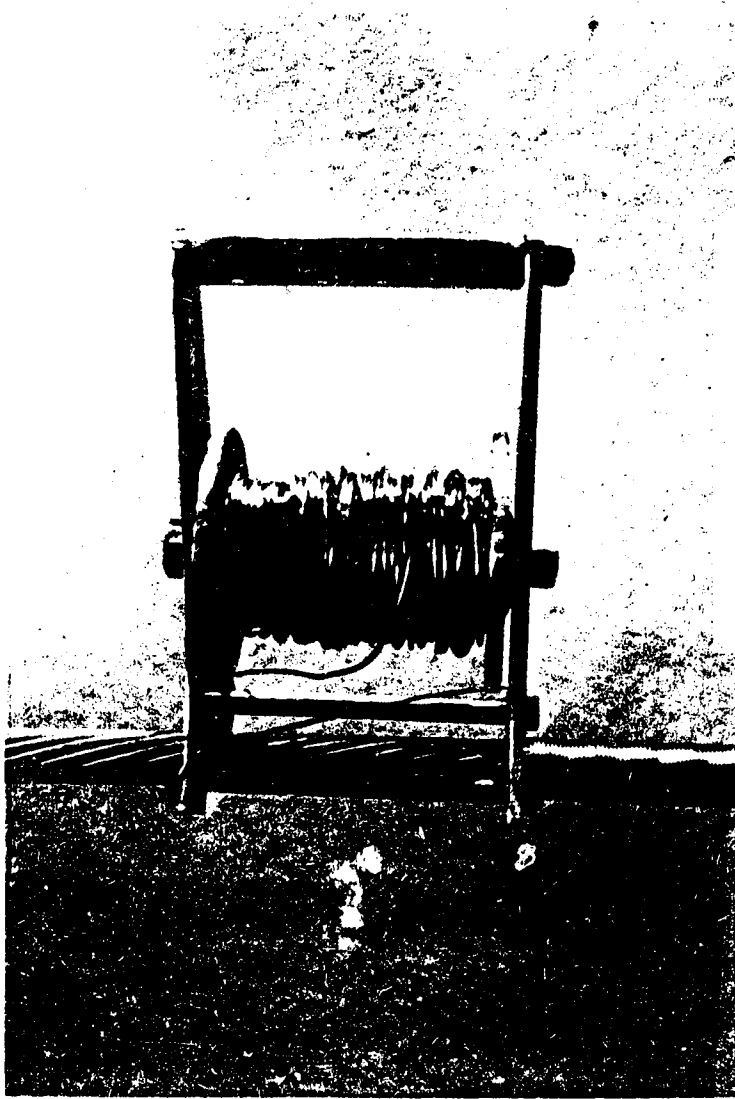
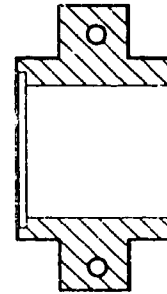
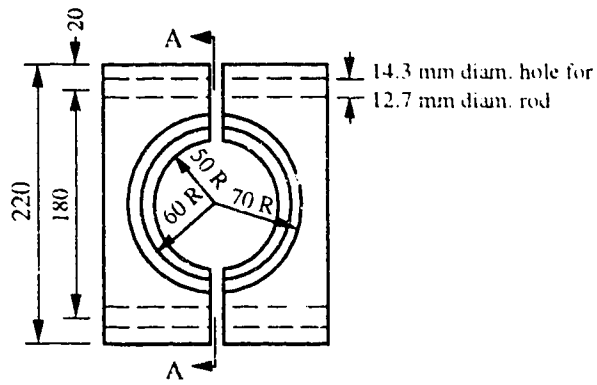


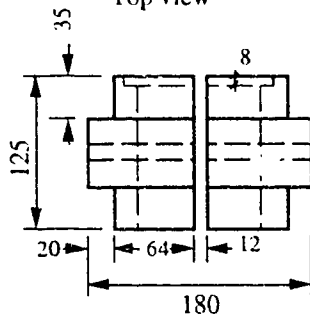
Figure 3.2 Seizing device



Top view

Section A-A

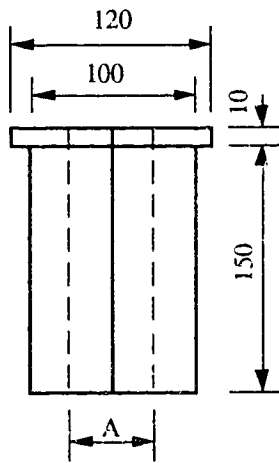
(a) Serving device



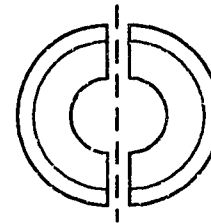
Front view

Notes

- (1) Material – G40-21M, 350W
- (2) A= 48.5 mm for 45 mm diam. strand
A= 29.5 mm for 25 mm diam. strand



Front view



Bottom view

(b) Clamp insert

Figure 3.3 Socketing clamp

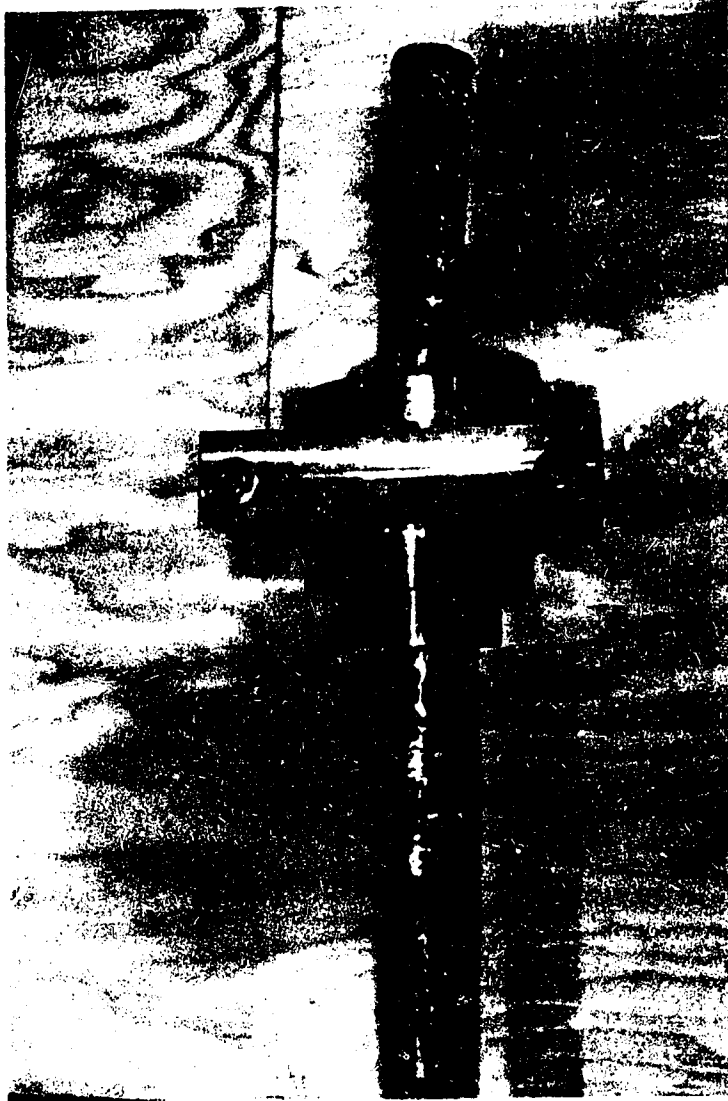


Figure 3.4 Seized and clamped specimen

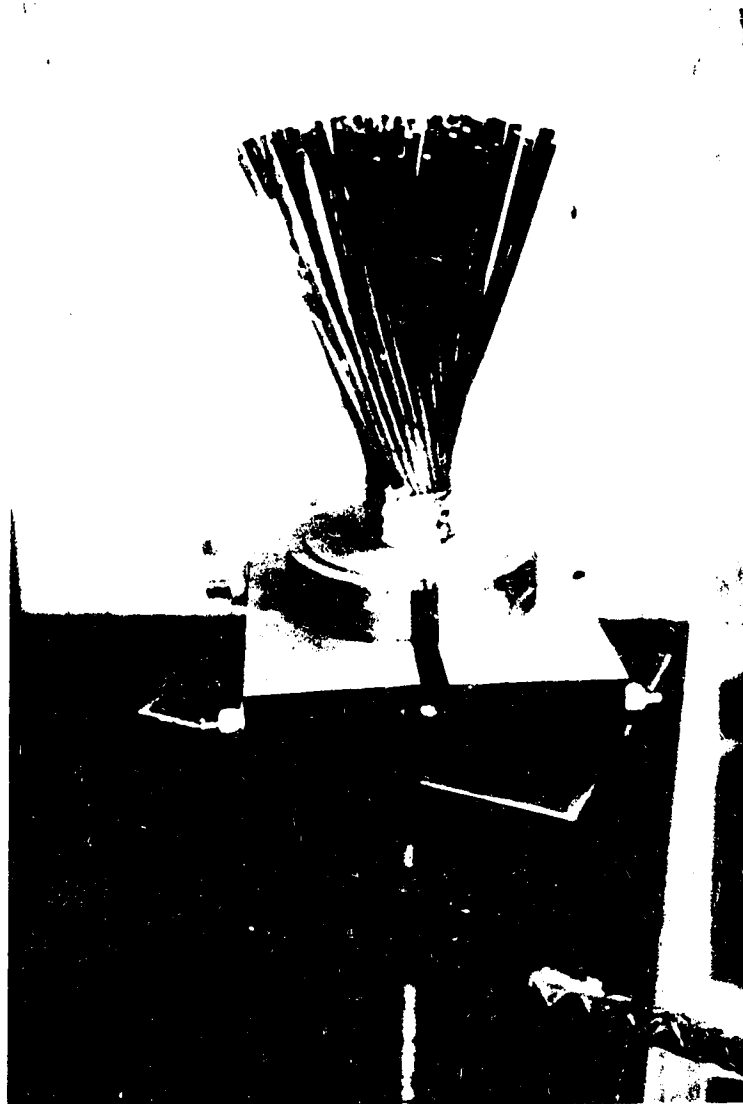


Figure 3.5 Spreading of individual wires around serving device



Figure 3.6 Socketing mold and vertical clamping device

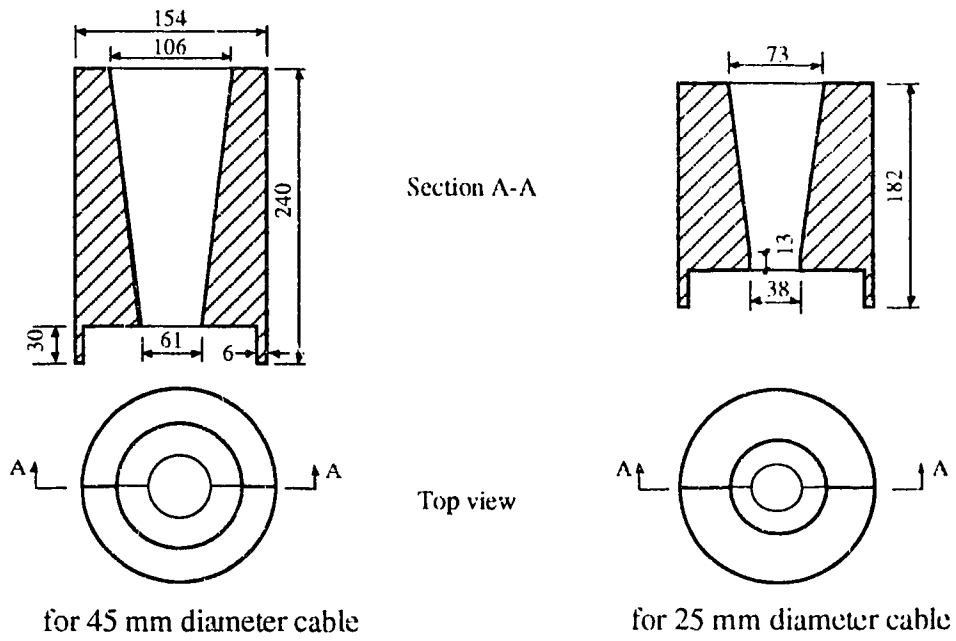


Figure 3.7 Split socket mold

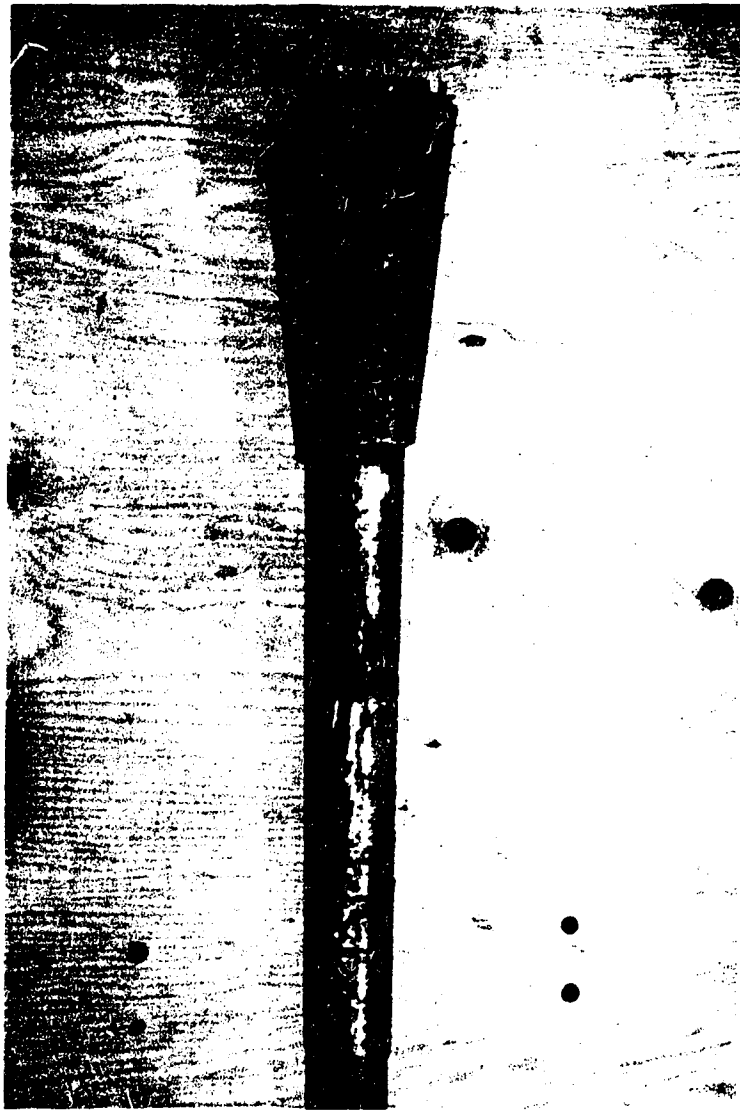


Figure 3.8 Finished socket for the 45 mm diameter specimens

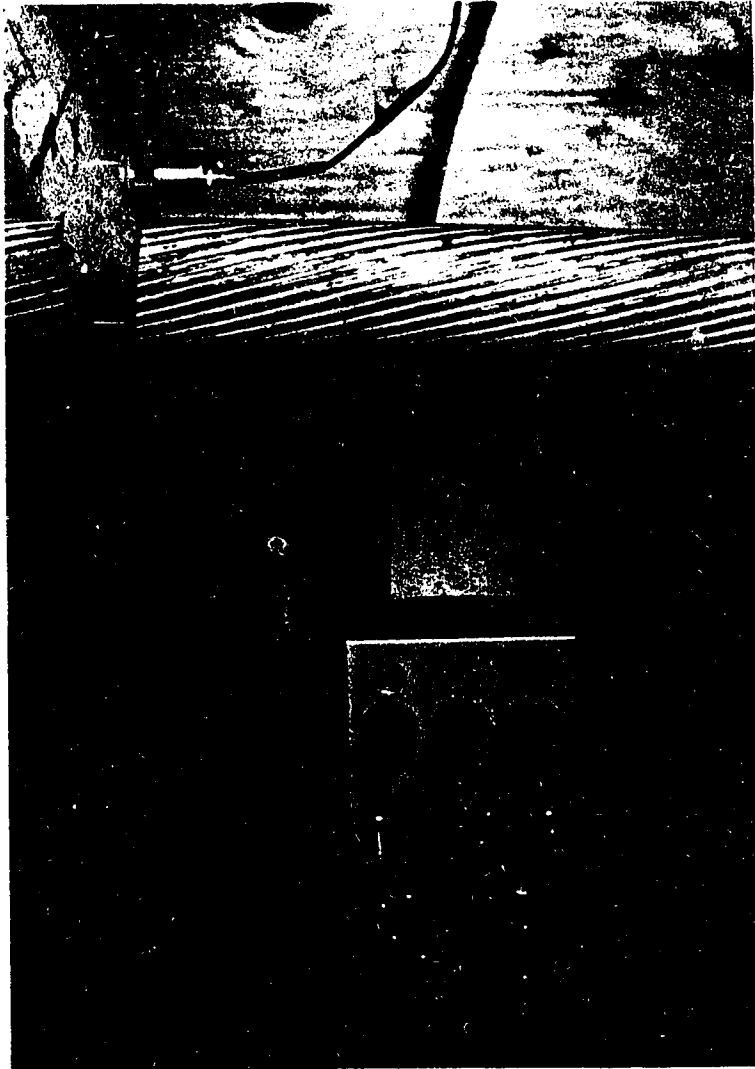


Figure 3.9 Accelerometer, bracket and charge pre-amplifier

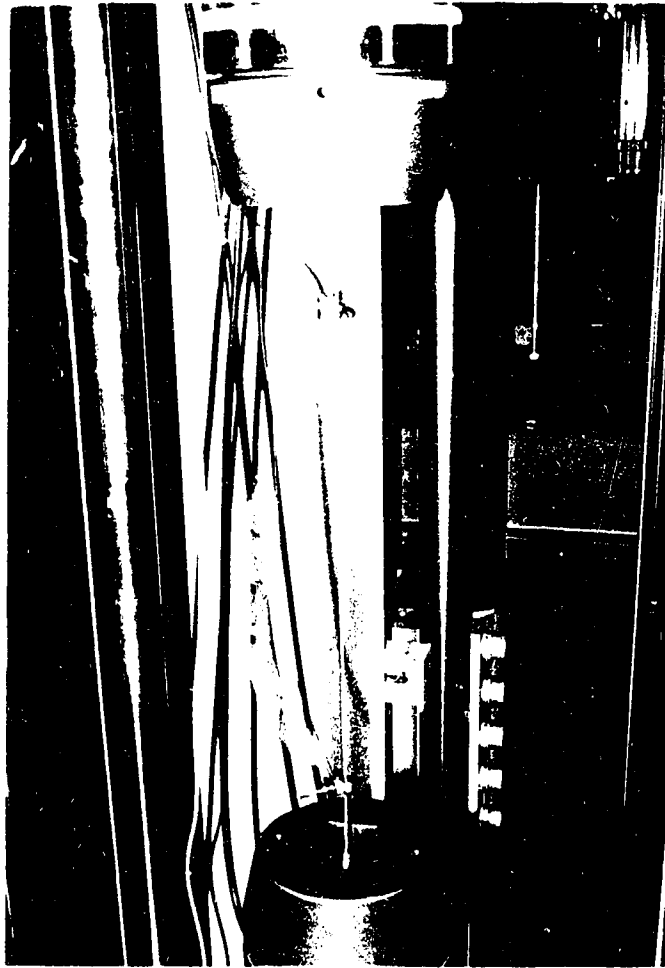


Figure 3.10 Single wire tensile test

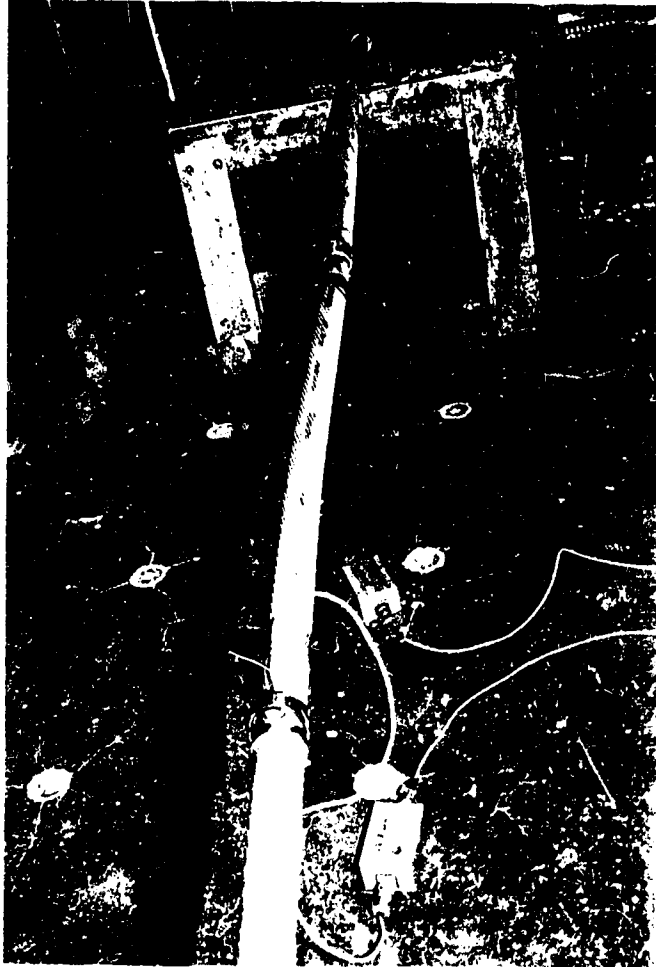


Figure 3.11 Acoustic emission transducer, wave attenuation test

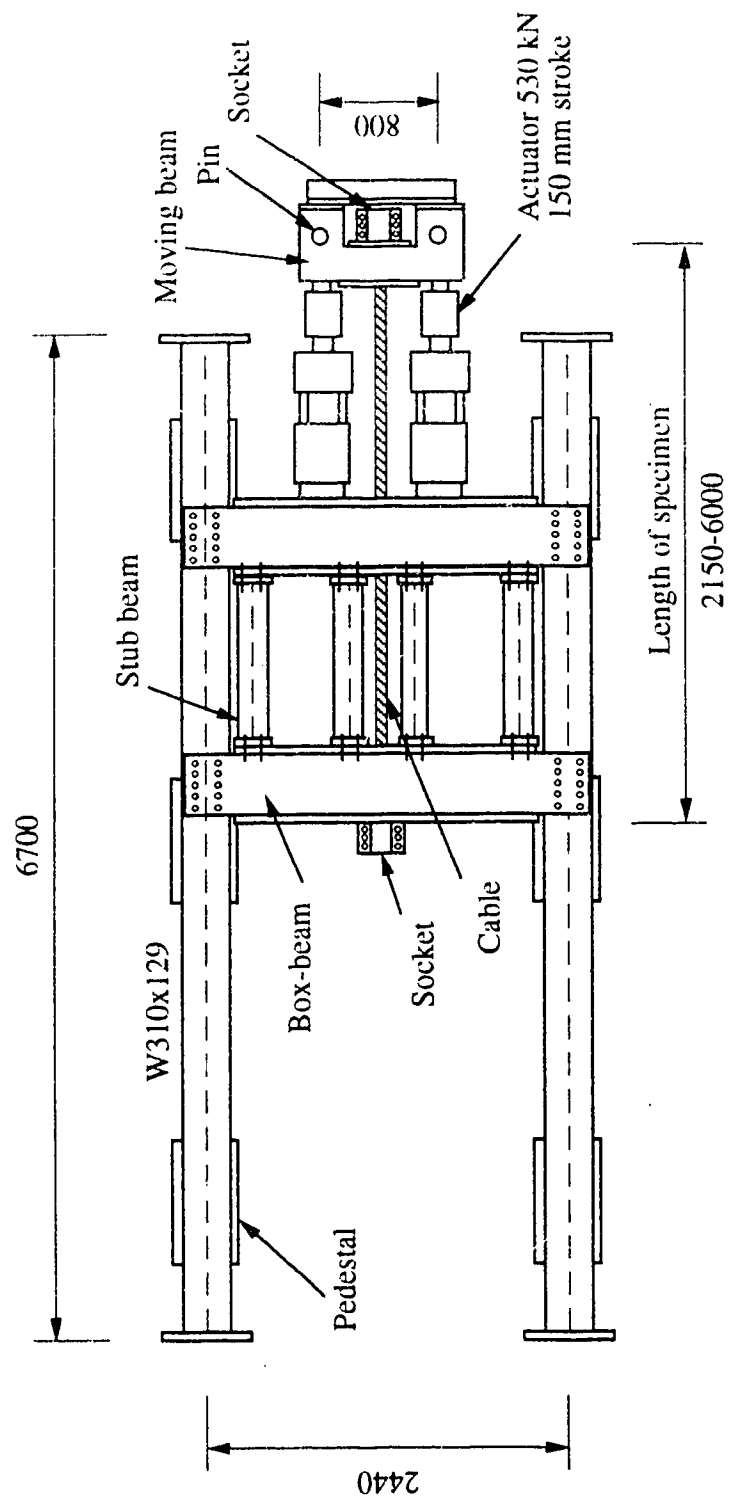


Figure 3.12 Plan view of axial fatigue test setup for cables

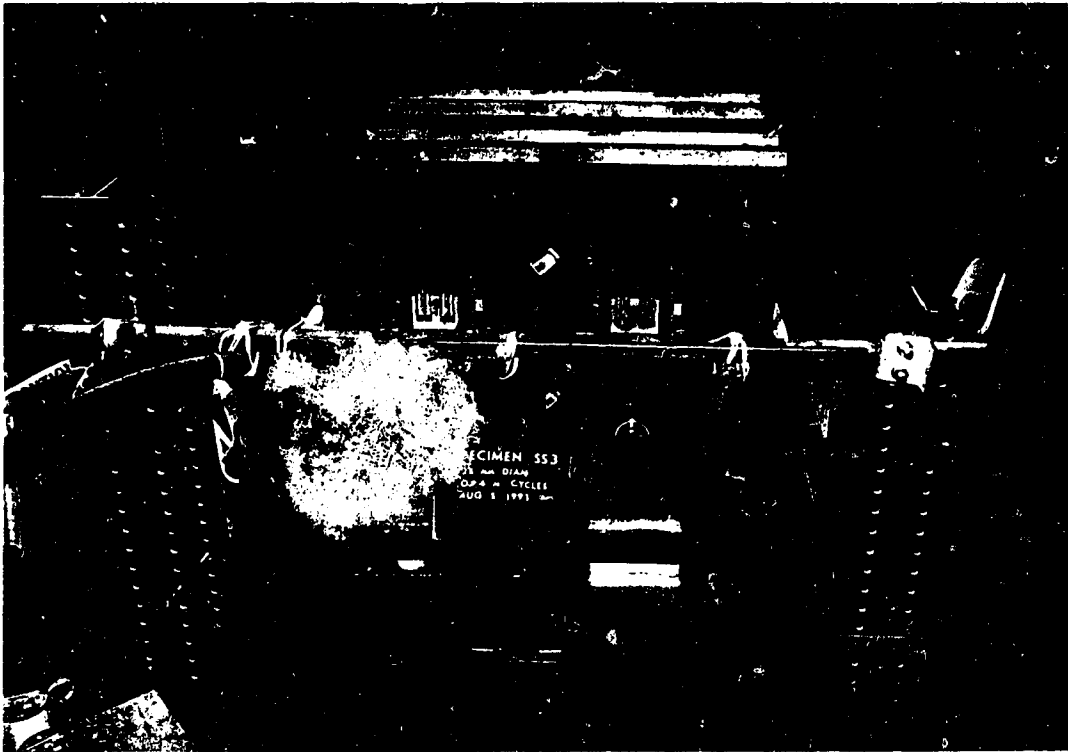


Figure 3.13 Axial fatigue testing apparatus for cables

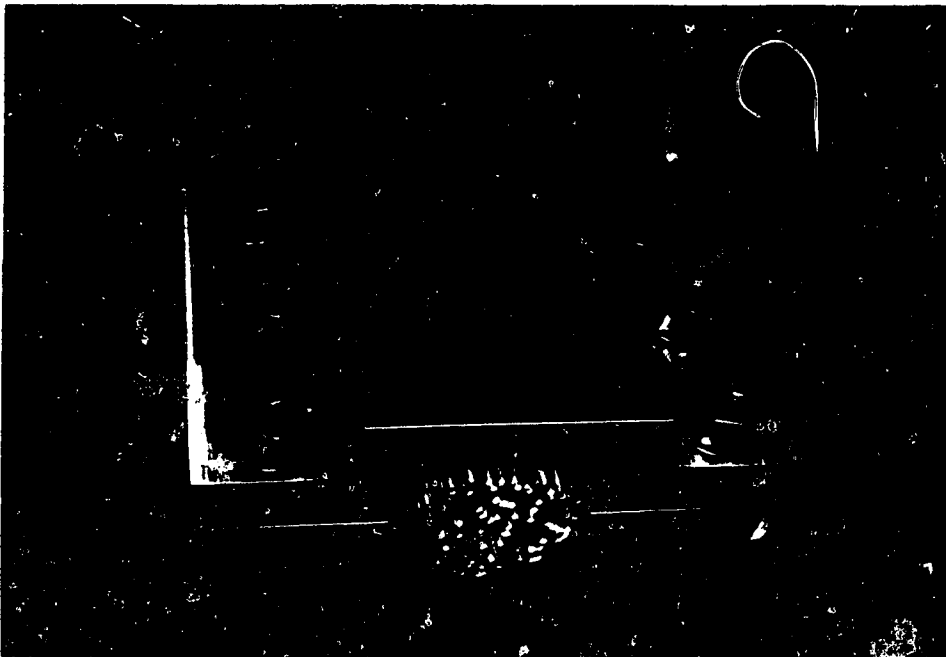


Figure 3.14 Connection of 45 mm diameter strand to supporting beam

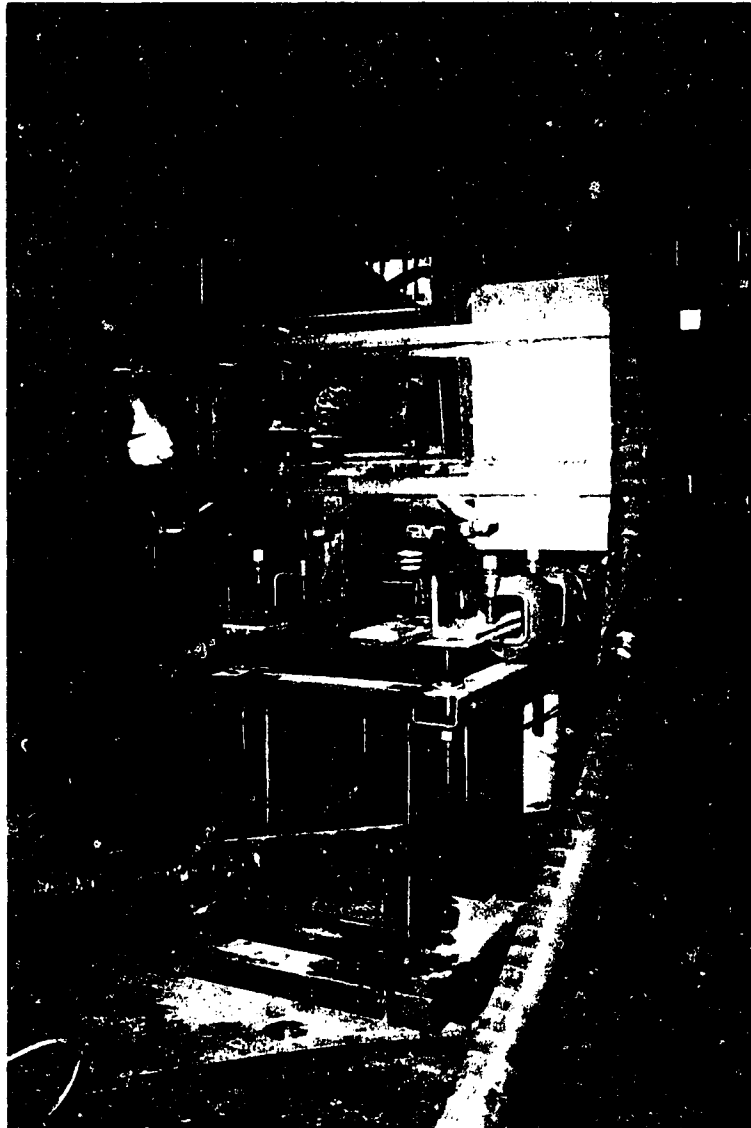


Figure 3.15 Moving beam roller support

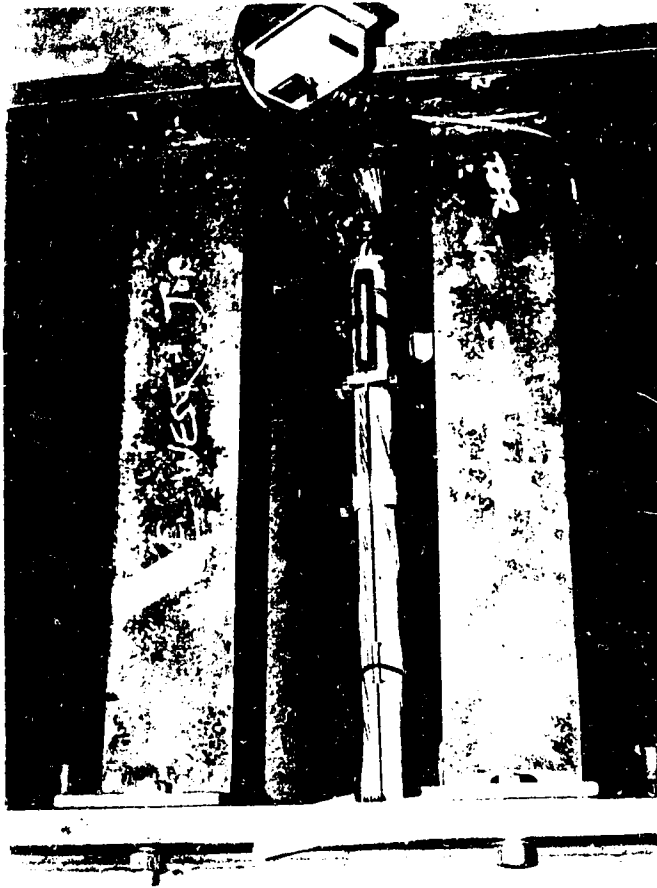


Figure 3.16 Instrumentation of a 45 mm diameter specimen

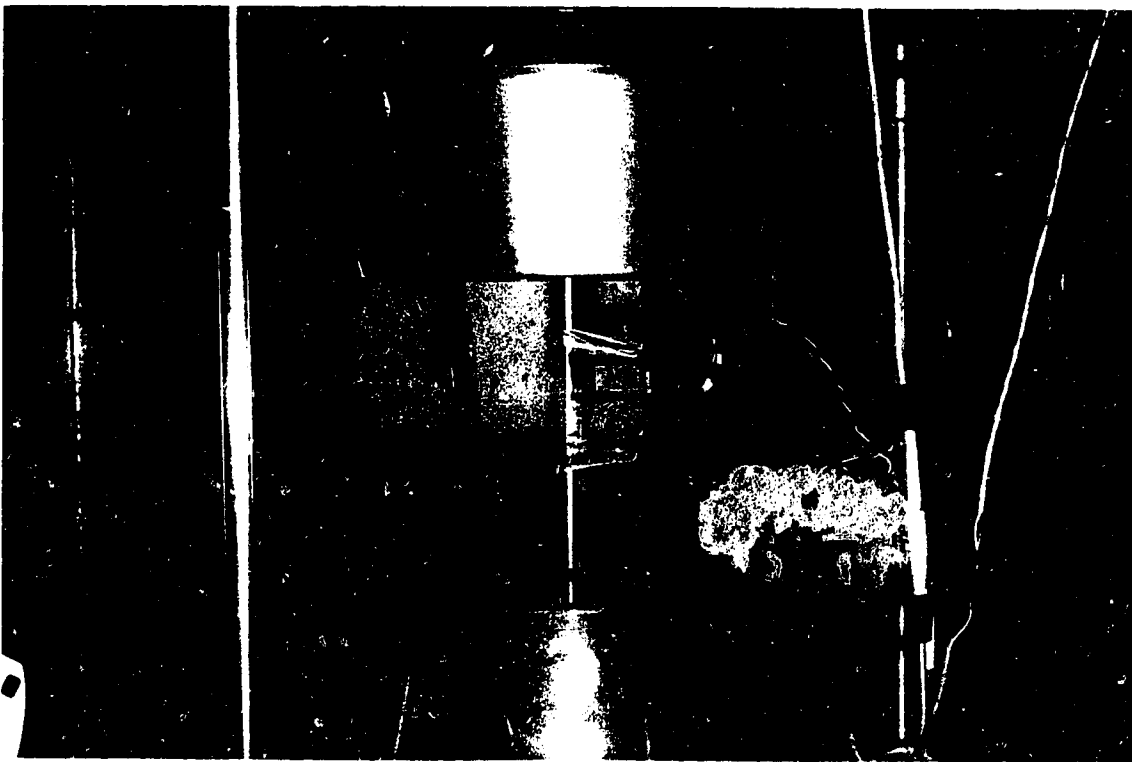


Figure 3.17 Individual wire coupon test

Chapter 4

Results of Experimental Program

4.1 Introduction

The experimental results obtained from the preliminary and the main test programs are presented in this Chapter. Results of secondary tests, such as material tests, calibration tests for the acoustic emission study, and fractographies, will also be presented.

The intention is to give the factual information and provide an overview of the axial fatigue behavior of multi-layered strands. Detailed examination of the different parameters that influence the performance of strands and the development of a failure criterion will be presented in following chapters.

4.2 Acoustic Emission Calibration Test Results

In order to assess the damage accumulated during the axial fatigue tests of the multi-layered strands, the number of breakages was monitored using two non-destructive procedures: accelerometers and acoustic emission (AE). For the AE, a series of preliminary (calibration) tests were required to investigate the AE signal characteristics, to set the criteria for sorting the five signal parameters, and to establish the attenuation of the AE event along the cable and between the different layers (Section 3.2.3.2). In the following sections, the results from the AE calibration tests are presented.

4.2.1 Acoustic Emission Signal Characteristics

Based on the single wire fracture tests (Section 3.2.3.2.1), the features of the wire fracture AE signal were derived. Figure 4.1 presents a typical AE signal captured from the oscilloscope and the AE unit during fracture of a single wire static test. The characteristic values of the signal parameters representing a wire fracture are:

- high amplitude signal with a peak ranging from 600 to 1200 micro-volts (mV)
- large event duration ranging from 2 to 6 micro-seconds (μ s)
- event energy ranging from 200 to 1000 micro-volts times seconds (mV.s)
- event count ranging from 400 to 2000

All of the above parameters vary within a frequency band of 100 to 300 kHz.

4.2.2 Signal Attenuation

The change of an AE signal as it travels between successive layers and along the cable is shown in Figures 4.2 to 4.4. The tests were conducted on a 45 mm diameter strand specimen and the AE signals were simulated by breaking 2H, 0.7 mm pencil leads on the outer layer of the specimen (see Section 3.2.3 2.2).

The graphs of Figure 4.2 show count rate, energy level, event duration, and peak amplitude as a function of cable layer. It can be concluded that the acoustic count rate, the energy level, and the peak amplitude were attenuated by about -10 dB as the signal travels from the outer to the core wire, while the duration was attenuated by only about -2 dB. The effect of the angular orientation of the AE event source in relation to the location of the transducer is given in Figure 4.3. It can be concluded that signal attenuation due to angular orientation is not significant for the signal parameters investigated. Attenuation of AE waves as they travel along the cable is a major concern. Figure 4.4 presents the recorded event patterns as captured from two transducers, located at 500 mm and 2500 mm from the AE event source. The change of the different signal parameters with the cable length is shown in Figure 4.5. Attenuation of acoustic parameters ranged from -4.0 to -5.3 dB per meter.

The results indicate that major attenuation occurs both between cable layers and along the cable. Although an outer wire breakage can easily be detected because of the high attenuation, it is more difficult to detect internal wire fractures. There may be up to a 25 dB difference when a wire breaks in the outer layer at one end of the cable as opposed to breakage of a core wire at the other end of the cable. From the attenuation tests it was also found that the speed of an AE wave is about 5.02 km/sec. This is a typical value for steel material, and agrees with the results reported by Woodward (Ref. 81).

4.2.3 Pulse Echo Test

A pulse echo test was conducted in order to investigate the potential of the AE device to detect pre-existing internal wire fractures. Access of the wires at one end of the cable is a pre-requisite for the method. Figure 4.6 clearly illustrates the promising results of the method. In this test, a broken wire was located at a distance of 3300 mm from the signal input end. By calculating the time interval between the two captured events and knowing the acoustic wave propagation speed, the exact location of the breakage could be estimated.

The disadvantages of the method are that all internal wires must be checked individually, and that access from at least one end of the cable is required. It should be noted that the

pulse echo test results presented in this research were based on a 3.3 meter long cable. The method need to be investigated further for real cable lengths (i.e. in excess of 100 meters).

4.3 Axial Fatigue Tests

Axial fatigue tests were conducted on sixteen multi-layered wire strand specimens. The specimens were subjected to cyclic tension. The parameters investigated were the stress range, the strand construction, and the specimen length-to-diameter ratio. Detailed information on the three test series SP, SL, and SS were presented in Chapter 3. In the following sections, the results obtained from the axial fatigue tests on multi-layered strand are presented. A summary of the test results for all three series is given in Table 4.1.

4.3.1 Preliminary Test SP1

A preliminary test (specimen SP1) was conducted in order to calibrate and check the fatigue test apparatus. The major problem found during the calibration concerned the two servo-hydraulic actuators used in parallel and in load control mode. This arrangement, together with the connection of the jacks and specimen with the front (moving) beam, created an unstable system. A small imperfection of the specimen center-line could generate a disturbing moment which resulted in out-of-phase movements between the two actuators. This created a high frequency vibration that produced secondary bending fatigue motion in the front termination of the cable. The out-of-phase problem of the actuators was resolved by introducing a stroke feedback circuit. This ensured in-phase stroke movements of the actuators during the load control test.

Because of the secondary bending of the front cable termination, most of the wire breaks of specimen SP1 occurred close to front socket. This is shown in Table 4.2, which gives the location of wire breaks for specimen SP1. A total of 34 broken wires having 39 wire breaks were detected. Figure 4.7 shows the fractured specimen after completion of the test. The condition of the third inner layer is shown in Figures 4.8 and 4.9 for the fixed and moving end, respectively.

The fatigue performance of the testing rig itself was also evaluated using the preliminary test SP1. Two poor details were noticed that eventually led to the formation of fatigue cracks. At approximately 2.2 million cycles, the front beam cracked at a cope that was present on the tension side of the beam. The cope was located at an abrupt change of cross-section. Stress concentration on the tensile side of the cope was the cause of this crack. The crack was gouged out and re-welded, and two 25 mm thick plates were added in order to increase the moment of inertia and decrease the sudden cross-sectional change of

the beam. The second fatigue problem appeared after 4.4 million cycles, when the two transverse box beams, which support the two actuators and the fixed termination of the specimen, started to crack at the bolted connection with the longitudinal beams. Those sixteen cracks were caused by the significant cross-sectional change at the connection. The twenty (25 mm diameter) high strength bolts used for each connection, created a fixity which restrained the end rotation. This problem was resolved by inter-connecting the two box beams with four stub columns. This stiffened the whole assembly and altered the load path. The poor connection detail was therefore by-passed.

It was also within the objectives of the preliminary experiment to finalize the instrumentation to be used during the main portion of the axial fatigue tests. The only reliable measurements obtained throughout the SPI test were the modulus of elasticity values derived from the static tests conducted at specific cycle intervals. The modulus of elasticity was based on the overall length of the specimen, which includes the socket movements inside the termination cones (end effects). Table A.1 of Appendix A and Figure 4.10 summarizes those results. It should be noted that during the static test this specimen was unloaded completely. This is contrary to what happens in reality. The principal effect of unloading is that fretting locations could change when the specimen is unloaded and then reloaded. Thus, if the specimen is unloaded during static tests unconservative results could be obtained for the constant amplitude axial fatigue test. Typical static test results, conducted at 5.9 million cycles are shown in Figure 4.11a. In Figure 4.11b, the computation of the modulus of elasticity is shown. This was done by linear regression of the ascending branch of the stress versus strain curve. The two features of the stress-strain curve of a cable, namely, the elastic hysteresis loop (during one cycle) and the viscous behavior at the beginning of the test, are also shown in Figure 4.11a. Those characteristics are due to the helical twist of the wires.

After the completion of the first test, it was decided to conduct all subsequent static tests at a load that was between the minimum and maximum values of the fluctuating load. Furthermore, an LVDT was placed in the free-length of specimen in order to obtain the free length elongation of the cable. The gauge length of the LVDT was approximately 1000 mm shorter than the overall length of the cable.

The accelerometers and the associated software for wire break detection were developed during this test so that they were subsequently able to successfully detect wire breaks during the axial fatigue tests. Finally, the configuration of the testing rig was finalized and its fatigue deficiencies were overcome.

4.3.2 Series SP

The strand make-up of the 45 mm diameter cable and the testing parameters were given in Tables 3.1 and 3.3, respectively. Series SP was considered to be the reference series and one of the objectives of that series was to establish the failure criterion. This was achieved by testing all 45 mm diameter specimens close to failure. The number of cycles at which the tests of SP series were discontinued are presented in Table 4.1.

With the exception of specimen SP1, both wire breaks and modulus of elasticity were used as damage parameters. These features were, therefore, continuously monitored throughout the test. The deterioration of the specimen stiffness was determined by performing static tests at specific cycle intervals. Both the free-length and the overall modulus of elasticity were determined. For specimens SP2, SP3, and SP4, the wire breakages were detected using two accelerometers. For the remaining tests in the SP series (tests SP5 to SP8) the wire breaks were detected by using both the accelerometers and the acoustic emission (AE) non-destructive methods.

Figures 4.12 and 4.13 show the detection of a broken wire for specimen SP5 using these methods. As can be seen from these figures, the interpretation of the accelerometer data does not require any special expertise since a wire breakage is well defined. The drawback of this method is that no specific information regarding the exact location (distance and layer) of the breakage is obtained. On the other hand, the acoustic emission system, which does locate the break with respect to length and layer, requires initial calibration tests (to set the window parameters of the acoustic event of a breakage) and special software in order to extract the wire breakage from all background noise.

The test data from the static tests and the detection of wire breaks are presented in tabular form in Appendix A. For every specimen, a table is given with the cycles at which the static test was conducted and the corresponding values of the overall modulus of elasticity, the free length modulus of elasticity, the number of wire breaks based on accelerometers, and the number of wire breaks based on AE (whenever they are available). Graphical representation of the test results are given in Figures 4.14 to 4.20. Two figures are presented for every specimen. Figure (a) shows the modulus of elasticity versus the number of cycles (a logarithmic scale), while Figure (b) gives the total number of wire breaks with the corresponding cycles (a logarithmic scale). These figures show that the reduction of the cross-sectional area (number of wire breaks) and the deterioration of the modulus of elasticity change significantly as the fatigue test progresses and that they can be used as damage parameters for the derivation of a failure criterion. Figures 4.17b to 4.20b

show that identification of wire breaks by the acoustic emission and accelerometer methods are in good agreement.

Test specimens SP1, SP2, SP4, and SP7 were dismantled after completion of the tests in order to investigate the number and location of wire breaks. The position of wire breaks for the disassembled specimens are given in Tables 4.2 to 4.5. Wire breaks were distributed more or less equally between the anchor portions and within the free length (away from the terminations). As can be seen from those tables, with the exception of specimen SP1, broken wires close to the terminations occurred invariably at the outside layer. This is indicative of a heavier stress concentration at the outside layer. Figure 4.21 shows the wire breaks at the outer layer of specimen SP2, close to the fixed termination. Internal breaks close to the moving socket of specimen SP1 can be explained from the secondary bending that occurred during calibration of the hydraulic actuators. As is evident from Tables 4.2 to 4.5, most of the wire breaks within the free length took place in the inner layers. Localized fretting fatigue at the interlayer contact patches appears to be the cause of those wire fractures. Figure 4.22 shows the interior wire breaks for layer 4 of specimen SP4.

For the 45 mm diameter specimens, the total recorded breakages from both the AE and ACC detection methods were not in good agreement with the actual number of breakages observed after disassembly. This is because the specimens of series SP were tested close to failure, with a possibility of several breakages occurring at nearly the same time. Because of the relatively long duration of AE and the ACC events from wire breakages, it can be expected that such events will overlap during the late stages of the test.

As can be seen from Tables 4.4 and 4.5, when the cables were disassembled it was observed that multiple breaks took place in individual wires. Such compound failure occurred on inner wires and within the free length of the cable. This phenomenon is the result of interwire friction. A typical multiple wire break failure is shown in Figure 4.22 for specimen SP4.

Figures 4.23 to 4.25 show the exterior condition of some of the specimens after testing had been discontinued. Specimen SP3, shown in Figure 4.23, was tested until complete failure of the specimen occurred (418 262 cycles). The failure was located at 450 mm away from the moving termination and was accompanied by extensive twisting of the whole wire bundle. A similar failure is shown in Figure 4.24 for specimen SP5. Other tests were discontinued before complete failure of the cable. As an example, specimen SP7, shown in

Figure 4.25, had only one exterior broken wire when the test was stopped at 2 124 100 cycles. The failure of specimen SP7 was characterized by a significant deterioration of the stiffness: the free-length modulus of elasticity decreased from 174 110 MPa at 1 889 400 cycles to 166 120 MPa at 2 124 100 cycles (see Table A.7 of Appendix A). As can be seen from Table 4.5, although only one broken wire was visible at the outside layer, a total of 78 wire breaks were subsequently located when dismantling the specimen. The interior wire breaks are shown in Figures 4.26 and 4.27 for layers 1, 2 and 3.

Figure 4.28 shows the excellent condition of the socket detail after completion of the test of specimen SP7. This termination behavior was typical for all specimens of SP series. Furthermore, the individual wires of specimens SP1 and SP2 had been marked at the socket location before the start of the test and it could be observed that there was no slippage between the wires and the socketing material as the test was carried out.

4.3.3 Series SL

Series SL consisted of five 25 mm diameter multi-layered strands, having a length-to-diameter ratio of 133. The strand make-up and the testing parameters were presented in Tables 3.2 and 3.3.

Since both non-destructive procedures, AE and ACC, were found to give similar results in predicting the wire breaks of SP series, only the simpler method, accelerometers, was used to detect wire breaks in the SL and SS test series. As had been done for the SP series, the stiffnesses of the specimens were monitored by performing static tests at specific time intervals. Each static test was conducted at a load that was between the minimum and the maximum values of the fluctuating load. The modulus of elasticity, either including or excluding end effects, was determined during each static test. The test data from the static tests and the detection of wire breaks are presented in Table A.9 of Appendix A.

Testing of SL1 specimen was carried out close to destruction in order to verify the correctness of the failure criterion that had been selected on the basis of SP series. Failure of SL1 was characterized by significant deterioration of the modulus of elasticity. Figure 4.29 a is a plot of the deterioration of the stiffness with respect to the number of cycles for this specimen. The number of wire breaks versus the number of cycles for the same specimen is given in Figure 4.29 b. With the exception of specimen SL1 and SL3, all SL series tests were discontinued when it was detected that a minimum of three wires (out of the nineteen wires) had broken. As can be seen from Table A.9, this corresponds to the

number of cycles at which the modulus of elasticity started to deteriorate significantly. The cycles at which the tests of SL series were discontinued are given in Table 4.1.

All specimens of the SL series were dismantled after completion of the tests in order to evaluate the validity of the accelerometer method. Table 4.6 and Figure 4.30 show the number and location of wire breaks. From a comparison between the total number of predicted and actual breakages, reported in Table 4.6, it can be concluded that the accelerometers performed satisfactorily. This comparison was possible because the fatigue tests of series SL were discontinued before a significant number of wires broke (which could lead to an overlapping of break events). With the exception of specimen SL4, all wire breaks of SL series occurred away from the terminations. This was probably a reflection of the 12 mm cylindrical transition region that was provided at the neck of the 25 mm diameter socket (see Figure 3.1). Specimen SL4 had all the wire breakages close to the moving end socket. This was due to slight out-of-phase movements of the two hydraulic jacks, that was induced as a result of re-calibration of the testing apparatus. Typical wire failures are shown in Figures 4.31 and 4.32 for the outside layer of specimens SL2 and SL5.

Specimen SL3, which was tested at a stress range of 207 MPa, reached a life of ten million cycles without any breakage. The test was discontinued and the specimen was then re-tested as specimen SL4 at a stress range equal to 517 MPa. It should be noted that at the end of test SL3 the fluctuating stress was increased to 517 MPa without unloading the specimen. The cycle indicator was zeroed and the new test was called SL4. The first breakage of SL4 occurred at 2.42 million cycles. This is higher than the life achieved by specimens SL1 and SL2, which were tested at the same stress range. This indicates that the 10 million cycles applied during the previous test, SL3, at a different stress range, did not damage the specimen. It must be assumed that the interwire fretting location changed in a significant way when higher stress range was applied. Thus, a variable amplitude axial fatigue test can be expected to last longer than an otherwise similar constant amplitude test. In turn, this indicates that a linear damage cumulative hypothesis will underestimate the total axial fatigue life.

4.3.4 Series SS

Series SS consisted of three 25 mm diameter specimens having a length-to-diameter ratio of 85. This series of tests were conducted in order to investigate the effect of the specimen length-to-diameter on the experimental results. Strand make-up and loading parameters were similar to those of SL series; they are presented in Tables 3.2 and 3.3.

The cycles at which the tests were discontinued are given in Table 4.1. With the exception of specimen SS2, failure was taken as a minimum of three wire breaks. Unfortunately, because of time limitations, testing of specimen SS2 had to be discontinued at 4.2 million cycles without any wire breakage having taken place.

For the SS series, static tests were conducted only at the beginning and the end of the test. The static test was carried between the minimum and maximum applied load and the modulus of elasticity, both including and excluding the end effects, was determined. Table A.10 of Appendix A summarizes the results from the static tests. During the cycling tests, the wire breaks were monitored using two accelerometers. The number of wire breaks at the time that a static test was conducted are also presented in Table A.10.

All three specimens of SS series were dismantled after completion of the tests. The location of the wire breaks in SS1 and SS3 are given in Table 4.6 and Figure 4.30. Wire breaks were located at the outside layer and were distributed more or less uniformly along the length of the cable.

4.4 Fractography

After completion of the axial fatigue tests, some specimens were dismantled and the fretting and fracture surfaces were investigated using both the optical and scanning electron microscope.

This examination showed that the mode of fatigue failure is fretting fatigue at the interlayer contact patches. Typical fretting surfaces for the 25 mm diameter specimens are shown in Figure 4.33. In Figure 4.34 fretting surfaces of a wire from the 45 mm diameter multi-layered strand are shown. The galvanizing coating was removed at the contact patches and pre-existing micro-cracks at the galvanize-wire interface come into the surface of the wire. Fatigue cracks, therefore, started mainly at the surface. Such a surface crack at a fretting patch can be seen at the right hand contact patch of the photomicrograph of Figure 4.34. A magnification of the crack is given in Figures 4.35 and 4.36.

It was hypothesized earlier that the interwire fretting location changed when the stress amplitude of specimen SL3 was increased from 207 MPa to the stress range of 517 MPa (specimen SL4). This hypothesis was found to be correct from microscopic examination of the wire surface. Figure 4.37 shows the two contact patches corresponding to the two-step variable amplitude test.

Microscopic examination of the wire fracture surfaces revealed three distinct regions, as shown in Figures 4.38 and 4.39. Region I, which contains the crack initiation site, consists of a fairly smooth flat surface of semi-elliptical shape, perpendicular to the loading direction. Substantial fretting debris (dark regions) are found in Region I. These are primarily iron oxides of the base metal. Corrosion products are involved in the case of metal fretting fatigue. Once the crack tip leaves the vicinity of the fretting region, it is no longer controlled by the fretting process but rather by the local stress field near the crack tip. The fracture surface of this Region II becomes somewhat coarser, indicating a faster crack propagation rate. In Figure 4.39, the beach marks are evident in the main fatigue crack propagation Region II. These markings are due to the two adjacent crack surfaces that open, close, and rub together during cycling loading.

Finally, in Region III, which consists of the final fracture region, an unstable crack propagated at an angle of approximately 45 degrees from the surface. At this stage, the state of stresses at the crack tip has become predominantly a state of plane stress, and the propagation rate has increased further. A typical fractography of the fracture Region III is given in Figure 4.40. It can easily be observed from this figure that the fracture surface consists of small dimples. This is typical of a ductile failure. In contrast to a cleavage failure, ductile fracture requires large plastic deformations associated with dislocation movements and slip displacements. The plastic deformation was confined to a small volume of material through which the crack propagated. The failure occurred with relatively little plastic deformation on a macro scale. The fracture is therefore considered as brittle in an engineering sense.

4.5 Metallogra

Examination of the metallographic specimens of wires, obtained from an outside layer, the fourth inner layer, and a center wire of the 45 mm diameter strand did not reveal anything unusual about the micro-structure of the cold drawn, unalloyed, eutectoid high carbon steel.

Figures 4.41 to 4.43 show typical micro-structure of an outside, inner and center wire, respectively. Those photomicrographs were obtained from a scanning electron microscope (SEM). All three samples gave very similar micro-structures. The directional grain orientation is an indication of plastic deformation induced from the cold working process. The crystallographic structure indicates a mixture of ferrite and pearlite. This is a typical appearance of eutectoid structural steels having 0.60% to 0.80% carbon content.

Hardness tests conducted on the three samples gave a Rockwell C hardness of 46, which corresponds to a tensile strength of 1500 MPa. This is another indication that all three samples had similar microstructures and mechanical properties.

The dip galvanizing process was used for the zinc coating of the wires. Figure 4.44, obtained from the SEM, shows the outside zinc layer, the zinc-iron interface and the cold drawn steel layers of a wire. As can be seen from this photomicrograph, microcracks pre-exist underneath the galvanizing. It is likely that those microcracks, which are potential sites of fatigue crack initiation, have arisen during the fabrication process from such factors as cold working or differential cooling during galvanizing.

4.6 Coupon Test Results

Typical stress versus strain curves for the four different diameter wires are shown in Figure 4.45. The results of all coupon tests are presented in Table 4.7. The modulus of elasticity was determined using the method of least squares from the strain gage extensometer and load readings recorded during test. Results for specimens that failed inside the loading grips were discarded. A typical coupon after fracture is shown in Figure 4.46.

Table 4.8 summarizes the average values of all coupon tests and compares them with the minimum requirements stated by the ASTM A586 Standard (Ref. 3). For zinc class A wires with a diameter larger than 2.794 mm (see also Table 1.2), the standard requires a minimum ultimate strength of 1520 MPa. Table 4.8 shows that all specimens met that requirements.

4.7 Chemical Analysis

The results of a chemical analysis is presented in Table 4.9. Average values (based on three samples) for carbon, silicon, chromium, and manganese contents were determined for the three different diameter wires used in the axial fatigue tests of the multi-layered strands. From the carbon content (between 0.60% to 0.79%), it was concluded that the steel wires used are eutectoid steels.

4.8 Summary

Experimental results obtained from the axial fatigue tests conducted on sixteen full-size multi-layered strands have been presented in this Chapter. The parameters investigated include the strand make-up, cable length, and stress range. The results of the main program indicated that, during the axial fatigue test, the cross-sectional area and the stiffness of the cable deteriorate. It is clear that the number of wire breaks and modulus of

elasticity can, therefore, be used to assess the damage accumulated on a cable and to establish a discard criterion.

Use of acoustic emission techniques and accelerometers to detect wire breaks during the fatigue tests was shown to provide comparable results. For specimens that were tested close to destruction (SP series), the non-destructive procedures were not able to detect the final number of wire breaks. This is because, close to failure, several breaks occur at the same time and the long duration AE and accelerometer events overlapped. However, for the experiments (SL and SS series) where the tests were not taken to destruction, the total number of wire breaks was successfully predicted using the accelerometer method.

Upon disassembling of the specimens, it was found that wire breaks were generally evenly distributed along the cables. Wire breaks within the free length were due to localized fretting fatigue at the interlayer contact patches. This was also observed in photomicrographs of fretting surfaces, which revealed that pre-existing microcracks at the zinc-iron interface of the contact patches propagate with loading cycles. Interlayer wire friction was found to be the cause of the multiple breaks that took place in individual internal wires.

Microscopic examination of the wire fracture surfaces revealed three distinct regions of the fretting fatigue failure: fretting fatigue initiation site, fatigue propagation region, and final fracture region. A substantial amount of fretting debris was observed in the first region. Although photomicrographs showed a ductile final fracture, from an engineering (macroscopic) sense the fracture can be considered as brittle since it is associated with relatively little plastic deformation.

From a simulated two-block amplitude tension fatigue test, it was concluded that a linear damage cumulative hypothesis will underestimate the total axial fatigue life. This is due to shifting of the fretting zone from one area to another as a different block load is applied. Microscopic examination of the fretting areas confirmed the validity of the above statement.

Metallographic examination, chemical analysis, and coupon tests on single wires showed that the steel wires that made up these cables are cold-drawn, eutectoid steels (0.6% C to 0.8% C) with mechanical properties conforming to the minimum requirements of the ASTM A586 standard.

Finally, from the preliminary calibration tests of the acoustic emission (AE) it was found that the AE wire breakage event is characterized by a high amplitude signal with large

duration, high energy range, and high count range. A major attenuation of the AE event occurs between different layers and along the cable. The pulse echo tests gave promising results in detecting existing wire breaks under the condition that one of the terminations of the cable is accessible.

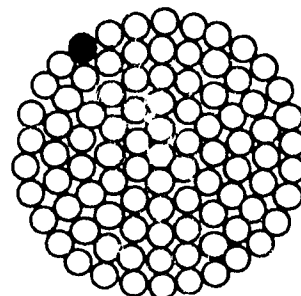
Table 4.1 Axial fatigue test results on multi-layered strands

Specimen Designation (Diameter)	Specimen Length (mm)	Stress Range (MPa)	Number of Cycles to Failure	Remarks Mode of Failure
SP1 (44.4 mm)	3315	303	8 200 360	Deterioration of modulus of elasticity
SP2 (44.4 mm)	3323	371	2 717 640	Deterioration of modulus of elasticity
SP3 (44.4 mm)	3336	371	418 262	Complete fracture of specimen
SP4 (44.4 mm)	3320	371	308 048	Deterioration of modulus of elasticity
SP5 (44.4 mm)	3323	303	9 371 997	Complete fracture of specimen
SP6 (44.4 mm)	3310	337	1 957 640	Deterioration of modulus of elasticity
SP7 (44.4 mm)	3328	337	2 124 100	Deterioration of modulus of elasticity
SP8 (44.4 mm)	3326	404	204 600	Deterioration of modulus of elasticity
SL1 (25.3 mm)	3357	310	566 300	More than three broken wires
SL2 (25.3 mm)	3376	310	635 860	More than three broken wires
SL3 (25.3 mm)	3379	207	10 000 000	Test was discontinued. No broken wires
SL4 (25.3 mm)	—	310	2 482 190	Retest of specimen SP3. More than three broken wires
SL5 (25.3 mm)	3387	362	245 740	Three broken wires
SS1 (25.3 mm)	2153	362	240 000	More than three broken wires
SS2 (25.3 mm)	2160	258	4 183 410	Test was discontinued. No broken wires
SS3 (25.3 mm)	2152	310	941 750	Three broken wires

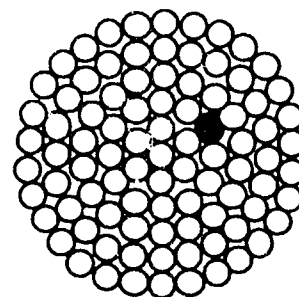
Table 4.2 Location of wire breaks for specimen SP1

Number of broken wires	Distance from fixed end (mm)	Layer
1	200	1 (out.)
2	3180, 3485	1
3	3455	1
4	3480	1
5-8	3510	1
9	3415, 3485	2
10-13	3455	2
14	3475, 3510	2
15, 16	3480	2
17-19	3490	2
20	3445	3
21-24	3455	3
25	3470	3
26	3485	3
27	930, 1190	4
28	3435, 3495	4
29, 30	3460	4
31, 32	3480	4
33	3485	5
34	3485	6
Breaks inside sockets		10
Breaks outside sockets		29
Total wire breakages		39

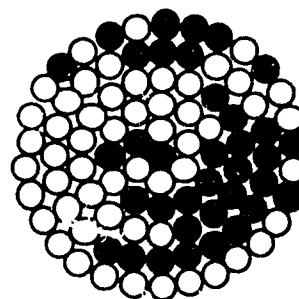
Total cable length (outside to outside) = 3710 mm



Broken wires close to fixed end



Broken wires within the free length

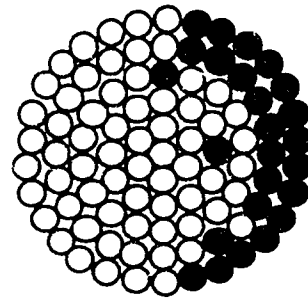


Broken wires close to moving end

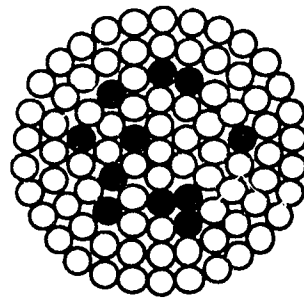
Table 4.3 Location of wire breaks for specimen SP2

Number of broken wires	Distance from fixed end (mm)	Layer
1-12	180	1 (out.)
13-14	190	1
15-18	3555	1
19-26	175	2
27	190	2
28	3555	2
29	3530	2
30	205, 3465	3
31	200, 1625	3
32	2265	3
33	2840	3
34	2850	3
35	310, 445	3
36	400	3
37	210	4
38	250, 640, 800, 1020	4
39	240	4
40	2548	4
41	240, 1025	5
Breaks inside sockets		31
Breaks outside sockets		17
Total wire breakages		48

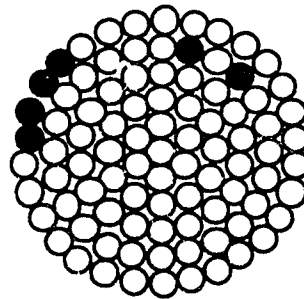
Total cable length (outside to outside) = 3730 mm



Broken wires close to fixed end



Broken wires within the free length

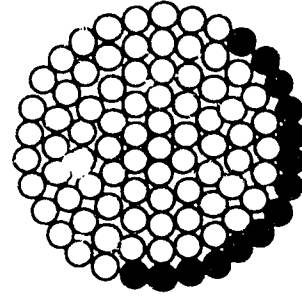


Broken wires close to moving end

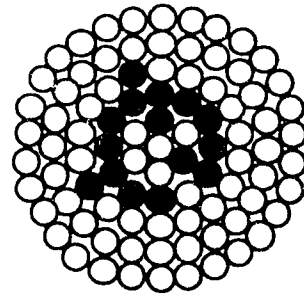
Table 4.4 Location of wire breaks for specimen SP4

Number of broken wires	Distance from fixed end (mm)	Layer
1-14	200	1 (out.)
15-18	3510	1
19	543	3
20	2085	3
21	355, 545, 935, 1365 1565, 1970, 2960	4
22	475, 615, 680, 780, 1080, 2265, 2495, 2915	4
23	850, 1850	4
24	1200, 1640, 1810 2765	4
25	1710, 2730	4
26	540, 2400, 2952	4
27	2105, 2945	4
28	2965, 3165	4
29	755, 1540, 3270	4
30	1010, 1255, 1760 2510, 2970	4
31	850, 1010, 3185	4
32	+30	5
33	2210	5
Breaks inside sockets		18
Breaks outside sockets		45
Total wire breakages		63

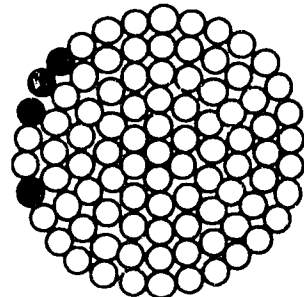
Total cable length (outside to outside) = 3710 mm



Broken wires close to fixed end



Broken wires within the free length



Broken wires close to moving end

Table 4.5 Location of wire breaks for specimen SP7

Number of broken wires	Distance from fixed end (mm)	Layer
1	2090	1 (out.)
2-12	2080	2
13, 14	500, 2070	3
15	1160, 2080	3
16-22	2080	3
23	550, 1145, 3120	4
24	550, 1125, 2080	4
25	550, 2080, 3220	4
26	500, 1165, 2080	4
27	500, 750, 1155, 2080	4
28	640, 1000, 1500, 2080, 3000	4
29	750, 1100, 2080, 2305	4
30	830	4
31	1050, 2050	4

Number of broken wires	Distance from fixed end (mm)	Layer
32	1155, 2060	4
33	1835	4
34	2080, 2854, 2904	4
35	640, 1100, 2080	5
36	680, 2080, 3075	5
37	2080, 3105	5
38	440, 1040, 2080	5
39	900, 1040, 2080	5
40	980, 2080	5
41	1040, 2080, 2600	6
Breaks closeto sockets		0
Breaks outside sockets		78
Total wire breakages		78

Total cable length = 3717 mm

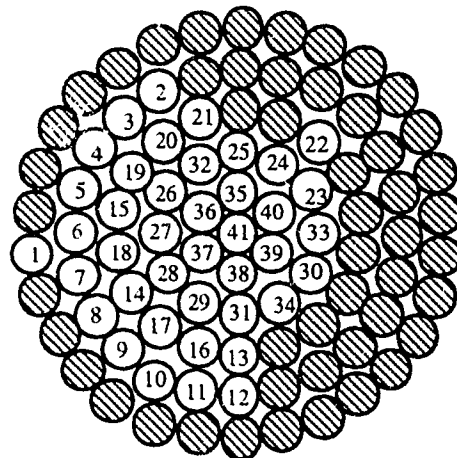


Table 4.6 Location of broken wires for 25 mm diameter specimens and comparison with accelerometer predictions

Broken Wires	Specimen SL1		Specimen SL2		Specimen SL4		Specimen SL5		Specimen SS1		Specimen SS3	
	dist.	layer	dist.	layer	dist.	layer	dist.	layer	dist.	layer	dist.	layer
1	1760	1	590	1	145	1	460		880	1	230	1
2	1910	1	2680	1	145	1	490	1	740	1	1400	1
3	2015	1	1227	1	145	1	3160	1	1925	1	1590	1
4	2000	1	2648	2	145	1			2030	1		
5	2505	1			145	1						
6	2495	1			145	1						
7	3335	1			150	2						
8	2530	2										
9	1975	2										
10	2720	3										
Breakages at sockets	0		0		7		0		0		1	
Breakages in free length	10		4		0		3		4		2	
Total No. of breakages	10		4		7		3		4		3	
Prediction: accelerometers	9 (90%)		4 (100%)		7 (100%)		3 (100%)		4 (100%)		3 (100%)	
Initial length	3357		3376		3378		3387		2153		2152	
Final length	3385		3405		3410		3415		2170		2165	

Notes: All dimensions are in millimeters (mm)

The distances of broken wires are measured from the outside of the moving sockets

The layers are numbered from outer towards inner layers

Table must be read in conjunction with Figure 4.30

Table 4.7 Results from coupon tests

Wire Diameter (mm)	Stress at 0.7% Extension (MPa)	Ultimate Tensile Strength (MPa)	Modulus of Elasticity (MPa)
4.041	1244	1637	203 710
4.025	1252	1715	205 420
4.036	1240	1649	202 930
4.298	1106	1640	192 440
4.308	1152	1624	197 730
4.320	1160	1629	194 860
5.085	1107	1610	194 200
5.033	1103	1613	212 330
5.050	1104	1612	194 300
5.265	1105	1613	197 540
5.255	1082	1610	195 300
5.258	1095	1614	198 250

Table 4.8 Mechanical properties of steel wires and comparison with ASTM A350 Standard

Wire Diameter (mm)	Measured Stress at 0.7% Strain (MPa)	Measured UTS ¹ (MPa)	Measured Modulus (MPa)	ASTM Stress at 0.7% Strain (MPa)	ASTM MUTS ² (MPa)	ASTM Elongation ³ (%)
4.034	1245	1667	204 020	1100	1520	4.0
4.315	1139	1631	195 010	1100	1520	4.0
5.056	1105	1612	200 280	1100	1520	4.0
5.260	1094	1612	197 030	1100	1520	4.0

(1) UTS = ultimate tensile strength

(2) MUTS = minimum ultimate tensile strength

(3) Elongation is based on 250 mm gauge length

Table 4.9 Chemical analysis of steel wire

Wire Diameter (mm)	% C	% Mn	% Cr	% Si
4.034	0.65	0.60	0.18	0.31
4.315	0.60	0.42	0.20	0.28
5.056	0.79	0.53	0.19	0.31

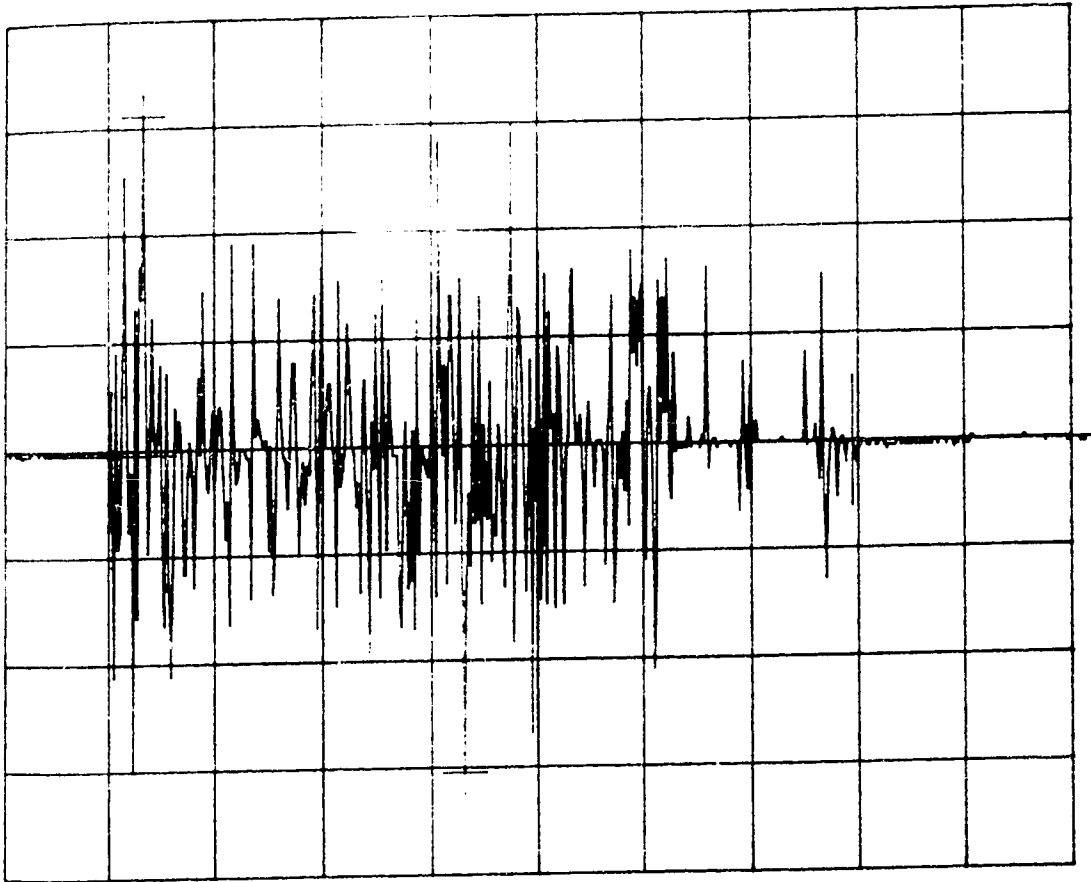


Figure 4.1 Typical acoustic emission signal during fracture of a single wire

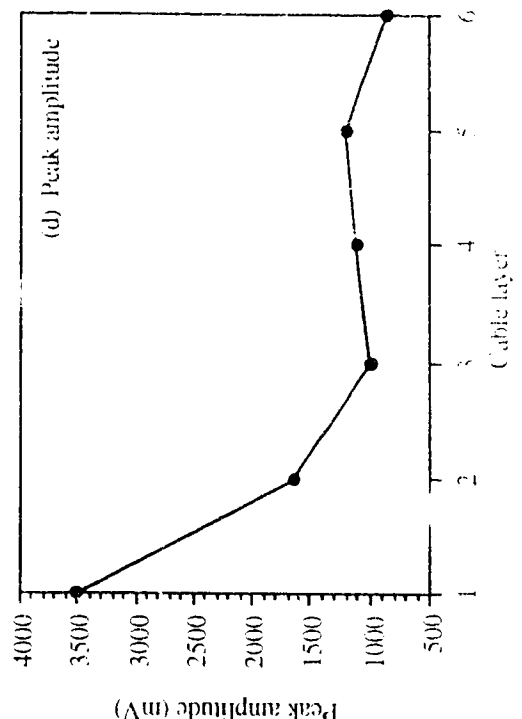
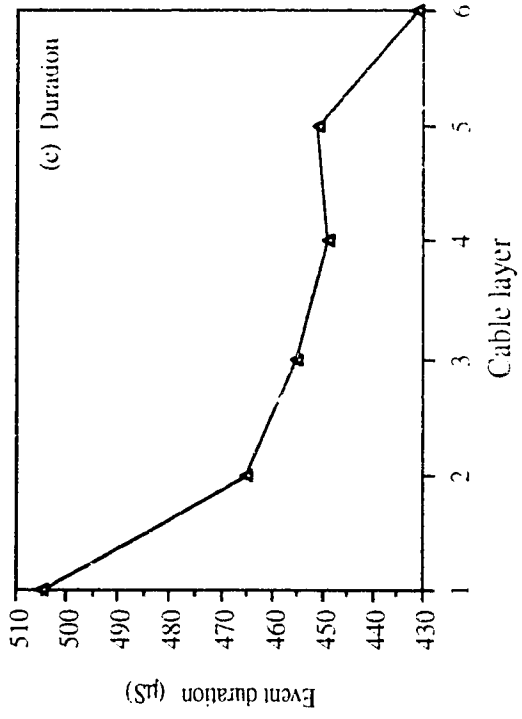
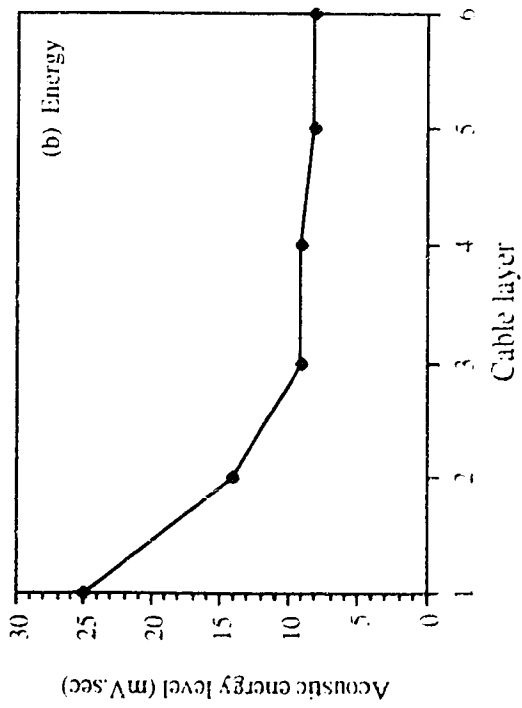
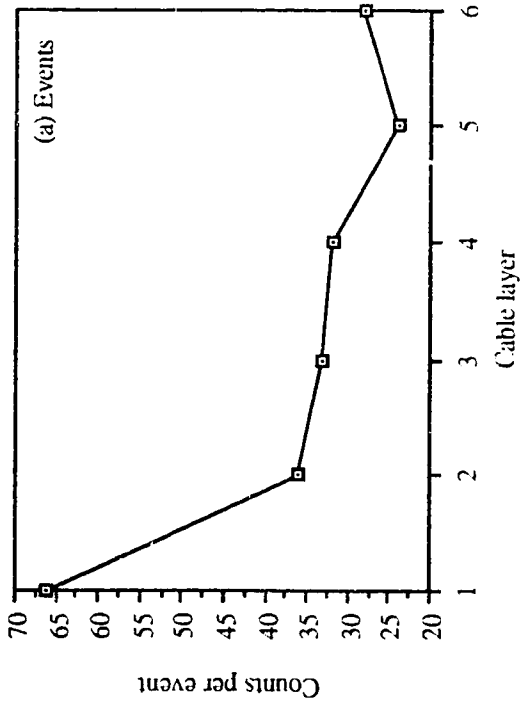


Figure 4.2 Attenuation of acoustic emission parameters through successive cable layers

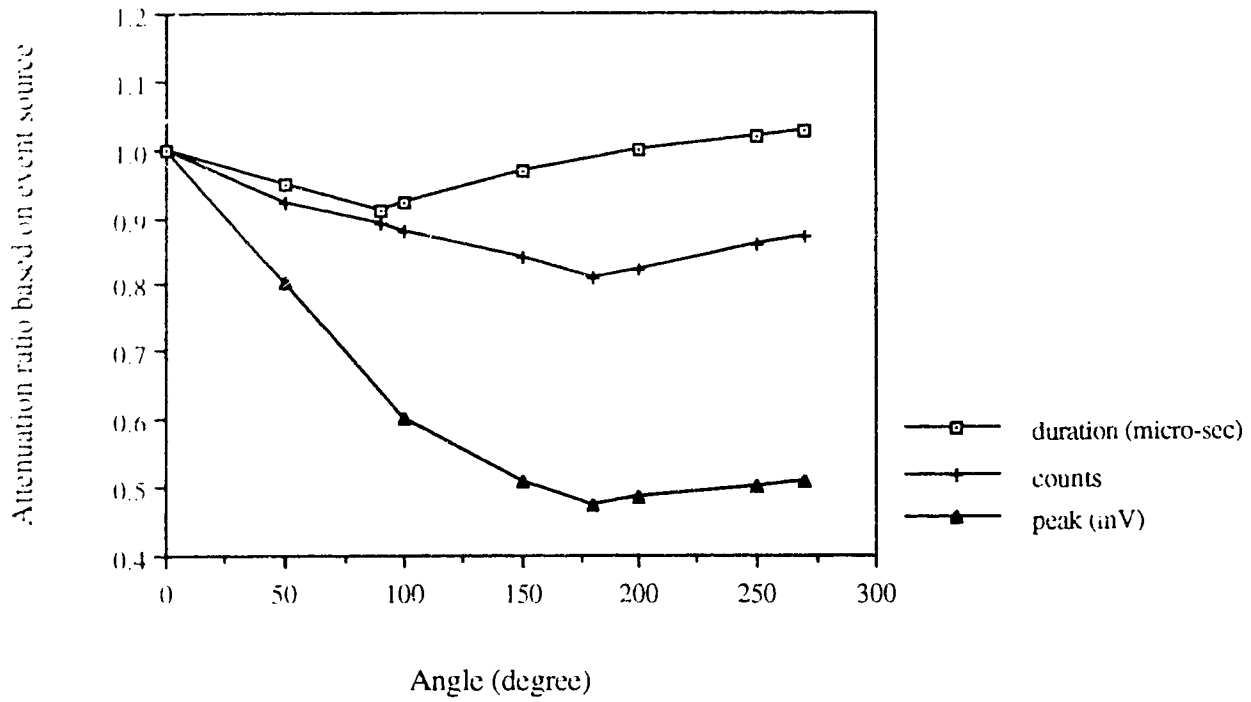


Figure 4.3 Attenuation of acoustic emission parameters with angular orientation

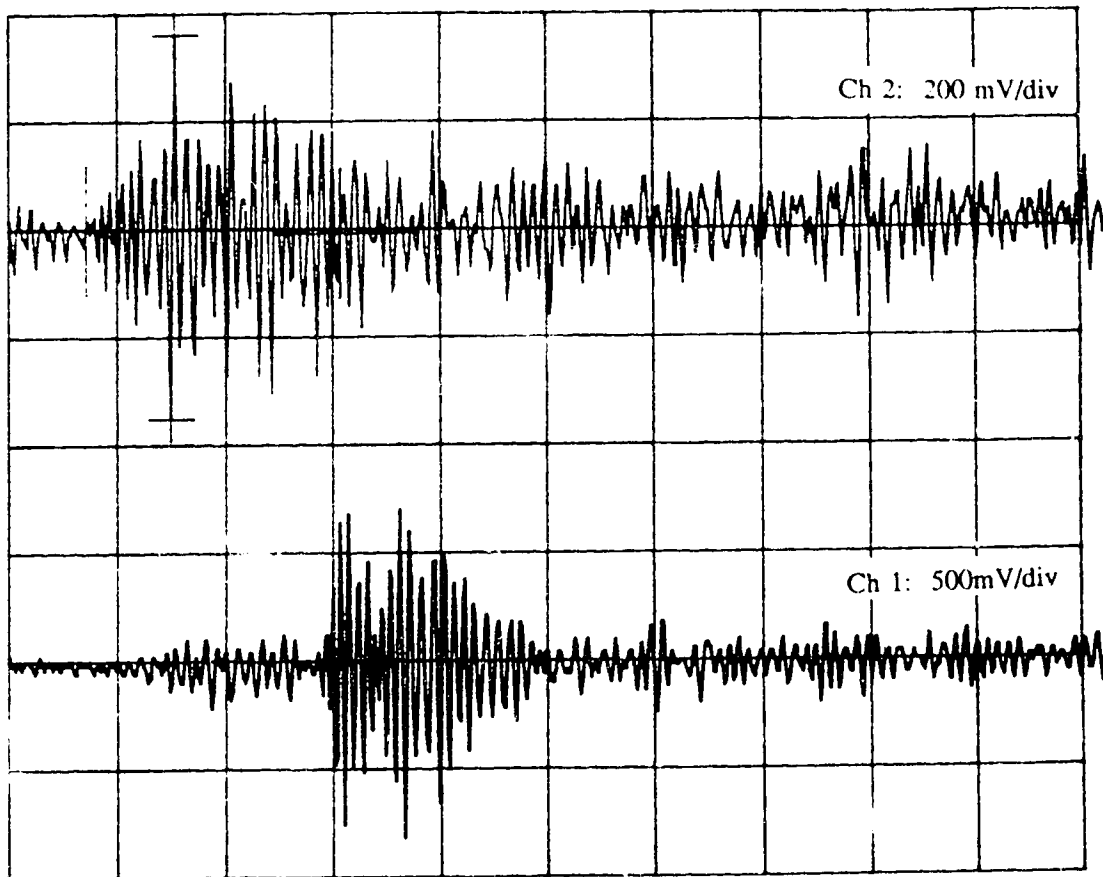


Figure 4.4 Recorded event patterns from two transducers located at 500 mm and 2500 mm from the acoustic emission event

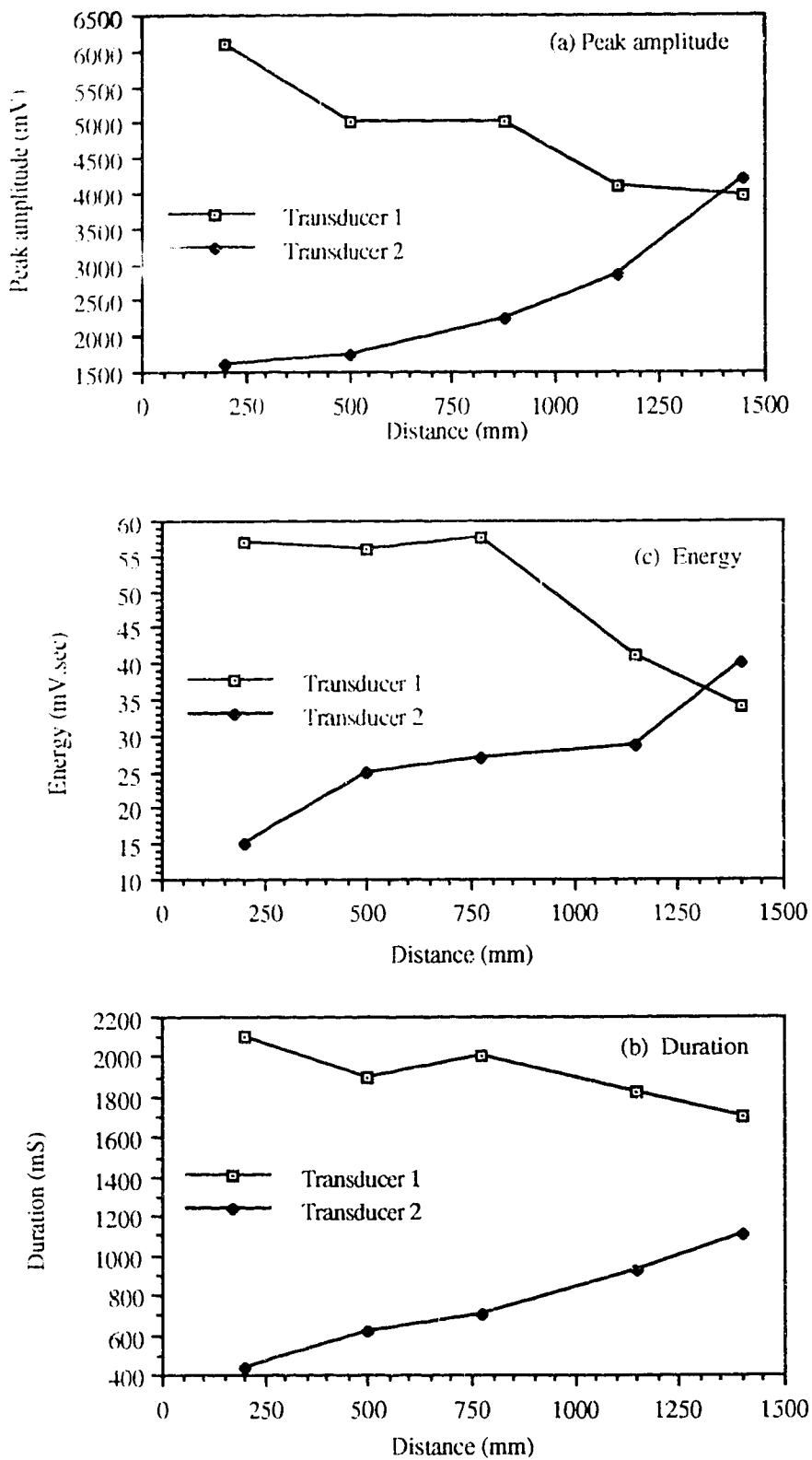


Figure 4.5 Attenuation of acoustic emission parameters with cable length

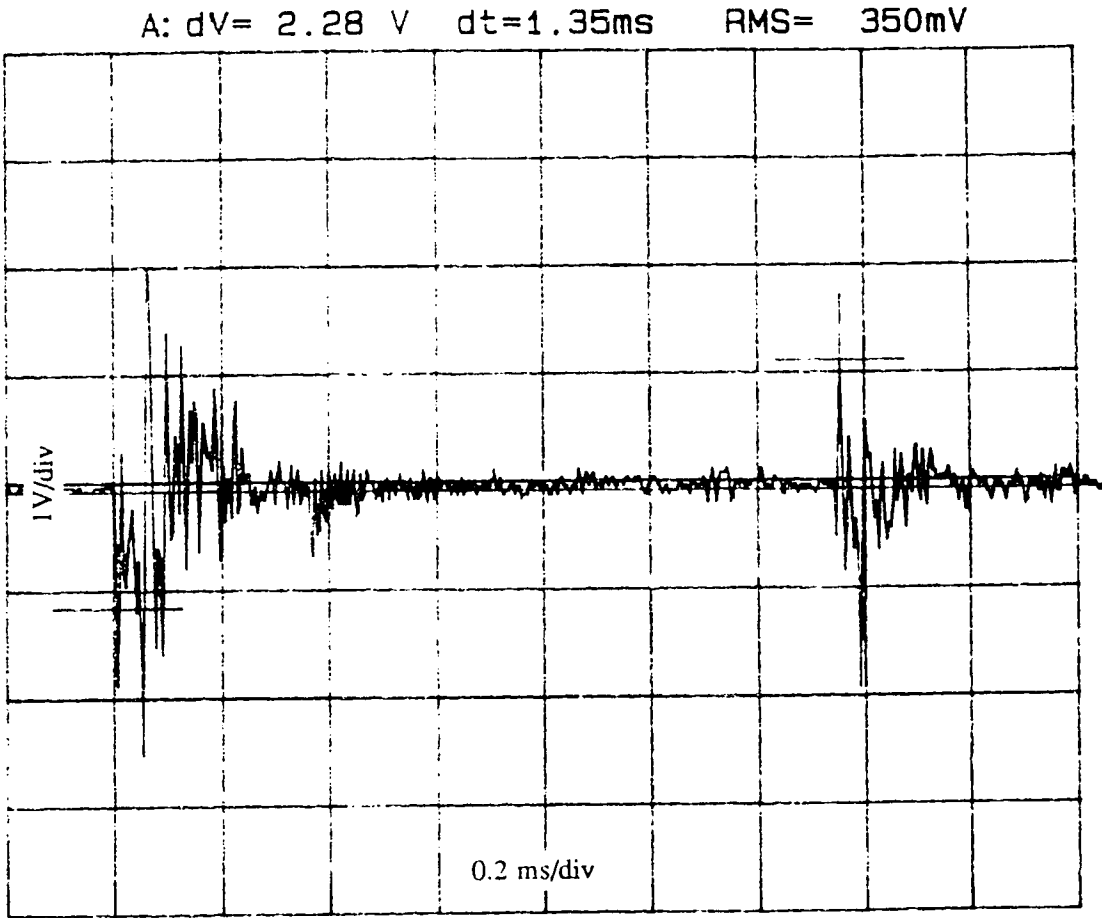


Figure 4.6 Input and reflected signals recorded during a pulse echo test



Figure 4.7 Specimen SP1 after completion of test

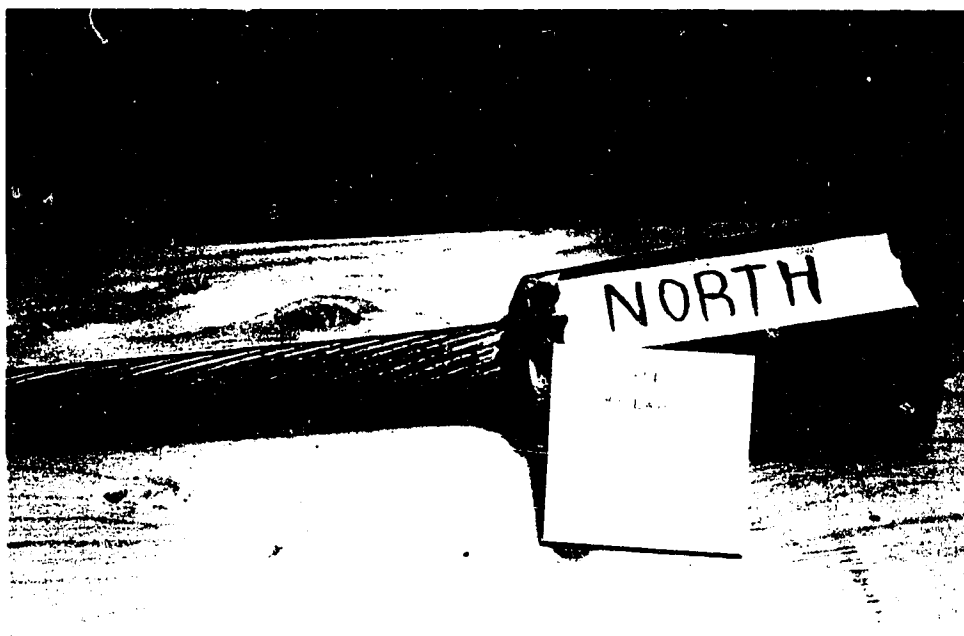


Figure 4.8 Internal condition of SPI close to fixed socket

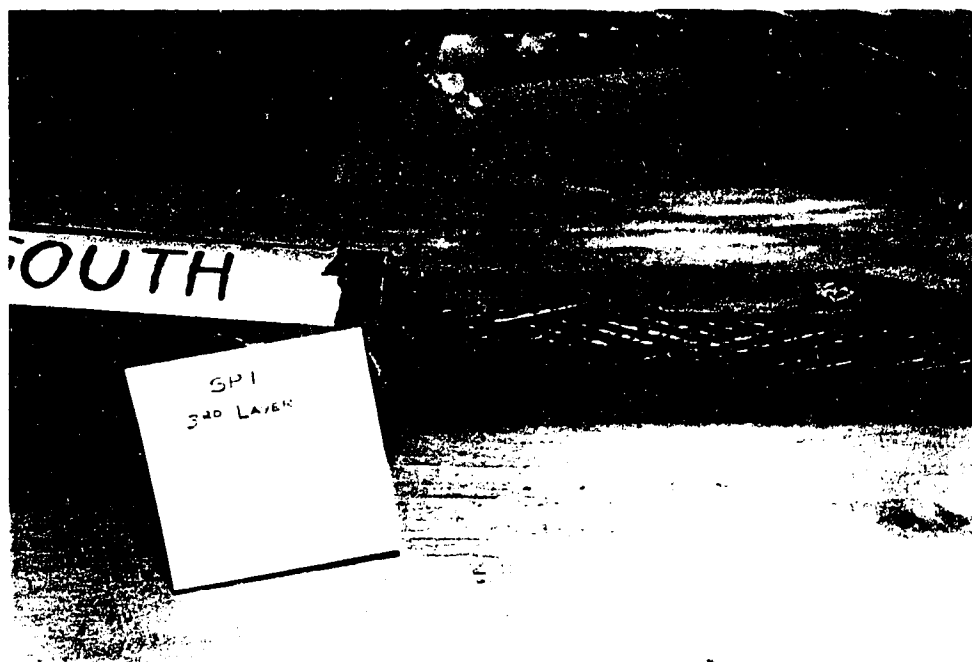


Figure 4.9 Internal wire breaks close to moving end for SPI

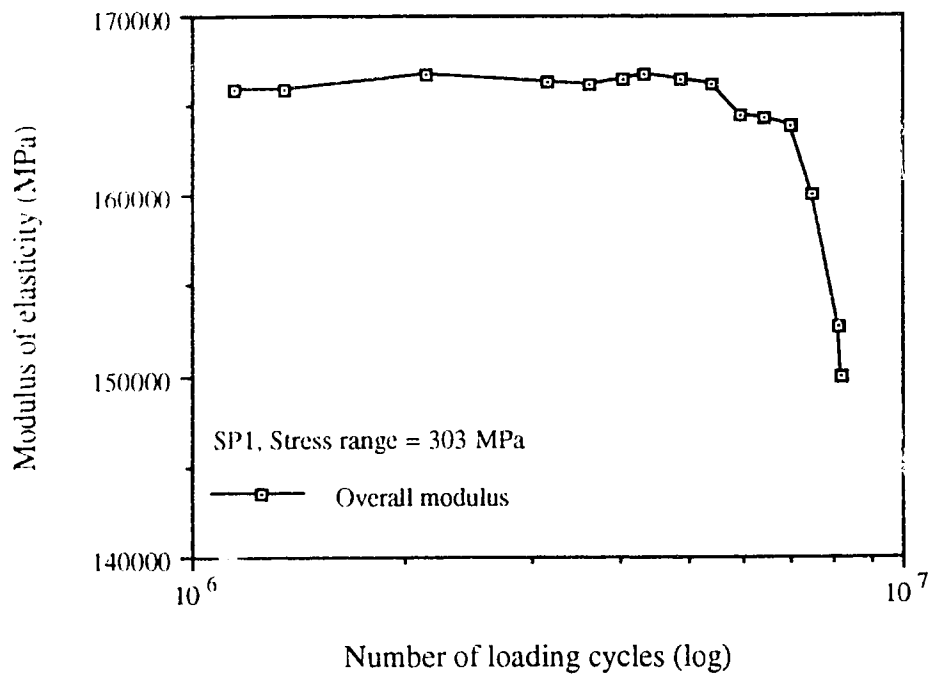


Figure 4.10 Modulus of elasticity versus fatigue life for SP1

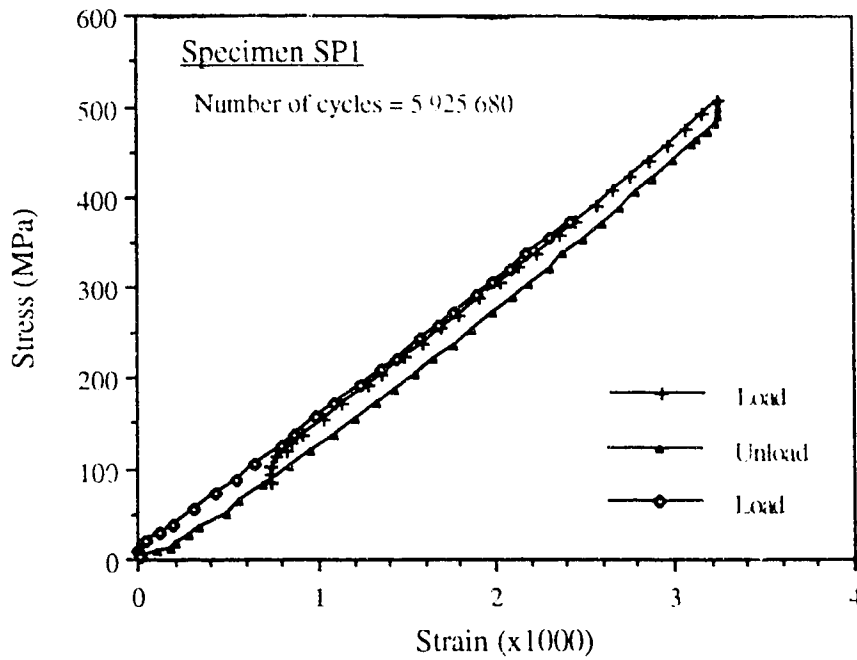


Figure 4.11a Stress-strain curve of specimen SP1 at 5 925 680 cycles

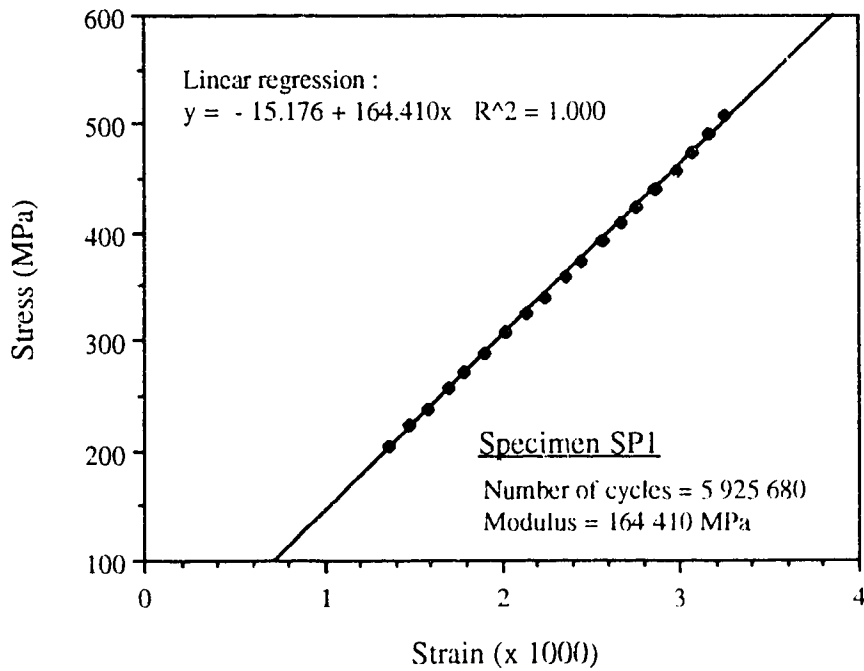


Figure 4.11b Typical computation of modulus of elasticity using linear regression

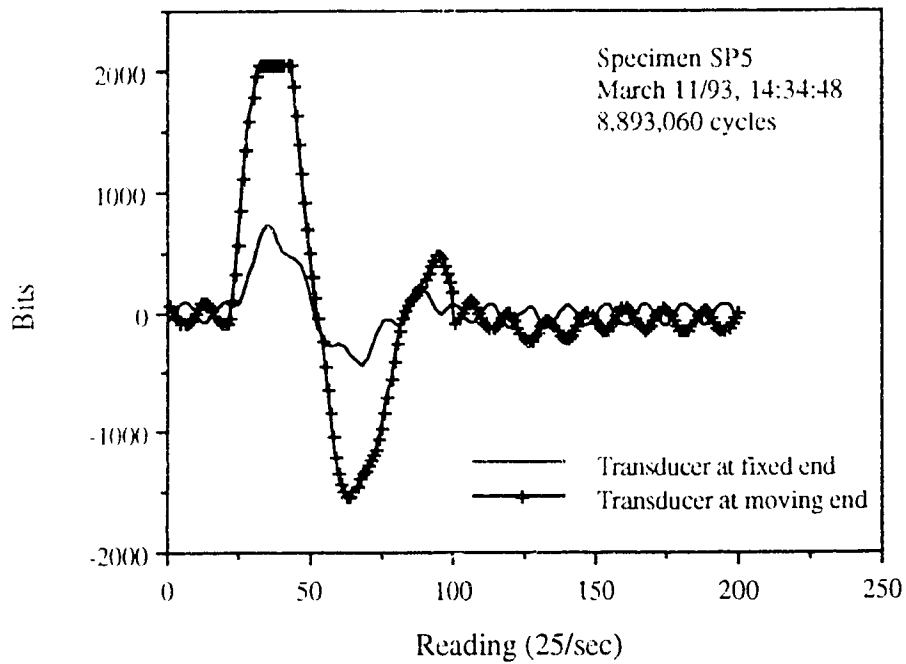


Figure 4.12 Detection of wire breakage based on accelerometers

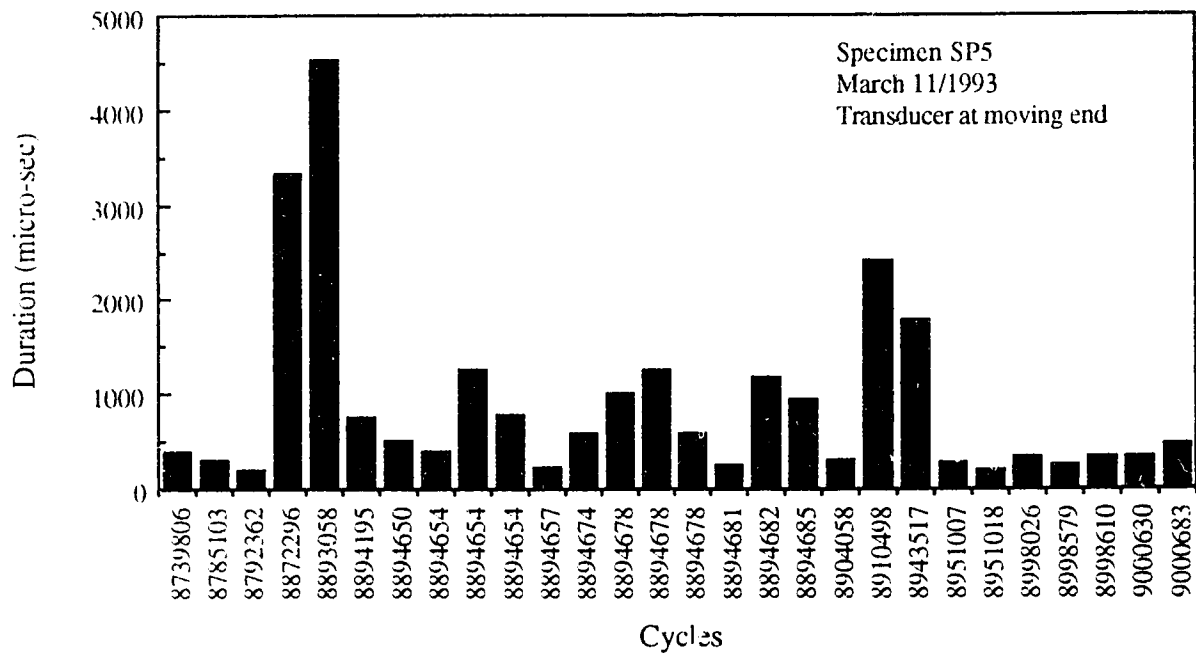


Figure 4.13 Detection of wire break based on acoustic emission events

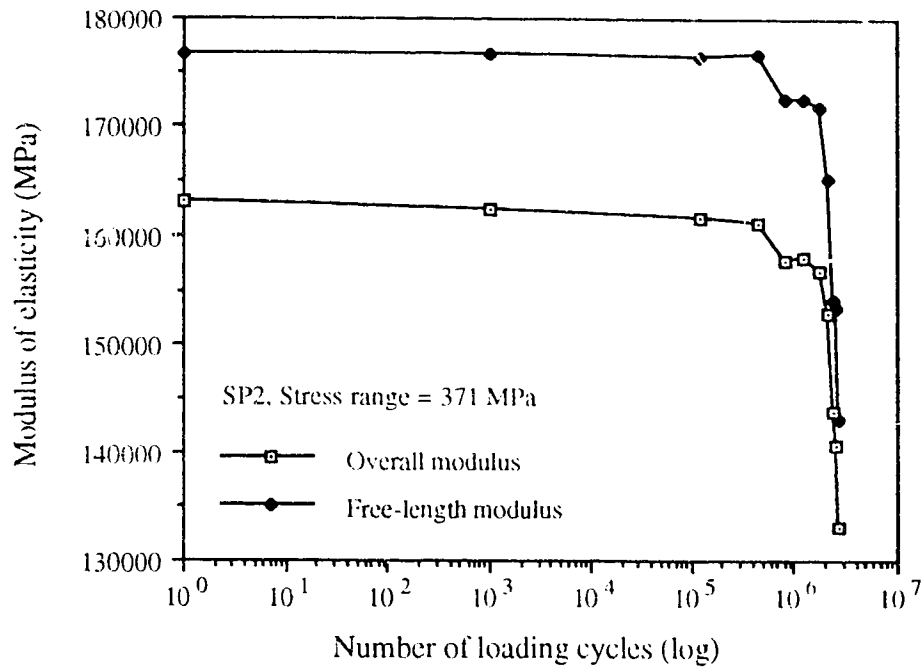


Figure 4.14a Modulus of elasticity versus cycles for SP2

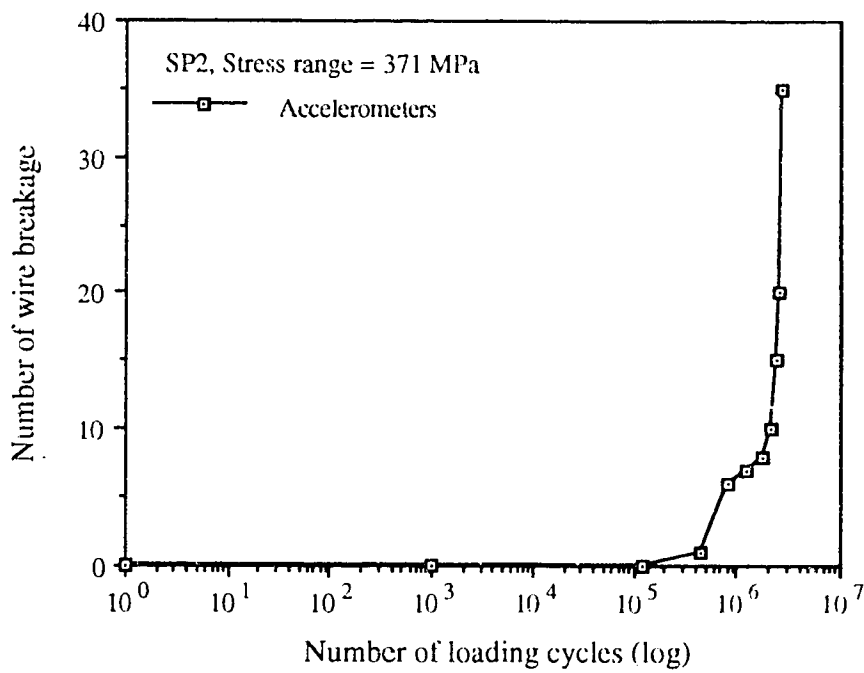


Figure 4.14b Wire breakage versus cycles for SP2

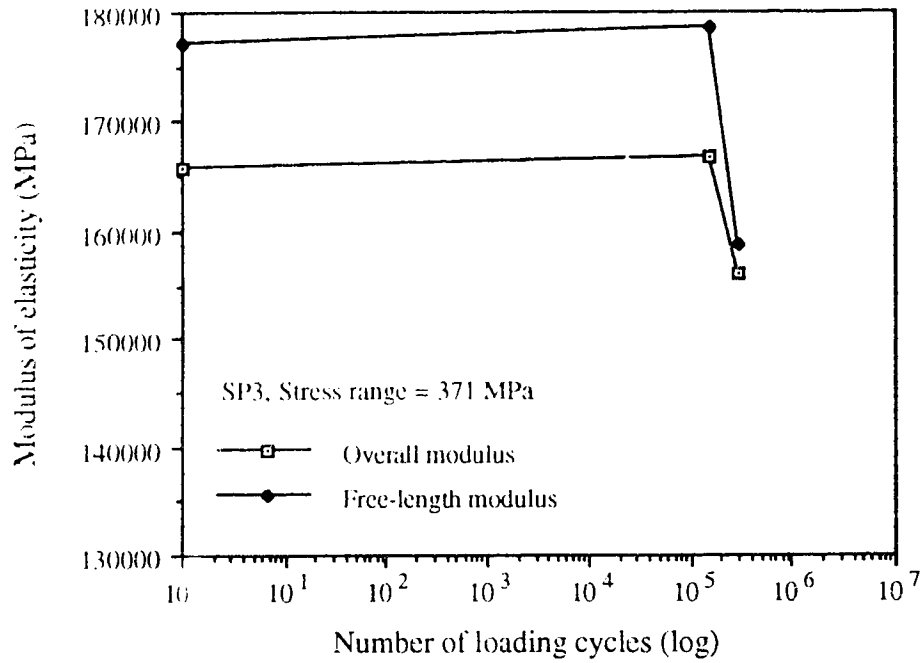


Figure 4.15a Modulus of elasticity versus cycles for SP3

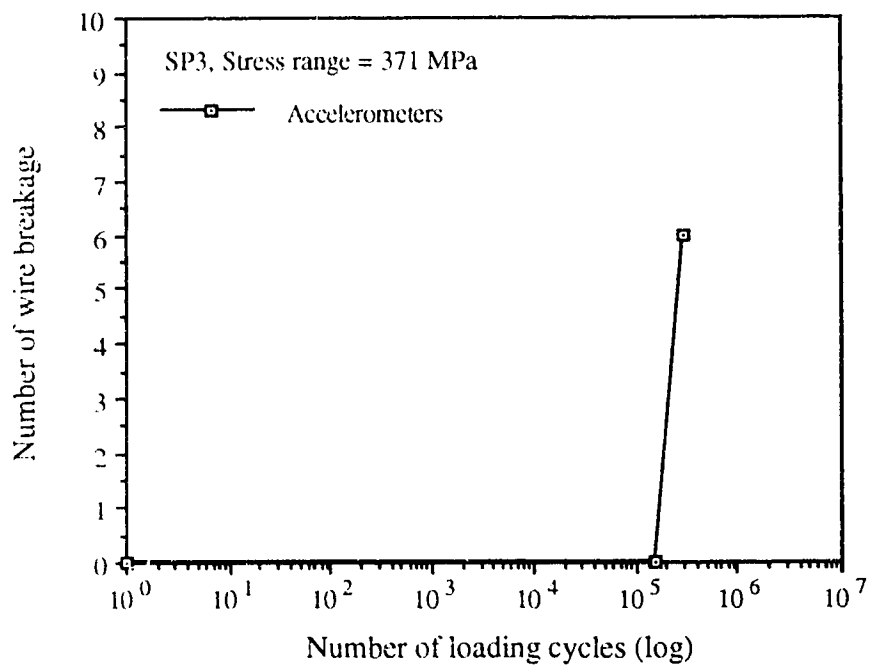


Figure 4.15b Wire breakage versus cycles for SP3

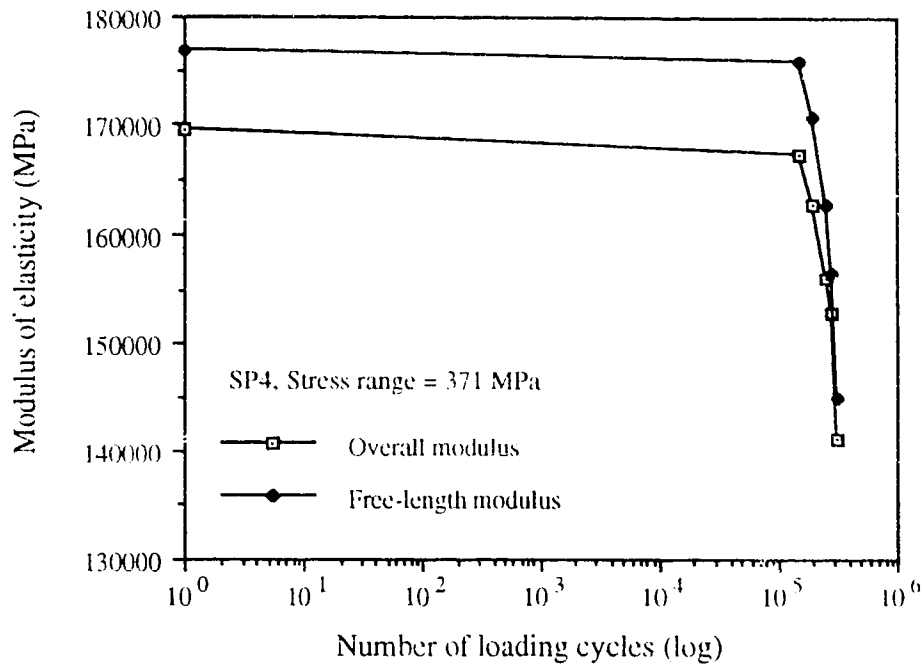


Figure 4.16a Modulus of elasticity versus cycles for SP4

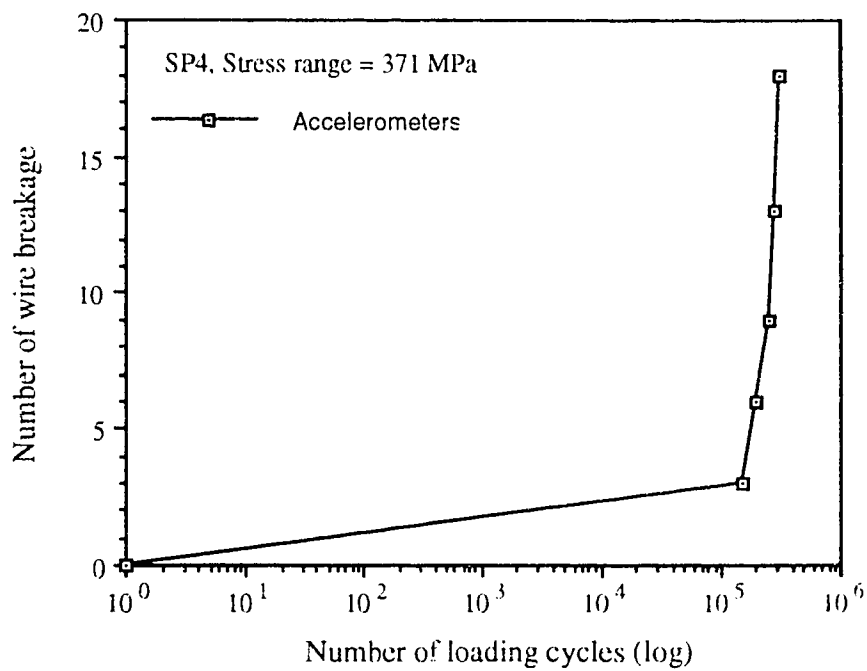


Figure 4.16b Wire breakage versus cycles for SP4

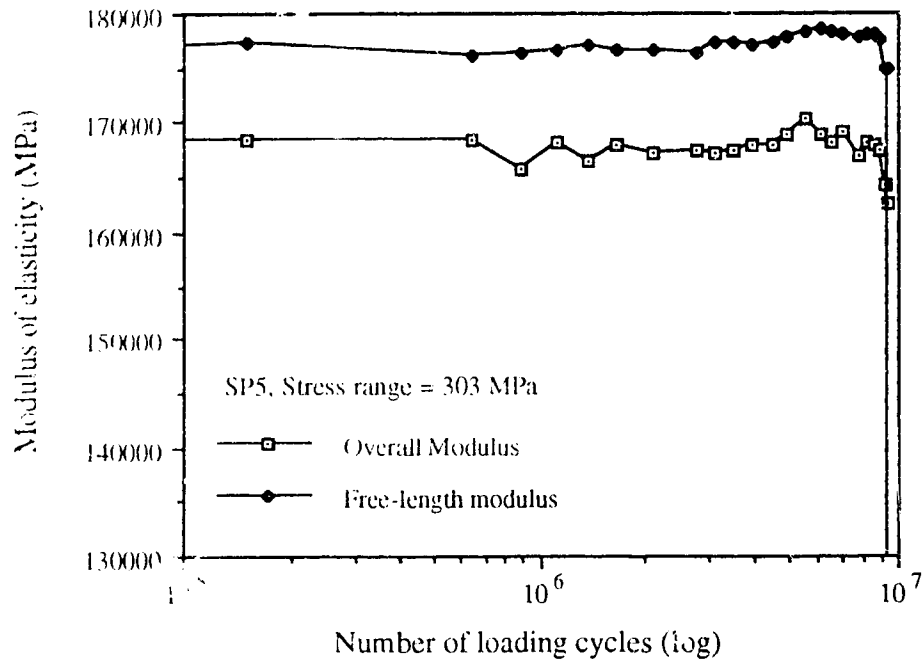


Figure 4.17a Modulus of elasticity versus cycles for SP5

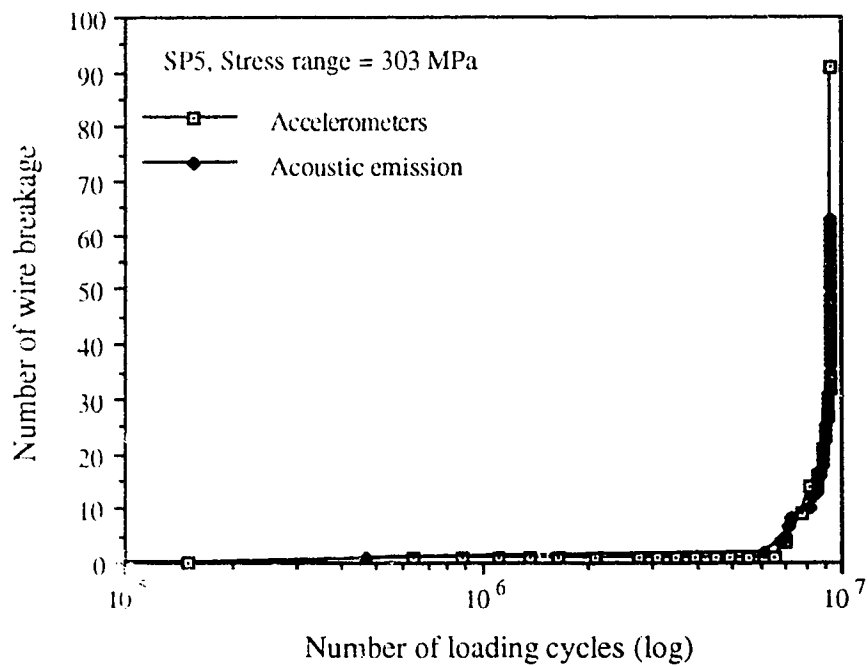


Figure 4.17b Wire breakage versus cycles for SP5

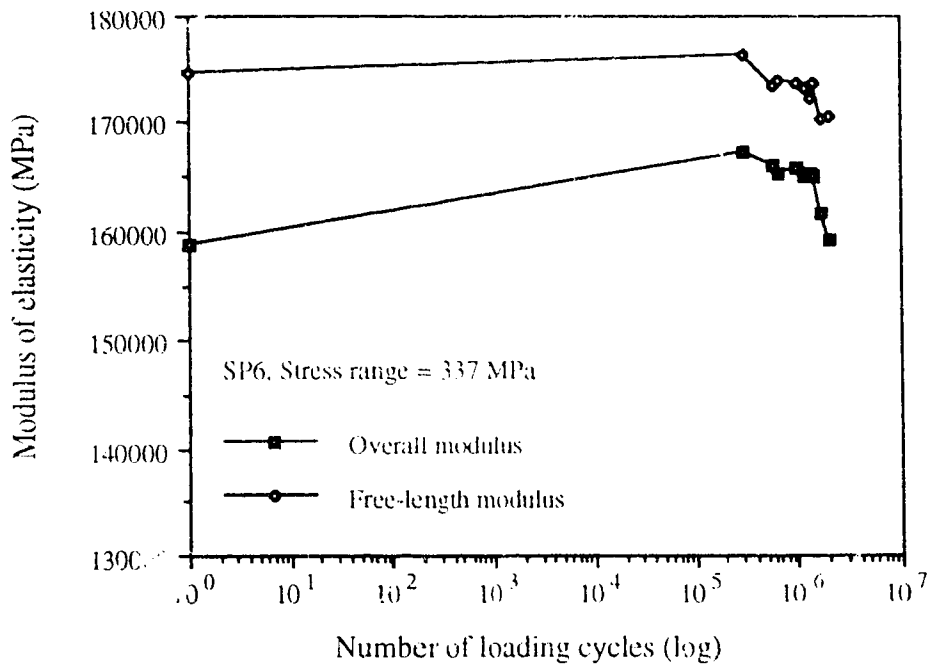


Figure 4.18a Modulus of elasticity versus cycles for SP6

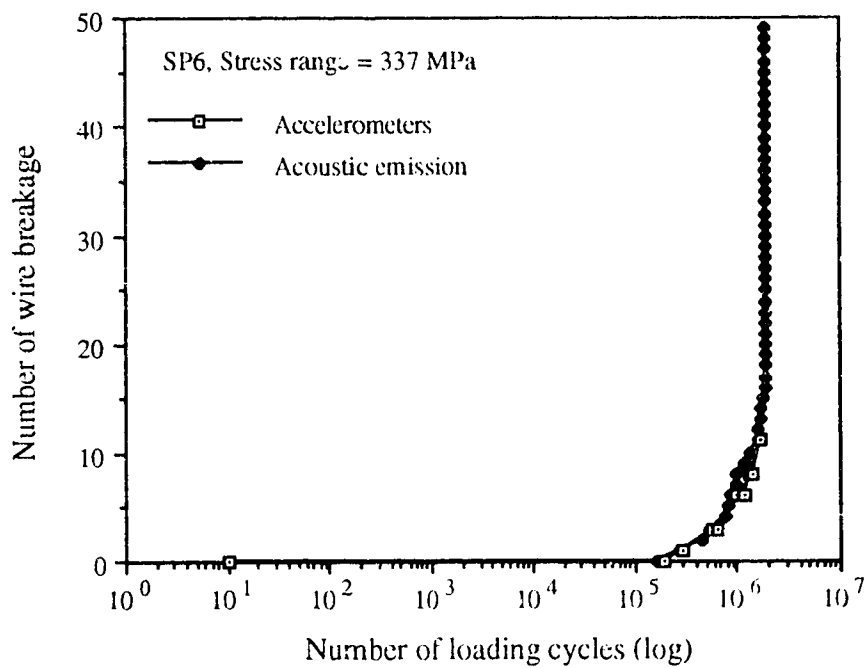


Figure 4.18b Wire breakage versus cycles for SP6

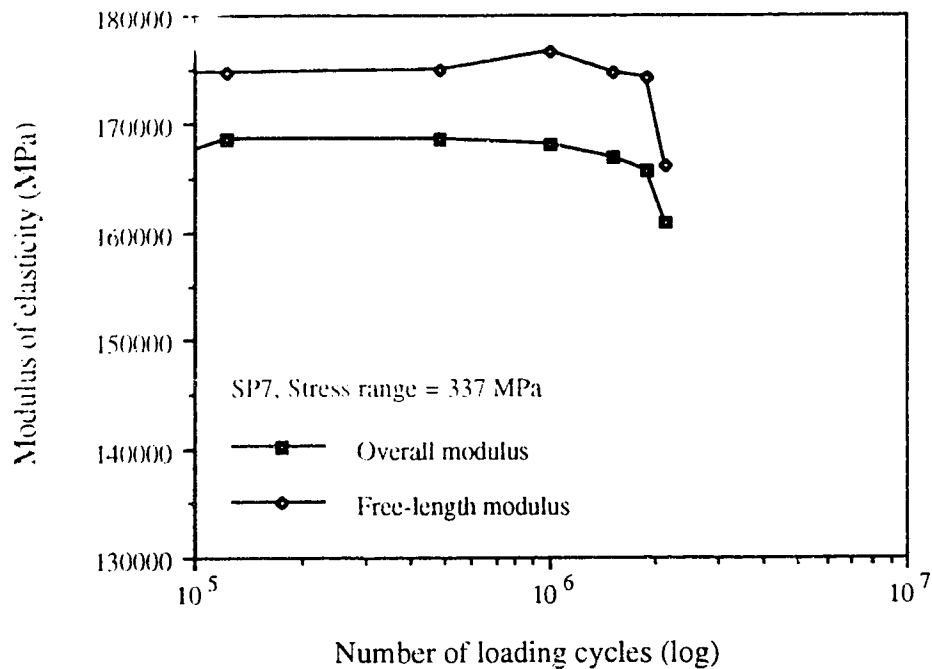


Figure 4.19a Modulus of elasticity versus cycles for SP7

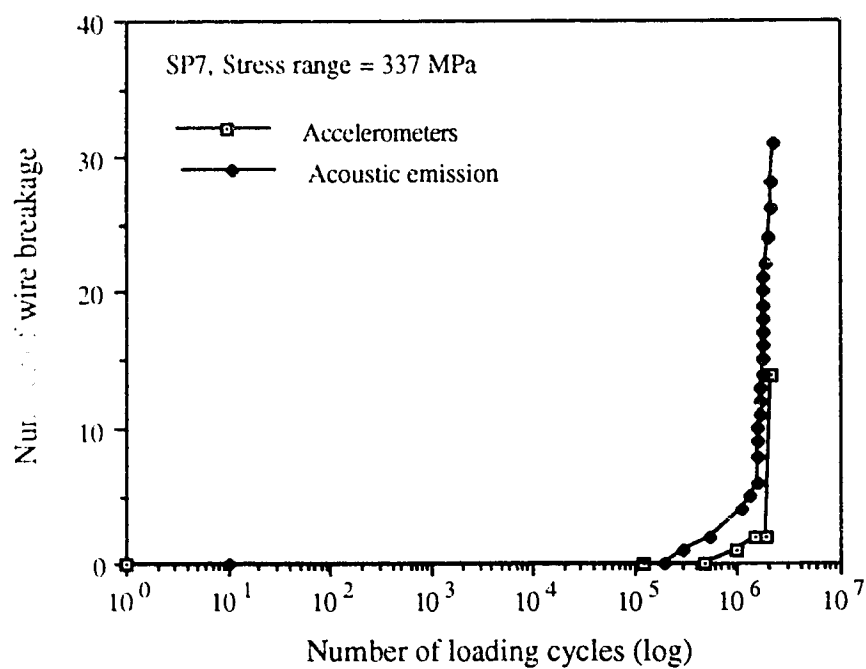


Figure 4.19b Wire breakage versus cycles for SP7

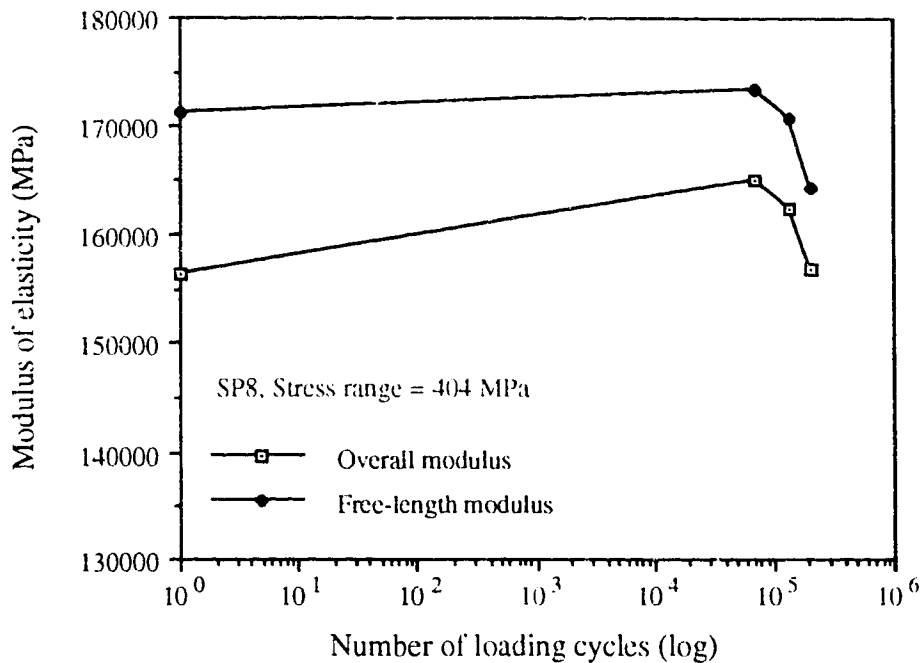


Figure 4.20a Modulus of elasticity versus cycles for SP8

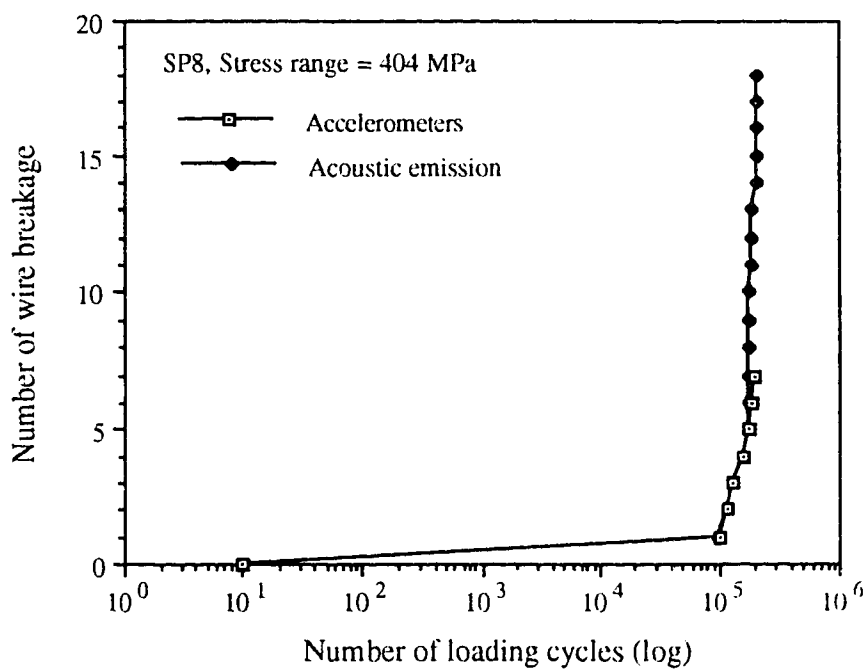


Figure 4.20b Wire breakage versus cycles for SP8



Figure 4.21 Wire breaks at the outer layer of SP2, close to the fixed termination



Figure 4.22 Internal multiple wire breaks for SP4, within the free length

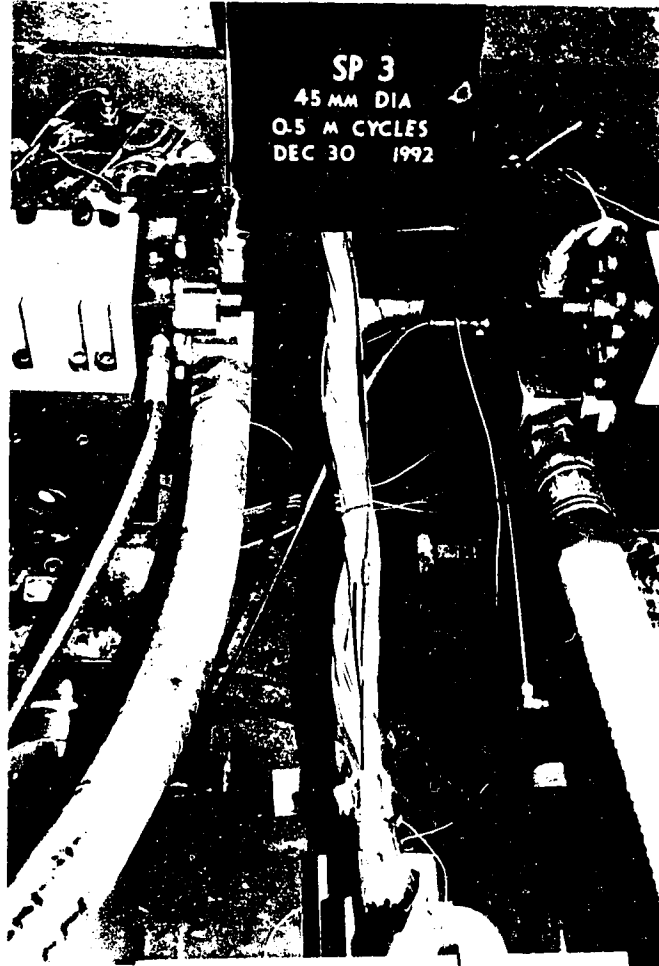


Figure 4.23 External condition of failed specimen SP3

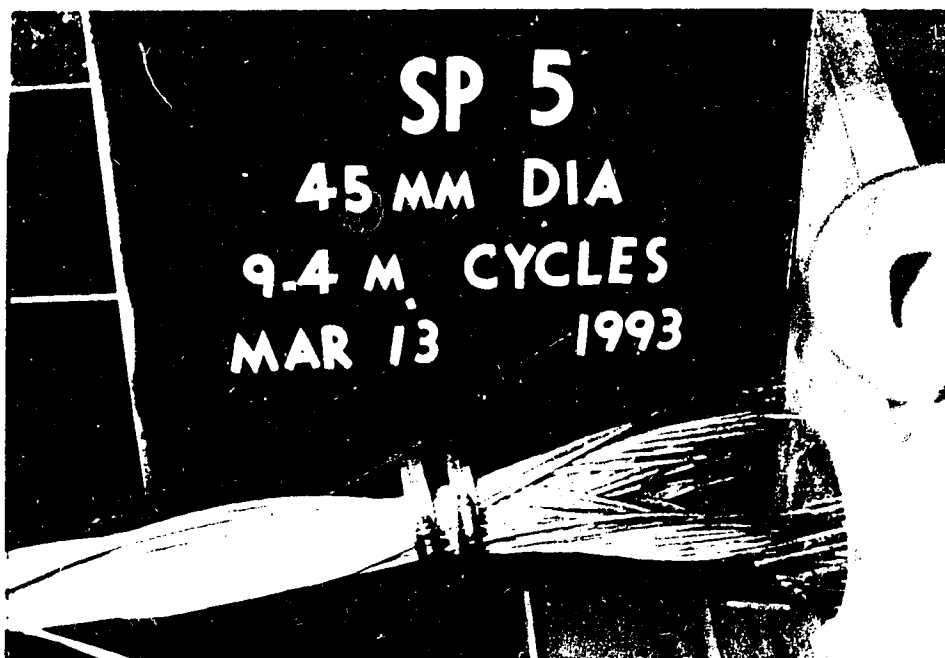


Figure 4.24 External condition of failed specimen SP5

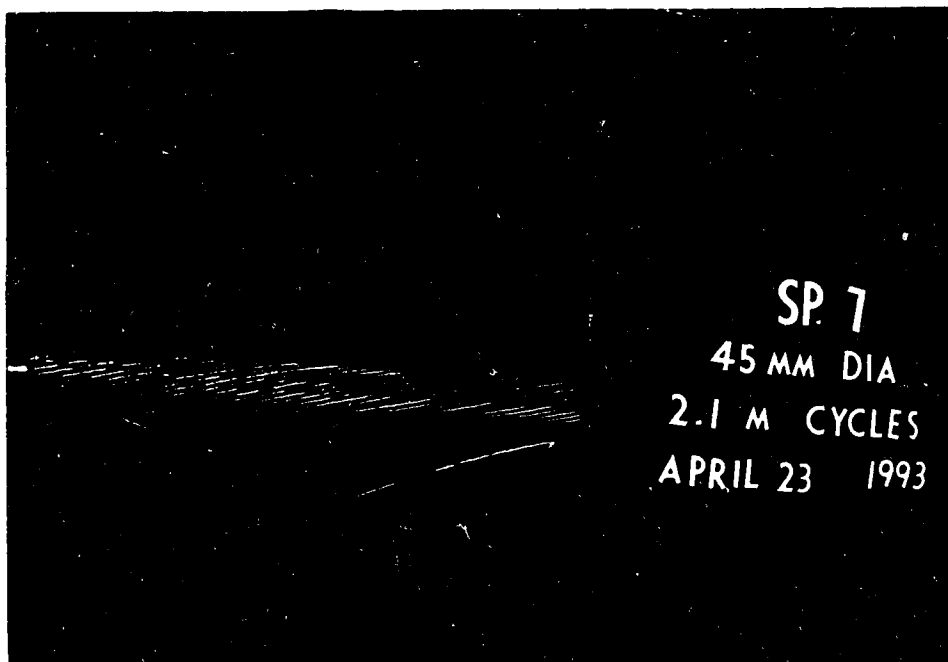


Figure 4.25 External condition of failed specimen SP7

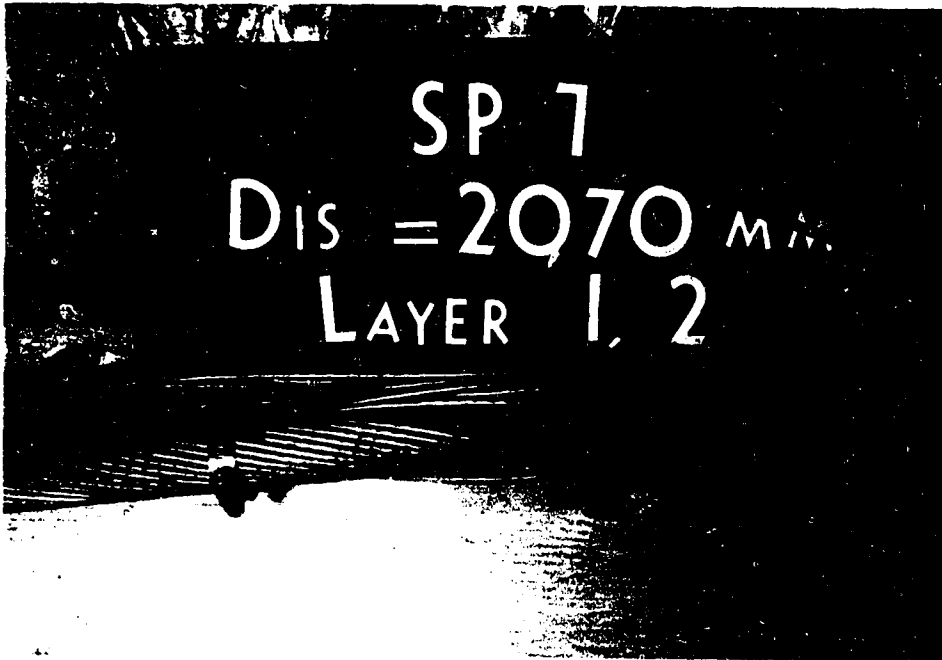


Figure 4.26 Internal wire breaks for specimen SP7—Layers 1,2

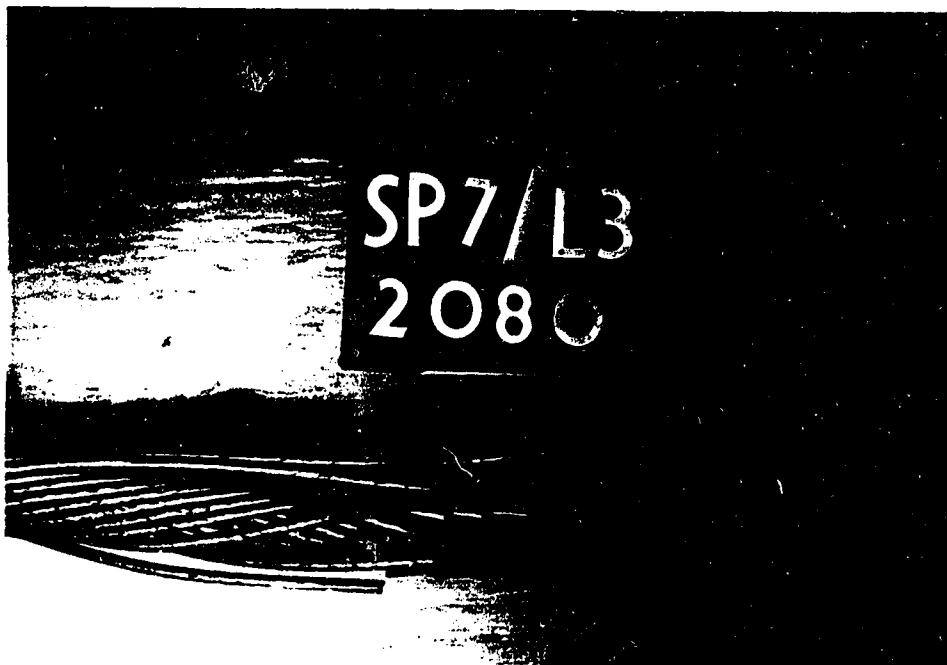


Figure 4.27 Internal wire breaks for specimen SP7—Layer 3

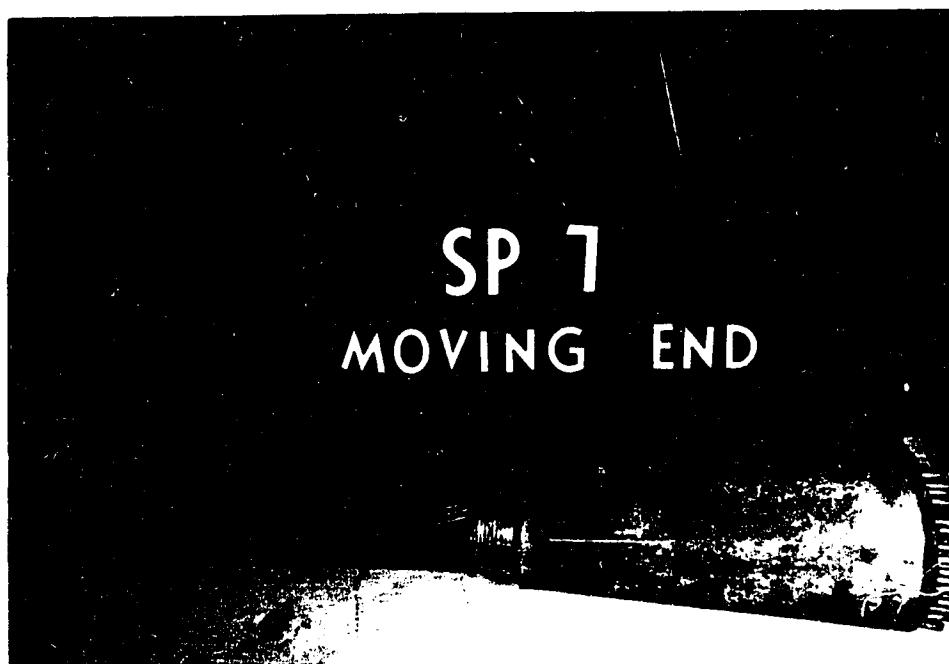


Figure 4.28 Socket condition after completion of SP7 test

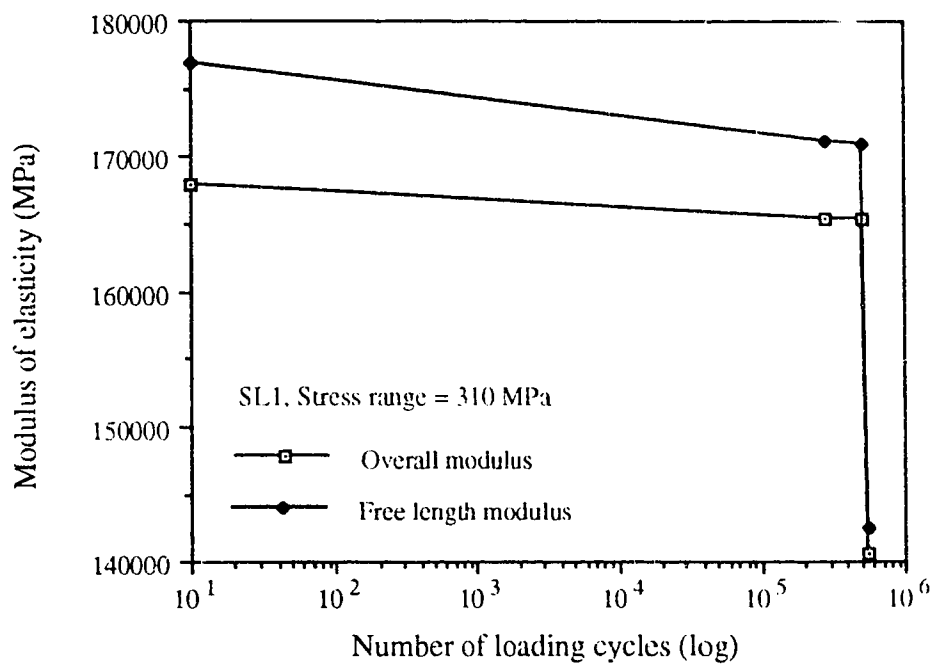


Figure 4.29a Modulus of elasticity versus cycles for SL1

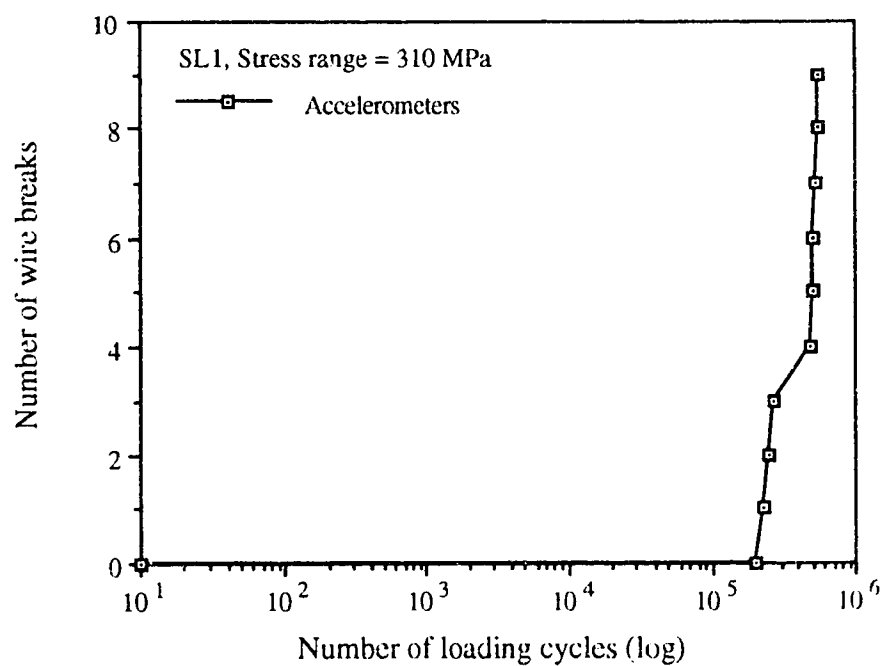
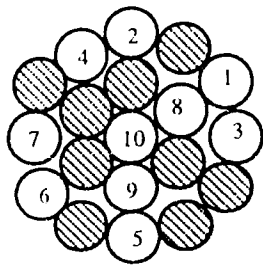
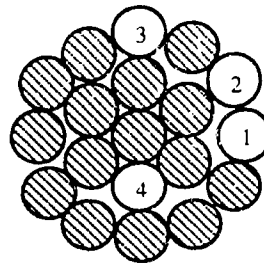


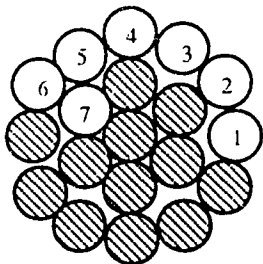
Figure 4.29b Wire breaks versus cycles for SL1



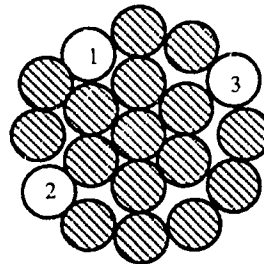
Specimen SL 1



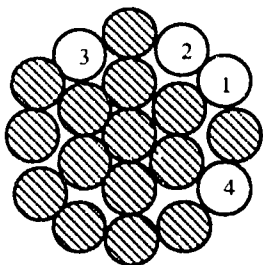
Specimen SL 2



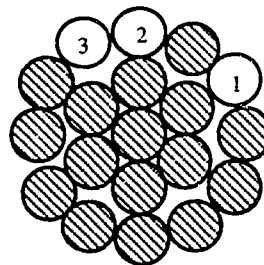
Specimen SL 4



Specimen SL 5



Specimen SS 1



Specimen SS 3

Figure 4.30 Location of wire breaks for 25 mm diameter specimens



Figure 4.31 External wire breaks for specimen SL2



Figure 4.32 External wire break for specimen SL5

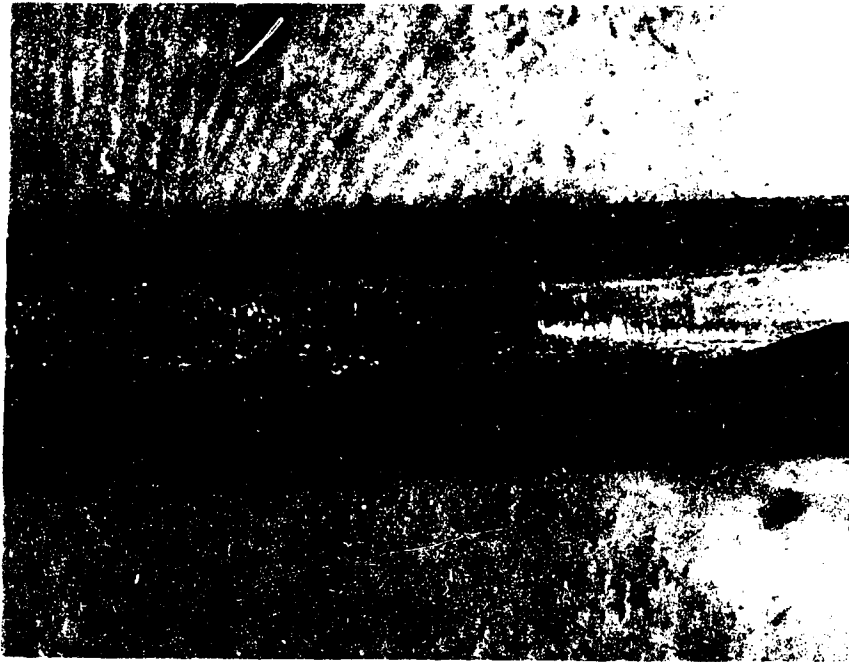


Figure 4.33 Photomicrograph of a fretting surface for specimen SL2—Layer 2

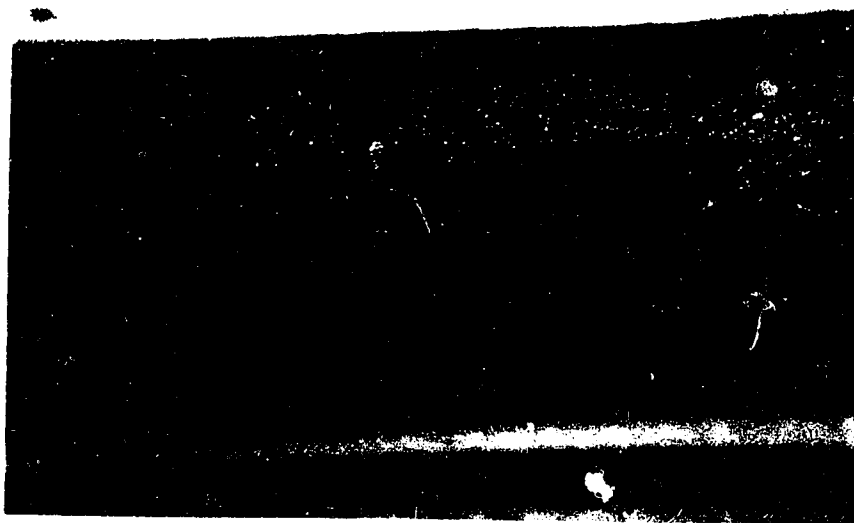


Figure 4.34 Photomicrograph of fretting surfaces for specimen SP7—Layer 5

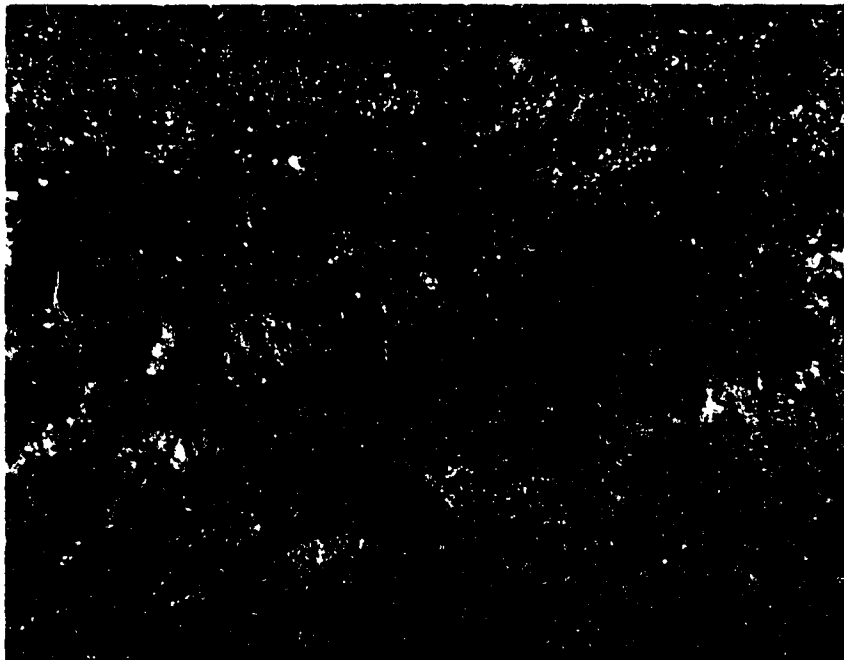


Figure 4.35 Photomicrograph of crack at a fretting surface of SP7—Layer 5

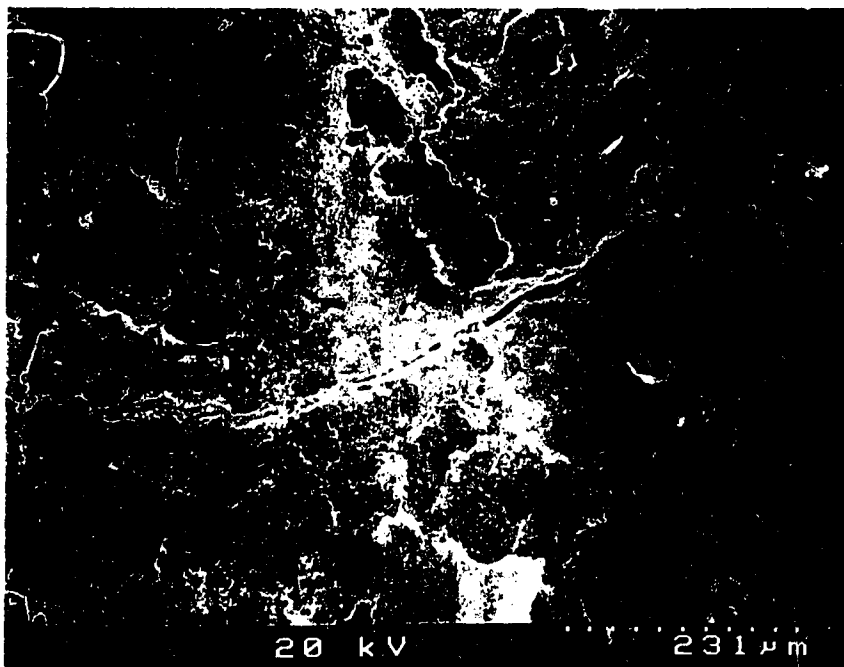


Figure 4.36 Electron photomicrograph of fretting surfaces for specimen SP7—Layer 5

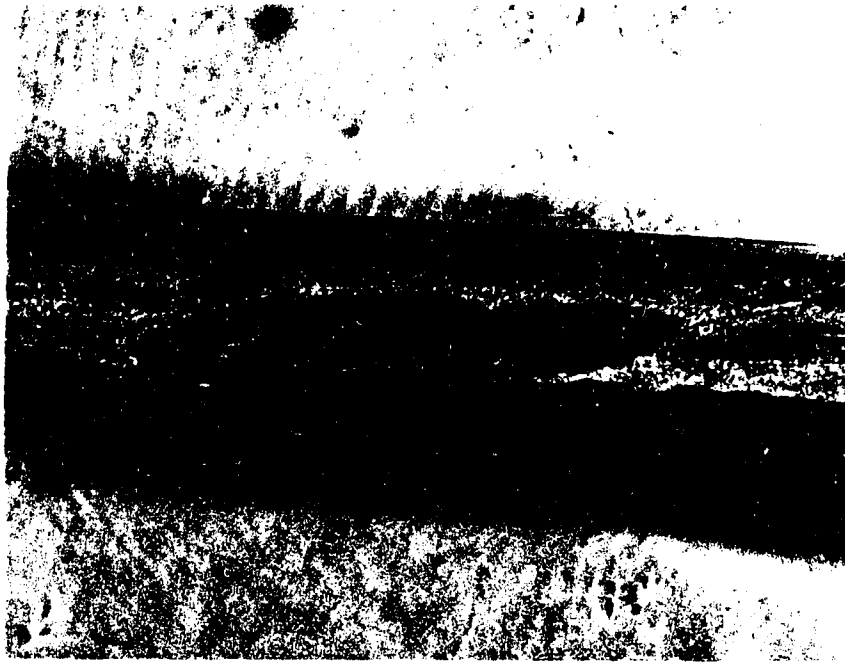


Figure 4.37 Interlayer fretting surfaces for SL4—Layer 2

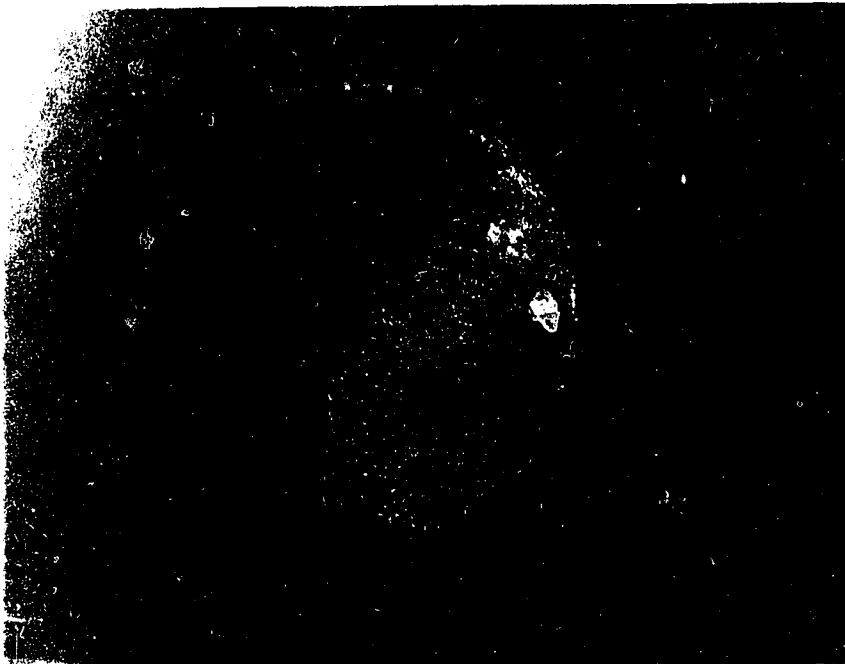


Figure 4.38 Typical wire fracture surface for SP7, layer 5

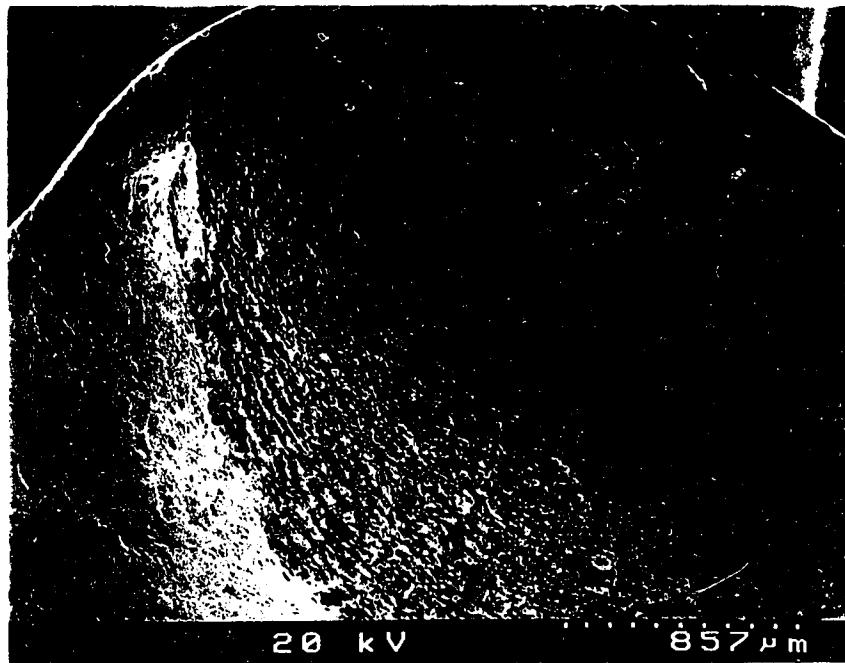


Figure 4.39 Electro photomicrograph of wire fracture surface for SP7—Layer 5

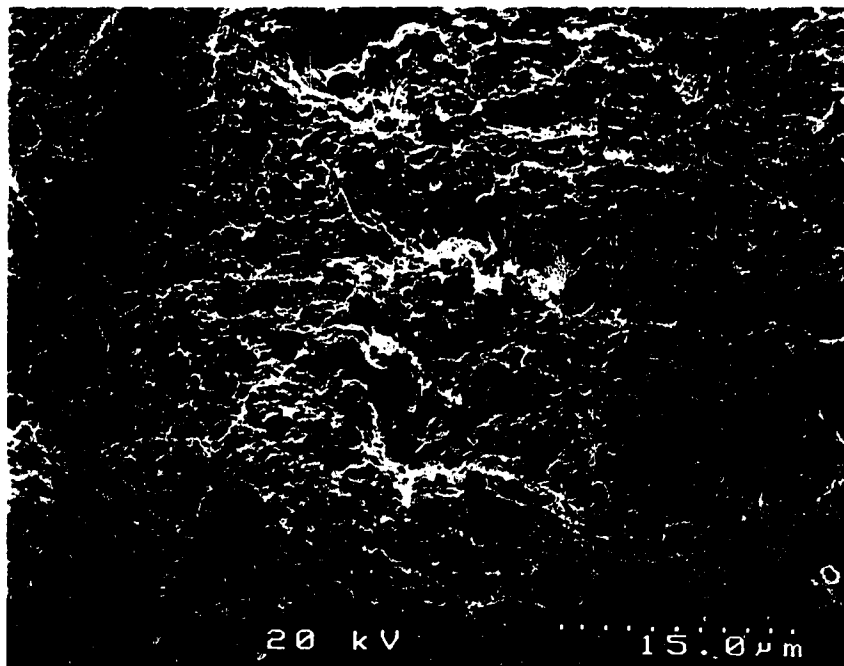


Figure 4.40 Ductile fracture of final fracture Region III

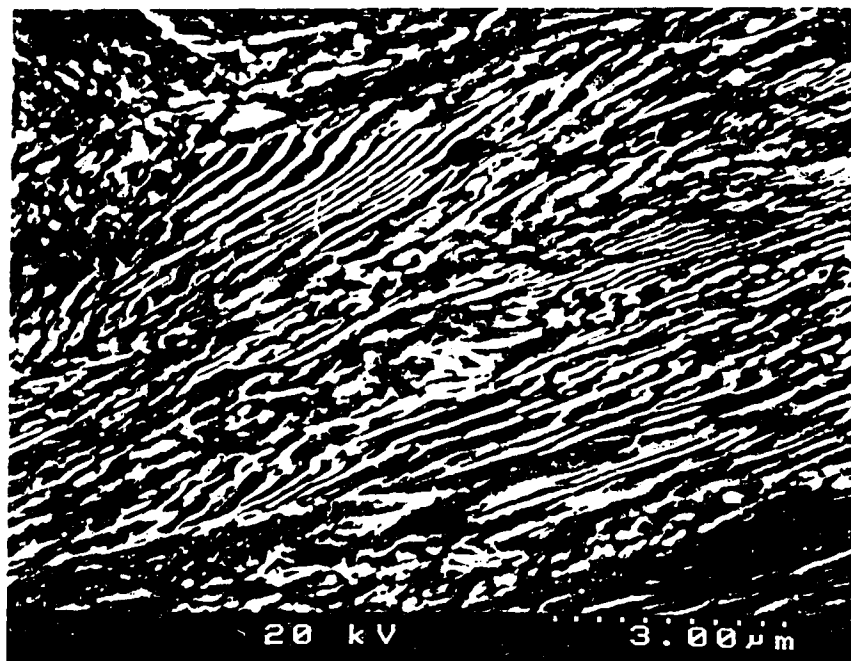


Figure 4.41 Microstructure of an outside 4.034 mm diameter wire

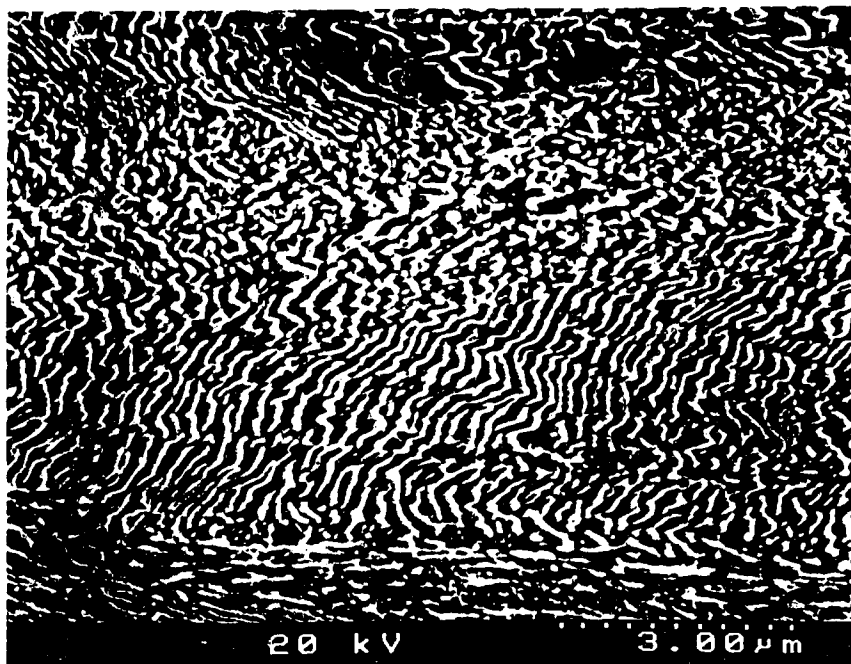


Figure 4.42 Microstructure of an internal 4.034 mm diameter wire—Layer 4

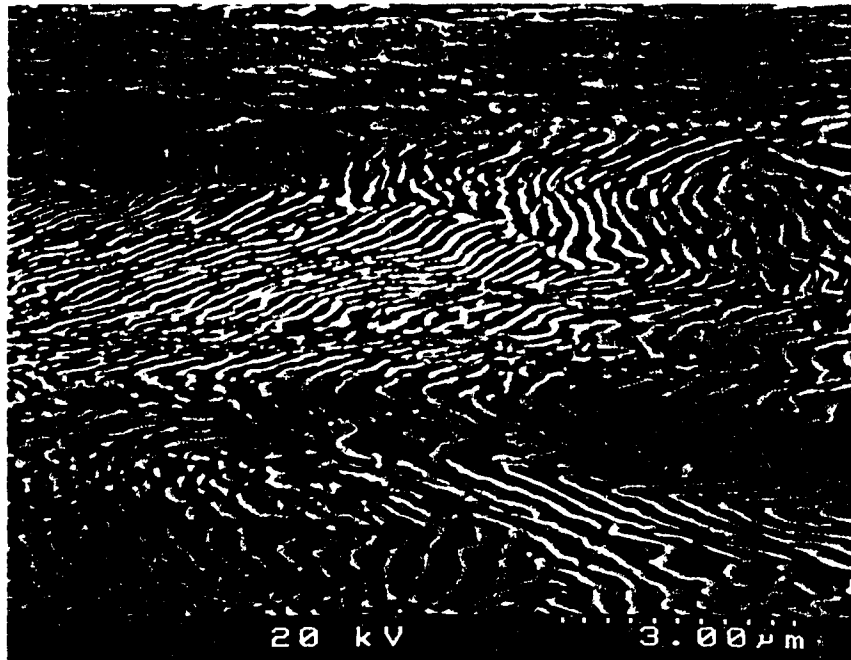


Figure 4.43 Microstructure of a 4.315 mm diameter center wire

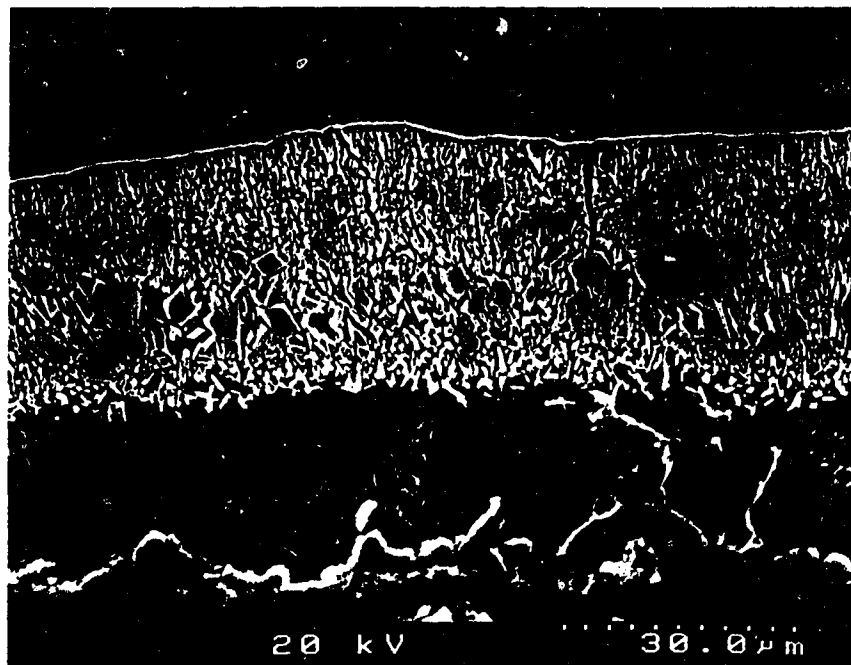
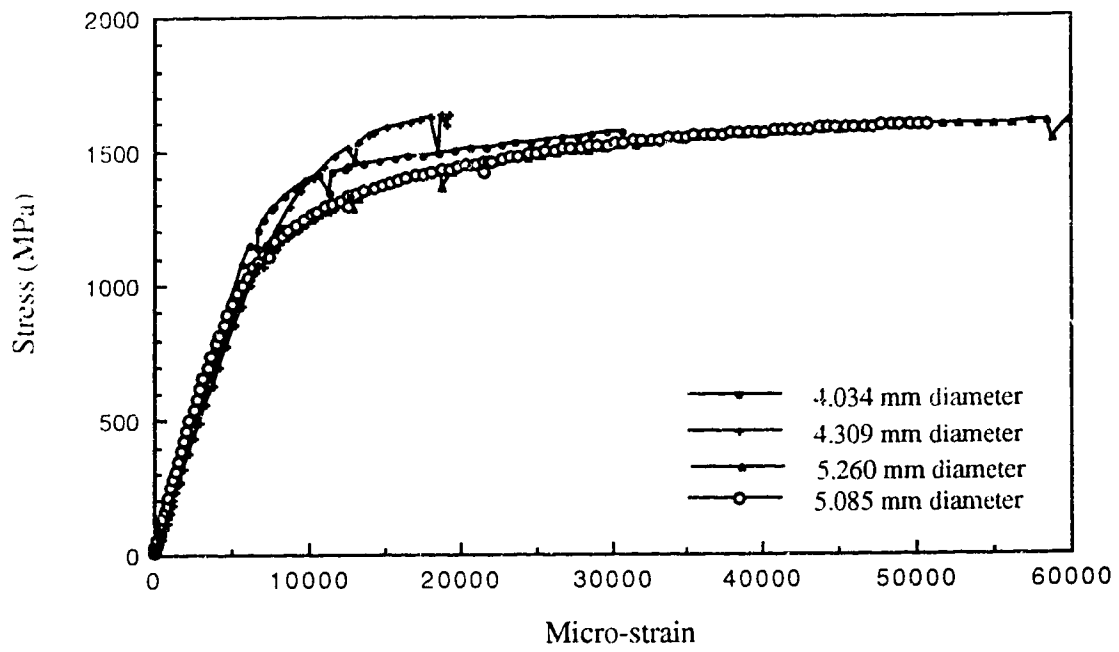


Figure 4.44 Microcracks at the zinc-iron interface of SP7—Center wire



Typical stress-strain curves for different diameter wires

Figure 4.45 Typical stress versus strain curves for steel wires



Figure 4.46 Typical fracture of steel wire coupon test

Chapter 5

Discussion of Test Results

5.1 Introduction

The criteria used to terminate the axial fatigue tests of the multi-layered wire strands were summarized in Table 4.1. For the 45 mm diameter strand, two specimens (SP3 and SP5) were tested to complete destruction. For six other specimens (SP1, SP2, SP4, and SP6 to SP8), testing was stopped after there was a large number of wire breaks and there was significant deterioration of the modulus of elasticity. For the eight 25 mm diameter cables tested, six were tested until a minimum of three wires (of 19) were broken. In the other two cases (SL3 and SS2), the tests were terminated before any wires broke.

In the first part of this Chapter, emphasis will be placed on developing a common discard criterion for the fatigue strength of multi-layered strands. Both the reduction of the cross-sectional area (number of wire breaks) and the deterioration of the modulus of elasticity (including or excluding the end effects) will be used to assess the fatigue damage accumulated by a strand.

After presenting a fatigue life data plot of all tests conducted at the University of Alberta, a regression analysis will be conducted and the parameters that might influence the fatigue performance of a cable will be identified. These include the strand make-up, the length of the test samples, the stress range, the testing frequency, and the specimen temperature. In addition, the performance of the terminations and a cumulative damage theory will be discussed.

5.2 Location of Wire Breaks

Based on examination of the disassembled specimens, it was observed (Section 4.3.2 to 4.3.4) that the wire breaks were distributed more or less randomly along the length of the cable. In order to further examine the periodicity of breaks over the cable length, dismantled specimens will be distinguished as to those that were tested close to destruction and those where testing was discontinued after a relatively small amount of breakage was detected. Starting with the latter category, Figure 5.1 gives the probability distribution of wire breaks along the cable length based on five disassembled specimens from the SL and SS series. These tests were terminated when a minimum of three wires had broken. (Note that specimen SL4 was excluded from the graphical compilation shown in Figure 5.1. Because of a re-calibration problem of the testing apparatus, which induced large secondary

bending movements around the socket region, specimen SL4 had all wire breaks located close to the moving end termination.) In order to conduct a frequency distribution, the class intervals must first be selected. There should be enough intervals to show the variability in the data. A rule of thumb is to use approximately as many as the square root of the number of observations (Ref. 86). Since the total number of break events in the probability distribution shown in Figure 5.1 was twenty-four, the cable length was subdivided into five equal segments. From this graph, it can be observed that the initial wire breaks have an almost equal probability of occurring anywhere along the length of the cable.

As the fatigue test progresses and the number of breaks increases, the cross-section area at a specific location along the cable will decrease to such an extent, that stresses in the remaining wires will be higher than they were initially. Thus, it can be expected that subsequent wire fractures will be concentrated predominantly at this location. If the test is carried out to destruction, this should also be the location of final fracture. The localized phenomenon described above is similar to the necking observed during a coupon test of structural steel, for example.

Specimens SP2, SP4, and SP7 of the SP series were tested close to destruction and can be used to examine the above hypothesis. These specimens were disassembled after completion of the test, and can, therefore, be used for a probability distribution analysis. (The preliminary specimen SP1, which was also dismantled after the test was terminated, was excluded from this probability analysis because out-of-phase movements of the actuators caused all wire breaks to occur close to the moving socket.) The probability distribution of wire breakage along the cable length for specimens SP2, SP4, and SP7 is shown graphically in Figure 5.2. The number of class intervals should be the square root of the number of observations, which is 7, 8, and 9 for specimens SP2 (48 breaks), SP4 (63 breaks), and SP7 (78 breaks), respectively. In the probability analysis reflected in Figure 5.2, an average of eight equal intervals were used to subdivide the length. Specimens SP2 and SP4 had 67% and 25% of the breakages, respectively, occurring at the first interval (close to the fixed end socket). On the other hand, specimen SP7 had 50% of wire breaks concentrated in the middle section (in the sixth length interval of Figure 5.2). With the same logic, specimen SP3 (not shown in Figure 5.2) failed completely at a location corresponding to the ninth length interval (500 mm from the moving end socket). It can be concluded that the final cable fracture can occur anywhere along the length of the cable.

Based on the examination above it was decided that all wire breaks of a specimen (close to or away from the termination) should be included in the data evaluation to be presented in the following sections of this Chapter. It is believed that this is realistic in cases where the end termination are typical of those used in the field and the specimens are long enough to compensate for end effects. These requirements will be discussed in Sections 5.5 and 5.9.

With respect to the distribution of wire breaks amongst the different layers, it was expected that the 25 mm and the 45 mm diameter strands would behave differently. The results are summarized in Tables 5.1 and 5.2 for the 45 mm and the 25 mm diameter strands, respectively. From Table 5.1 it can be seen that 33% of the wires of the large diameter cable are located in the outside layer and 67% are internal wires. Based on the available small statistical sample derived from the dismantled specimens SP2, SP4, and SP7, which is summarized in Table 5.1, it can be concluded that, as an average, 22.5% of the total breaks were external. It should also be noticed that the majority of the wire breaks were recorded in the fourth inner layer (41%). For most of these results, there is a large standard deviation, however.

The 25 mm diameter strand had 63.2% of the wires located in the external layer. This is shown in Table 5.2. The results of the examination conducted on the five specimens of SL and SS series that were later disassembled showed that 89% of the wire breaks occurred in the outer layer.

A different fatigue life should be expected between the two different cable make-ups. Since the majority of wires of the 25 mm diameter strand are exposed (that is, in the outer layer), its fatigue life is more susceptible to flaws and kinks that are introduced during handling of the cable. In addition, the small diameter cable consists of fewer and larger diameter individual wires than does the 45 mm cable. A single external wire break in the 25 mm diameter strand represents 8.3% of the exposed wires. In comparison, for the 45 mm diameter cable one exterior wire break will represent only 3.3% of the exposed wires.

5.3 Modulus of Elasticity

From the static tests performed at specific time intervals, the stiffness of the specimens including and excluding the end effects was obtained. The results were summarized in Appendix A. As is shown in the Tables of Appendix A, the overall modulus of elasticity is consistently lower than the corresponding free-length modulus of elasticity. This is because of the relative movements (wedge action) occurring between the cable and the sockets at the termination region.

The response of the cable stiffness during the fatigue cyclic loading can be subdivided in three distinct regions. They are shown schematically in Figure 5.3.

Region I, the pre-stretching region, reflects the initial loading cycles. In this region, the modulus of elasticity increases as cycles are applied. This phenomenon is due to the constructional stretching of the cable (see Section 1.14), and it is caused by the settlement of the wires in the strands as the load is applied. In a very short time (around 10 cycles, approximately) the stiffness should stabilize. The number of cycles at which the modulus of elasticity stabilizes depends on the cable make-up, the maximum applied load, and any initial pre-stretching that might have been done. Region I represents a small portion of the fatigue life of the cable and, in the case of pre-stretched cables, Region I does not even exist. This region is not of any significant importance for the designer.

Region II in Figure 5.3 represents the cable stiffness under serviceability conditions. The modulus of elasticity in this region is the value assumed by designers when sizing the cable, and it should remain fairly constant throughout its life. Region II covers the largest portion of the fatigue life of a cable. Tables 5.3 and 5.4 summarize the average values and the standard deviations of the modulus of elasticity for Region II for all the specimens tested. Both the overall and the free-length modulus of elasticity are presented. Mean values of the modulus of elasticity for specimens with the same strand make-up are also given in the Tables

The averaged experimental free-length modulus of elasticity can be compared with the simplified equation proposed by Raouf (Ref. 40):

$$E_{\text{full-slip}} = E_s \left(-0.26442 - 2.004046 H + 6.5735 H^2 - 3.3068 H^3 \right) \quad (5.1)$$

where E_s is the modulus of elasticity for the steel wire and H is the Hruska parameter, given by the following expression:

$$H = \sum_{i=1}^N \frac{A_i}{A_T} \cos^4 \alpha_i, \quad \text{with } 0.70 < H \leq 1.0 \quad (5.2)$$

$$A_i = n_i \frac{\pi D_i^2}{4 \cos \alpha_i}, \quad i \leq (N - 1) \quad (5.3)$$

$$A_T = A_C + \sum_{i=1}^{N-1} A_i \quad (5.4)$$

where N is the total number of layers including the core wire; α_i is the lay angle in layer i whose net steel area is A_i ; A_C is the steel area for the core wire; n_i is the number of wires in layer i ; and D_i is the wire diameter of layer i .

The modulus of elasticity of the individual wires for the strands investigated was presented in Table 4.8. Average values of 203 900 MPa and 200 030 MPa were obtained for the 45 mm and the 25 mm diameter cables, respectively. The Hruska parameter can be easily calculated from Eq. 5.2 to Eq. 5.4 based on the strand make-up given in Tables 3.1 and 3.2. It was found to be 0.884 and 0.908 for the 45 mm and the 25 mm diameter cable construction, respectively. Finally, the free-length, full-slip modulus of elasticity can be computed from Eq. 5.1. The results are also presented in Tables 5.3 and 5.4. The ratio of the predicted value to the test result was found to be 1.061 and 1.022 for the 45 mm and 25 mm diameter strands, respectively.

It should be noted that, because of interwire frictional phenomena, the effective axial stiffness of a strand is a function of the applied load. For small variations in load, the changes in the contact forces will be so small that friction is not overcome. For large variations in axial load, full interwire slippage can take place. These two extremes are referred to as *no-slip* and *full-slip* modulus of elasticity. Equation 5.1 estimates the full-slip modulus. The no-slip modulus does not have any practical application since it corresponds to very small loads (even smaller than the pretension load). However, for completeness of the discussion, the fitted polynomial proposed by Raoof (Ref. 40) for the no-slip modulus is presented:

$$\Gamma = \frac{E_{\text{no-slip}}}{E_{\text{full-slip}}} = 3.998 - 7.916 K_1 + 7.238 K_1^2 - 2.321 K_1^3 \quad (5.5)$$

$$\text{where } K_1 = E_{\text{full-slip}}/E_s, \quad 0.40 < K_1 \leq 1.0 \quad (5.6)$$

Finally, in the last region shown in Figure 5.3, the so-called failure Region III, the modulus of elasticity starts to deteriorate rapidly as load cycles continue to be applied. The reduction of the stiffness is accompanied by an elongation of the cable and individual wire breaks. For the design of standing cables, a precise length and a well-defined modulus of elasticity are required. Thus, in Region III the cable has reached the serviceability limit and is in imminent danger of failure. The cycles corresponding to the intersection between Regions II and III can reasonably be considered as failure, and this is of major interest to researchers. In the experiments conducted at the University of Alberta, Regions II and III

were clearly defined, as can be seen from Figures 4.14 (a) to 4.20 (a), which were given in Chapter 4.

5.4 Discard Criterion

The test results of specimens SP2 to SP8 and SL1 will be used for the development of a discard criterion for multi-layered strands. Those particular tests were carried out close to destruction and their fatigue damage was assessed by monitoring both the deterioration of the modulus of elasticity and the number of breaks versus cycles. It was decided (see Section 5.2) that all wire fractures along the cable will be considered in the data evaluation. To be consistent with the above, the overall modulus of elasticity was used instead of the free-length modulus. This will most likely represent the wire breaks that occurred along the length of the cable, close to or away from the terminations.

In the following discussion, double ordinate graphs will be used for the graphical representation of the variation of the fatigue parameters with cycles, and they are shown on Figures 5.4 to 5.11. The abscissa of the graphs represents the number of loading cycles on a logarithmic scale. The ordinate on the left is the deterioration of the overall modulus of elasticity as a percentage of the average serviceability modulus (Region II) given in Tables 5.3 and 5.4. The ordinate on the right side of the graphs is the percentage of broken wires. The percentage is calculated with respect to the total number of individual wires, which is 91 for the 45 mm (series SP) and 19 for the 25 mm (series SL and SS) diameter strands.

The initial portion of the graphs shown in Figures 5.4 to 5.11, which is relatively flat, corresponds to the Region II (Serviceability) of the life of the cable (see Figure 5.3). Region III (Failure) of that general description is the nearly-vertical portion of the graphs depicted in Figures 5.4 and 5.11. As was discussed in Section 5.3, the intersection between these two lines (or somewhere in the transition region between them), could reasonably be considered as the limit of the usefulness of the cable.

Figures 5.4 to 5.11 show that there is a gradual transition from Region II to Region III and that the serviceability limit is not uniquely defined. A failure that lies within the transition region will therefore have to be selected. It can be concluded from Figures 5.4 to 5.11 that after somewhere between 1% and 10% of the wires were broken, the modulus of elasticity deteriorates rapidly and the rate of wire fractures increases significantly. The Acoustic Emission (AE) system also showed that after somewhere between 5% to 10% of wire breaks, a relatively high and constant signal rate was observed. This high event rate can be referred as a damage period and covered about the last 25% to 40% of the total fatigue life

of specimen. The occurrence of a linear damage period implies that at this stage the specimen deteriorates continuously and gradually, while subjected to the constant cyclic loading. In the following discussion, a value of 5% wire breaks is chosen as a failure criterion.

Similar observations and results have also been reported in the literature. Hanzawa et al. (Ref. 55 and 56) used a 5% failure criterion in order to establish the fatigue life of their tested specimens. Waters, Eggar and Plant (Ref.54) found that the modulus of elasticity remained constant until 6 to 10 wire breaks were observed. At that point, the modulus of elasticity started to reduce considerably as successive breakages occurred. Nakamura and Hosokawa (Ref. 68) also considered a specimen to be damaged when 5% of the wires were broken.

A quantitative representation of the fatigue parameters at specific time intervals is given on Table 5.5. At 5% wire breaks, the overall modulus of elasticity is reduced by an average of 2.33%. It is worth noticing that the percentage of stiffness loss is not directly equivalent to the percentage of wire breaks. As it was explained in Chapter 4, this reflects the multiple break type of failure and the existence of interwire friction, which allow a broken wire to redevelop its full carrying capacity within a relatively short length. In addition, from the same Table, it can be concluded that 5% wire breaks corresponds to an average of 57% of strand life. (Strand life, in this Table, is taken as the termination of the test, at which point there was either complete fracture of the sample or large deterioration of the modulus and cross-section. It is not the serviceability limit or failure criterion.)

Based on the above, use of the 5% wire breakage failure criterion can be supported. A dimensionless representation of the fatigue life versus the percentage of wire breaks is given in Figure 5.12 for all specimens (SP2 to SP8 and SL1) that were used for the derivation of the failure criterion. In Figure 5.12, failure N_f was considered to be the loading cycles corresponding to 5% wire breaks. The good correlation of all test data in the dimensionless representation of Figure 5.12 can be considered as evidence of the validity of the failure criterion used.

Because of the phenomenon of multiple breaks, the application of the 5% wire breaks criterion also depends on the length of the sample. For example, 5% wire breaks on a 300 meter long cable is less significant than 5% breakage on a 3 meter long specimen. Obviously, the discard criterion should always be referred to a *standard gauge length*. This standard gauge length, expressed in terms of length-to-exterior lay ratio, should be

established in order to standardize the fatigue test procedures and the acceptance criteria for cables. From a practical point of view, this is the minimum length of a specimen that can be tested without introducing any end effects that might adversely affect the fatigue life of the specimen. In addition, the standard gauge length should be somewhat longer than the recovery length (minimum distance between two consecutive breaks on the same wires) or, to simplify it, a few times longer than the lay length. From the experiments conducted at the University of Alberta, it appears that the specimens should have a minimum length-to-exterior lay ratio greater than about six (see also Section 5.5).

Based on the 5% breakage criterion, all specimens of SL and SS series would be considered as having reached their fatigue life when one broken wire (5% of 19 wires = 1 wire) has been detected.

As an alternative, the fatigue test of a strand could be considered completed when the modulus of elasticity of the strand starts to deteriorate. From the test results presented above (see Table 5.5), a 2.3% deterioration of the modulus of elasticity could be used as a discard criterion. Based on this criterion, the fatigue life of specimen SP1, for example, is the number of loading cycles corresponding to an overall modulus of elasticity of

$$\left(1 - \frac{2.3}{100}\right) \times 166\,379 = 162\,550 \text{ MPa}$$

From a linear interpolation between the values given in Table A.1, the fatigue life of specimen SP1 is found to be around 7.2 million cycles, approximately.

Table 5.6 and Figure 5.13 present the axial fatigue results for all three series of tests conducted at the University of Alberta, a total of 15 individual results. Note that the stress range is given as percentage of the minimum ultimate tensile strength (UTS), as tabulated in ASTM A586 Standard (Ref. 3). This standard format is used to represent axial fatigue test of cables because it facilitates comparison of fatigue data from different sources.

5.5 Effect of Length of the Specimen

The length effect was experimentally investigated only with respect to its influence in the test results. The question is, how short can a specimen be before the end terminations affect the fatigue results? The size effect problem, which is the extrapolation of any test results to predict the fatigue life of a cable that may be hundreds of times longer, was not investigated experimentally.

The length effect was investigated comparing SL specimens with those of SS series. Specimens of both series were prepared from the same 25 mm diameter cable and were

tested at similar stress ranges. The only difference between SL and SS series was the length-to-exterior lay ratio, which was 12.8 and 8.2, respectively. Because of the limited number of specimens tested at different length-to-diameter ratios, a statistical analysis (i.e. regression analysis) is not justified. Only direct comparison between specimens having different length-to-exterior lay ratio and tested under similar conditions will be presented.

From a comparison of specimens SS1 with SL5 and of SS3 with SL1 and SL2, it can be concluded that similar fatigue lives were obtained from both length-to-diameter ratios tested. Therefore, based on these data, the fatigue test results did not depend on the length tested, and the termination region had no influence on the fatigue life of these test specimens.

It is therefore proposed that a minimum specimen length-to-exterior lay ratio of 8 is appropriate for physical testing of cables. More tests are required in order to further substantiate and refine this value, however.

5.6 Regression Analysis and Effect of Strand Make-up

In order to provide information on the quantitative effect of stress range and strand make-up on the fatigue life under constant mean stress, a regression analysis of the test data is required. Because of the limited number of specimens tested at each stress level, assumptions had to be made regarding the shape of the distribution of fatigue life values. Based on the statistical model used by other authors (Tilly, Ref. 16; Raoof, Ref. 63; Paulson et al., Ref. 71) for the evaluation of fatigue tests, it was concluded that a log-normal distribution of fatigue life with respect to stress range could be assumed.

Regression analysis will be conducted for the two different cable constructions. In Section 5.5 it was concluded that the length of the specimens did not have any effect on the fatigue life. All specimens of the SL and SS series, which are made from the same cable, could therefore be grouped together for the regression analysis of the 25 mm diameter strand. Similarly, the specimens of SP series will be used for the statistical analysis of the 45 mm diameter strand. For the specimens that did not fail (SL3 and SS2), the total number of cycles when the test was terminated was used. This will provide a conservative estimate of their fatigue life for the analysis.

In the statistical method used to analyze the results, the logarithmic values of the fatigue lives and the percentage of stress range-to-ultimate tensile strength (UTS) ratio were used for the dependent and independent variables, respectively. The coefficient of determination, r^2 , was used as a measure of goodness of fit for the regression line. This

coefficient represents the portion of the total variability that is accounted for by the fitted simple linear regression model. A value of unity would be expected if the model fits the test data perfectly. The model is expressed as follows:

$$\log N = b_0 + b_1 \log S_r + \varepsilon \quad (5.7)$$

where N is the number of cycles to failure, S_r is the ratio of stress range to UTS (expressed in percent), and ε is the error term. The constants b_0 and b_1 are determined from a least squares regression analysis (Ref. 86). Appendix B gives the details of the regression analysis. Using the model of Eq. (5.7) gives

$$\text{for 45 mm strand:} \quad \log N = 24.85 - 13.58 \log S_r \quad (5.8)$$

$$\text{for 25 mm strand:} \quad \log N = 16.12 - 7.72 \log S_r \quad (5.9)$$

The coefficient of determination, r^2 , was found to be 0.905 and 0.768 for the 45 mm and the 25 mm strand, respectively. The results from the regression analysis are plotted in Figure 5.14.

From a comparison of the coefficients of determination, it is clear that there is a larger scatter for the 25 mm diameter cables than for the 45 mm diameter cables. In addition, from Figure 5.14 it can be seen that the regression line of the 25 mm strand has a steeper slope than does the 45 mm diameter strand. This translates to a lower fatigue life for the 25 mm strand, especially for high cycles. As it was discussed in Section 5.2 the lower fatigue life of the 25 mm diameter strand is probably due to the fact that the smaller strand consists of fewer and larger diameter individual wires. Its fatigue life is therefore more susceptible to flaws and kinks that are introduced during handling of the cable. This is also supported by the fact that the first wire break and the majority of the breaks occurred in the exposed layer of the small diameter specimens.

Equations 5.8 and 5.9 represent an estimate of the mean fatigue life for values of stress range between 15% and 29% of UTS and a constant mean stress of 25% of UTS (350 MPa approximately) for the 45 mm and 25 mm diameter strand, respectively. Confidence limits of the estimate can be formed using the variance of the estimate. The variance of $\log N$, estimated by the regression line of Eq. 5.7, is defined as the sum of squares of the deviations divided by the number of degrees of freedom available for calculating the regression line.

A confidence interval delimited by a number of standard error of estimate from the mean can be constructed as

$$\log N \pm n s_e \quad (5.10)$$

where n is an arbitrary number and s_e is the standard error of estimate (equivalent to the standard deviation for a set of data), given as

$$s_e = \sqrt{\frac{1}{n-2} \sum_{i=1}^n (y_i - \hat{y}_i)^2} \quad (5.11)$$

and where y_i is a measured value of $\log N$, and \hat{y}_i is the corresponding value of $\log N$ predicted by the regression line (Eq. 5.8 and 5.9). The interval delimited by two standard errors of the estimate was found to be —

$$\text{for 45 mm strand:} \quad \log N = 24.85 - 13.58 \log S_r \pm 0.43 \quad (5.12a)$$

$$\text{or} \quad 10^{24.42} S_r^{-13.58} \leq N \leq 10^{25.26} S_r^{-13.58} \quad (5.12b)$$

$$\text{and for 25 mm strand:} \quad \log N = 16.12 - 7.72 \log S_r \pm 0.73 \quad (5.13a)$$

$$\text{or} \quad 10^{15.39} S_r^{-7.72} \leq N \leq 10^{16.85} S_r^{-7.72} \quad (5.13b)$$

5.7 Effect of Stress Range on Fatigue Life

The effect of stress range was investigated experimentally by keeping the mean stress constant at a value of 25% of the specified minimum ultimate tensile strength (UTS), or 350 MPa, and varying the stress range level between 14.8% of UTS (207 MPa) and 28.7% (404 MPa).

The effect of stress range can be quantitatively investigated using the same regression analysis of fatigue data presented in Section 5.6. A log-normal distribution of fatigue life was assumed and Eqs. 5.8 and 5.9 were thus derived for the 45 mm and 25 mm diameter strand, respectively.

In order to determine whether $\log N$ is dependent upon $\log S_r$, a significance test for the slope of the regression expressions 5.8 and 5.9 was performed (Ref. 86). The dependence test is conducted using the 't' test statistic parameter

$$t = \frac{|b_1|}{s_b} \quad (5.14)$$

where b_1 is the slope of the regression line (Eq. 5.7) and s_b the standard deviation of the slope given by

$$s_b = \sqrt{\frac{S_{yy} - b_1 S_{xy}}{(n-2) S_{xx}}} \quad (5.15)$$

and

$$S_{xy} = \sum_{i=1}^n (x_i y_i) - \frac{\left(\sum_{i=1}^n x_i\right)\left(\sum_{i=1}^n y_i\right)}{n} \quad (5.16a)$$

$$S_{yy} = \sum_{i=1}^n (y_i^2) - \frac{\left(\sum_{i=1}^n y_i\right)^2}{n} \quad (5.16b)$$

$$S_{xx} = \sum_{i=1}^n (x_i^2) - \frac{\left(\sum_{i=1}^n x_i\right)^2}{n} \quad (5.16c)$$

The calculated value from Eq. 5.14 is compared with the tabulated value of the Student's distribution, $t_{\alpha/2, n-2}$, for a level of significance of $\alpha = 0.05$ and a number of degrees of freedom of $n-2$. The Student's distribution value was obtained from Table A.4 of Appendix A of Ref. 86. For both the 25 mm and the 45 mm diameter strands, $n = 8$ and $\alpha = 0.05$. The comparison gave

$$\text{for 45 mm strand, } t = 7.56 > t_{0.025,6} = 2.45 \quad (5.17)$$

$$\text{for 25 mm strand, } t = 4.46 > t_{0.025,6} = 2.45 \quad (5.18)$$

Therefore, it can be concluded that, with a risk of $\alpha = 0.05$, the stress range has a significant effect on the fatigue life of the specimen.

Since strand make-up appears to have an influence on the fatigue life of a cable (Section 5.6), it may be statistically incorrect to group such sets of data in order to use a least squares regression analysis to get mean life and safe life curves. However, following the path of other researchers, it is desirable to use large samples for the statistical analysis, and

therefore the test data from both strand make-ups will be treated as a single population. The regression analysis with all test data (sixteen in total) gave the following mean curve:

$$\log N = 15.26 - 6.88 \log R \quad (5.19)$$

The large scatter observed in the test data is reflected by a low coefficient of determination, r^2 , of 0.554. This is largely a reflection that two different strand constructions being examined in the regression. The results from the regression analysis are plotted in Figure 5.15.

Next, the dependence of $\log N$ upon $\log S_r$ was checked using the significance "t" test. The t value, computed from Eq. 5.14 to Eq. 5.16, was compared to the tabulated value of the Student's distribution, $t_{\alpha/2, n-2}$, for a level of significance of $\alpha = 0.05$ and a number of degrees of freedom of $n - 2 = 14$. From the comparison it was found that

$$t = 4.17 > t_{0.025, 14} = 2.15 \quad (5.20)$$

Since the calculated t is greater than the tabulated value of $t_{\alpha/2, n-2}$, it can be concluded that $\log N$ is dependent on $\log S_r$, even for different cable constructions. The comparison of experimental data from different strand construction is therefore justified. A design equation based on a regression analysis will be of a general use only if it is derived from a data bank that consists of large variety of strand make-up.

The confidence interval of Eq. 5.20 delimited by two standard errors of the estimate was calculated using Eq. 5.10 and 5.11 and can be expressed as

$$\log N = 15.26 - 6.88 \log S_r \pm 0.90 \quad (5.21a)$$

$$\text{or} \quad 10^{14.36} S_r^{-6.88} \leq N \leq 10^{16.16} S_r^{-6.88} \quad (5.21b)$$

Figure 5.15 shows the test data with the mean regression line of Eq. 5.20 and the two standard deviation confidence interval described by Eq. 5.21.

As mentioned earlier (Section 5.6), the regression analysis was performed using all the test data obtained in this study, including the discontinued experiments. It was, therefore, assumed that the fatigue limit, defined as the stress below which failure does not occur, is less than the minimum stress range (14.77% of UTS) used in the experimental investigation. The statistical problem of accurately determining a fatigue limit is complicated by the fact that the value of fatigue limit for any given specimen cannot be

measured. A specimen can only be tested at a particular stress range and, if failure occurs, it is known that the fatigue limit is somewhere below the stress range of the test. When determining the fatigue limit, it must be recognized that each test specimen has its own fatigue limit.

Two statistical methods have been recommended for making a statistical estimate of the fatigue limit (Committee E-9 on Fatigue, 1963, Ref. 87), the Probit analysis and the staircase method. A minimum of 50 test specimens is recommended in order to determine the fatigue limit using the Probit method, while a minimum of 30 specimens is recommended when using the staircase method. Because of the large number of test specimens required to obtain a good estimate of the fatigue limit, no attempt has been made in this study to determine a fatigue limit using statistical analysis. Assuming the fatigue limit to lie at the minimum stress range used in the experimental program would be unconservative and, in order to get a reliable estimate of the fatigue limit, more test data are required. Moreover, the existence of any fatigue limit at all, for components subjected to fretting fatigue has been questioned by some researchers (Esslinger, Ref. 45).

5.8 Effect of Specimen Temperature and Test Frequency

The temperature variation with respect to the ambient temperature throughout the cycling test was recorded using a temperature probe located on the outside layer of the specimens. A typical graphical representation of the temperature change during test (cable temperature vs. ambient temperature) is presented in Figure 5.16 for specimen SP5. Test SP5 started at a frequency of 2.0 Hz. After 30 000 cycles, the temperature difference stabilized at 5 °C. At 514 000 cycles, the frequency was increased to 3.0 Hz. This was accompanied by a 1.5 °C increment in the temperature difference. At 1.8 million cycles, the frequency was raised further, to 3.5 Hz. The temperature difference between the specimen and the environment reached the value of 9.0 °C at 7.9 million cycles. This temperature difference then remained fairly constant until complete fracture of the specimen occurred at 9.4 million cycles. The maximum temperature experienced by the specimen during the test was 33.6 °C. From the temperature monitoring of all specimens it was found that with a maximum testing frequency of 3.5 Hz the temperature difference stabilized at a value of about 10 °C.

Only the average temperature of the outside layer was recorded. Of course, the interwire fretting locations experience higher temperatures, but this could not be recorded with the available instrumentation.

Although the testing frequency ranged between 1.5 Hz to 3.5 Hz, depending upon the loading characteristics of a given test specimen, it is believed that this did not have any significant effect on the experimental results. Esslinger (Ref. 88) observed an influence of the test frequency on the fatigue test results for specimens tested at relatively high stress ranges (600 MPa to 800 MPa) when the frequency was raised from 3.5 Hz to 105 Hz. It was observed that, at lower frequency, higher plastic strain ranges appears, which led to a shorter life. Esslinger believes that the effect of testing frequency vanishes as the stress range approaches the fatigue limit. Such a large variation in the frequency never occurred on the experiments conducted at the University of Alberta.

5.9 Performance of Cable Termination

Although an investigation of the effect of the end clamping devices used was not one of the specific objectives of the present research program, their importance to the success of the axial fatigue tests was realized from the beginning and special attention was given to designing them. The socket detail that was developed at the University of Alberta was presented in Section 3.2.1.

Sockets designed for fatigue tests of cables should be similar to the ones used in real structures. The socketing material, the dimensions of the cone, and bearing clamping plates used in the physical tests conducted at the University of Alberta were similar to those found on real structures. Cold socketing material was used since it is considered to have a higher fatigue performance than zinc alloy hot pouring metal, which has often been used in the past.

The most important characteristics of a well-designed socketing system for fatigue tests is the avoidance of stress and fracture concentration in the termination region of the sample. Because a uniform distribution of breakages along the dismantled specimens (see Section 5.2 and Figure 5.1) was observed in these tests, it can be concluded that the above requirement was satisfied. Finally, from the individual wires of specimens SP1 and SP2, which were marked at the socket locations, it was concluded that slippage did not occur between the wires and the socketing material.

5.10 Cumulative Fatigue Damage

In the majority of fatigue tests, uniform load cycles are applied to the specimen until the cumulative effect of all cycles eventually produces failure (unless the stress range is below the endurance limit). This is called constant amplitude testing. When the load cycles are applied in an irregular manner (a condition which likely prevails in bridges as different type

of vehicles cross), the cumulative effect of these events can also lead to fatigue failure. This is called variable amplitude loading. Fatigue effects of loading events other than uniform cycles are referred to as cumulative damage.

A cumulative fatigue damage theory is necessary to account for the previous damage history and loading sequence effect. Two types of cumulative damage theories exist: linear and non-linear. Linear methods assume that the damage rate of each cycle is independent of the load history. In contrast, non-linear models account for load interactions. Although non-linear models are more realistic, such models are generally semi-empirical in nature and, consequently, those laws can be used with confidence only for the cases in which the parameters were applicable. A great number of variable amplitude tests need to be conducted for the derivation of a non-linear damage theory, since different combinations of loading sequences need to be investigated. Furthermore, since non-linear models account for loading sequence, a good knowledge of the loading spectrum applicable to the problem at hand is imperative if the model is to yield satisfactory results.

The cumulative fatigue damage theory that is customarily used in civil engineering practice is the linear theory proposed by Palmgren in 1924 and further developed by Miner in 1945 (Fuchs and Stephens, Ref. 41). In spite of the inability of the Palmgren-Miner law to account for the loading sequence, it is used extensively, mostly for its simplicity. According to this model, the fatigue damage sustained under one cycle of loading is $1/N_f$, where N_f is the fatigue life under uniform load cycling. The total damage from all stress range levels that are applied to the details is, of course, the sum of all such occurrences:

$$\sum \frac{n_i}{N_{fi}} = 1 \quad (5.22)$$

where n_i = number of cycles that take place at stress range level i

N_{fi} = number of cycles that would cause failure at stress range level i

In order to experimentally derive a cumulative damage theory, variable amplitude tests are required. They are time consuming and costly tests and require knowledge of the expected history as primary input. Potts et al. (Ref. 53) reported the results of a variable amplitude tension fatigue test program conducted on 19 mm diameter ropes. The Miner damage summation was found to range between 1.25 and 1.43 at the time of failure. This indicated that linear damage cumulative hypothesis consistently underestimated the total axial fatigue life. Shifting of the fretting zone from one area to the other as the different block loads were applied was used to explain the high values of the Miner summation.

The two-step variable amplitude test conducted at the University of Alberta (Section 4.3.3) also showed that the linear damage cumulative hypothesis will underestimate the total axial fatigue life. Photomicrographs of the fretting areas (Figure 4.37) confirm that the location of the fretting patches change as the level of the cycling load changes. Obviously, more variable amplitude tests will be required in order to establish a cumulative damage expression. Until then, the lower bound of the damage sum suggested by Potts (Ref. 53) should be used:

$$\sum \frac{n_i}{N_{fi}} = 1.25 \quad (5.23)$$

Table 5.1 Distribution of breaks by layer for the 45 mm diameter strand

	Layer ¹ 1	Layer 2	Layer 3	Layer 4	Layer 5	Layer 6
Wire Distribution	33%	26.3%	19.8%	15.2%	6.6%	1.1%
Specimen SP2	37.2%	22.9%	20.8%	14.6%	4.2%	0%
Specimen SP4	28.6%	0%	3.2%	65.1%	3.2%	0%
Specimen SP7	1.3%	14.1%	16.7%	43.6%	20.5%	3.8%
Average	22.5%	12.3%	13.6%	41.1%	9.3%	1.3%
Standard Deviation	15.4%	9.4%	7.5%	20.7%	7.9%	1.8%

(1) Layers are numbered from outer towards inner layers.

Table 5.2 Distribution of breaks by layer for the 25 mm diameter strand

	Layer ¹ 1	Layer 2	Layer 3
Wire Distribution	63.1%	31.6%	5.3%
Specimen SL1	70%	20%	10%
Specimen SL2	75%	25%	0%
Specimen SL5	100%	0%	0%
Specimen SS1	100%	0%	0%
Specimen SS3	100%	0%	0%
Average	89%	9%	2%
Standard Deviation	13.6%	11.1%	4%

(1) Layers are numbered from outer towards inner layers.

Table 5.3 Modulus of elasticity of 45 mm strand and comparison with Raouf's prediction

		Overall Modulus of Elasticity (MPa)		Free-length Modulus of Elasticity (MPa)	
Specimen	No. ¹	Arithmetic Mean Value	Standard Deviation	Arithmetic Mean Value	Standard Deviation
SP1	7	166 379	254	—	
SP2	4	162 057	797	176 578	100
SP3	2	166 345	686	177 825	1068
SP4	2	168 515	1605	176 340	566
SP5	20	167 929	974	177 362	746
SP6	2	167 100	240	176 410	85
SP7	3	168 493	266	175 860	1216
SP8	2	163 695	1888	171 887	1467
Average		166 863	868	176 744	784
Raouf's Analytical Prediction for Free-length Modulus				166 572	
Test / Prediction Ratio				$176\,744 / 166\,572 = 1.061$	

(1) Total number of static tests conducted in Region II.

Table 5.4 Modulus of elasticity of 25 mm strand and comparison with Raouf's prediction

Specimen	Mean Value of Overall Modulus of Elasticity ₁ (MPa)	Mean Value of Free Length Modulus of Elasticity (MPa)
SL1	167 800	176 910
SL2	167 080	176 570
SL3	172 300	176 130
SL4	169 730	177 310
SL5	172 210	173 840
SS1	162 155	174 590
SS2	159 525	177 610
SS3	164 550	172 480
Mean Value	166 919	175 680
Standard Deviation	4608	1840
Raouf's Analytical Prediction for Free-length Modulus		171 940
Test / Prediction Ratio		$175\,680 / 171\,940 =$ $= 1.022$

- (1) Since typically only two static tests were conducted for each specimen in Region II, standard deviations for the mean value of the modulus of elasticity are not presented.

Table 5.5 Wire breaks and modulus of elasticity at specific cycle intervals

Specimen	1 st Break Cycles	1 st Break Modulus ¹ (MPa)	5% Breaks Cycles	5% Breaks Modulus (MPa)	Reduction of Modulus ² (%)	End of Test Cycles	End of Test Modulus (MPa)	% of Fatigue Life at 5% Breaks ³
SP2	422 000	161 250	661 054	157 700	2.69	2 717	133 020	25
SP3	232 752	166 830	284 374	157 841 ⁴	5.11	418 262	— 5	68
SP4	93 782	167 380	180 475	162 830	3.37	308 048	141 190	58
SP5	470 000	168 860	6 942 000	167 380	0.33	9 372 000	— 5	74
SP6	286 218	167 270	810 410	165 330	1.06	1 957 640	159 180	41
SP7	293 909	168 720	1 345 617	165 700	1.66	2 121 100	160 910	63
SP8	97 022	165 030	178 624	158 981 ⁴	2.88	204 600	156 810	87
SL1 ⁶	226 578	165 280	226 578	165 280	1.5	566 300	140 640	40
			Average		2.33	Average		57
			Sample Standard Deviation		1.51	Sample Standard Deviation		20.41

- (1) Overall modulus of elasticity.
- (2) The reduction is with respect to the overall modulus of elasticity given on Tables 5.3 and 5.4.
- (3) Percentage of the ratio of cycles at 5% breaks divided by the cycles at the end of test.
- (4) Linear interpolation was used.
- (5) Complete failure of specimen. Modulus of elasticity is not available.
- (6) For the 25 mm diameter strand the first wire break corresponds to 5% wire breaks.

Table 5.6 Axial fatigue life of tests conducted at the University of Alberta

Specimen	Stress Range (% of UTS ¹)	Fatigue Life (cycles ²)
SP1	21.50	7 200 000
SP2	26.33	661 100
SP3	26.33	284 400
SP4	26.33	180 500
SP5	21.50	6 942 000
SP6	23.92	810 400
SP7	23.92	1 345 600
SP8	28.67	178 600
SL1	22.11	226 600
SL2	22.11	306 100
SL3	14.77	10 000 000 ³
SL4	22.11	2 424 400
SL5	25.82	180 000
SS1	25.82	180 500
SS2	18.40	4 183 000 ³
SS3	22.11	276 290

(1) The minimum ultimate tensile strength as per ASTM A586 is 1409 MPa for SP specimens and 1402 MPa for SL and SS specimens.

(2) The number of cycles are rounded to the closest 100 cycles.

(3) Test was discontinued with no broken wires.

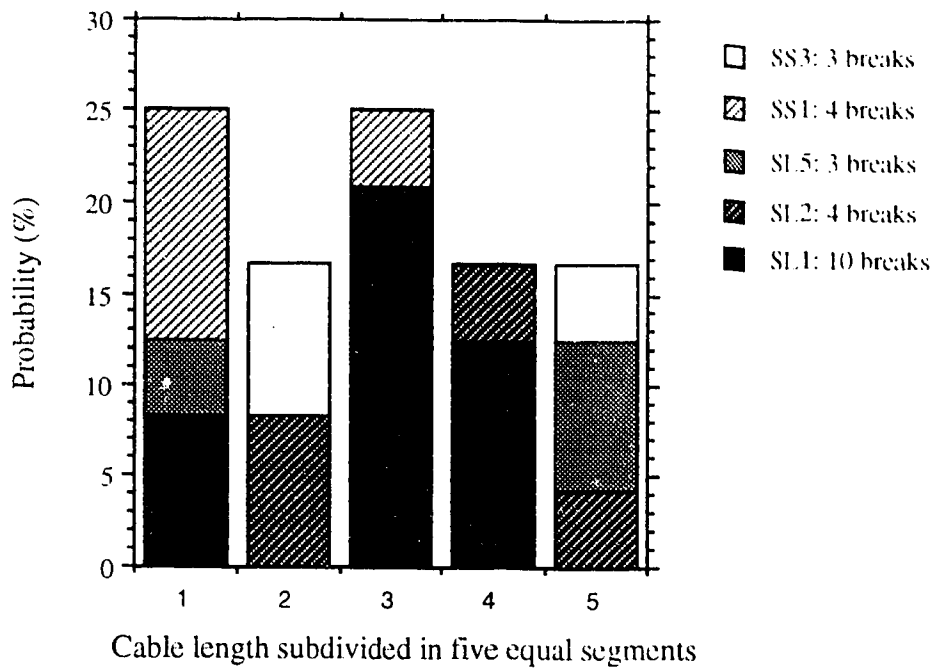


Figure 5.1 Probability distribution of wire breaks along cables of SL and SS series

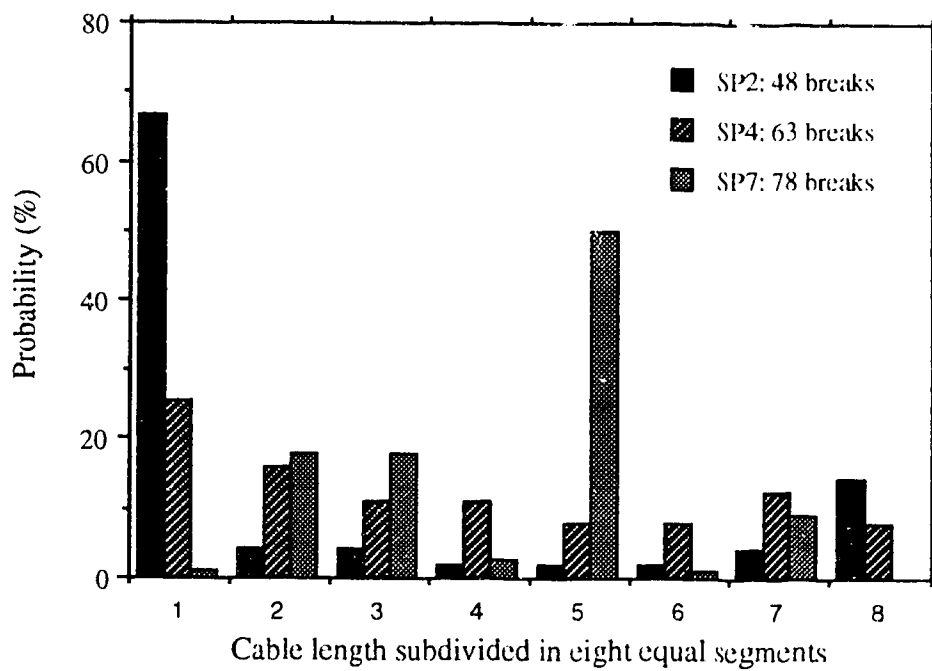


Figure 5.2 Probability distribution of wire breaks along the cable (SP2, SP4, and SP7)

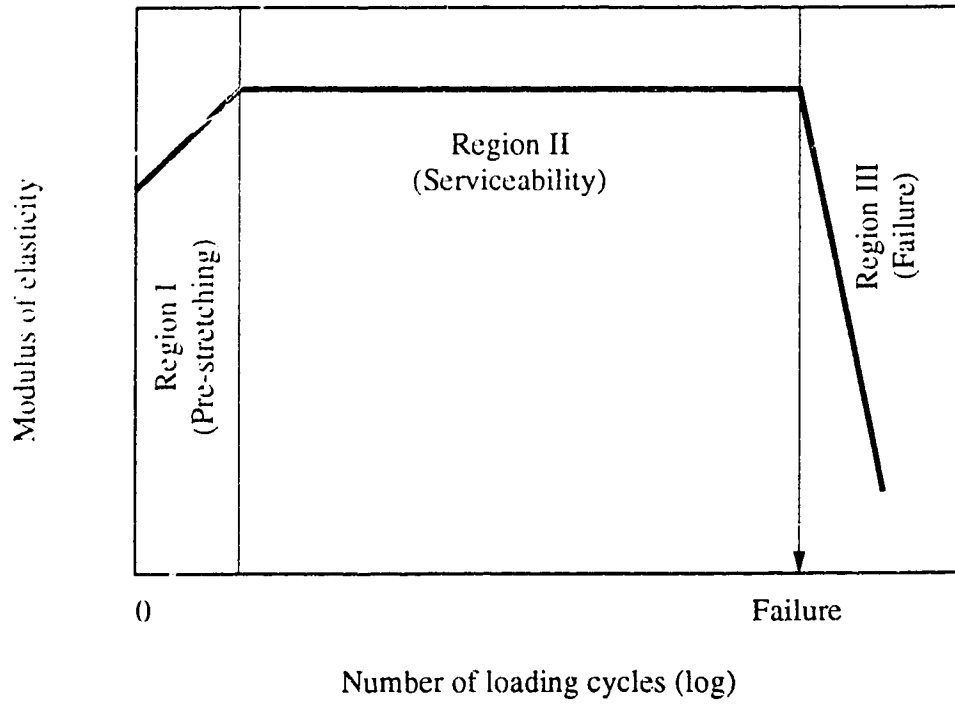


Figure 5.3 Schematic representation of cable stiffness change with fatigue cycles

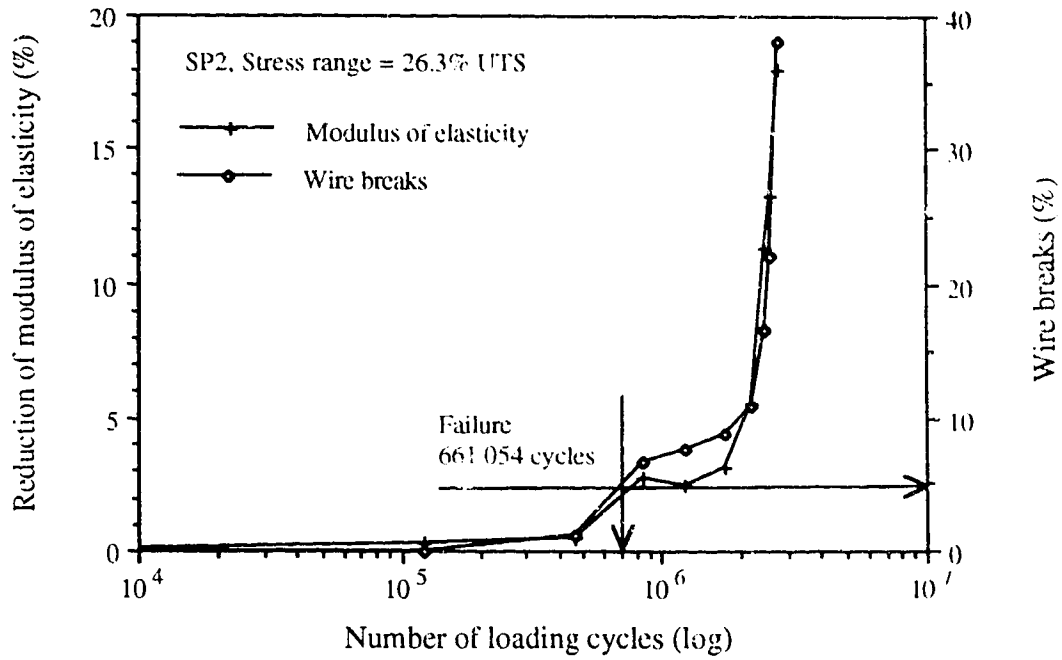


Figure 5.4 Fatigue parameters versus life for specimen SP2

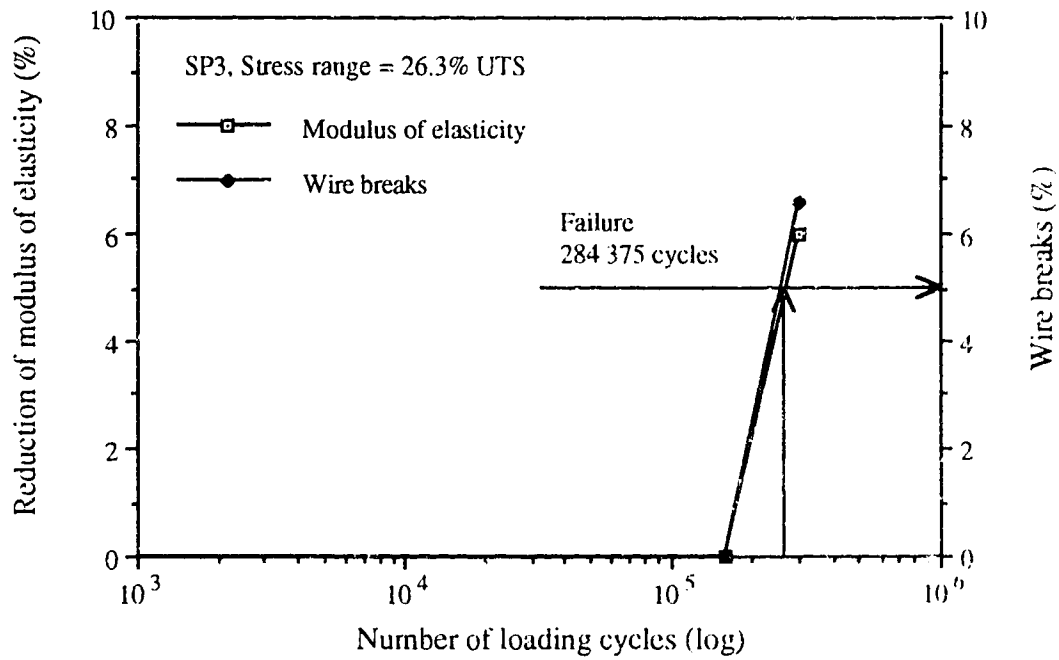


Figure 5.5 Fatigue parameters versus life for specimen SP3

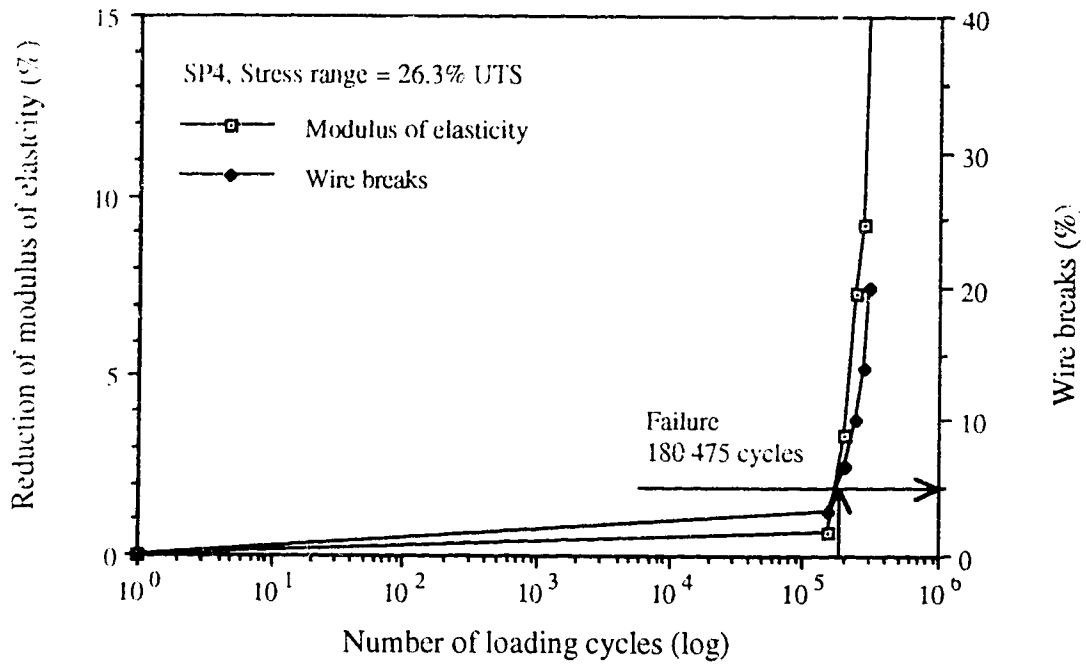


Figure 5.6 Fatigue parameters versus life for specimen SP4

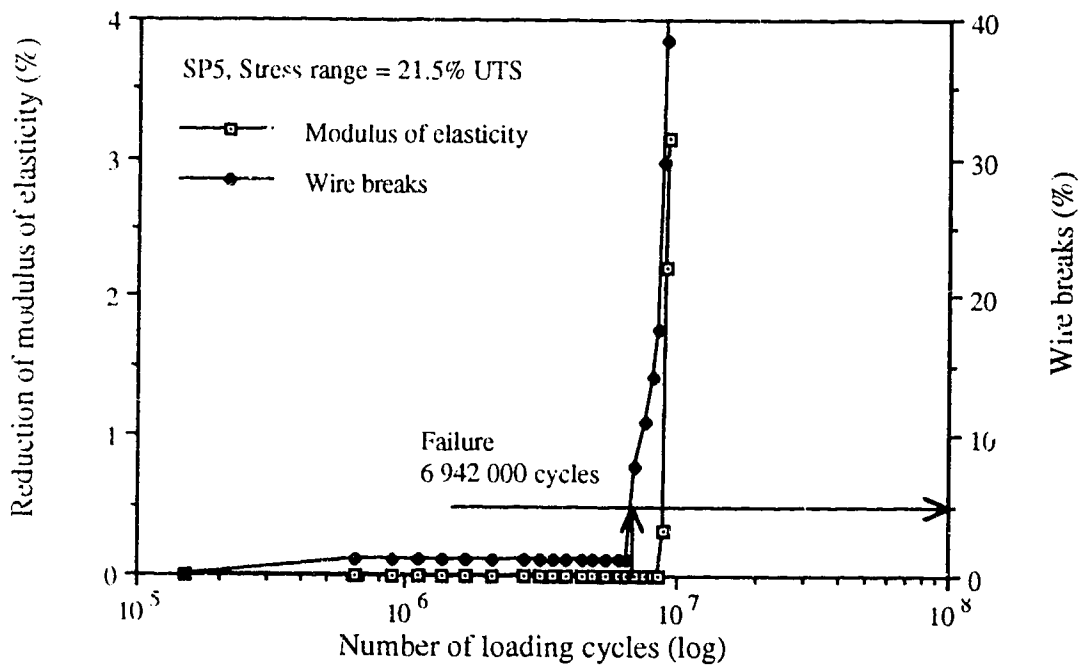


Figure 5.7 Fatigue parameters versus life for specimen SP5

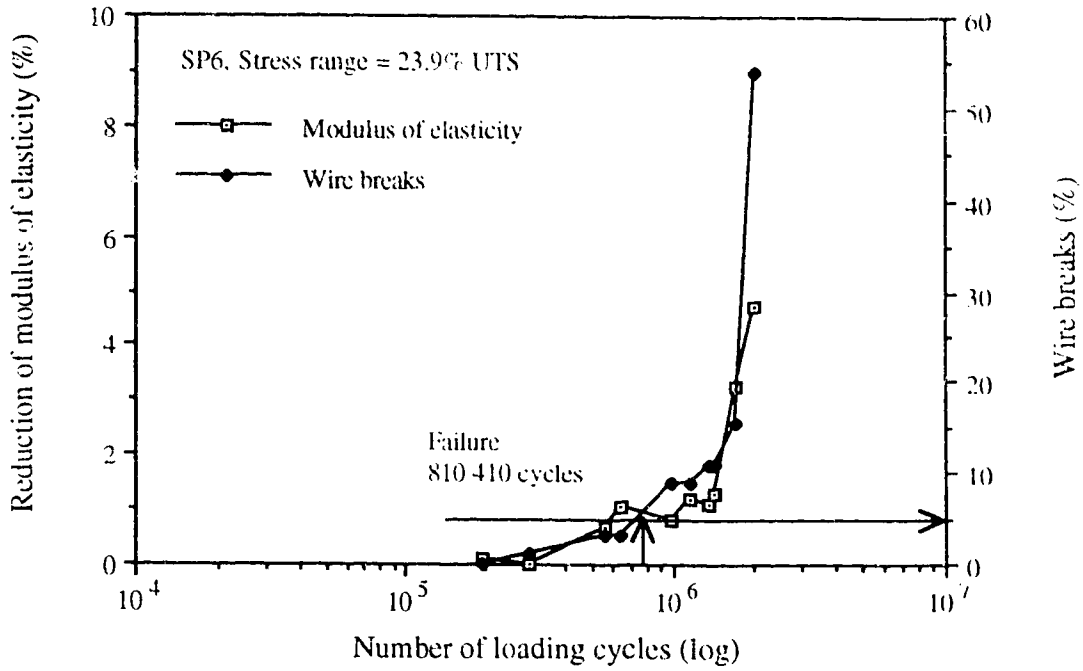


Figure 5.8 Fatigue parameters versus life for specimen SP6

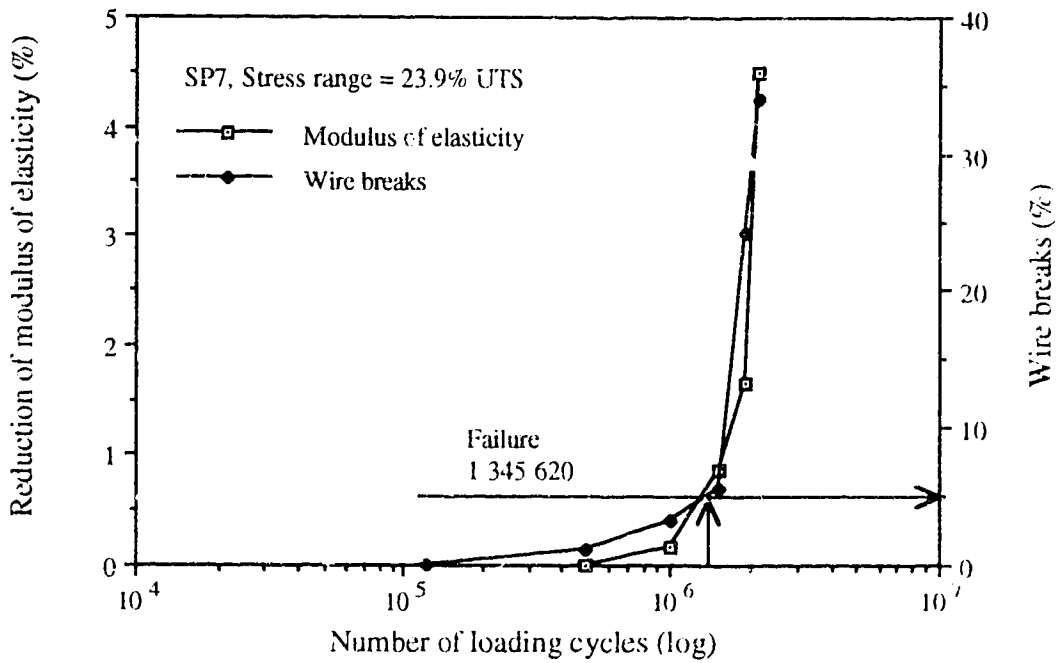


Figure 5.9 Fatigue parameters versus life for specimen SP7

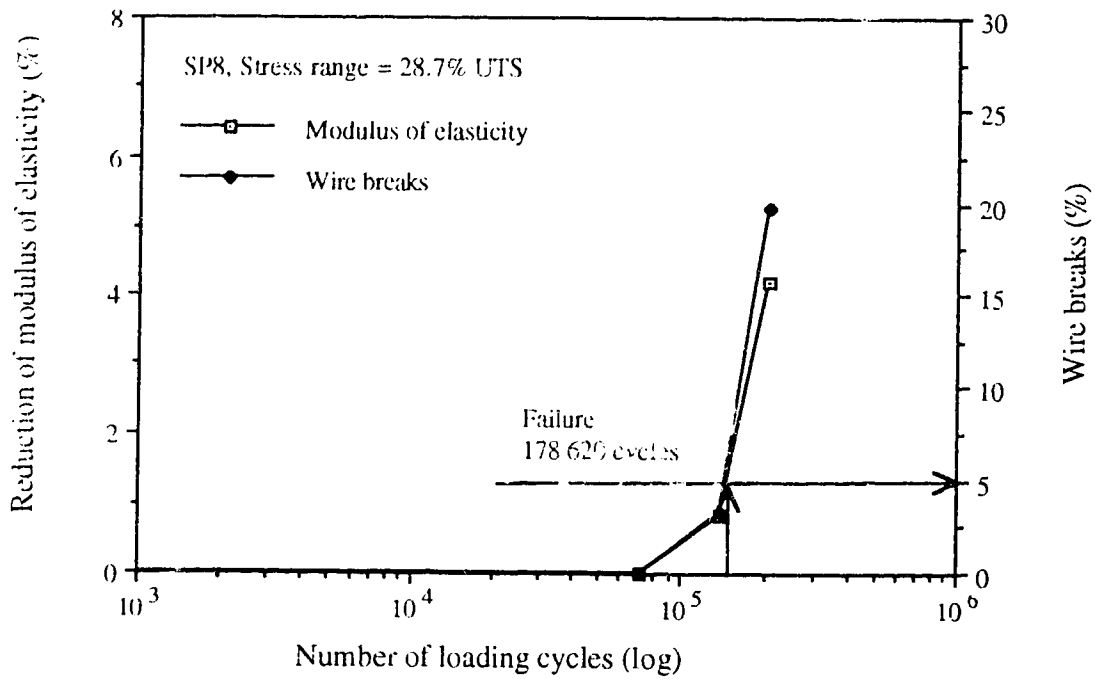


Figure 5.10 Fatigue parameters versus life for specimen SP8

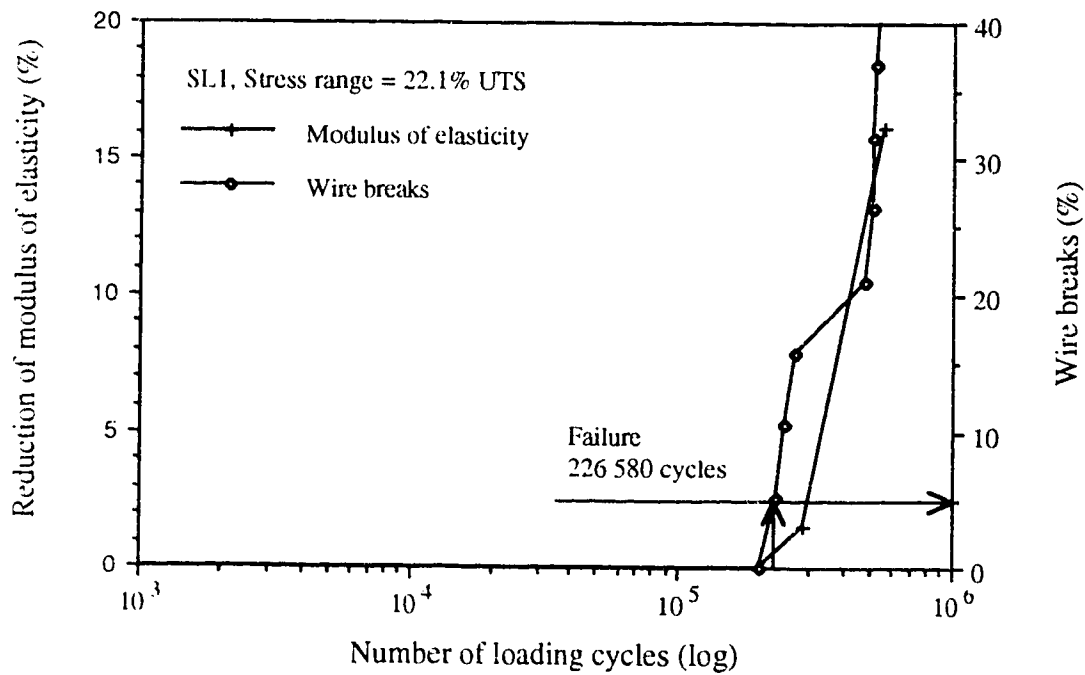


Figure 5.11 Fatigue parameters versus life of specimen SL1

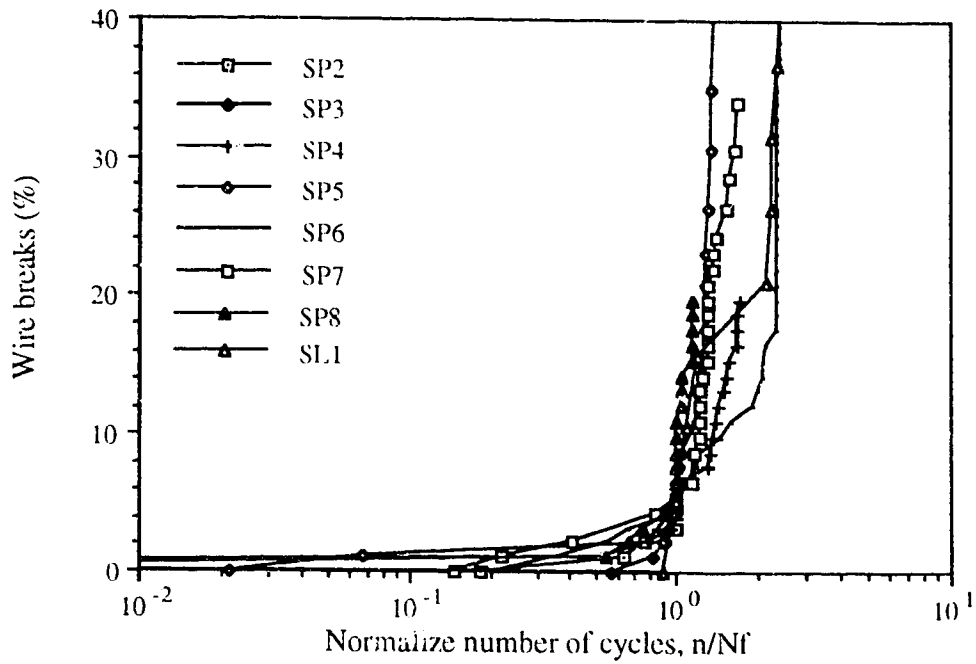


Figure 5.12 Dimensionless representation of fatigue life versus wire breaks

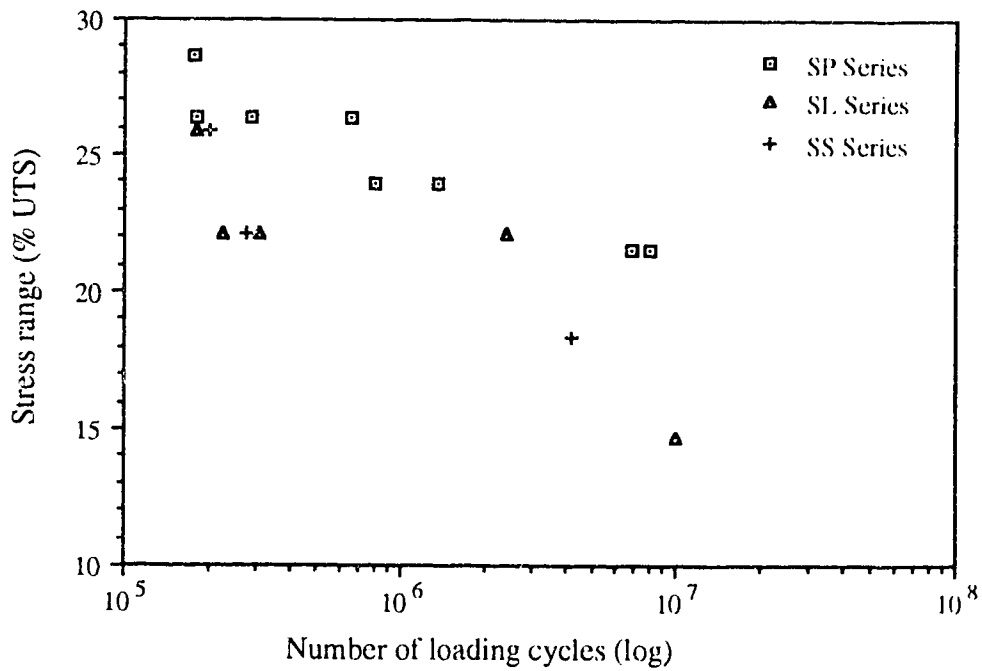


Figure 5.13 Axial fatigue life versus stress range (S-N curve)

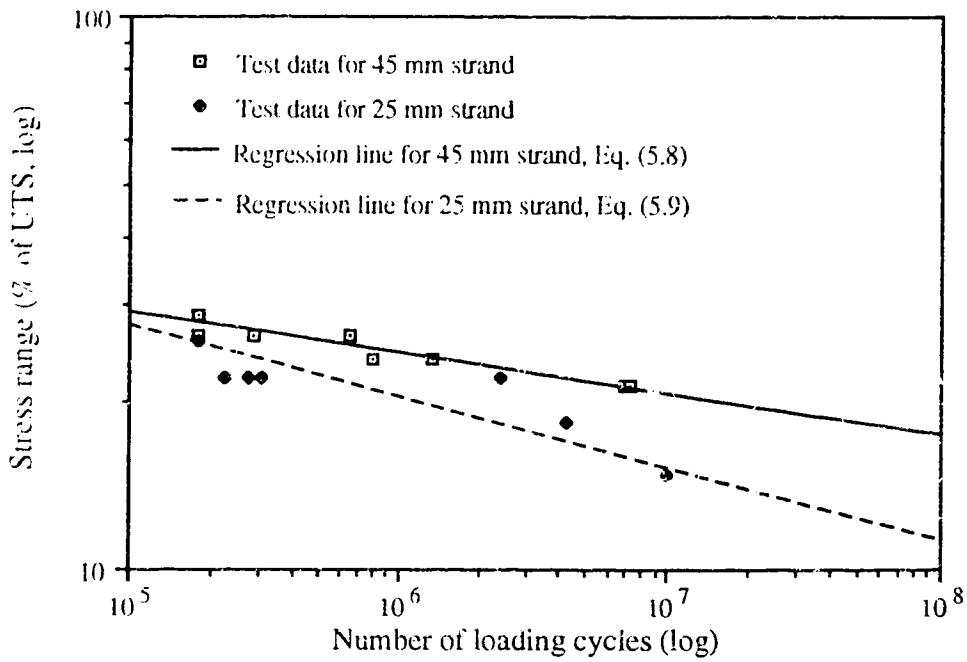


Figure 5.14 Effect of strand make-up

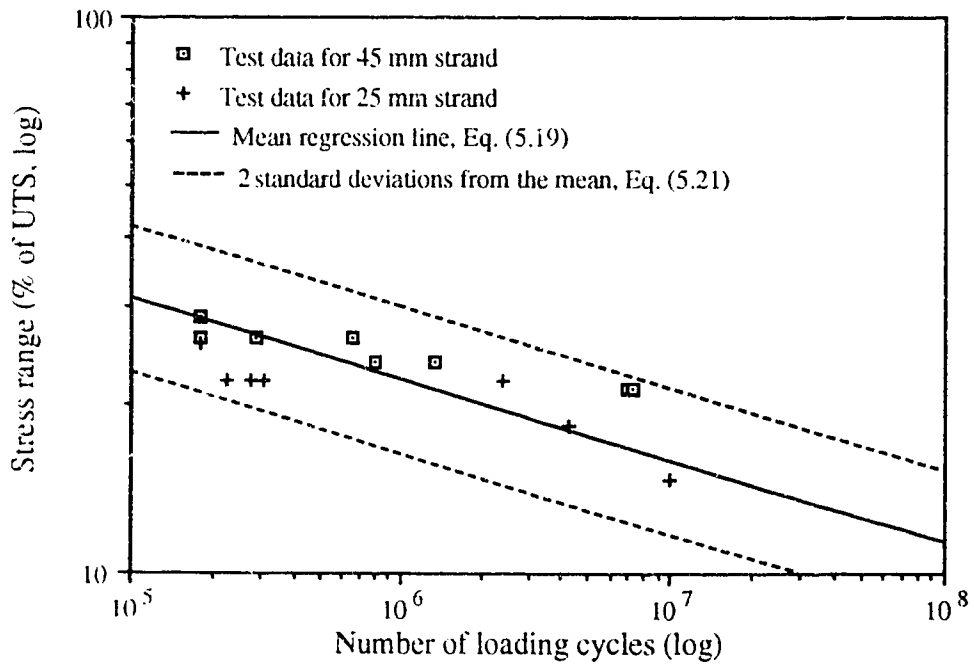


Figure 5.15 S-N curve for all test data

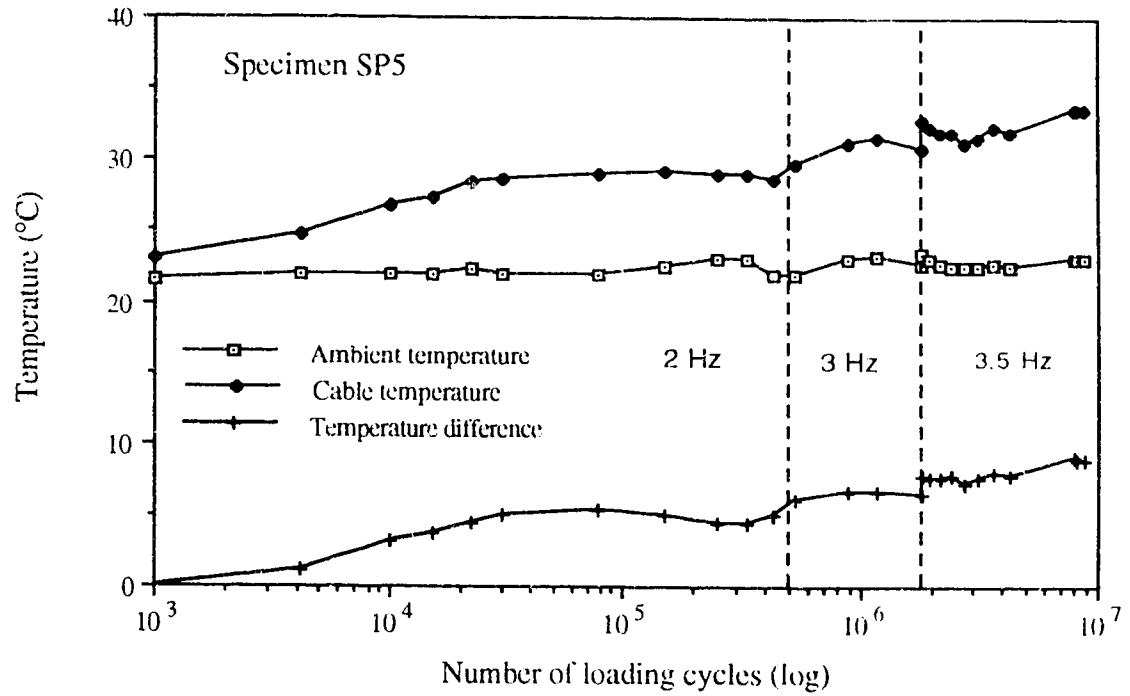


Figure 5.16 Effect of testing frequency on specimen temperature

Chapter 6

Comparison of Test Results with Work of Other Investigators

6.1 Introduction

Experimental evidence for the reduction of fatigue strength as it is affected by cable length was presented in Section 2.4. Since full length cables cannot be tested because of physical limitations, the effect of length on the fatigue life of a real cable must be investigated using statistical techniques.

In the first part of this Chapter, the mathematical model developed by Castillo et al. (Ref. 50) will be used to extrapolate the fatigue strength of tested specimens to practical real lengths and to predict the fatigue life of a bridge cable based on tests of limited duration (runout tests). This five-parameter model was briefly presented in Section 2.4.1.

Also in this Chapter, a selective review of the literature concerned with the axial fatigue performance of strands will be presented. The objective is to compare and evaluate the work presented here in light of other work conducted in the same area, and also to attempt to pool the available fatigue data into one data base from which design guidelines can be formulated. Finally, the most commonly used design curves will be compared with the selected data from the literature.

6.2 Castillo et al. Statistical Model

Castillo et al. (Ref. 50) proposed a mathematical model for analyzing fatigue data of wires, strands, and cables based on statistical requirements (stability, limit and compatibility conditions) and physical requirements (i.e. endurance limit).

Physical requirements — The model should be able to reproduce the real statistical properties of the experimental data. Experimental evidence from a large number of fatigue tests of single wires presented by Birkenmaier and Narayanan (Ref. 19) and Castillo et al. (Ref. 50) indicates:

- a non-linear relation between the median of N (number of cycles) and $\Delta\sigma$ (stress range)
- a standard deviation function that increases with decreasing $\Delta\sigma$, and
- the existence of an endurance limit.

According to Castillo, it is reasonable to take the size (length) effect into consideration using the weakest link principle (see also section 2.4.1). This principle states that the fatigue strength of a cable of length L (composed of n imaginary pieces of length L_0) will be that of the weakest connected sub-element, i.e.

$$N = \min(N_1, N_2, \dots, N_n) \quad (6.1)$$

where N is the number of cycles to failure of the cable and N_i (with $i = 1, 2, \dots, n$) is the number of cycles to failure for the sub-elements.

The flaws in the material located at the fretting location (and which produce the fatigue failure) can be assumed to be either systematically or independently distributed along the wire. In the first case, there is a statistical dependence between neighboring pieces, but independence can be assumed for distant ones. In the second, the statistical independence can be assumed throughout. If the fabrication process is regular and the storage and manipulation process is homogeneous, it is reasonable to assume the same distribution for the fatigue strength of different pieces. Knowing the cumulative distribution function (cdf), $F_{L_0}(x)$, for the sub-elements (i.e. test data) of length L_0 , the cdf, $F_L(x)$, of the cable with length L can be derived from:

$$F_L(x) = 1 - [1 - F_{L_0}(x)]^{(L/L_0)} \quad (6.2)$$

Stability condition — The cdf of $\Delta\sigma$ for a given N , $F(\Delta\sigma; N)$, and the cdf of N for a given $\Delta\sigma$, $E(N; \Delta\sigma)$, must be stable for any arbitrary length. If the length effect is expressed using Eq. (6.2), the stability requirement implies that both cdf, $F_{L_0}(\Delta\sigma; N)$ and $F_L(\Delta\sigma; N)$ or $E_{L_0}(N; \Delta\sigma)$ and $E_L(N; \Delta\sigma)$ must belong to the same family.

Limit condition — If the length of the sub-elements goes to zero, or the number of pieces goes to infinity, the families of the cdf must be asymptotic. For the case of independence or asymptotic independence between the number of cycles to failure or the stress range for different sub-elements, only three limit distributions are possible: Gumbel, Weibull and Frechet. The Frechet distribution was excluded because of its negative character of lifetime. Due to the simplicity of the Weibull distribution, and the fact that a Gumbel distribution can be approximated by Weibull distribution, Castillo et al. decided to use the Weibull distribution:

$$E(N; \Delta\sigma, L_0) = 1 - \exp \left\{ - \left[\frac{N - N_0(\Delta\sigma, L_0)}{N_a(\Delta\sigma, L_0)} \right]^{b(\Delta\sigma, L_0)} \right\} \quad (6.3)$$

where, $E(N; \Delta\sigma, L_0)$ is the cdf of N for given $\Delta\sigma$, and $N_0(\Delta\sigma, L_0)$, $N_a(\Delta\sigma, L_0)$ and $b(\Delta\sigma, L_0)$ are functions of $\Delta\sigma$ and L_0 , to be determined.

or

$$F(\Delta\sigma; N, L_0) = 1 - \exp \left\{ - \left[\frac{\Delta\sigma - \Delta\sigma_0(N, L_0)}{\Delta\sigma_a(N, L_0)} \right]^{a(N, L_0)} \right\} \quad (6.4)$$

where, $F(\Delta\sigma; N, L_0)$ is the cdf of $\Delta\sigma$ for given N , and $\Delta\sigma_0(N, L_0)$, $\Delta\sigma_a(N, L_0)$ and $a(N, L_0)$ are functions of N and L_0 , to be determined.

Compatibility condition — This requirement is satisfied if, and only if,

$$F(\Delta\sigma; N) = E(N; \Delta\sigma) \quad \text{for } \forall \Delta\sigma \text{ and } N \quad (6.5)$$

By substituting the Weibull expressions (6.3) and (6.4) into Eq.(6.2) and (6.5), Castillo et al. derived the following five-parameter statistical model:

$$(N - B)(\Delta\sigma - C) = D \left[- \frac{L_0}{L} \ln(1 - P) \right]^{1/A} - E \quad (6.6)$$

where P is the percentile, L_0 is the reference length, and L the cable length. The five statistical parameters A, B, C, D, E are designated as follows:

- A is the Weibull shape or slope parameter
- B is the asymptotic N (cycles) limit
- C is the endurance limit
- D is the scale fitting parameter obtained for chosen reference length L_0
- E is a constant defining the $\Delta\sigma$ vs N threshold curve (asymptotic curve, zero probability of failure curve).

Equation (6.6) is a series of equilateral hyperbolas, with asymptotes $N = B$ and $\Delta\sigma = C$. It is possible for both limit values, B and C , to become zero.

The analytical formulation of Eq. 6.6 can be found in Ref. 50, which is the work conducted by E. Castillo, A.F. Canteli, V. Esslinger, and B. Thürlimann.

It should be noted that more work will be required in order to determine the distribution that most accurately describes the fatigue life of multi-layered wire strands. This could be done by analyzing statistically significant populations of cables from different manufacturers.

6.2.1 Development of the Program FANOW

A computer program, called ZURICH, for the evaluation of the five-parameter statistical model presented in Section 6.2 was first implemented for Macintosh computer and later rewritten for DOS-environment by F.M. Rodrigez at the Technical University of Dijon in 1989. The program was subsequently adapted and modified by the Swiss Federal Laboratories for Materials Testing and Research (EMPA). During the translation of the error messages and help texts from the Spanish language to English, the name of the program was changed to FANOW (Fatigue ANalysis Of Wires). A copy of the latest revision of FANOW software was obtained from EMPA by the University of Alberta. This program will be used in this Chapter for the statistical evaluation of the effect of length on the axial fatigue life of strands.

The program FANOW requires a minimum of three data sets at different stress ranges in order to be able to run. A set of data consists of the stress range and number of cycles to failure. A different form of Castillo model, Eq. (6.6), was adopted in the computer formulation:

$$(\ln N - B)(\ln \Delta\sigma - C) = D \left[-\frac{L_0}{L} \ln(1 - P) \right]^{1/A} + E \quad (6.7)$$

In the first step, the experimental data are used to calculate the parameters (constants) of the Weibull distribution in order to define its shape, the endurance limit, and the asymptotic limit of the number of cycles to failure. Once the five parameters A, B, C, D, and E are evaluated, the model allows the designer to determine a set of different failure probability curves (depending on the values of the percentile, P, inserted in Eq. (6.7)). The ratio L/L_0 is used to account for the length effect (L_0 is the length of the tested specimens and L the length of the actual cable).

The Castillo et al. model has also the capability to account for runout tests. (Runouts are tests that have been discontinued before failure occurred.) Information from runouts is incomplete, and contains the uncertainty as to whether the specimen will actually fail or not. The program FANOW assumes that the specimen will fail some time later and predicts the number of cycles at which this failure will occur. The user needs only to specify the number of cycles that represent this runout limit.

6.2.2 Castillo Model for the 45 mm Diameter Strand

A data file with all eight test results of SP series (as given in Table 5.6 of Chapter 5) was created for the statistical analysis using the FANOW program. The runout limit was chosen to be 10 million cycles. Table 6.1 gives the five parameters that were estimated using the FANOW software. Equation (6.7) can then be written as follows:

$$(\ln N - 7.6927)(\ln \Delta\sigma - 5.3798) = 0.3419 \left[-\frac{L_0}{L} \ln(1-P) \right] \left(\frac{1}{1.1145} \right) + 2.3651 \quad (6.8)$$

Using the calculated parameters, the following fatigue properties were obtained:

- endurance limit: $(\Delta\sigma)_e = e^{5.3798} = 217 \text{ MPa}$
- threshold cycles: $(N)_{TH} = e^{7.6927} = 2192 \text{ cycles}$

The percentile $\Delta\sigma$ vs. N curves can be obtained from Eq. (6.8) or from the following modified expression

$$N = \exp \left(\frac{K_{P, L_0/L} + 2.365}{\ln \Delta\sigma - 5.380} + 7.693 \right) \quad (6.9)$$

$$\text{where } K_{P, L_0/L} = 0.3419 \left[-\frac{L_0}{L} \ln(1-P) \right] \left(\frac{1}{1.1145} \right) \quad (6.10)$$

The constant $K_{P, L_0/L}$ is given in Table 6.1 for different values of percentile, P , and length ratio, L_0/L . A graphical representation of the field of percentile curves is given in Figures 6.1 to 6.4. It should be mentioned that all graphs in this Chapter are presented in a semi-logarithmic form. (The abscissa gives the number of loading cycles on a logarithmic scale and the ordinate the stress range on a normal scale.) This representation was chosen in order to facilitate the comparison of the data. (A logarithmic versus logarithmic graphical representation will have the tendency to cluster and overlap the data, making visual comparison more difficult.)

Figure 6.1 gives various percentile curves ($P = 0.5, 0.95, 0.05$ and 0) for a length ratio $L_0/L = 1$. In Figure 6.2 the 5th percentile curve of the Castillo model is compared with the lower limit (two-standard deviation from the mean) of the linear $\log \Delta\sigma$ vs. $\log N$ model derived in Chapter 5 (Eq. 5.12b) for the SP Series of data. From Figure 6.2, it is evident that the linear $\log \Delta\sigma$ vs. $\log N$ model provides a conservative estimate of the fatigue life of the 45 mm diameter strand.

The length effect is investigated by varying the length ratio, L_0/L , in Eq. (6.10) and keeping the percentile constant. Two different percentiles were examined, and these are displayed in Figures 6.3 and 6.4. In Figure 6.3, the median ($P = 50\%$) percentile curves were generated for length ratios equal to 1, 0.1, and 0. Since the length of the test specimens was 3.3 meters, these length ratios correspond to hypothetical cable lengths of 3.3 meters, 33 meters, and infinity, respectively. The effect of the cable length is obvious from Figure 6.3: as the length increases, the fatigue strength of the cable decreases.

The length effect was also investigated for the 5th percentile curve, and length ratios equal to 1 and zero. The results are shown in Figure 6.4. It can be seen, that for the 5th percentile curve, the effect of the actual length of the cable is negligible. A comparison of Figure 6.4 and Figure 6.3 shows that the influence of the length diminishes as the probability of failure approaches zero. This is because, as the probability of failure decreases, the percentile curve approaches the asymptotic curve, which is independent of the length since $K_{p, L_0/L} = 0$. A conservative design equation for the fatigue strength of the 45 mm diameter strand which will account for the effect of length could be obtained by using the 5th percentile curve of an infinite long cable ($L_0/L = 0$). (Note, that the above curve corresponds to the zero percentile curve, since from Eq. (6.10) $K_{0.05,0} = 0$.) In this case, Eq. (6.9) could be simplified significantly and the following design equation was derived:

$$(\ln N - 7.693) \cdot (\ln \Delta \sigma - 5.380) = 2.365 \quad (6.11a)$$

or

$$N = \exp\left(\frac{2.365}{\ln \Delta \sigma - 5.380} + 7.693\right) \quad (6.11b)$$

6.2.3 Castillo Model for the 25 mm Diameter Strand

The statistical analysis described in Section 6.2.2 was repeated for the 25 mm diameter strand. The specimens from both SL and SS series were considered. This was possible since it was found (see Section 5.5), that the specimen length had no influence upon the fatigue strength within the test range. Moreover, only the two extreme length ratios ($L_0/L = 1$ and 0) will be used for the investigation of the length effect so that the exact specimen length is not required. The input file required to run the program was based on the test results presented in Table 5.6 (with the exception that the actual stress ranges in MPa must be used instead of the percentage values shown in Table 5.6). The runout limit was chosen to be 4 million cycles, since specimen SS2 was discontinued at 4.18 million cycles. The

five parameters estimated using the FANOW software are presented in Table 6.1. The equation of the percentile curves is:

$$(\ln N + 8.3068)(\ln \Delta\sigma - 2.8307) = 1.6010 \left[-\frac{L_0}{L} \ln(1-P) \right] \left(\frac{1}{0.8629} \right) + 60.0095 \quad (6.12)$$

Using these parameters the following fatigue properties are obtained:

- endurance limit: $(\Delta\sigma)_e = e^{2.3307} = 17 \text{ MPa}$
- threshold cycles: $(N)_{TH} = e^{-8.3068} = 0 \text{ cycles}$

The percentile $\Delta\sigma$ vs. N curves can be obtained using the following modification of expression (6.12):

$$N = \exp \left(\frac{K_{P, L_0/L} + 60.0095}{\ln \Delta\sigma - 2.8307} - 8.3068 \right) \quad (6.13)$$

$$\text{where } K_{P, L_0/L} = 1.6010 \left[-\frac{L_0}{L} \ln(1-P) \right] \left(\frac{1}{0.8629} \right) \quad (6.14)$$

Table 6.1 gives the constant $K_{P, L_0/L}$ for different values of percentile, P , and length ratio, L_0/L . A graphical representation of the field of probability failure curves for the 25 mm diameter strand is shown in Figure 6.5.

In Figure 6.6, the 5th percentile curve of Castillo model for the 25 mm diameter can be compared with the lower limit (two-standard deviation from the mean) of the linear $\log \Delta\sigma$ vs. $\log N$ model (for SL and SS Series), described in Section 5.6 (Eq. 5.13b). As it was the case for the 45 mm diameter cable, the linear $\log \Delta\sigma$ vs. $\log N$ regression gives more conservative results. Part of the explanation is that the $\log \Delta\sigma$ vs. $\log N$ model considers the runout tests as failed specimens.

The length effect was investigated for the median (50%) and the 5th percentile curves. These results are presented in Figures 6.7 and 6.8, respectively. The two extreme cases, a cable having a length equal to the test sample and a cable having an infinite length, were investigated. The effect of the length is clearly shown on the median percentile curves of Figure 6.7. However, the effect of length is hardly noticeable for the 5th percentile curves, shown in Figure 6.8. As was explained in Section 6.4, this reflects of the asymptotic behavior of the Weibull distribution from which Castillo model was derived. The 5th percentile curve of an infinitely long cable, which is statistically equivalent to the zero

percentile curve, could therefore be used to predict the fatigue life of an actual cable (given that it has the same strand make-up as the 25 mm diameter cable that was tested).

$$(\ln N + 8.307)(\ln \Delta\sigma - 2.831) = 60.010 \quad (6.15a)$$

$$N = \exp\left(\frac{60.010}{\ln \Delta\sigma - 2.831} - 8.307\right) \quad (6.15b)$$

The 5th percentile curve of an infinitely long cable (Eq. 6.15) was chosen for design purposes because of its simpler format as compared to expressions 6.12 to 6.14, and the fact that it conservatively takes into account the effect of the actual length of the cable.

6.2.4 Castillo Model for all Tests Conducted at the University of Alberta

For completeness of the discussion presented in the previous two Sections (6.2.2 and 6.2.3), the FANOW program was run with an input file containing the experimental results of all three experimental series (SP, SL, and SS). A runout limit of 4 million cycles was used for this run. The values of the five parameters are given in Table 6.1. The percentile curves are given by the following expression:

$$(\ln N + 25786.658)(\ln \Delta\sigma + 4100.615) = 7334.354 \left[-\frac{L_0}{L} \ln(1 - P) \right]^{\left(\frac{1}{0.8852}\right)} + 105939704 \quad (6.16)$$

The endurance limit and the threshold cycles are:

- endurance limit: $(\Delta\sigma)_e = e^{-4100.615} = 0 \text{ MPa}$
- threshold cycles: $(N)_{T:H} = e^{-25786.658} = 0 \text{ cycles}$

Eq. (6.16) can be written in the following form:

$$N = \exp\left(\frac{K_{P, L_0/L} + 105939704}{\ln \Delta\sigma + 4100.615} - 25786.658\right) \quad (6.17)$$

$$\text{where } K_{P, L_0/L} = 7334.354 \left[-\frac{L_0}{L} \ln(1 - P) \right]^{\left(\frac{1}{0.885}\right)} \quad (6.18)$$

Because the number of cycles calculated from Eqs. 6.16 and 6.17 was found to be very sensitive to the exact value of the constants, it is imperative to keep three significant digits for all constants.

The results of the parametric study that was conducted based on Eqs. 6.16 to 6.18, are summarized in Table 6.1 and in Figures 6.9 to 6.12. Figure 6.9 shows the percentile curves for a length ratio, $L_o/L = 1$. A comparison between the 5th percentile curve and the two standard deviation confidence lower limit of the linear $\log \Delta\sigma$ vs. $\log N$ model (Eq. 5.21a), shown in Figure 6.10, reveals again that the prediction of the test results obtained on the basis of a linear regression analysis are conservative, especially for low cycles. Finally, from Figures 6.11 and 6.12, it can be concluded that the effect of cable length, although significant (Figure 6.11) for the median curve, diminishes as the probability of failure approaches zero.

The 5th percentile curve of an infinitely long cable will, therefore, be a conservative estimate of the fatigue life of an actual cable (having the same make-up with the 25 mm or 45 mm diameter strands that were tested). Note, that the 5th percentile curve of an infinite long cable is statistically equivalent to the zero percentile curve, and therefore the following simplified design equations can be derived:

$$(\ln N + 25786.658)(\ln \Delta\sigma + 4100.615) = 105939704 \quad (6.19)$$

$$N = \exp\left(\frac{105939704}{\ln \Delta\sigma + 4100.615} - 25786.658\right) \quad (6.20)$$

6.3 Inclusion of Previous Experimental Data

On the basis of the literature reviewed in Chapter 2 (see Section 2.3.3), it was concluded that the fatigue data of cables should be categorized according to the type of cable. In the following discussion, only fatigue data for multi-layered and seven-wire strands will be presented and compared with the test results obtained in the present investigation. Those results will be also compared with the existing design recommendations.

6.3.1 Experimental Work of Tilly (Ref. 16, Ref. 89)

Tilly conducted axial fatigue tests on four different configurations of multi-layered strands and for diameters between 35 mm to 70 mm. Based on the characteristic strengths of 928 kN to 3590 kN reported by Tilly, the ultimate tensile stress was estimated to range between 1226 MPa and 1273 MPa. The results in Tilly's report are expressed as a percent of the characteristic strength of the strand. In order to obtain the absolute stress ranges, the average value of 1250 MPa was used as the ultimate tensile stress.

For the end termination of the Tilly specimens, the wires were bushed and low-melting-temperature alloy was cast into steel sockets. The cable length between sockets was

3 meters and the failure criterion was five broken wires. During the axial fatigue tests, the mean load varied between 20% to 38% of the ultimate tensile strength, and stress ranges of 10% to 28% of the ultimate tensile strength were applied. The results are summarized in Table C.1 of Appendix C. It should be noted that the values given in Table C.1 were obtained from a graphical presentation in Ref. 89 (Figure 9). The exact values were not reported in Tilly publication.

Tilly observed that after the first wire fracture, at N_1 cycles, the additional number of cycles to five fractures ranged from $0.5 N_1$ to $2 N_1$. In addition, runout tests of up to 5 million cycles were recorded, and there was no evidence of endurance limit within the condition tested.

A regression analysis performed by Tilly gave the following lower-bound fatigue life expression:

$$N = 2 \cdot 10^9 S_r^{-3.3} \quad (6.21)$$

where S_r is the load range expressed as a percentage of the ultimate tensile strength and N is the number of cycles to failure. It should be noted that this lower bound equation was derived on the basis of the fatigue results of three different cable configurations: multi-layered strands, stranded ropes and locked coil cable. Expression (6.21) could, therefore, be used for the axial fatigue prediction of wire ropes, multi-layered strands and locked coil cables. In the literature review of Chapter 2, it was suggested that fatigue life equations should be categorized depending the type of cable.

The experimental work of Tilly is compared with the test results obtained at the University of Alberta in Figure 6.13. In the same figure, the lower bound fatigue expression (6.21), suggested by Tilly, is compared with the lower bound regression expression derived for all experimental data obtained at the University of Alberta (Eq. 5.21). It can be seen that the strands tested at the University of Alberta had a higher fatigue performance than those tested by Tilly, especially in the high cycle fatigue range. This observation is also reflected in the prediction equation proposed by Tilly, which gives more conservative results when compared to the lower-bound Eq. (5.21).

6.3.2 Experimental Work of Hobbs and Ghavami (Ref. 64)

Hobbs and Ghavami (Ref. 64) conducted axial fatigue tests on fifteen multi-layered strands that had diameters from 16 mm to 32 mm. The twelve specimens with 16 mm diameter had a test length of 1055 mm. The cable construction consisted of 1x19 galvanized wires

of 3.2 mm diameter. The UTS of the strand was 234 kN, or 1531 MPa. The three 38 mm diameter specimens, which had a test length of 6000 mm, were taken from an existing mast. They consisted of five layers of wires (92 in total), 3.5 mm in diameter, over a 5 mm diameter king wire. The UTS of the (1x92) strand was 1230 kN, which corresponds to an ultimate tensile stress of 1375 MPa.

All specimens were terminated using zinc-poured sockets, and were tested using a pair of hydraulic actuators of 500 kN capacity each. This setup is very similar to the one presented in this investigation. Wire failure observations were made "by ear, eye, and shock contact," and tests were discontinued when the specimens were unable to carry the applied mean load. Fatigue failures for all the specimens occurred at the strand/socket interface, with the first observed breakage invariably in the outer layer. This type of failure probably reflects the socketing material used and the geometry of the socket. As was noted in Section 1.1.5.2, the high temperatures of hot-poured sockets has a tendency to reduce the fatigue strength of the wires at the socket interface. Furthermore, the geometry of the socket could create high concentration stresses at the outside layer wires that could lead to premature fatigue failures. Nevertheless, because of the general lack of fatigue data on multi-layered strands, it was decided to use the experimental data obtained by Hobbs and Ghavami. The premature failures at the socket locations will give design curves on the conservative side.

Hobbs and Ghavami concluded that fatigue life is insensitive to mean load and that the number of cycles from first wire fracture to overall failure increases with the number of wires. The latter could be explained by the fact that the loss of cross-section from one breakage is less significant for large diameter strand (which has more wires) than for smaller diameter cable.

The fatigue data obtained by Hobbs and Ghavami are summarized in Table C.2 of Appendix C. It should be noted that the fatigue lives presented in Table C.2 are only approximate, since they were read from a graph given in Ref. 64.

In Figure 6.14, the experimental work of Hobbs and Ghavami is compared with the test data obtained in this investigation. From this comparison it can be concluded that the multi-layered strands tested at the University of Alberta, gave consistently higher fatigue lives for comparable stress ranges. This is probably a reflection of the cold-socketing end termination that was used in the present investigation, which produces a fairly uniform

distribution of wire fractures along the cable. It appears that, in effect, Ghavami and Hobbs tested the end termination rather than the free length.

The lower-bound regression expression (Eq. 5.21) derived from all test data obtained in the present investigation is also given in Figure 6.14. It can be seen that six out of the fifteen data reported by Ghavami and Hobbs are on the unsafe side of the curve.

6.3.3 Experimental Work of Raof (Ref. 72)

In order to confirm the validity of his analytical model for fatigue strength prediction of cables from first principles, Raof (Ref. 72) conducted axial fatigue tests on multi-layered strands. Raof tested 51 mm diameter strand consisting of 139 wires helically wound in six layers. All wires, with the exception of the core wires, were 4 mm in diameter. The independent core consisted of 19 wires with diameters ranging from 2.31 to 3.00 mm. The ultimate tensile strength of the strand was 2160 kN or 1330 MPa.

The criterion for fatigue initiation, which is considered by Raof to be the useful service life of a cable, was the occurrence of the first wire failure in the outer layer. Based on the results obtained at the University of Alberta and those reported by Tilly (see Section 2.3.1) it is believed that the failure criterion used by Raof is very conservative, especially for large diameter multi-layered strands consisting of a large number of wires. Epoxy resin was used for the end terminations, and all the wire fractures occurred away from the ends, that is, within the free length of the cable.

The test results obtained by Raof are summarized in Table C.3 of Appendix C. Figure 6.15 shows a comparison of test results reported by Raof and those presented in this investigation. As can be seen from this Figure, with the exception of two data, the lower-bound Eq. (5.21) could be used to predict the test data presented by Raof.

6.4 Comparison of Test Data with Existing Design Curves

A linear logarithmic regression analysis of all the test data reviewed in Section 6.3 (see also Appendix C) and the test data obtained in the present investigation, was carried out. This represents a total of 53 test results. Details of the regression analysis method are presented in Table B.4 of Appendix B. An estimate of the mean fatigue life for stress ranges between 140 MPa and 630 MPa is:

$$\log N = 10.751 - 3.814 \log S_r \quad (6.22)$$

where N is the number of cycles to failure and S_r is the stress range-to-UTS ratio expressed in percent. The coefficient of determination, r^2 , for these data is 0.638. The dependence of $\log N$ with $\log S_r$ was again checked by conducting a significance test for the slope of the regression Eq. 6.22. (See Section 5.7 for the details of the significance test). The comparison of the "t" statistic parameter (see Eq. 5.14) with the tabulated value of Student's distribution, $t_{\alpha/2, n-2}$, for a level of significance of $\alpha = 0.05$ and a number of degrees of freedom of $(n - 2) = (53 - 2) = 51$ gave:

$$t = 9.49 > t_{\alpha/2, n-2} = 1.99 \quad (6.23)$$

Thus, it can be concluded that, with a risk of $\alpha = 0.05$, the stress range has a significant effect on the fatigue life of the specimen. The interval delimited by two standard errors of the estimate is:

$$\log N = 10.751 - 3.814 \log S_r \pm 0.884 \quad (6.24a)$$

$$\text{or} \quad 10^{9.867} S_r^{-3.814} \leq N \leq 10^{11.635} S_r^{-3.814} \quad (6.24b)$$

The lower bound regression line (Eq. 6.24) is shown in Figure 6.16. Note that representative ultimate tensile strength value of 1400 MPa, which is typical for stranded cables (ASTM A586, Ref. 3), was used in preparing the data represented in Figure 6.16. The regression analysis was performed using all the test data, including the discontinued experiments. This, together with the more conservative failure criteria used in some cases (i.e., Raoof, Ref. 72) will result in a conservative design curve.

The five-parameter statistical model developed by Castillo et al. (see Ref. 50), which accounts for the effect of length, was also used to develop a prediction of the fatigue life of all test data. The FANOW program (see Section 6.2.1) in this case gave the following statistical model:

$$(\ln N + 46224.468)(\ln \Delta\sigma + 11443.354) = 16306.167 \left\{ -\frac{L_0}{L} \ln(1 - P) \right\}^{\frac{1}{1.368}} + 5.296 \times 10^8 \quad (6.25)$$

The run-out limit selected was 2 million cycles and test specimens that were discontinued before reaching this limit were taken into account in this length effect analysis. As was explained in Section 6.2, in order to account for the effect of length the the 5th percentile curve for an infinitely long cable should be used as a safe estimate of the fatigue life of an actual cable. This is statistically equivalent to the zero-percentile curve of Eq. 6.25.

Moreover, the zero-percentile curve will simplify Eq. 6.25 to an expression that could easily be used for design purposes. Hence:

$$N = \exp\left(\frac{529362.591}{(\ln \Delta\sigma + 11443.3537)} - 46224.4681\right) \quad (6.26)$$

It should be noted that Eqs. (6.25) and (6.26) are very sensitive to the exact values of their parameters, and for this reason at least three significant digits were kept for all constants.

The results obtained using the data bank collected in the present investigation can also be compared with the most commonly used fatigue design specifications for multi-layered strand. Those were reviewed in Section 2.3.4, and, for completeness of this Chapter, will be given again as follows:

American Petroleum Institute (API)

$$N \left(\frac{R}{100}\right)^{4.09} = 731 \quad (6.27)$$

Post-Tensioning Institute (PTI)

$$N = 1.4 \times 10^{13} (\Delta\sigma)^{-3.27} \quad (6.28)$$

Tilly lower bound curve

$$N = 2 \times 10^9 R^{-3.3} \quad (6.29)$$

where R is the load range expressed as a percentage of the minimum ultimate tensile strength, $\Delta\sigma$ is the stress range in MPa, and N is the fatigue life in cycles. The fatigue life predictions given by Eq. 6.27 to Eq. 6.29 are also plotted in Figure 6.16.

From a comparison of the design curves shown in Figure 6.16, it can be concluded that the equation proposed by the American Petroleum Institute (Eq. 6.27) gives unsafe results for both high and low cycle fatigue. The lower bound expressions suggested by PTI (Eq. 6.28), Tilly (Eq. 6.29), and the present regression analysis (Eq. 6.24) are in reasonably good agreement, especially in the high cycle fatigue range.

The effect of cable length is taken into consideration using the percentile curves of the Castillo et al. statistical model (Eq. 6.25). It is believed that the 5th percentile curve corresponding to an infinite long cable should be used to safely take into account the effect

of the length of the cable. Equation 6.25 was therefore simplified into the form given by Eq. 6.26. From the comparison shown in Figure 6.16, it can be seen that Castillo design curve gave less conservative results in the high cycle fatigue as compared to the PTI design recommendation. An explanation of this lies in the fact that runout tests are considered as failed specimens in all models except the Castillo model. In the Castillo et al. model runout tests are treated as statistically incomplete data and the E-M-algorithm method (Ref. 50) is used to assign an expected failure number of cycles to all discontinued tests.

6.5 Simplified Design Equation

The effect of length has been safely taken into consideration in Eq. 6.26, since it represents the 5th percentile curve of an infinite long cable. The expectation life of runout tests has also been adopted in this expression. It is, therefore, believed that Eq. 6.26 reflects the important aspects related to the fatigue performance of multi-layered strands, and it can be safely used by designers to estimate the axial fatigue life of those components.

Equation 6.26 is sensitive to the exact values of its constants, and the following simplification is proposed for design purposes:

$$N = 10^{15.162} \Delta\sigma^{-4.038} \quad (6.30a)$$

$$\text{Endurance limit} \quad \Delta\sigma = 105 \text{ MPa}, \quad (6.30b)$$

A comparison between this approximation (Eq. 6.30) and the 5th percentile curve of an infinitely long cable (Eq. 6.26) is presented in Figure 6.17. Good agreement is observed in both low and high cycle fatigue ranges.

Table 6.1 Parameters of Castillo Model

Parameters	SP Series	SL and SS Series	SP, SL and SS Series
A	1.1145	0.8629	0.8852
B	7.6927	-8.3068	-25786.6583
C	5.3798	2.8307	-4100.6147
D	0.3419	1.6010	7334.3543
E	2.3651	60.0095	1.059397×10^8
Endurance Limit (MPa)	217	17	0
Threshold Curve (Cycles)	2192	0	0
$K_{Lo/L=1, P=0.5}$	2.6112	61.0565	1.05944×10^8
$K_{Lo/L=0.1, P=0.5}$	2.4563	60.0821	1.05940×10^8
$K_{Lo/L=0.01, P=0.5}$	2.3767	60.0145	1.05940×10^8
$K_{Lo/L=1, P=0.05}$	2.3889	60.0607	1.05940×10^8
$K_{Lo/L=0.1, P=0.05}$	2.3681	60.0131	1.059397×10^8
$K_{Lo/L=0.01, P=0.05}$	2.3655	60.0097	1.059397×10^8
$K_{Lo/L=0, P}$ or $K_{Lo/L, P=0}$	2.3651	60.0095	1.059397×10^8

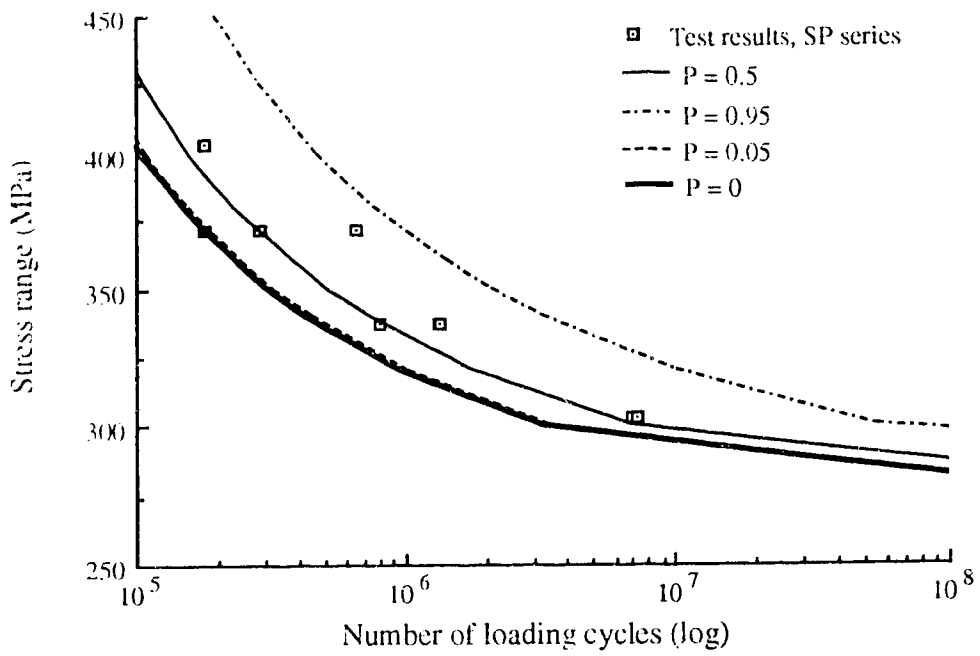


Figure 6.1 Castillo et al. model for the 45 mm diameter strand, $L_o/L = 1$

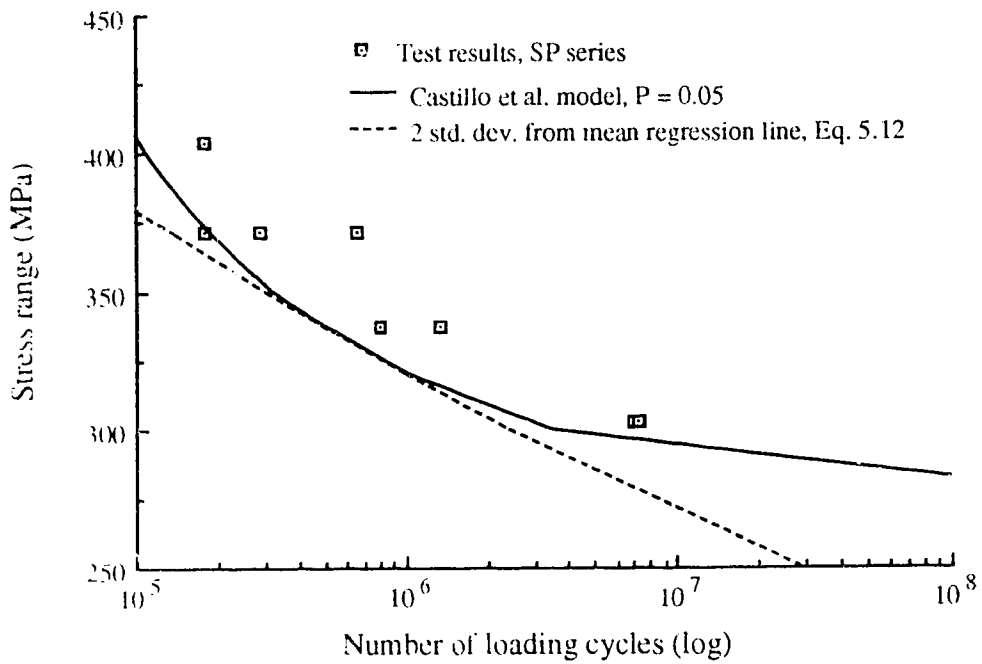


Figure 6.2 Comparison of statistical models for 45 mm diameter strand

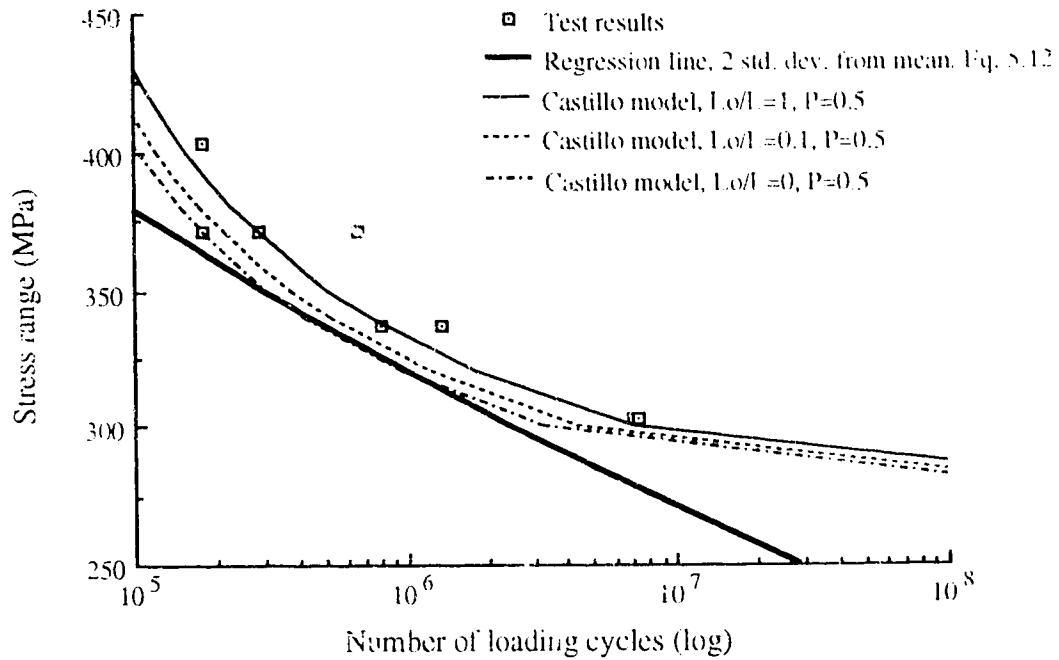


Figure 6.3 Length effect of 45 mm diameter strand, for $P = 0.5$

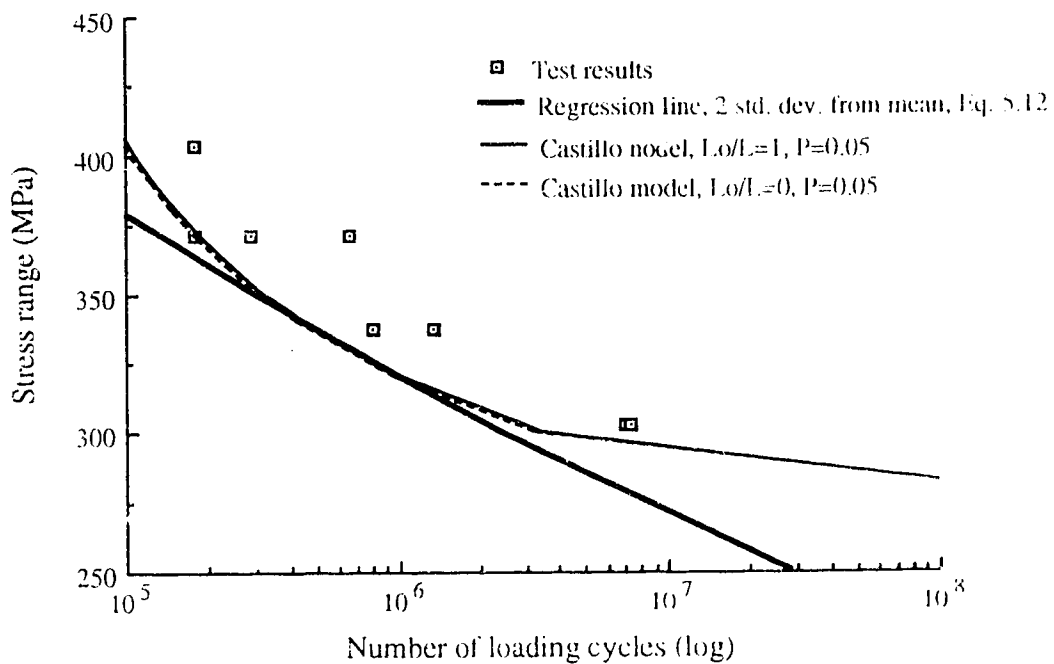


Figure 6.4 Length effect on 45 mm diameter strand, for $P = 0.05$

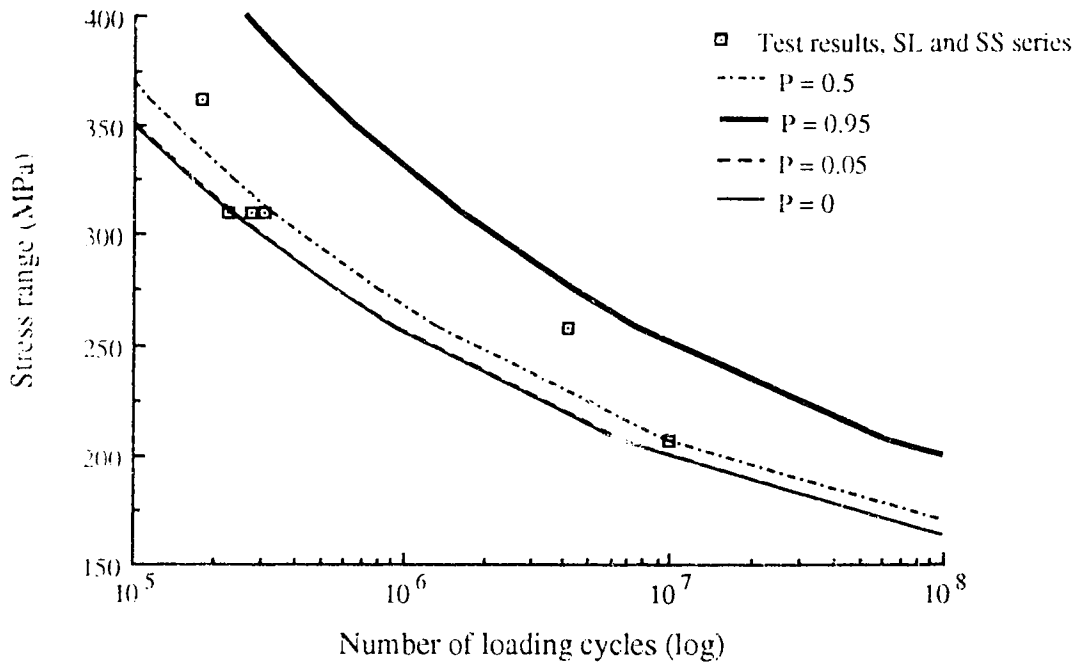


Figure 6.5 Castillo et al. model for the 25 mm diameter strand, $L_o/L = 1$

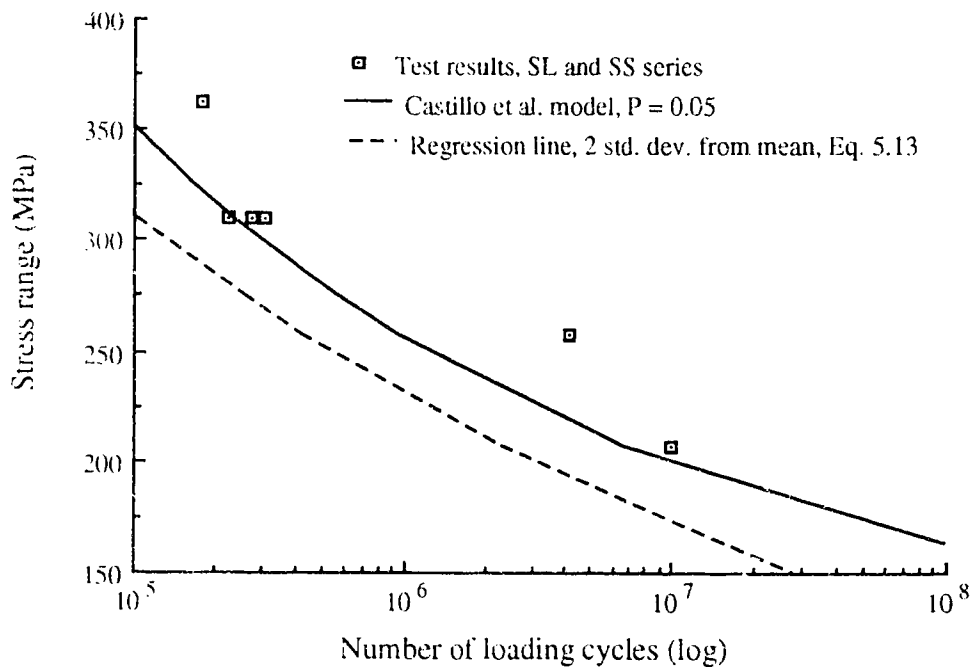


Figure 6.6 Comparison of statistical models for 25 mm diameter strand

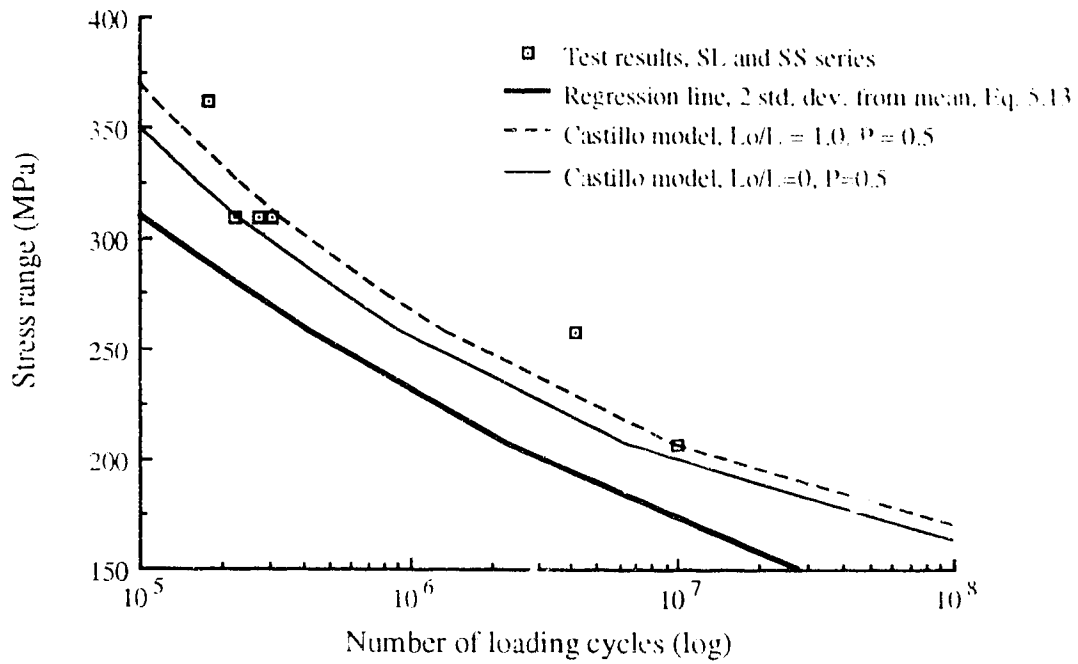


Figure 6.7 Length effect for the 25 mm diameter strand, $P = 0.5$

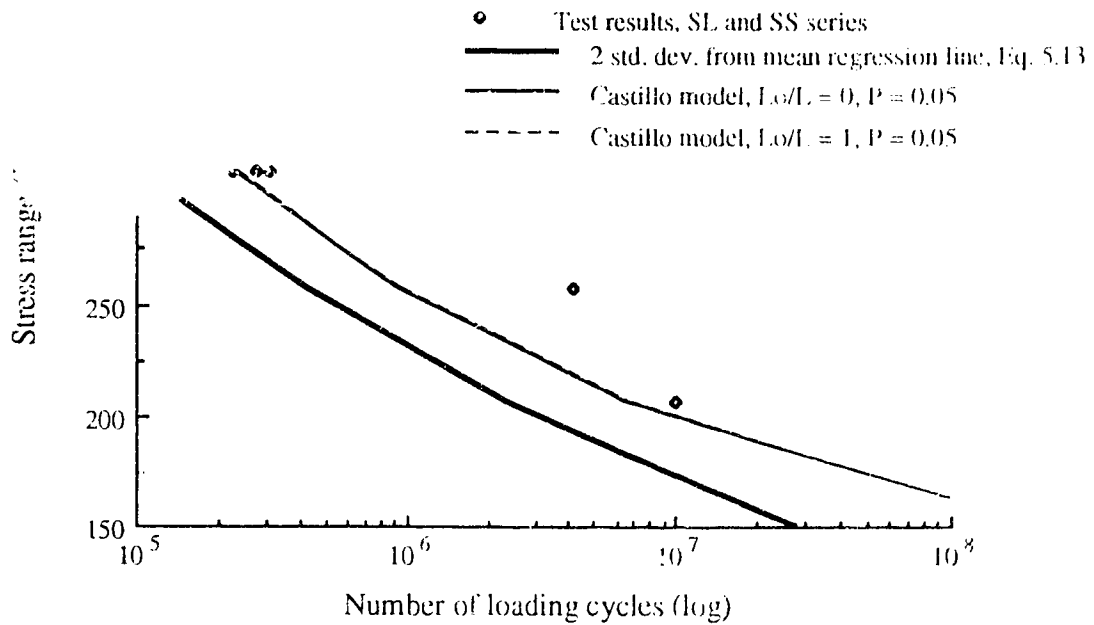


Figure 6.8 Length effect for the 25 mm diameter strand, $P = 0.05$

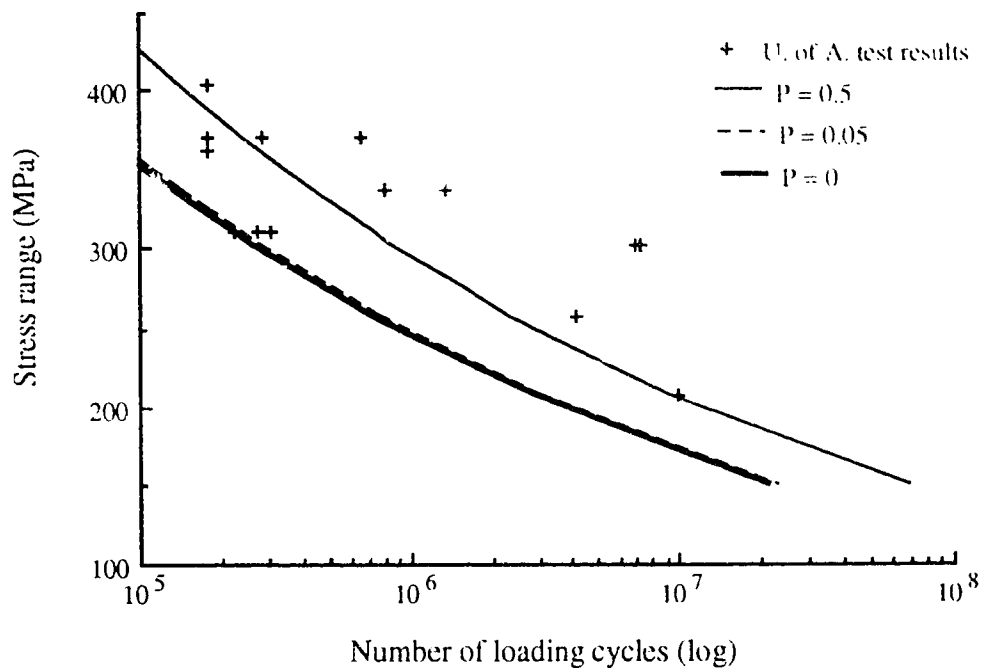


Figure 6.9 Castillo et al. model for SP, SL, and SS series, $Lo/L = 1$

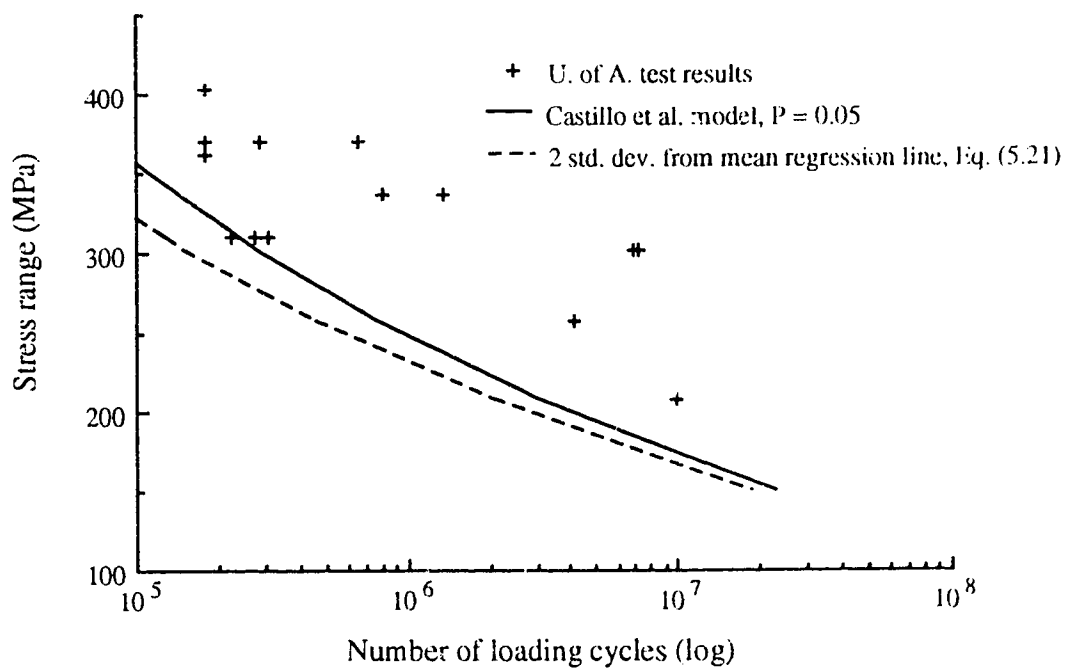
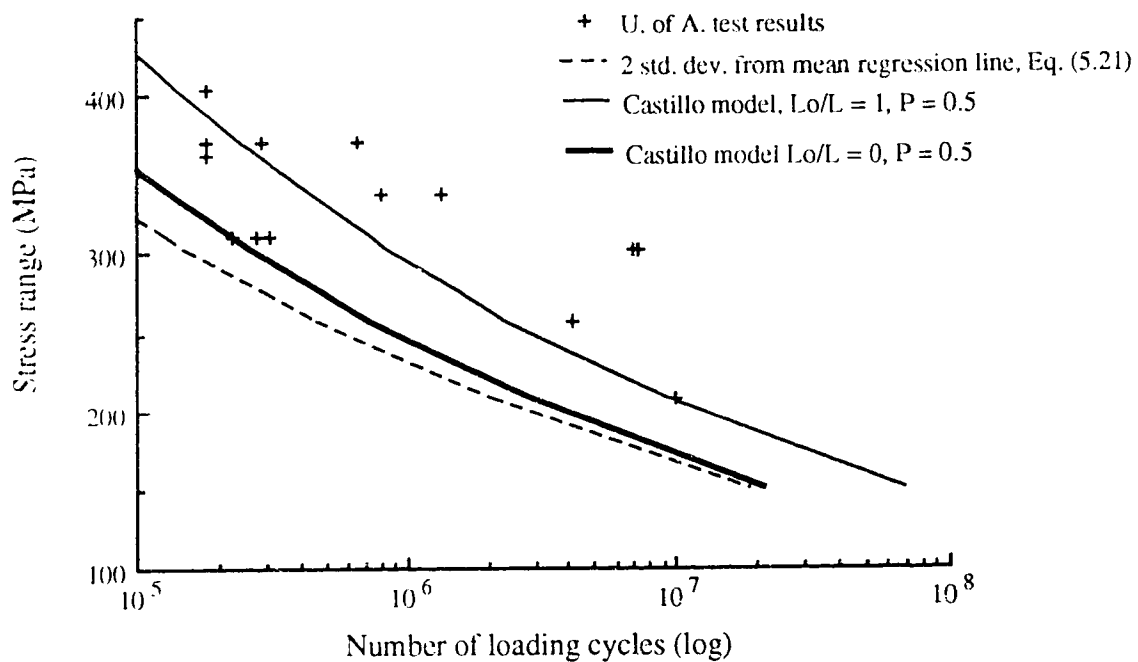
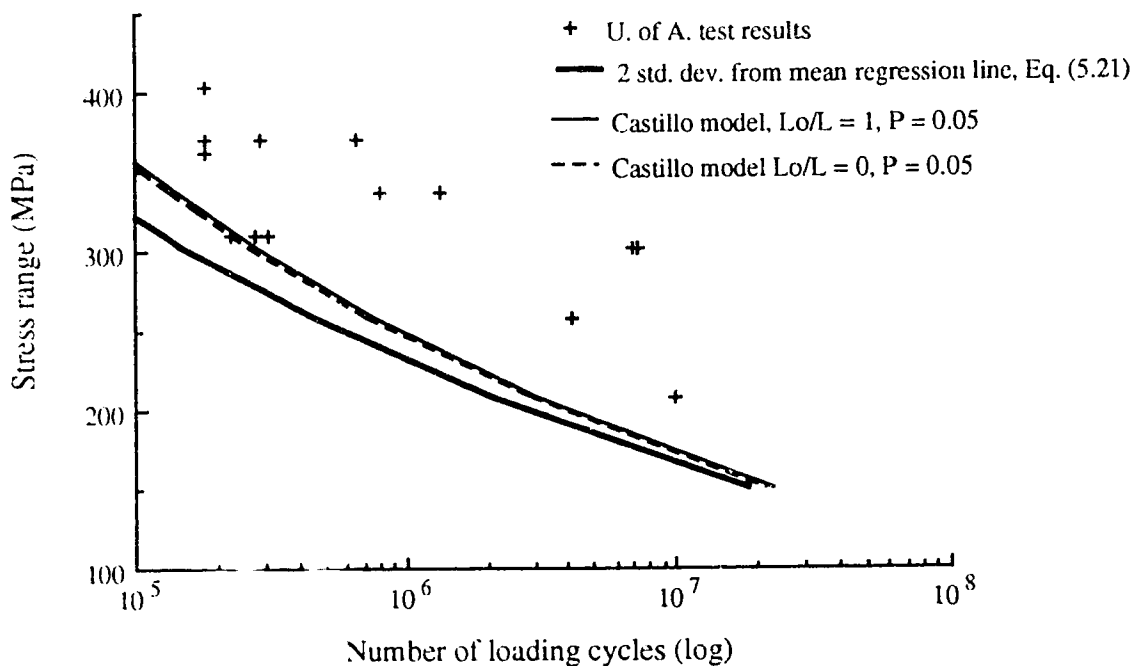


Figure 6.10 Comparison of statistical models for SP, SL, SS series

Figure 6.11 Length effect for SP, SL and SS series, $P = 0.5$ Figure 6.12 Length effect for SP, SL and SS series, $P = 0.05$

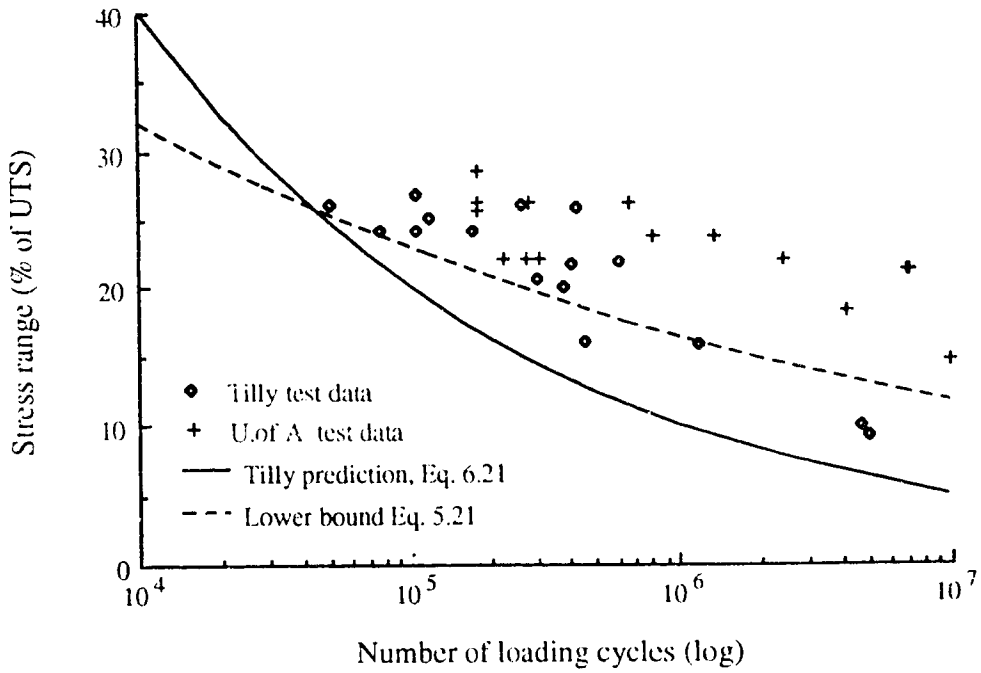


Figure 6.13 Comparison with Tilly test data

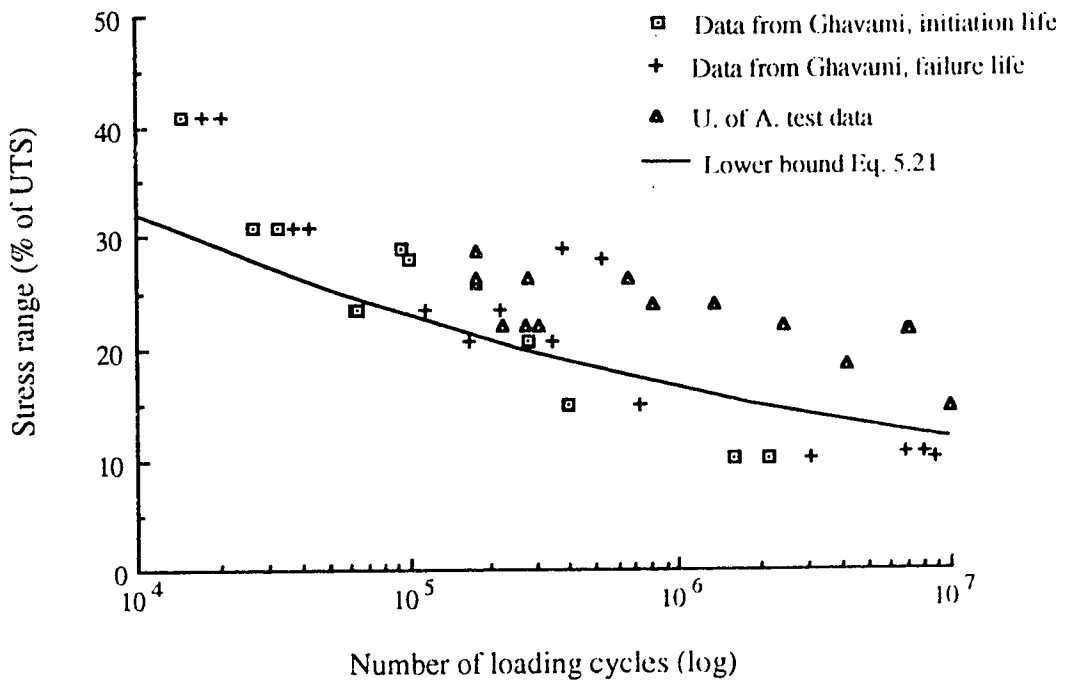


Figure 6.14 Comparison with Hobbs and Ghavami test data

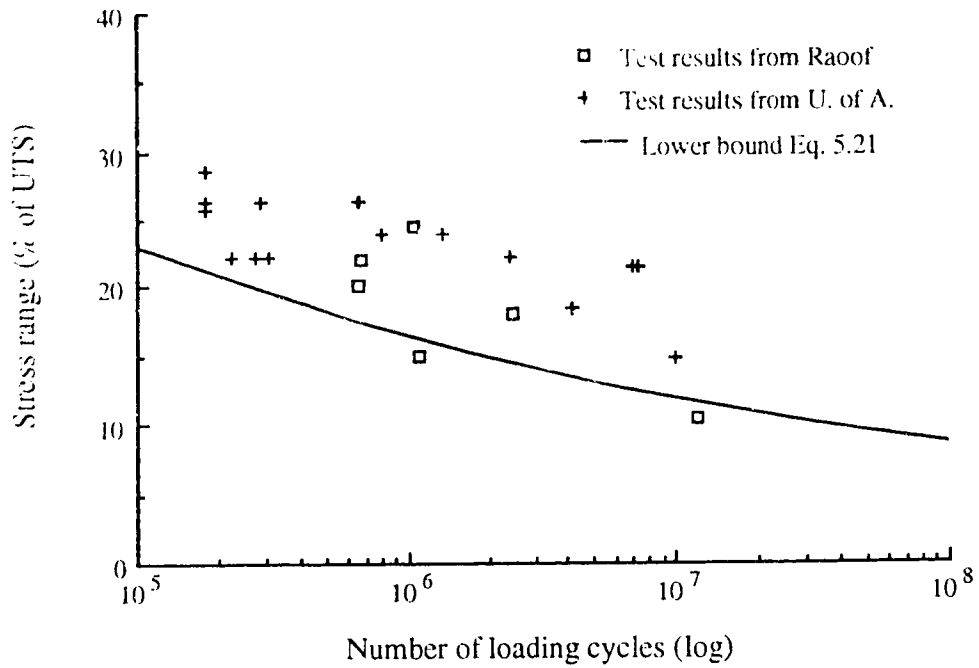


Figure 6.15 Comparison with Raouf test data

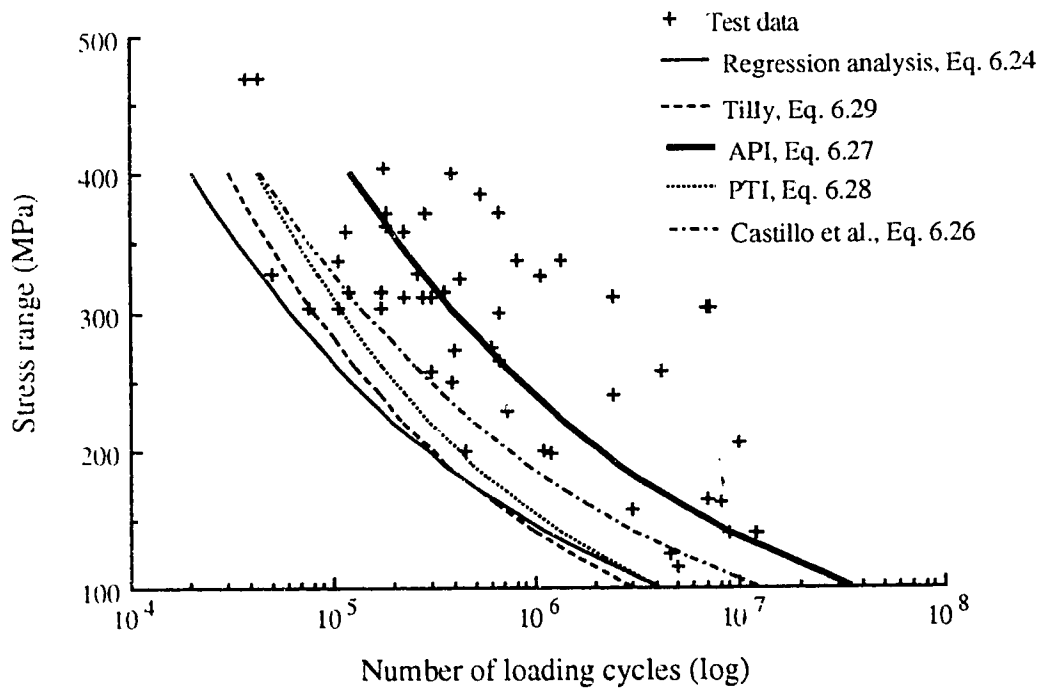


Figure 6.16 Comparison of test data with design curves

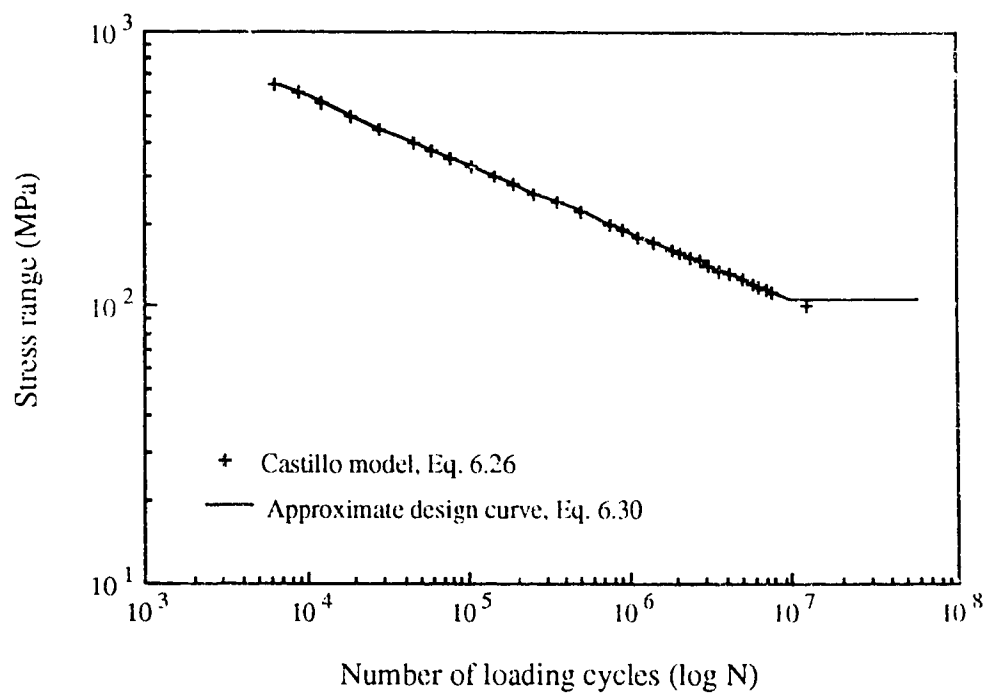


Figure 6.17 Comparison of Castillo et al. model with approximate design curve

Chapter 7 Summary, Conclusions, and Recommendations

7.1 Summary

The fatigue performance of multi-layered structural strands subjected to axial cyclic loading has been investigated. The methodology used was to carry out a literature survey, conduct physical tests, compare test data with selected results and design models from the literature, and, finally, to develop design rules for the fatigue evaluation of multi-layered strands.

The literature review indicated that the fatigue data on cables exhibit a large degree of scatter. This is mainly due to the different discard criteria used by researchers and to inappropriate test parameters, such as insufficient length of the test samples and socket details that may have caused premature failure at the socket location. Moreover, very few investigators have tested cables to destruction, and many of the reported data have been discontinued at two million cycles. This is unrealistically low for steel cables in bridge applications. The size effect problem, which relates to the extrapolation of test results to determine the fatigue strength of cables having lengths of several hundred meters, was also reviewed using the Castillo et al. statistical model. This is a five-parameter, Weibull model that uses the weakest link principle and assumes statistical independence between the sub-elements that form the actual cable. Finally, the available design procedures were also examined. Only the Post-Tensioning Institute (PTI) and the American Petroleum Institute (API) give guidelines for the fatigue life evaluation of steel cables. The rules they provide were developed using only experimental data, and they do not account for the effect of cable length. The API design rules appear to give unsafe results for both high and low cycle fatigue.

An experimental program was established in order to develop a failure criterion, to obtain fatigue life data for large diameter strands in the low stress range region, and to investigate the effect of stress range, strand make-up (i.e., layers, wire diameter, lay length, cable diameter, etc.) and length-to-diameter ratio of the specimens. The test setup was designed to permit large diameter cables to be tested in constant axial cyclic loading. The main program consisted of three series. The eight specimens of the SP series were 45 mm diameter galvanized strand with a length of around 3300 mm. All specimens of SP series were tested close to destruction and this enabled the results to be used to establish a failure criterion. Series SL and SS consisted of five and three specimens, respectively, each of

19 individual wires, 25 mm diameter galvanized strand. Specimens in the SL series had a length of 3375 mm and those of SS series had a length of 2150 mm. SS and SL series were used to investigate the effect of strand make-up and specimen length. For all series the mean stress was kept constant at 350 MPa and the stress range took various values of between 207 MPa and 404 MPa.

The wire breaks that occurred during testing, were detected using two non-destructive methods: accelerometers and acoustic emission system. The deterioration of the stiffness, which was also used to establish the end of the test, was determined by performing static tests at specific time intervals.

After completion of testing, some specimens were disassembled in order to investigate the wire break distribution along the cable and to confirm the validity of the non-destructive predictions. Microscopic examination of fractured surfaces of individual wires was conducted in order to study the fatigue failure mechanism.

The test results obtained in the investigation presented herein were compared with the work of other researchers and selected fatigue data were pooled into one database (a total of 53 test data), which was then compared with the most commonly used design curves. It was found that the specimens tested in the present research program gave consistently higher fatigue lives (especially in the high cycle regime) as compared with the test results reported by Tilly, Hobbs and Ghavami, and Raoof et al.

A comparison of the existing design curves (American Petroleum Institute, Eq. 6.27; Post-Tensioning Institute, Eq. 6.28; and Tilly lower bound, Eq. 6.29) with the selected database and the lower bound Eq. 6.24, confirmed that the equation proposed by the American Petroleum Institute gives unsafe results for both high and low cycle fatigue. The lower bound expressions suggested by the Post-Tensioning Institute, Tilly, and the regression analysis of the selected data bank (Eq. 6.24) are in reasonably good agreement with one another.

The extrapolation of fatigue strength of multi-layered strands from test lengths to practical lengths was investigated analytically using the Castillo et al. statistical model. This model is based on the weakest link principle and assumes statistical independence between test samples. All data from the selected data bank (53 in total) were used for the calibration of Castillo five parameter model. The runout limit was selected as to be 2 million cycles. Finally, the Castillo model was simplified and design recommendations were proposed for

the evaluation of the axial fatigue life of multi-layered strands. These recommendations include the effect of cable length and consider runout tests.

7.2 Conclusions

Based on the number of specimens tested in this program and the analytical study presented herein, the following conclusions are presented.

7.2.1 Effect of Testing Parameters

The effect of stress range on the fatigue performance of multi-layered strands was found to be significant. The number of cycles to failure decreases when the applied stress range increases. This was confirmed by all experimental studies presented herein. The effect of stress range in air was also quantitatively depicted by the statistical analysis conducted on the fatigue data base. The following simplified expression describes the relationship between the number of cycles to failure and the applied stress range:

$$\log N = 15.16 - 4.04 \log \Delta\sigma \quad (6.30a)$$

where N is the fatigue life in cycles, and $\Delta\sigma$ the stress range in MPa.

The effect of strand make-up was also found to be significant. A lower fatigue life was observed for smaller diameter strands. Since the majority of wires of a small strand are exposed (that is, in the outer layer), its fatigue life is more susceptible to flaws and kinks that may be introduced during handling of the cable. In general, small diameter cables consist of fewer and larger diameter individual wires as compared with larger diameter cables. Based on the rule of 5% wire breaks (see Section 7.2.5), an occasional broken wire of a multi-layered strand that has fewer than 20 individual wires should be considered as failure, and the strand should be replaced.

Similar fatigue lives were obtained for the two different length-to-exterior lay ratios tested in this program (12.8 and 8.2). Within these data, the fatigue results did not show a dependence upon the length tested, and the termination region also had no influence on the fatigue life of the specimens. It is therefore proposed that a minimum length-to-lay ratio of 8 should be used for physical testing of multi-layered strands.

Although the testing frequency did influence the average temperature of the specimen, it is believed that, for frequencies between 1.5 Hz to 3.5 Hz, this does not have any significant effect on the experimental results.

Cold-socketing material should be used for the termination details, since it is considered to have better fatigue performance than a hot-poured socket. The dimensions and detail of the socket to be used should be similar to the ones used in real structures. From the uniform distribution of wire breaks along the dismantled specimens, it can be concluded that the socket detail used in the present experimental investigation performed satisfactorily.

7.2.2 Detection of Wire Breaks

Acoustic emission techniques and use of accelerometers to detect wire breaks during the fatigue tests gave comparable results. For specimens that were tested close to destruction (SP series), the non-destructive procedures were not able to detect the final number of wire breaks. This is because, close to failure, several breaks occur at the same time and the long duration acoustic emission and accelerometer events overlapped. However, for the experiments (SL and SS series) where the tests were not taken to destruction, the total number of wire breaks was successfully predicted using the accelerometer method.

The ability of the accelerometers and acoustic emission to detect pre-existing internal wire fractures is an important question. In this program, promising results were obtained when a pulse echo test was carried out on one of the specimen using acoustic emission. By calculating the time interval between two captured events and knowing the acoustic wave propagation speed, the existence and location of a break could be estimated. The disadvantages of this method are that all internal wires must be checked individually and that access from at least one end of the cable is required.

7.4.3 Cumulative Fatigue Damage

From a simulated two-block amplitude tension fatigue test, it was concluded that a linear damage cumulative hypothesis will underestimate the total axial fatigue life. This is because the fretting zone shifts from one area to another as a different block load is applied. Photomicrographs of the fretting areas confirmed the hypothesis. Obviously, more variable amplitude tests will be required in order to establish a cumulative damage expression. Until then, the lower bound of the damage summation suggested by Potts (Ref. 53) should be used:

$$\sum \frac{n_i}{N_{fi}} = 1.25 \quad (5.23)$$

7.2.4 Distribution of Wire Breaks and Failure Mechanism

Upon disassembling of the specimens, it was found that wire breaks were generally evenly distributed along the cables. Wire breaks within the free length were the consequence of

localized fretting fatigue at the interlayer contact patches. This was observed in photomicrographs of fretting surfaces, which revealed that pre-existing microcracks at the zinc-iron interface of the contact patches propagate with loading cycles. Interlayer wire friction was found to be the cause of the multiple breaks that took place in individual internal wires.

Microscopic examination of the wire fractured surfaces revealed the three distinct regions of the fretting fatigue failure; fretting fatigue initiation site, fatigue propagation region, and final fracture region. A substantial amount of fretting debris was observed in the first region. Although the photomicrographs showed a ductile final fracture, from an engineering (macroscopic) perspective the fracture can be considered as brittle since it is associated with relatively little plastic deformation.

7.2.5 Discard Criterion

The test program indicated that the cross-sectional area and the stiffness of the cable deteriorate significantly with the number of cycles. Those features were used to establish the failure criterion. Based on the limited number of specimens tested close to destruction, it was concluded that the service limit of a multi-layered strand is reached when about 5% of the total number of wires are broken. This discard criterion was associated with a test length of at least six times the exterior lay length (see Section 7.2.1). More tests will be required to further refine this length.

The percentage of stiffness loss is not directly equivalent to the percentage of wire breaks. At 5% wire breaks the reduction of the overall modulus of elasticity was found to be 2.3%. This is due to the multiple break type of failure and the existence of interwire friction, which allows a broken wire to redevelop its full carrying capacity within a relatively short length.

7.2.6 Length Effect

The extrapolation of fatigue strength of multi-layered strands from test lengths to the actual lengths was investigated analytically using the Castillo et al. statistical model. This analysis showed that the fatigue life of a cable decreases with cable length. However, the effect of length diminishes as the probability of failure approaches zero. This is because, as the probability of failure decreases, the percentile curves of the Castillo et al. model approaches an asymptotic curve which is independent of the length.

For design purposes, the effect of length can be taken into account by using the 5th percentile curve of an infinitely long cable.

7.3 Recommendations

The recommendations made in this section are divided into two parts: design recommendations, which provide some design guidelines and replacement criteria for multi-layered strands, and recommendations for future research.

7.3.1 Design Recommendations

Based on the experimental and analytical work presented herein, the following design recommendations are made:

1. The fatigue life in air of galvanized multi-layered wire strands subjected to axial cyclic loading can be predicted using the following expressions:

$$\log N = 15.16 - 4.04 \log \Delta\sigma \quad (6.30a)$$

$$\text{endurance limit} \quad \Delta\sigma = 105 \text{ MPa} \quad (6.30b)$$

where N is the number of cycles to failure and $\Delta\sigma$ the applied stress range in MPa. It should be noted that length effect and runout tests were taken into consideration in the development of Eq. 6.30.

2. In case of variable amplitude stress range, the total damage from all stress range levels that are applied to the strand can be taken into consideration using the following cumulative fatigue damage expression:

$$\sum \frac{n_i}{N_{fi}} = 1.25 \quad (5.23)$$

where n_i = number of cycles that take place at stress range level i

N_{fi} = number of cycles that would cause failure at stress range level i
(N_{fi} can be obtained from expression.6.30).

3. Existing multi-layered strands should be replaced when non-destructive inspection of the cable reveals that 5% of the total number of wires are broken within a minimum length of six times the exterior lay length. Alternatively, when a previous record of the modulus of elasticity for a particular cable make-up exists, the strand in service should be replaced if a static test reveals any deterioration (say, 2%) of the modulus of elasticity. The gauge length for estimating the modulus of elasticity should be at least 3 to 5 times the exterior lay length.

7.3.2 Recommendations for Future Research

In the work presented herein an attempt was made to provide design recommendations for the axial fatigue strength evaluation of multi-layered wire strands. However, during this process it was realized that many questions related to the fatigue performance of cables remain unanswered and more research need to be conducted in several areas.

1. Most of the available fatigue data on cables have been obtained from tests conducted in air (with effects of corrosion not being included). Since bridge strands are often located in a hostile environment, further experimental research should be conducted on axial fatigue of cables in a corrosive environment. It is difficult to investigate the influence of corrosion using accelerated test programs. This is because corrosion is a time-dependent process and is best investigated in real time. Reliable test results can be obtained when samples become available from structures that are dismantled after time in service. Tilly (Ref. 89) concluded that the performance of severely corroded strand can be about two standard deviations below the lower bound obtained for specimens tested in air. This needs to be confirmed with additional testing and incorporated into design recommendations.
2. Only multi-layered strands were used for the derivation of the lower bound equations proposed herein. Similar research should be conducted for wire ropes and parallel wire strands. From the literature survey, it was concluded that multi-layered strands have significantly higher fatigue performance than do wire ropes. Parallel wire ropes, on the other hand, have a completely different failure mechanism from that of stranded cable. Failure criteria and design curves will have to be developed for the different types of cables.
3. From the two-step variable amplitude test conducted in the present investigation, it was concluded that the linear damage cumulative hypothesis will underestimate the total axial fatigue life of cables subjected to variable amplitude loading. Additional tests will be required in order to establish a reliable cumulative damage expression.
4. The majority of statistical models that are used for the extrapolation of fatigue data from test lengths to cables of real length uses the independence or the weakened asymptotic independence assumptions. It has been demonstrated (Castillo et al., Ref. 50) that for short lengths independence does not hold. However, for large testing lengths, physical and theoretical reasons justify this assumption. Thus, it is extremely important to

determine a threshold value of length above which the assumption of asymptotic behavior can be used.

5. The end termination of samples is always one of the critical points in a fatigue test. Specimens where the wire fractures are predominantly in the termination region must be disregarded in cases where the free length is to be investigated. It should be noted that for short test specimens the termination region takes up a relatively large proportion of the free length. How short can a specimen be before the end termination affects the fatigue results? From the limited number of tests conducted in this investigation it was found that the minimum length-to-diameter ratio should be 85. More tests will be required in order to further substantiate and refine this value.
6. Although cables in bridge applications are primarily subjected to tension, load fluctuations caused by combinations of deck traffic loading, relative movements between main cables and the deck, and lateral wind loads cause cyclic tension and cyclic secondary bending of the cable. Observations on bridges in service indicated that secondary bending is significant close to the anchorage points. The socketing material (cold-casting versus hot-casting sockets), the socket geometry (to minimize stress concentration), and vibration damping devices are some of the parameters that may need to be investigated. After the secondary bending fatigue is established, the problem of combination of axial fatigue with cyclic fatigue will have to be studied.
7. A knowledge of the fatigue design stress range and the actual loading experienced by bridge cables is important in order to assess the actual performance of a cable. Birdsall (Ref. 18) was able to obtain the design stress range of cables in some bridges. More field data on loading of cables needs to be obtained in order to derive representative load spectrum that could be used in a future variable amplitude test program.
8. Both acoustic emission and accelerometer non-destructive procedures are able to predict wire breaks at the instance of occurrence. The ability of these methods to detect pre-existing internal wire fracture is questionable. However promising results were obtained when a pulse echo test was performed on one of the specimen using the acoustic emission technique. The pulse echo test result presented in this research was based on a three meter long cable. The attenuation of the acoustic emission event along the cable and between layers is critical when the length and size of the cable increases. The potential of the pulse echo test should be further investigated using real cable lengths (e.g., in excess of 100 meters).

To conclude, the research presented herein showed that the axial fatigue performance of cables is affected by many parameters. The investigation of each individual parameter could be considered as a research topic. It is believed that future research will be required to investigate the importance of parameters such as cable make-up, lubrication, corrosion protection and testing environment, axial fatigue of individual wires, length-to-diameter ratio of test specimens, termination conditions, mean stress, cable vibration, and test frequency.

List of References

1. Podolny, W. Jr., and Scalzi, J.B., 1976, "Construction and design of cable-stayed bridges," John Wiley and Sons, p. 189-218.
2. Gimsing, N.J., 1983, "Cable supported bridges: concept and design," John Wiley and Sons, p. 57-78.
3. ASTM-Designation A586-86, May 1986, "Standard specification for zinc-coated parallel and helical steel wire structural strand," American Society for Testing and Materials, Philadelphia.
4. ASTM-Designation A603-88, Nov. 1988, "Standard specification for zinc-coated steel structural wire rope," American Society for Testing and Materials, Philadelphia.
5. ASTM-Designation A722-88a, Apr. 1989, "Standard specification for uncoated high-strength steel bar for prestressing concrete," American Society for Testing and Materials, Philadelphia.
6. ASTM-Designation A421-80, Dec. 1980, "Standard specification for uncoated stress-relieved steel wire for prestressed concrete," American Society for Testing and Materials, Philadelphia.
7. ASTM-Designation A416-88b, Dec. 1988, "Standard specification for steel strand, uncoated seven-wire stress-relieved for prestressed concrete," American Society for Testing and Materials, Philadelphia.
8. Wire Rope Industries Ltd., 1991, "General wire rope catalogue," Surrey, B.C..
9. Troitsky, 1977, "Cable-stayed bridges: theory and design," Crosby Lockwood Staples, p. 136-141.
10. Shinko Wire Co., Ltd., 1992, "HiAm and DINA high fatigue resistant cables for cable-stayed bridges," Nakahama, Amagasaki, Japan.
11. Watson, S.C. and D. Stafford, Apr. 1988, "Cables in trouble," Civil Engineering, ASCE, Vol. 58, No. 4, p.38-41.

12. Ministry of Transportation, Province of Ontario, 1988, "Ontario Highway Bridge Design Code – III," Downsview, Canada.
13. American Association of State Highway and Transportation Officials, Apr. 1992, "Standard Specifications for Highway Bridges," 4th Draft Edition, AASHTO, Washington, D.C..
14. American Petroleum Institute, May 1991, "Draft API recommended practice for design, analysis, and maintenance of mooring for floating production systems." API 2FP1 (RP2FP1), First Edition.
15. Post -Tensioning Institute, 1993, "Recommendations for stay cable design, testing and installation."
16. Tilly, G.P., June 1990, "Long term serviceability of bridge cables," Proceedings of the 2nd Symposium on Strait Crossings. Edited by J. Krokeborg, Trondheim, Norway, p.347-354.
17. Phoenix, S.L., H.H. Johnson and W. McGuire, June 1986, "Condition of steel cable after period of service," Journal of Structural Engineering, ASCE, Vol. 112, No. 6, p. 1263-1279.
18. Birdsall, B.,1992, "Lessons to be learned from the history of suspension bridge suspenders," Length Effect on Fatigue of Wires and Strands, IABSE Workshop, El Paular, Madrid, IABSE Report, Vol. 66, p. 139-145.
19. Birkenmaier, M. and R. Narayanan, 1982, "Fatigue resistance of large high tensile steel stay tendons," Fatigue of Steel and Concrete Structures, IABSE Colloquium, Lausanne, Switzerland, p. 663-672.
20. Hruska, F.H., 1951, "Calculation of stresses in wire ropes," Wire and Wire Products, Vol. 26, p. 76-767, 799-801.
21. Hruska, F.H., May 1952, "Radial forces in wire ropes," Wire and Wire Products, Vol. 27, p. 459-463.
22. Hruska, F.H., May 1953, "Tangetial forces in wire rope," Wire and Wire Products, Vol. 28, p. 455-460.

23. Leissa, A.W., Mar. 1959, "Contact stresses in wire ropes," *Wire and Wire Products*, Vol. 34, No. 3, p. 307-314, 372.
24. Starkey, W.L. and H.A. Cress, 1959, "An analysis of critical stresses and mode of failure of a wire rope," *Journal of Engineering for Industry, Transactions, ASME*, Vol. 81, Series B, No. 4, p. 307-316.
25. Durelli, A.J. and S. Machida, July 1973, "Response of epoxy oversized models of strands to axial and torsional loads," *Experimental Mechanics*, Vol. 13, p. 313-321.
26. Costello, G.A. and J.W. Phillips, OTC. 1974, "A more exact theory for twisted wire cables," *Journal of Engineering Mechanics Division, ASCE*, Vol. 100, p. 1096-1099.
27. Costello, G.A. and J.W. Phillips, Feb. 1976, "Effective modulus of twisted wire cables," *Journal of Engineering Mechanics Division, ASCE*, Vol. 102, p. 171-181.
28. Costello, G.A. and S.K. Sinha, May 1977a, "Static behavior of wire ropes," *Advances in Civil Engineering Through Engineering Mechanics, Proceeding Second Annual Engineering Mechanics Division Specialty Conference, North Carolina State University, Raleigh*, p. 475-478.
29. Costello, G.A. and S.K. Sinha, 1977b, "Torsional stiffness of twisted wire cables," *Journal of Engineering Mechanics Division, ASCE*, Vol. 103, p. 766-770.
30. Costello, G.A. and R.E. Miller, Aug. 1979, "Lay effect of wire rope," *Journal of Engineering Mechanics Division, ASCE*, Vol. 105, p. 597-608.
31. Love, A.E.H., 1927, "Treatise on the mathematical theory of elasticity," 4th ed. Cambridge, (and Dover Publications, New York, 1944).
32. Knapp, R.H., 1979, "Derivation of a new stiffness matrix for helically armored cables considering tension and torsion," *International Journal of Numerical Methods in Engineering*, Vol. 14, p. 515-529.
33. Hobbs, R.E. and M. Raouf, 1982, "Interwire slippage and fatigue prediction in stranded cables for TLP tethers," *Behavior of Offshore Structures*, Edited by C.

- Chryssostomidis and J. Connor, Hemisphere, McGraw Hill, New York Vol. 2, p. 77-99.
34. Raof, M. and R.E. Hobbs, July 1988, "Analysis of multilayered structural strands," *Journal of Engineering Mechanics*, ASCE, Vol. 114, No. 7, p. 1166-1182.
 35. Hobbs, R.E. and M. Raof, Dec. 1984, "Hysteresis in bridge strand," *Proceedings of the Institute of Civil Engineers*, Part 2, Vol. 77, p. 445-464.
 36. Raof, M. and R.E. Hobbs, Dec. 1989, "Torsional stiffness and hysteresis in spiral strands," *Proceedings of the Institute of Civil Engineers*, Part 2, Vol. 87, p. 501-515.
 37. Raof, M., 1990, "Effect of hydrostatic pressure on strand behavior," *Journal of Strain Analysis*, Institute of Mechanical Engineers, Vol. 25, No 2, p. 75-84.
 38. Raof, M., Dec. 1990, "Simple formulae for spiral strands and multi-strand ropes," *Proceedings of the Institute of Civil Engineers*, Part 2, Vol. 88, p. 527-542.
 39. Raof, M., 1991, "Methods of analysing large spiral strands," *Journal of Strain Analysis*, Institute of Mechanical Engineers, Vol. 26, No 3, p. 165-174.
 40. Raof, M. and Y.P. Huang, Nov. 1992, "Simplified methods for analysing steel strands," *Journal of the Institution of Structural Engineers*, Vol. 70, No 22, p. 390-397.
 41. Fuchs, H.O. and R.I. Stephens, 1980, "Metal fatigue in engineering," John Wiley and Sons Publication, Chapter 3.
 42. Waterhouse, R.B., M. Takeuchi and A.P. van Gool, Aug. 1989, "The relative effects of hot dip galvanising and electrodeposited zinc on the fretting-fatigue behavior of roping steel wires in seawater," *Transaction of the Institute of Metal Finishing*, Vol. 67, No. 3, p. 63-66.
 43. Verpoest, I., E. Aernoudt, A. Deruyttere and M. De Bondt, 1985, "The fatigue threshold, surface condition and fatigue limit of steel wire," *International Journal of Fatigue*, Vol. 7, No. 4, p. 199-214.

44. Waterhouse, R.B., 1972, "Fretting corrosion," Pergamon Press, Chapter 1.
45. Esslinger, V., 1992, "Fatigue testing of wires and strands: test procedures and experimental studies," Length Effect on Fatigue of Wires and Strands, IABSE Workshop, El Poular, Madrid, IABSE Report, Vol. 66, p. 33-50.
46. Gabriel, K., 1992, "Failure mechanisms in fatigue," Length Effect on Fatigue of Wires and Strands, IABSE Workshop, El Poular, Madrid, IABSE Report, Vol. 66, p. 51-72.
47. Llorca, J., J.M. Varona, V. Sanchez-Galvez and F. Gutierrez Solana, 1989, "Fatigue behavior of wire ropes," Materials and Structures, Vol. 22, p. 411-419.
48. Bahke, E., 1980a, "Principles defining the strength of wire ropes and chains," Part I, Wire, Vol. 29, No. 2, p. 54-61.
49. Bahke, E., 1980b, "Principles defining the strength of wire ropes and chains," Part II, Wire, Vol. 30, No. 3, p. 168-178.
50. Castillo, E., A. Fernandez-Canteli., V. Esslinger and B. Thurlimann, 1985, "Statistical model for fatigue analysis of wires, strands and cables," IABSE Proceedings P-82/85, Zurich, p. 1-40.
51. Watt, D.G., May 1941, "Fatigue test on zinc-coated steel wire," Wire and Wire Products, Vol. 16, p. 280-285, 294,295.
52. Thorpe, T.W. and A.Rance, May 1983, "The tensile fatigue of wire rope: a new approach," Proceedings of the 15th Annual Offshore Technology Conference, Houston, Texas, OTC 4638, p. 483-490.
53. Potts, A.E., C.R. Chaplin and N.R.H. Tantrum, May 1988, "Factors influencing the endurance of steel wire ropes for mooring offshore structures," Proceedings of the 20th Annual Offshore Technology Conference, Houston, Texas, OTC 5718, p. 321-331.
54. Waters, D., D. Eggar and H. Plant, May 1985, "Developments in fatigue assessments of large-diameter wire ropes used in offshore moorings," Proceedings of the 17th Annual Offshore Technology Conference, Houston, Texas, OTC 5000, p. 361-366.

55. Hanzawa, M., H. Yokota, Y. Toda and K. Yokoyama, June 1982, "Fatigue behavior of large diameter wire ropes," *Journal of the Society of Petroleum Engineers*, Vol. 22, No. 3, p. 420-428.
56. Hanzawa, M., H. Yokota, Y. Toda and K. Yokoyama, May 1981, "Fatigue behavior of large diameter wire ropes," *Proceedings of the 13th Annual Offshore Technology Conference*, Houston, Texas, OTC 3999, p. 435-442.
57. Berge, S., 1985a, "Axial stiffness and fatigue strength of 76 mm diameter steel rope," Report MK/R87, University of Trondheim.
58. Berge, S., 1985b "Axial stiffness and fatigue strength of 32 mm diameter steel rope," Report MK.R88, University of Trondheim.
59. Lucht, W.A. and F.W. Donecker, May 1977, "Factors affecting wire rope life in a marine environment," *Proceedings of the 9th Annual Offshore Technology Conference*, Houston, Texas, OTC 2924, p. 361-366.
60. Casey, N.F. and D.M. Waters, May 1987, "Fatigue testing of large wire ropes," *Wire Industry*, Vol. 54, No. 641, p. 300-303.
61. Casey, N.F. and D.M. Waters, May 1988, "Fatigue behaviour of large diameter wire ropes," *Wire Industry*, Vol. 55, No. 653, p. 371-378.
62. Ronson, K.T., May 1980, "Ropes for deep water mooring," *Proceedings of the 12th Annual Offshore Technology Conference*, Houston, Texas, OTC 3850, p. 485-496.
63. Raof, M., 1992, "A critical review of draft API recommended practice 2FP1 regarding fatigue life estimation of moorings," *Materials Engineering*, ASME, Vol. III-B, 1992 OMAE, p. 521-532.
64. Hobbs, R.E. and K. Ghavami, Apr. 1982, "The fatigue of structural wire strands," *International Journal of Fatigue*, Vol. 4, p. 69-72.
65. Yeung, Y. and J. Walton, July 1986, "Accelerated fatigue testing of wire ropes," *Wire Industry*, Vol. 53, No. 631, p.490-493.

66. Smith, H.L., F.R. Stonesifer and E.R. Seibert, May 1978, "Increase in fatigue life of wire rope through periodic overloads," Proceedings of the 10th Annual Offshore Technology Conference, Houston, Texas, OTC 3256, p. 1771-1778.
67. Stonesifer, F.R. and H.L. Smith, May 1979, "Tensile fatigue in wire rope," Proceedings of the 11th Annual Offshore Technology Conference, Houston, Texas, OTC 3419, p. 539-545.
68. Nakamura, S. and H. Hosokawa, Oct. 1989, "A study on the fatigue design of parallel wire strands on cable-stayed bridges," Proceedings of the Japan Society of Civil Engineers, Vol. 6, No. 2, p. 157-166.
69. Birkenmaier, M., May 1980, "Fatigue resistant tendons for cable-stayed construction," IABSE Proceedings P-30/80, Part 2, p. 65-79.
70. Takena, K., C. Miki, H. Shimokawa and K. Samamoto, Mar. 1992, "Fatigue resistance of large-diameter cable for cable-stayed bridges," Journal of Structural Engineering, ASCE, Vol. 118, No. 3, p. 701-715.
71. Paulson, C., K.H. Frank, and J.E. Breen, Apr. 1983, "A fatigue study of prestressing strand," Research Report 300-1, Center for Transportation Research, The University of Texas at Austin.
72. Raof, M., Oct. 1990, "Axial fatigue of multilayered strands," Journal of Engineering Mechanics, ASCE, Vol. 116, No. 10, p. 2083-2099.
73. Raof, M., Mar. 1991, "Axial fatigue life prediction of structural cables from first principles," Proceedings of the Institute of Civil Engineers, Part 2, Vol. 91, p. 19-38.
74. Knapp, R.H. and E.Y.C. Chiu, Mar. 1988, "Tension fatigue model for helically armored cables," Journal of Energy Resources Technology, ASME, Vol. 110, p.12-18.
75. Boresi, A.P., O.M. Sidebottom, F.B. Seely and J.O. Smith, 1978, "Advanced mechanics of materials," 3rd Edition, Chapter 14, John Wiley.
76. Fernandez-Canteli, A., E. Castillo and A. Arguelles, 1992, "Length Effect on Fatigue of Wires and Prestressing Steels," Length Effect on Fatigue of Wires and

- Strands, IABSE Workshop, El Paular, Madrid, IABSE Report, Vol. 66, p. 125-135.
77. Babel, H., 1979, "Destructive and non-destructive test methods to determine the life of wire ropes—Part 1," *Wire*, Vol. 28, No. 6, p. 263-270.
 78. Babel, H., 1980, "Destructive and non-destructive test methods to determine the life of wire ropes—Part 2," *Wire*, Vol. 29, No. 1, p. 38-44.
 79. Weischedel, H.R., Sept. 1985, "The inspection of wire ropes in service," *Wire Journal International*, Vol. 18, No. 9, p. 180-195.
 80. The European Working Group on Acoustic Emission, Aug. 1985, "Codes for acoustic emission examination," *NDT International*, Vol. 18, No. 4, p. 185-194.
 81. Taylor, J.L. and N.F. Casey, Jan. 1984, "The acoustic emission of steel wire ropes," *Wire Industry*, Vol. 51, No. 601, p. 79-82.
 82. Casey, N.F., K.M. Holford and J.L. Taylor, Sept. 1988, "Wire break detection during the tensile fatigue testing of 40 mm diameter wire rope," *British Journal of Non-Destructive Testing*, Vol. 30, No. 5, p. 338-341.
 83. Woodward, R.J., July 1989, "Detecting fractures in steel cables," *Wire Industry*, Vol.56, No. 667, p. 401-405.
 84. Brüel and Kjær manual on vibration transducers.
 85. Monac International, July 1993, "Progress report on acoustic emission monitoring of steel cables," Internal Report.
 86. Wadsworth, H.M., 1990, "Handbook of statistical methods for engineers and scientists," M^c Graw Hill, Sections 2 and 13.
 87. Committee E-9 on Fatigue, 1963, "A guide for fatigue testing and statistical analysis of fatigue data," ASTM Special Technical Publication No. 91, Second Edition, American Society for Testing and Materials, Philadelphia.
 88. Esslinger, V., 1992, "Experimental execution and results of fatigue test with prestressing steel," Length Effect on Fatigue Wires and Strands, IABSE Workshop, El Paular, Madrid, IABSE Report, Vol. 66, p. 147-156.

89. Tilly, G.P., 1988, "Performance of bridge cables," 1st Oleg Kerensky Memorial Conference, Houston, Texas, 539-545.
90. Casey, N.F., Dec. 1991, "An approach to the fatigue life prediction of large diameter wire ropes," OIPEEC Bulletin, No. 62, published by the Department of Engineering, Reading University, Reading, U.K.

Appendix A

Test Data from Static Tests and Wire Breakage Detection

Table A.1 Test data for specimen SP1

Number of Cycles	Overall Modulus of Elasticity (MPa)
1 150 370	165 750
1 350 280	165 800
2 130 750	166 710
3 175 760	166 280
3 622 150	166 090
4 035 040	166 400
4 350 430	166 670
4 882 980	166 430
5 417 650	166 070
5 925 680	164 410
6 440 140	164 200
6 978 610	163 720
7 474 460	160 000
8 147 530	152 730
8 200 360	149 990

Table A.2 Test data for specimen SP2

Number of Cycles	Overall Modulus of Elasticity (MPa)	Free Length Modulus of Elasticity (MPa)	Total Number of Breaks (Accelerometers)
10	162 990	176 620	0
1000	159 430	176 610	0
121 470	161 560	176 430	0
467 880	161 250	176 650	1
846 560	157 700	172 620	6
1 230 880	158 040	172 500	7
1 739 870	156 920	171 890	9
2 189 150	153 060	165 260	10
2 420 730	143 680	154 220	15
2 579 310	140 560	153 490	20
2 717 640	133 020	143 110	35

Table A.3 Test data for specimen SP3

Number of Cycles	Overall Modulus of Elasticity (MPa)	Free Length Modulus of Elasticity (MPa)	Total Number of Breaks (Accelerometers)
10	165 860	177 070	0
160 000	166 830	178 580	0
299 670	156 140	158 630	6
418 260	0	0	—

Table A.4 Test data for specimen SP4

Number of Cycles	Overall Modulus of Elasticity (MPa)	Free Length Modulus of Elasticity (MPa)	Total Number of Breaks (Accelerometers)
10	169 650	176 740	0
154 520	167 380	175 940	3
200 000	162 830	170 850	6
250 000	156 090	162 950	9
277 100	152 990	156 510	13
308 048	141 190	144 980	18

Table A.5 Test data for specimen SP5

Number of Cycles	Overall Modulus of Elasticity (MPa)	Free Length Modulus (MPa)	Wire Breaks (Accelerometers)	Wire Breaks (Acoustic Emission)
1	166 550	170 210	0	0
150 000	168 450	177 290	0	0
642 550	168 380	176 060	1	1
877 860	165 740	176 270	1	1
1 120 000	168 260	176 580	1	1
1 368 000	166 550	177 030	1	1
1 653 000	167 960	176 620	1	1
2 099 020	167 310	176 530	1	1
2 762 340	167 430	176 410	1	1
3 115 540	167 250	177 420	1	1
3 468 000	167 530	177 350	1	1
3 930 610	167 920	177 090	1	1
4 529 250	167 940	177 350	1	1
4 939 700	168 860	177 710	1	1
5 490 700	170 260	178 270	1	1
6 109 710	168 960	178 610	1	1
6 543 390	168 080	178 400	1	2
7 019 960	169 250	178 110	4	5
7 718 110	166 940	177 750	9	8
8 216 190	168 110	177 970	14	10
8 587 900	167 950	178 080	16	13
8 924 900	167 380	177 700	21	21
9 217 800	164 190	174 910	27	29
9 319 020	162 630	175 030	32	33
9 372 000	—	—	—	63

Table A.6 Test data for specimen SP6

Number of Cycles	Overall Modulus of Elasticity (MPa)	Free Length Modulus (MPa)	Wire Breaks (Accelerometers)	Wire Breaks (Acoustic Emission)
1	158 790	174 800	0	0
291 540	167 270	176 470	1	1
558 870	165 970	173 430	3	3
635 860	165 330	173 970	3	3
985 590	165 760	173 840	6	8
1 155 690	165 120	173 140	6	8
1 362 590	165 300	172 370	8	10
1 417 410	164 930	173 740	8	10
1 703 520	161 640	170 310	11	14
1 957 640	159 180	170 620	-	49

Table A.7 Test data for specimen SP7

Number of Cycles	Overall Modulus of Elasticity (MPa)	Free Length Modulus (MPa)	Wire Breaks (Accelerometers)	Wire Breaks (Acoustic Emission)
1	113 050	167 850	0	0
122 230	168 560	174 650	0	0
488 510	168 720	175 000	0	1
1 001 320	168 200	176 720	1	3
1 513 930	167 050	174 770	2	5
1 889 400	165 700	174 110	2	22
2 124 100	160 910	166 120	14	31

Table A.8 Test data for specimen SP8

Number of Cycles	Overall Modulus of Elasticity (MPa)	Free Length Modulus (MPa)	Wire Breaks (Accelerometers)	Wire Breaks (Acoustic Emission)
1	156 330	171 280	0	0
71 790	165 030	173 560	0	0
138 180	162 360	170 820	3	3
204 600	156 810	164 410	6	18

Table A.9 Test data for series SL

Specimen	Number of Cycles	Overall Modulus of Elasticity (MPa)	Free Length Modulus (MPa)	Total Number of Breaks (Accelerometers)
SL1	10	167 800	176 910	0
	282 870	165 280	171 170	3
	504 000	165 270	170 890	4
	553 470	140 640	142 430	7
	566 300	—	—	9
SL2	10	166 650	176 250	0
	250 140	167 510	176 890	0
	462 560	165 380	171 300	2
	635 860	162 910	168 510	4
SL3	10	172 590	175 370	0
	9 824 000	172 010	176 890	0
SL4	1 413 150	169 730	177 310	0
	2 482 190	—	—	7
SL5	10	172 210	173 840	0
	226 680	169 680	177 310	2
	245 740	164 610	178 030	3

Table A.10 Test data for series SS

Specimen	Number of Cycles	Overall Modulus of Elasticity (MPa)	Free Length Modulus (MPa)	Total Number of Breaks (Accelerometers)
SS1	10	162 155	174 590	0
	240 000	144 280	156 450	3
SS2	10	159 510	176 760	0
	4 183 410	159 540	178 460	0
SS3	10	164 550	172 480	0
	941 750	141 130	150 020	3

Appendix B

Statistical Analysis of Test Data

Statistical Analysis of Test Data

B.1 Regression Analysis

Statistical analysis of the test data was performed in order to find the relation between the fatigue life of multi-layered strand (dependent variable) and the stress range (independent variable). The regression analysis was conducted using the method of least squares.

This appendix serves as a supplement to Chapters 5 and 6. It presents the data used to obtain the regression models presented in Chapters 5 and 6. Tables B.1 to B.3 present the test data obtained in the experimental program conducted at the University of Alberta and outlined in Chapters 3 and 4. Table B.4 gives the statistical analysis of all test data reviewed from the literature survey presented in Chapter 6 and in Appendix C. The test data obtained in the present investigation were also included in the analysis presented in Table B.4.

The simple and linear model used for the regression analysis was

$$y = b_0 + b_1 x \quad (\text{B-1})$$

where x is the independent variable and y is the dependent variable. The constants b_0 and b_1 are the y -intercept and the slope of the line, respectively. Using the method of least squares, the slope b_1 of the best fit is obtained from (Ref. 86)

$$b_1 = \frac{n \sum_{i=1}^n (x_i y_i) - \sum_{i=1}^n x_i \sum_{i=1}^n y_i}{n \sum_{i=1}^n x_i^2 - \left(\sum_{i=1}^n x_i \right)^2} \quad (\text{B-2})$$

where n is the number of data points, x_i is the i -th value of the independent variable, and y_i is the i -th measured value of the dependent variable. The values for the sums used in Eq. (B-2) are tabulated in the Tables presented in this Appendix. The value of b_0 can be obtained from:

$$b_0 = \bar{y} - b_1 \bar{x} \quad (\text{B-3})$$

where \bar{y} is the mean value of y and \bar{x} is the mean of x .

The goodness of fit of the regression model is measured using the coefficient of determination, r^2 , given by (Ref. 86)

$$r^2 = b_1 \frac{S_{xy}}{S_{yy}} \quad (\text{B-4.a})$$

where,

$$S_{xy} = \sum_{i=1}^n (x_i y_i) - \frac{\left(\sum_{i=1}^n x_i \right) \left(\sum_{i=1}^n y_i \right)}{n} \quad (\text{B-4.b})$$

$$S_{yy} = \sum_{i=1}^n (y_i^2) - \frac{\left(\sum_{i=1}^n y_i \right)^2}{n} \quad (\text{B-4.c})$$

If all the points are located on the regression line, then r^2 would equal unity. An r^2 value of zero indicates that y is not linearly predicted in any useful way by x . Ideally, a value of r^2 close to unity is required, but there is no dividing line that separates "acceptable" r^2 values from "unacceptable" values.

Table B.1 Regression analysis for SP series

Stress Range Sr (% UTS)	N	log Sr (Xi)	log N (Yi)	Xi ²	Yi ²	XiYi
21.50	7200000	1.332	6.857	1.775	47.023	9.137
26.33	661054	1.420	5.820	2.018	33.875	8.267
26.33	284374	1.420	5.454	2.018	29.745	7.747
26.33	180475	1.420	5.256	2.018	27.630	7.466
21.50	6942000	1.332	6.841	1.775	46.806	9.116
23.92	810410	1.379	5.909	1.901	34.913	8.147
23.92	1345617	1.379	6.129	1.901	37.564	8.450
28.67	178624	1.457	5.252	2.124	27.583	7.654

Sum =	11.141	47.519	15.530	285.138	65.985
Average =	1.393	5.940			

b1 = -13.576	Sxy = -0.192	R ² = 0.905
b0 = 24.847	Sxx = 0.014	Sigma = 0.214
n = 8	Syy = 2.882	t = 7.558

Table B.2 Regression analysis for SL and SS series

Stress Range Sr (% UTS)	N	log Sr (Xi)	log N (Yi)	Xi ²	Yi ²	NiYi
22.11	226578	1.345	5.355	1.808	28.678	7.201
22.11	306125	1.345	5.486	1.808	30.095	7.376
14.75	10000000	1.169	7.000	1.366	49.000	8.182
22.11	2424370	1.345	6.385	1.808	40.763	8.585
25.82	179974	1.412	5.255	1.994	27.617	7.420
25.82	180402	1.412	5.256	1.994	27.628	7.422
18.40	4200000	1.265	6.623	1.600	43.867	8.377
22.11	276290	1.345	5.441	1.808	29.608	7.316

Sum =	10.636	46.802	14.185	277.258	61.878
Average =	1.329	5.850			

b1 = -7.7245046	Sxy = -0.344	R ² = 0.768
b0 = 16.119833	Sxx = 0.045	Sigma = 0.365
n = 8	Syy = 3.457	t = 4.462

Table B.3 Regression analysis for SP, SL and SS series

Stress Range Sr (% UTS)	N	log Sr (Xi)	log N (Yi)	Xi ²	Yi ²	XiYi
21.50	7200000	1.332	6.857	1.775	47.023	9.137
26.33	661054	1.420	5.820	2.018	33.875	8.267
26.33	284374	1.420	5.454	2.018	29.745	7.747
26.33	180475	1.420	5.256	2.018	27.630	7.466
21.50	6942000	1.332	6.841	1.775	46.806	9.116
23.92	810410	1.379	5.909	1.901	34.913	8.147
23.92	1345617	1.379	6.129	1.901	37.564	8.450
28.67	178624	1.457	5.252	2.124	27.583	7.654
22.11	226578	1.345	5.355	1.808	28.678	7.201
22.11	306125	1.345	5.486	1.808	30.095	7.376
14.75	10000000	1.169	7.000	1.366	49.000	8.182
22.11	2424370	1.345	6.385	1.808	40.763	8.585
25.82	179974	1.412	5.255	1.994	27.617	7.420
25.82	180402	1.412	5.256	1.994	27.628	7.422
18.40	4200000	1.265	6.623	1.600	43.867	8.377
22.11	276290	1.345	5.441	1.808	29.608	7.316

Sum =	21.777	94.321	29.715	562.396	127.863
Average =	1.361	5.895			

b1 = -6.879	Sxy = -0.513	R ² = 0.554
b0 = 15.258	Sxx = 0.075	Sigma = 0.450
n = 16	Syy = 6.371	t = 4.172

Table B.4 Regression analysis of all test data

Stress Range Sr (% UTS)	N	log Sr (Xi)	log N (Yi)	X_i^2	Y_i^2	$X_i Y_i$
26.20	50000	1.418	4.699	2.012	22.080	6.665
27.00	104800	1.431	5.020	2.049	25.204	7.186
26.20	263700	1.418	5.421	2.012	29.388	7.689
25.90	422400	1.413	5.626	1.997	31.649	7.951
24.20	76400	1.384	4.883	1.915	23.845	6.757
24.20	105000	1.384	5.021	1.915	25.212	6.948
25.20	119100	1.401	5.076	1.964	25.765	7.113
24.20	172500	1.384	5.237	1.915	27.424	7.247
20.60	301700	1.314	5.480	1.726	30.026	7.199
20.00	379300	1.301	5.579	1.693	31.125	7.258
21.80	400300	1.338	5.602	1.791	31.387	7.499
22.00	607600	1.342	5.784	1.802	33.450	7.764
16.10	451800	1.207	5.655	1.456	31.978	6.825
10.00	4641600	1.000	6.667	1.000	44.444	6.667
15.90	1183300	1.201	6.073	1.443	36.882	7.296
9.20	5000000	0.964	6.699	0.929	44.876	6.456
21.50	7200000	1.332	6.857	1.775	47.023	9.137
26.33	661100	1.420	5.820	2.018	33.876	8.267
26.33	284400	1.420	5.454	2.018	29.745	7.747
26.33	180500	1.420	5.256	2.018	27.631	7.467
21.50	6942000	1.332	6.841	1.775	46.806	9.116
23.92	810400	1.379	5.909	1.901	34.913	8.147
23.92	1345600	1.379	6.129	1.901	37.564	8.450
28.67	178600	1.457	5.252	2.124	27.582	7.654
22.11	226600	1.345	5.355	1.808	28.679	7.201
22.11	306100	1.345	5.486	1.808	30.095	7.376
14.77	10000000	1.169	7.000	1.367	49.000	8.186
22.11	2424400	1.345	6.385	1.808	40.763	8.585
25.82	180000	1.412	5.255	1.994	27.618	7.420
25.82	180500	1.412	5.256	1.994	27.631	7.422
18.40	4183000	1.265	6.621	1.600	43.844	8.375
22.11	276290	1.345	5.441	1.808	29.608	7.316
41.10	17460	1.614	4.242	2.604	17.995	6.846
41.10	20400	1.614	4.310	2.604	18.573	6.955
30.70	37500	1.487	4.574	2.212	20.922	6.802
30.70	42660	1.487	4.630	2.212	21.437	6.885
23.40	115000	1.369	5.061	1.875	25.611	6.929
23.40	221300	1.369	5.345	1.875	28.569	7.318
20.50	170000	1.312	5.230	1.721	27.358	6.861
20.50	347000	1.312	5.540	1.721	30.695	7.268

15.00	724000	1.176	5.860	1.383	34.337	6.892
10.30	3040000	1.013	6.483	1.026	42.028	6.566
10.70	6900000	1.029	6.839	1.060	46.770	7.040
10.60	8010000	1.025	6.904	1.051	47.650	7.078
29.00	380200	1.462	5.580	2.139	31.137	8.160
28.00	531000	1.447	5.725	2.094	32.777	8.285
10.10	8810000	1.004	6.945	1.009	48.233	6.975
20.00	660000	1.301	5.820	1.693	33.867	7.571
22.00	667000	1.342	5.824	1.802	33.920	7.818
24.50	1050000	1.389	6.021	1.930	36.255	8.364
15.00	1110000	1.176	6.045	1.383	36.546	7.110
18.00	2450000	1.255	6.389	1.576	40.821	8.020
10.50	11800000	1.021	7.072	1.043	50.012	7.222

Sum =	69.8861125	303.279298	93.3460817	1762.63355	395.35307
Average =	1.3186059	5.7222509			

b1 =	-3.8135707	Sxy =	-4.5528	R ² =	0.63848139
bo =	10.7508477	Sxx =	1.19384177	Sigma =	0.43904729
n =	53	Syy =	27.1933133	t =	9.49060462

Appendix C

Experimental Data from Literature

Table C.1 Fatigue test data from Tilly (Ref. 89)

Stress Range Ratio (% UTS)	Stress Range (MPa)	Number of Cycles
26.2	327.50	50 000
27.0	337.50	104 800
26.2	327.50	263 700
25.9	323.75	422 400
24.2	302.50	76 400
24.2	302.50	105 000
25.2	315.00	119 100
24.2	302.50	172 500
20.6	257.50	301 700
20.0	250.00	379 300
21.8	272.50	400 300
22.0	275.00	607 600
16.1	201.25	451 800
10.0	125.00	4 641 600
15.9	198.75	1 183 300
9.2	115.00	5 000 000

23.9	323.75	422 400
24.2	302.50	76 400
24.2	302.50	105 000
25.2	315.00	119 100
24.2	302.50	172 500
20.6	257.50	301 700
20.0	250.00	379 300
21.8	272.50	400 300
22.0	275.00	607 600
16.1	201.25	451 800
10.0	125.00	4 641 600
15.9	198.75	1 183 300
9.2	115.00	5 000 000



23.9	323.75	422 400
24.2	302.50	76 400
24.2	302.50	105 000
25.2	315.00	119 100
24.2	302.50	172 500
20.6	257.50	301 700
20.0	250.00	379 300
21.8	272.50	400 300
22.0	275.00	607 600
16.1	201.25	451 800
10.0	125.00	4 641 600
15.9	198.75	1 183 300
9.2	115.00	5 000 000

